NTNU
Norwegian University of
Science and Technology

Numerical Implementation and Evaluation of a Set of Population Balance Breakage Closures

Vidar Torarin Skjervold

Chemical Engineering and Biotechnology
Submission date: June 2016
Supervisor: Hugo Atle Jakobsen, IKP
Co-supervisor: Jannike Solsvik, IKP

Norwegian University of Science and Technology
Department of Chemical Engineering

Abstract

The population balance equation (PBE) can be used to model multiphase processes, where one or more dispersed phases are distributed in a continuous medium. In such systems, the interfacial area is an important quantity, because it governs the rate of mass, heat and momentum transfer between the phases. Applying the PBE to multiphase systems gives a more accurate description of the interfacial area, and is therefore an important tool in the modelling of several types of chemical engineering equipment. In order to solve the PBE, constitutive equations known as breakage closures must be specified. Without accurate and robust breakage closures, it is difficult to accurately predict the size distributions in multiphase processes using the PBE.

Despite the considerable efforts that have been invested in developing breakage closures, there does not seem to be consensus in the literature on the underlying physics of the breakage mechanism. The objective of this thesis was to perform an evaluation of a set of breakage closures, to determine their suitability as constitutive equations in the population balance equation. Emphasis was placed on selecting regularly used closures that were designed for turbulent systems. The closures were evaluated with regard to computational time, conserving properties, the ability to reproduce experimental data and their performance as closures in a simplified PBE test case. All closures were extended to the wide energy spectrum of turbulence, and the extended models were also included in the evaluation.

Based on the evaluation, it was concluded that the models of Coulaloglou and Tavlarides (1977), Han et al. (2011) and Becker et al. (2014) were most suitable as constitutive equations in the PBE. Additionally, a modified version of Martínez-Bazán et al., where a breakage probability was introduced to make the breakage frequency profile less steep, performed well. These closures were computationally efficient, volume and number conserving, in acceptable agreement with at least one of the experimental data series and gave plausible solutions of the PBE test case without causing numerical difficulties. To ensure that the breakage closures are valid in all ranges of turbulence, the wide energy spectrum versions should be used. The capillary criterion was identified as an important breakage constraint, because it avoids accumulation of particles at the smallest particle size in the mass density function.

All of the studied closures apply *a priori* assumptions of the number of daughters formed in the breakage process. Introducing a relation that calculates the number of produced daughters based on the system properties and mother particle size was identified as a possible way of improving the breakage closures. However, introducing such a relation involves some challenges, and a method for reducing the model complexity by dividing the daughter population into groups based on the particle size was presented. When applying this method, care should be taken to ensure that the redistribution density function is both

volume and number conserving. New breakage closures based on this concept should be developed and evaluated, to determine if the prediction of the number of daughters makes the models more physically realistic.

In the literature, there is a general lack of experimental data for the breakage frequencies and probability density functions for bubbles and droplets. In order to enable proper evaluation of the breakage closures, it should be made a priority to perform experiments on the breakage frequencies and redistribution functions for both bubbles and droplets in several systems for a wide range of particle sizes.

Sammendrag

Populasjonsbalansen kan brukes til å modellere flerfaseprosesser, hvor en eller flere dispergerte faser er fordelt i et kontinuerlig medium. Arealet mellom fasene er en viktig størrelse i slike systemer, fordi det styrer overføringen av masse, varme og moment mellom fasene. Populasjonsbalansen gir en mer nøyaktig beskrivelse av arealet mellom fasene, og er derfor et viktig verktøy i modelleringen av kjemitekniske enheter. For å løse populasjonsbalansen må ytterligere likninger som beskriver oppbrytningen av partiklene i den dispergerte fasen være kjent. Dersom disse likningene ikke er nøyaktige og robuste er det vanskelig å oppnå en nøyaktig beskrivelse av flerfasesystemer ved å bruke populasjonsbalansen.

På tross av den betraktelige innsatsen som har blitt investert i å utvikle modeller som beskriver oppbrytningen av partikler, virker det å være uenighet i litteraturen om hvilke fysiske prinsipper som ligger bak oppbrytningsmekanismen. Målet med denne oppgaven er å gjennomføre en evaluering av en rekke oppbrytningsmodeller, for å vurdere modellenes egnethet som funksjoner i populasjonsbalansen. I evalueringen ble det valgt å fokusere på modeller for turbulente systemer som jevnlig benyttes i litteraturen. Modellene ble evaluert i forhold til beregningstid, konserverende egenskaper, evne til å reprodusere eksperimentelle data og oppførsel i et forenklet populasjonsbalansesystem. En utvidelse av alle modellene til hele det turbulente energispekteret ble foretatt, og de utvidede modellene ble også inkludert i evalueringen.

Basert på evalueringen ble det konkludert at modellene til Coulaloglou og Tavlarides (1977), Han et al. (2011) og Becker et al. (2014) var best egnet som oppbrytningsfunksjoner i populasjonsbalansen. En utvidet versjon av Martínez-Bazán et al., hvor oppbrytningsfrekvensen ble gjort mindre spiss ved å introdusere en oppbrytningssannsynlighet, viste også gode resultater i evalueringen. Disse modellene var beregningseffektive, volum- og antallkonserverende, i akseptabel overensstemmelse med minst ett av de eksperimentelle dataseriene og bidro til plausible løsninger av populasjonsbalansen uten numeriske problemer. De utvidede modellene som er gyldige i hele det turbulente energispekteret burde benyttes. Kapillærkriteriet ble identifisert som viktig, ettersom det unngår akkumulering av partikler på den minste mulige partikkelstørrelsen.

Alle de studerte modellene antar *a priori* hvor mange datterpartikler som dannes i oppbrytningsprosessen. Å introdusere en relasjon som beregner antall døtre basert på systemegenskaper og morstørrelse ble identifisert som en mulig forbedring av oppbrytningsmodellene. Innføringen av en slik relasjon medfører noen utfordringer, og en metode for å redusere kompleksiteten til modellene ved å dele datterpartiklene inn i grupper basert på størrelse ble presentert. Ved bruk av denne metoden må det passes på at fordelingsfunksjonen blir volum- og antallkonserverende. Nye modeller basert på dette konseptet burde utvikles og evalueres, for å fastslå om beregning av antall døtre gjør modellene mer fysisk korrekte.

Det er mangel på eksperimentelle data for oppbrytningsfrekvenser og fordelingsfunksjoner for både bobler og dråper i litteraturen. Dette gjør det vanskelig å gjennomføre ordentlige evalueringer av oppbrytningsmodellene, og det burde derfor være en prioritet å gjennomføre eksperimenter på oppbrytningsfrekvenser og fordelingsfunksjoner for flere typer systemer og mange partikkelstørrelser.

Preface

This Master's thesis was written in the spring of 2016. It concludes the 5 year Master's program in Chemical Engineering and Biotechnology at the Norwegian University of Science and Technology, leading to the degree of M.Sc. in Chemical Engineering. My final year at NTNU was spent as a part of the research group in Environmental Engineering and Reactor Technology within the Department of Chemical Engineering. The work performed in this thesis is a continuation of the specialization project carried out in the fall of 2015.

I would like to thank my supervisors, Dr. Jannike Solsvik and Professor Hugo Jakobsen for your support throughout this last year. The dedication and passion you show towards your work is truly a source of inspiration. Our weekly meetings often lasted much longer than intended, but hopefully you also learned something from our long discussions and my seemingly endless list of questions. I certainly did!

I would also like to thank my classmates, who have made these five years at NTNU fly by. A special thanks to Mathias for many breaks, discussions, laughs and also for proofreading my thesis. Last, but not least, I am grateful for the support and encouragement I have always received from my family and Cathrine.

Declaration of Compliance

I declare that this is an independent work according to the exam regulations of the Norwegian University of Science and Technology (NTNU).

Trondheim, June 19, 2016

Vidar T. Skjervold

Table of Contents

List of Figures

Nomenclature

Acronym	Explanation
PBE	Population balance equation
CFD	Computational fluid dynamics

Alias	Explanation
AW	Air-water system
BE	Original closure of Becker et al. (2014)
BEW	Wide energy spectrum version of Becker et al. (2014)
CT	Original closure of Coulaloglou and Tavlarides (1977)
CTW	Wide energy spectrum version of Coulaloglou and Tavlarides (1977)
DW	Dodecane-water system
H11	Original closure of Han et al. (2011)
H11W	Wide energy spectrum version of Han et al. (2011)
H15	Original closure of Han et al. (2015)
H15M	Modified version of Han et al. (2015)
LI	Original closure of Liao (2013) and Liao et al. (2015)
LIW	Wide energy spectrum version of Liao (2013) and Liao et al. (2015)
LS	Original closure of Luo and Svendsen (1996)
LSW	Wide energy spectrum version of Luo and Svendsen (1996)
MB	Original closure of Martínez-Bazán et al.
MBW	Wide energy spectrum version of Martínez-Bazán et al.
PW I	Petroleum-water system I
PW II	Petroleum-water system II
SO	Original closure of Solsvik et al. (2013)
SOW	Wide energy spectrum version of Solsvik et al. (2013)
TW	Toluene-water system
XI	Original closure of Xing et al. (2015)
XIW	Wide energy spectrum version of Xing et al. (2015)

List of Latin Symbols

Symbol	Description	Unit
A	Statistical event in Poisson process	[-]
a	Short semiaxis of ellipsoidal intermediate	[m]
B	Statistical event in Poisson process	[-]
B_B	Breakage birth term in PBE	$[\mathrm{m}^{-4}\mathrm{s}^{-1}]$
		$[\mathrm{kgm}^{-4}\mathrm{s}^{-1}]$
B_D	Breakage death term in PBE	$[\mathrm{m}^{-4}\mathrm{s}^{-1}]$
		$[\mathrm{kgm}^{-4}\mathrm{s}^{-1}]$
b	Breakage frequency	$[\mathrm{s}^{-1}]$
	Long semiaxis of ellipsoidal intermediate	[m]
C	Constant	[-]
Ca	Capillary number	[-]
$\mathrm{Ca_c}$	Continuous phase capillary number = $\overline{\sigma}_{\mu,c}/\overline{\sigma}_s$	[-]
$\mathrm{Ca_d}$	Dispersed phase capillary number = $\overline{\sigma}_{\mu,d}/\overline{\sigma}_s$	[-]
C_0	Dimensionless oscillation ratio of Han et al. (2011)	[-]
	Constant used in Han et al. (2015)	[-]
C_1	Constant	[-]
C_B	Coalescence birth term in PBE	$[\mathrm{m}^{-4}\mathrm{s}^{-1}]$
		$[\mathrm{kgm}^{-4}\mathrm{s}^{-1}]$
C_D	Coalescence death term in PBE	$[\mathrm{m}^{-4}\mathrm{s}^{-1}]$
		$[\mathrm{kgm}^{-4}\mathrm{s}^{-1}]$
C_L	Constant in energy spectrum of Pope (2000)	[-]
C_q	Constant in Han et al. (2015)	[-]
C_t	Constant in Han et al. (2015)	[-]
C_η	Constant in energy spectrum of Pope (2000)	[-]
c	Coalescence frequency	$[\mathrm{s}^{-1}]$
c_d	Surface energy density increase coefficient	[-]
$c_{d,m}$	Surface energy density increase coefficient for process m	[-]
c_f	Surface area increase coefficient	[-]
$c_{f,m}$	Surface area increase coefficient for process m	[-]
c_i	Constant, i = 1,2,3,4,5,6	[-]
D	Diameter of impeller	[m]
E	Turbulent energy spectrum	$[\mathrm{Jmkg}^{-1}]$
	Turbulent kinetic energy	[J]
$\overline{E}$	Mean turbulent kinetic energy	[J]
$E_{\text{available}}$	Available energy of an eddy	[J]
E_{crit}	Critical energy required for breakup	[J]
E_s	Surface energy of fluid particle	[J]
$\overline{E}_s$	Surface energy of fluid particle	[J]
E_λ	Eddy kinetic energy	[J]
E_μ	Viscous energy inside a drop	[J]

Symbol	Description	Unit
f_d	Diameter fraction = ω/ξ	[-]
$f_{d,n}$	Diameter based number density function	$[\mathrm{m}^{-4}]$
$f_{d,m}$	Diameter based mass density function	$[\mathrm{kgm}^{-4}]$
f_L	Dimensionless function from Pope (2000)	[-]
f_v	Volume fraction = V_ω/V_ξ	[-]
f_v'	Unmodified volume fraction of Xing et al. (2015)	[-]
$f_{v,m}$	Volume fraction of daughter m	[-]
f_η	Dimensionless function from Pope (2000)	[-]
g	Gravitational constant, 9.81	$[\mathrm{ms}^{-2}]$
h_{DSD}	Breakage redistribution density function	$[\mathrm{m}^{-1}]$
$h_{m,\mathrm{DSD}}$	Breakage redistribution density function for process m	$[\mathrm{m}^{-1}]$
J	Source term in PBE	$[\mathrm{m}^{-4}\mathrm{s}^{-1}]$
		$[\mathrm{kgm}^{-4}\mathrm{s}^{-1}]$
K_b	Constant used in Liao et al. (2015)	[-]
K_c	Contraction loss coefficient of Xing et al. (2015)	[-]
K_e	Expansion loss coefficient of Xing et al. (2015)	[-]
K_g	Constant used in breakage frequency of Martínez-Bazán et al.	[-]
k	Turbulent eddy kinetic energy	$[\mathrm{Jkg}^{-1}]$
L	Integral length scale	[m]
	Dimensionless length scale of Lehr et al. (2002)	[-]
Mo	Morton number	[-]
M_d	Molecular weight of dispersed phase	$[\mathrm{kgmol}^{-1}]$
N	Number of drops	[-]
	Number of daughters	[-]
n	Number density of fluid particles	$[\mathrm{m}^{-3}]$
	Constant used in Liao et al. (2015)	[-]
n_r	Rotational speed of impeller	$[\mathrm{ms}^{-1}]$
n_{sm}	Number density of smallest daughter particles	$[\mathrm{m}^{-3}]$
n_κ	Number density of eddies	$[\mathrm{m}^{3}]$
n_λ	Number density of eddies	$[\mathrm{m}^{-3}]$
P	Probability of Poisson process	[-]
P_0	Constant in energy spectrum of Pope (2000)	[-]
P_b	Breakage probability	[-]
$P_{b,m}$	Breakage probability of process m	[-]
P_{breakage}	Breakage probability used to modify Martínez-Bazán et al.	[-]
P_{DSD}	Probability density function	$[\mathrm{m}^{-1}]$
P^*_{DSD}	Dimensionless probability density function	[-]
P_E	Kinetic energy distribution	$[\mathrm{J}^{-1}]$
$P_{E,\mathrm{2D}}$	Kinetic energy distribution	$[\mathrm{J}^{-1}]$
$P_{\lvert\mathbf{v}\rvert_{2D}}$	Two-dimensional speed distribution	$[\mathrm{sm}^{-1}]$
p	Pressure	[Pa]
p_0	Ambient pressure	[Pa]
	Initial pressure	[Pa]
p_i	Pressure inside spherical part i	[Pa]

Symbol	Description	Unit
p_{neck}	Pressure inside neck	[Pa]
R	Universal gas constant = 8.314	[$\text{JK}^{-1}\text{mol}^{-1}$]
Re_{D}	Reynolds number for agitation system = $D^2 n_r \rho_c / \mu_c$	[-]
Re_L	Integral scale Reynolds number	[-]
R_i	Radius of curvature for spherical part i	[m]
$\mathbf{r}$	Vector of external coordinates	[m]
r_d	Length scale in Sawford and Hunt (1986)	[m]
r_L	Length scale in Sawford and Hunt (1986)	[m]
S	Surface area of ellipsoidal intermediate	[m^2]
$\overline{S}$	Shear rate	[s^{-1}]
S_d	Shape factor of Han et al. (2015)	[-]
T	Temperature	[K]
t	Time coordinate	[s]
t_b	Breakage time	[s]
$t_{b,k}$	Breakage time of mechanism k	[s]
t_i	Time scale i of Xing et al. (2015), $i = 1, 2$	[s]
U_λ	Continuous phase velocity of Xing et al. (2015)	[ms^{-1}]
V_1	Volume of spherical part 1 in Xing et al. (2015)	[m^3]
V_ξ	Volume of mother particle	[m^3]
V_ω	Volume of daughter particle	[m^3]
V_ω^*	Dimensionless daughter volume	[-]
$V_{\omega,\text{max}}^*$	Maximum dimensionless daughter volume	[-]
$V_{\omega,\text{min}}^*$	Minimum dimensionless daughter volume	[-]
v	Speed	[ms^{-1}]
	Root mean square fluctuating velocity	[ms^{-1}]
$v_{b,k}$	Breakage velocity of mechanism k	[ms^{-1}]
v_i	Velocity in direction $i = x, y, z$	[ms^{-1}]
v_{neck}	Velocity inside neck	[ms^{-1}]
v_{plus}	Additional shrinking velocity of Xing et al. (2015)	[ms^{-1}]
$\mathbf{v_r}$	Vector of velocities in external coordinates	[ms^{-1}]
$\overline{v}_{\text{rel}}$	Relative velocity between fluid particle and eddy	[ms^{-1}]
$v_{\text{rms},2D}$	Root mean square velocity	[ms^{-1}]
v_{T}	Terminal velocity	[ms^{-1}]
v_z	Continuous phase velocity in z-direction	[ms^{-1}]
v_η	Kolmogorov velocity scale	[ms^{-1}]
v_ξ	Growth velocity of internal coordinate	[ms^{-1}]
	Characteristic velocity of eddy of size ξ	[ms^{-1}]
v_κ	Eddy velocity	[ms^{-1}]
v_λ	Eddy velocity	[ms^{-1}]
$\overline{v}_\lambda$	Mean eddy velocity	[ms^{-1}]
We_{D}	Weber number for agitation system = $\rho_c n_r^2 D^3 / \sigma$	[-]
We_{t}	Weber number = $\overline{\sigma}_t / \overline{\sigma}_s$	[-]
z	Axial coordinate	[m]
z_{min}	Minimum value of axial coordinate	[m]
z_{max}	Column length	[m]

List of Greek Symbols

Symbol	Description	Unit
α_d	Dispersed phase volume fraction	[-]
β	Constant in structure function of Martínez-Bazán et al.	[-]
β_2	Constant in energy spectrum of Pope (2000)	[-]
γ	Breakup probability function of Xing et al. (2015)	[-]
$\dot{\gamma}_{\text{eddy}}$	Eddy shear strain	[s^{-1}]
$\dot{\gamma}_{\text{shear}}$	Mean shear strain rate	[s^{-1}]
ΔE_s	Surface energy increase	[J]
ΔN	Change in number of drops	[-]
Δv	Change in velocity	[ms^{-1}]
Δv_b	Characteristic breakage velocity	[ms^{-1}]
Δv_{min}	Minimum relative velocity of oscillation	[ms^{-1}]
$\Delta \sigma_{ti}$	Excess stress associated with daughter i	[Pa]
$\overline{\delta}$	Mean surface oscillation distance of droplets	[m]
$\overline{\delta v^2}$	Structure function	[m^2s^{-2}]
$\nabla_{\mathbf{r}}$	Del operator in external coordinates	[m^{-1}]
∇_{ξ}	Del operator in internal coordinate	[m^{-1}]
ε	Turbulent dissipation rate	[Wkg^{-1}]
ζ	Particle diameter	[m]
	Dimensionless eddy size = λ/ξ	[-]
	Dimensionless quantity = b^2/a^2	[-]
ζ_{min}	Minimum dimensionless eddy size = λ_{min}/ξ	[-]
η	Kolmogorov length scale	[m]
κ	Wave number	[m^{-1}]
Λ	Dimensionless quantity = ξ_{crit}/ξ	[-]
λ	Turbulent eddy size	[m]
	Intensity parameter in Poisson process	[-]
λ_{min}	Minimum eddy size	[m]
μ_c	Dynamic viscosity of continuous phase	[Pa s]
μ_d	Dynamic viscosity of dispersed phase	[Pa s]
ν	Number of daughters	[-]
	Kinematic viscosity	[m^2s^{-1}]
ν_c	Kinematic viscosity of continuous phase	[m^2s^{-1}]
ξ	Particle diameter	[m]
ξ'	Dimensionless particle diameter	[-]
ξ_{crit}	Critical particle diameter	[m]
ξ_{max}	Maximum particle diameter	[m]
ξ_{min}	Minimum particle diameter	[m]
ξ_{neck}	Diameter of neck	[m]
ρ_c	Continuous phase density	[kgm^{-3}]
ρ_d	Dispersed phase density	[kgm^{-3}]

Symbol	Description	Unit
σ	Surface tension	[Nm^{-1}]
$\overline{\sigma}_{\text{crit}}$	Critical stress	[Pa]
$\overline{\sigma}_{\text{eddy}}$	Eddy shear stress	[Pa]
$\overline{\sigma}_{\text{inter}}$	Stress due to interfacial slip	[Pa]
$\overline{\sigma}_s$	Surface restoring stress	[Pa]
$\overline{\sigma}_{\text{shear}}$	Laminar velocity shear stress	[Pa]
$\overline{\sigma}_t$	Turbulent deforming stress	[Pa]
$\overline{\sigma}_{\text{turb}}$	Turbulent fluctuating stress	[Pa]
σ_v^2	Variance in velocity	[$\mathrm{m}^2\mathrm{s}^{-2}$]
$\overline{\sigma}_{\mu,c}$	Continuous phase viscous stress	[Pa]
$\overline{\sigma}_{\mu,d}$	Dispersed phase viscous stress	[Pa]
τ	Time interval	[s]
τ_η	Kolmogorov time scale	[m]
τ_μ	Viscous shear stress	[Pa]
χ	Inner coordinate in PBE	[m]
	Dimensionless energy	[-]
χ_c	Critical dimensionless energy	[-]
$\chi_{c,m}$	Critical dimensionless energy for breakage process m	[-]
Ω	Breakage density	[$\mathrm{m}^{-3}\mathrm{s}^{-1}$]
Ω_m	Breakage density of process m	[$\mathrm{m}^{-3}\mathrm{s}^{-1}$]
ω	Daughter particle diameter	[m]
ω^*	Dimensionless daughter size = ω/ξ	[-]
ω^*_{max}	Maximum dimensionless daughter size	[-]
ω^*_{min}	Minimum dimensionless daughter size	[-]
ω_{col}	Collision frequency	[$\mathrm{m}^{-3}\mathrm{s}^{-1}$]
ω_{inter}	Interaction frequency	[$\mathrm{m}^{-3}\mathrm{s}^{-1}$]
ω_{sm}	Diameter of smallest daughter	[m]

Chapter 1

Introduction

The population balance equation (PBE) is an integro-differential equation that can be applied in many branches of science and engineering. It is used to model multiphase processes, where one or more dispersed phases are distributed in a continuous medium. In such systems, the interfacial area is an important quantity, because it governs the rate of mass, heat and momentum transfer between the phases. The PBE gives the size distribution of dispersed phase particles, from which the interfacial area can easily be computed. Thus, applying the PBE facilitates more accurate modelling of multiphase systems. Polymerization, aerosols, crystallization, emulsification, boiling, chemical reactors and separators are examples of possible applications of the PBE (Solsvik and Jakobsen, 2015).

In this chapter, an introduction to the population balance framework will be given. The constitutive equations needed in order to solve the PBE will be outlined, before breakage closures are treated in greater detail. An overview of the mechanisms for fluid particle breakage used in the literature will be given. The majority of breakage closures are designed for turbulent systems, and a short introduction to the domains of turbulence is therefore also included in this chapter. Finally, the objectives of the thesis will be presented.

1.1 The Population Balance Equation

The PBE is usually identified as the equation derived simultaneously by Randolph (1964) and Hulburt and Katz (1964). As described in the review of Solsvik and Jakobsen (2015), the population balance uses a density function defined in a phase space to balance a population of entities that can undergo continuous change. The phase space consists of the spatial coordinates, also called the *external coordinates*, the property coordinates, often referred to as the *inner coordinates*, and a time variable. It is common to use the size of

entities, e.g. the volume, diameter or mass, as the inner coordinate. However, other properties, such as chemical composition, energy content, age and chemical activity can also be applied.

In multiphase systems, the dispersed phase entities are often in continuous motion, thus changing their position in the external coordinate system. There are several mechanisms that can lead to changes in the inner coordinates, e.g. expansion, compression, evaporation and condensation. Such mechanisms are associated with a velocity in the property space, often referred to as a *growth velocity*. Additionally, changes in the inner coordinate may occur as a result of particle-particle and particle-continuous phase interactions. Such interactions cause particle *coalescence* and *breakage*, leading to the death and birth of particles within the inner coordinate domain. In Figure 1.1, the four breakage and coalescence events that lead to the birth and death of entities with inner coordinate χ are illustrated.

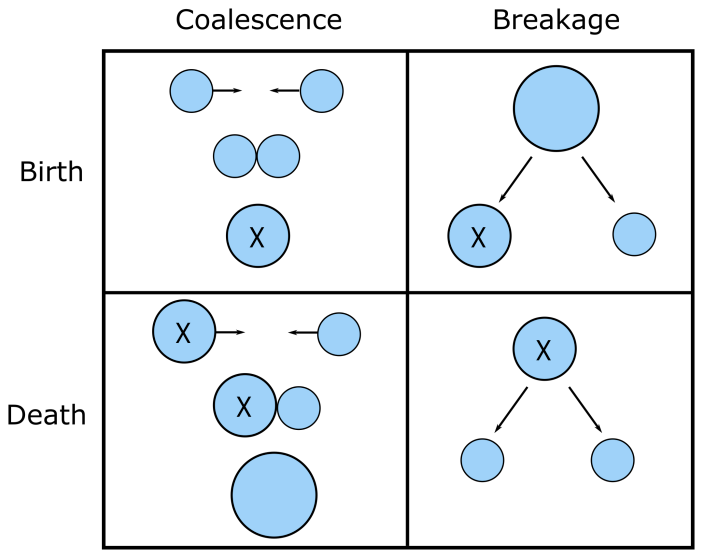

Figure 1.1: The four breakage and coalescence events that lead to the death and birth of entities of size χ.

Mathematically, the PBE consists of an accumulation term, a convective term in both the external and internal coordinates and a source term. The density function can be chosen as a *number density function*, representing the number of dispersed phase entities with a certain inner coordinate per unit volume. If the particle diameter is chosen as the inner coordinate, the unit of the number density function is $1/\left(\mathrm{m} \times \mathrm{m}^3\right)$. In this case, the

population balance can be written as (Solsvik and Jakobsen, 2013):

$$\frac{\partial f_{d,n}(\xi,\mathbf{r},t)}{\partial t}+\nabla_{\mathbf{r}}\cdot\left[\mathbf{v}_{\mathbf{r}}(\xi,\mathbf{r},t)\,f_{d,n}(\xi,\mathbf{r},t)\right]+\nabla_{\xi}\cdot\left[v_{\xi}(\xi,\mathbf{r},t)\,f_{d,n}(\xi,\mathbf{r},t)\right]=J(\xi,\mathbf{r},t) \tag{1.1}$$

Where $f_{d,n}$ is the diameter based number density function, $\mathbf{v_r}$ is the velocity in the external coordinates in $\mathbf{r}$ and v_ξ is the growth velocity in the inner coordinate, here chosen to be the diameter ξ. $J(\xi,\mathbf{r},t)$ is the source term, which accounts for the death and birth of entities through breakage and coalescence events. The source term can be written as:

$$J(\xi,\mathbf{r},t)=B_B(\xi,\mathbf{r},t)-B_D(\xi,\mathbf{r},t)+C_B(\xi,\mathbf{r},t)-C_D(\xi,\mathbf{r},t) \tag{1.2}$$

Where B and C denotes a breakage and coalescence event, and the subscripts B and D denote a birth and death event, respectively. As described in Solsvik and Jakobsen (2015), the expressions for the source terms can be derived from mechanistic principles. The particles formed in the breakage and coalescence events must be inside the domain $[\xi_{\text{min}},\xi_{\text{max}}]$. Otherwise, mass will disappear from the system.

The birth of particles of size ξ due to breakage can only occur when particles larger than ξ break:

$$B_B(\xi,\mathbf{r},t)=\int_{\xi}^{\xi_{\text{max}}}h_{\text{DSD}}(\xi,\zeta)\,b(\zeta)\,f_{d,n}(\zeta,\mathbf{r},t)\,\mathrm{d}\zeta \tag{1.3}$$

The breakage death term is simpler than the breakage birth term: if a particle of size ξ breaks, the number of particles of size ξ in the system will be reduced. Thus, the breakage death term can be written as:

$$B_D(\xi,\mathbf{r},t)=b(\xi)\,f_{d,n}(\xi,\mathbf{r},t) \tag{1.4}$$

Similarly, coalescence between a particle of size ξ and another particle will reduce the number of particles of size ξ in the system. This gives the coalescence death term:

$$C_D(\xi,\mathbf{r},t)=f_{d,n}(\xi,\mathbf{r},t)\int_{\xi_{\text{min}}}^{\left(\xi_{\text{max}}^3-\xi^3\right)^{1/3}}c(\xi,\zeta)\,f_{d,n}(\zeta,\mathbf{r},t)\,\mathrm{d}\zeta \tag{1.5}$$

Coalescence of two particles smaller than ξ can lead to the birth of a particle of size ξ. If binary coalescence is assumed, the coalescence birth term can be written as:

$$C_B(\xi,\mathbf{r},t)=\frac{\xi^2}{2}\int_{\xi_{\text{min}}}^{\xi}\frac{c\left(\left[\xi^3-\zeta^3\right]^{1/3},\zeta\right)}{\left[\xi^3-\zeta^3\right]^{2/3}}f_{d,n}(\zeta,\mathbf{r},t)\times f_{d,n}\left(\left[\xi^3-\zeta^3\right]^{1/3},\mathbf{r},t\right)\mathrm{d}\zeta \tag{1.6}$$

As can be seen from equation (1.3)-(1.6), constitutive equations are needed to be able to solve the PBE. The breakage frequency $b(\xi)$ represents the fraction of particles that break per unit time (Solsvik and Jakobsen, 2013):

$$b(\xi)=\frac{\text{Number of particles of size }\xi\text{ that break per unit time}}{\text{Total number of particles of size }\xi} \tag{1.7}$$

The breakage redistribution density function gives information on how likely the formation of a particle of size ξ from a breaking particle of size ζ is (Solsvik and Jakobsen, 2013):

$$h_{\mathrm{DSD}}\left(\xi,\zeta\right)\mathrm{d}\xi = \frac{\text{Number of particles that are formed of size } \left[\xi,\xi+\mathrm{d}\xi\right]}{\text{Total number of particles of size } \zeta \text{ that break}} \tag{1.8}$$

The breakage redistribution density function can be written as the product of the average number of daughters formed in the breakage process, ν, and the normalized probability density function, P_{DSD} (Solsvik and Jakobsen, 2015):

$$h_{\mathrm{DSD}}\left(\xi,\zeta\right) = \nu P_{\mathrm{DSD}}\left(\xi,\zeta\right) \tag{1.9}$$

Where the probability density function can be interpreted as (Solsvik and Jakobsen, 2013):

$$P_{\mathrm{DSD}}\left(\xi,\zeta\right)\mathrm{d}\xi = \frac{\text{Number of particles that are formed of size } \left[\xi,\xi+\mathrm{d}\xi\right]}{\text{Total number of particles that appear in the interval } \left[\xi_{\mathrm{min}},\zeta\right]} \tag{1.10}$$

Together, the breakage frequency and breakage redistribution density function form what is often referred to as a *breakage closure* or *breakage kernel*.

In the coalescence source terms, the coalescence frequency, $c\left(\xi,\zeta\right)$ is required. This function gives the number of particles that are formed due to coalescence per unit time. A constitutive equation for the growth velocity of dispersed phase entities must also be provided in order to obtain a solvable equation system.

1.2 Mechanisms of Fluid Particle Breakage

In the literature, numerous breakage closures have been presented over the previous decades. Several reviews on breakage closures have been carried out, e.g. by Lasheras et al. (2002), Jakobsen et al. (2005), Liao and Lucas (2009) and Solsvik et al. (2013). Several of the closures apply fundamentally different assumptions, especially in connection with the breakage mechanism. Liao and Lucas (2009) and Solsvik et al. (2013) both identify four different categories of fluid particle breakage mechanisms applied in the literature. These are *turbulent motions and stresses*, *viscous shear stresses*, *shearing-off processes* and *interfacial instabilities*. In this section, an overview of these mechanisms will be provided.

1.2.1 Turbulent Motions and Stresses

Most of the breakage closures available in the literature are developed for turbulent systems. In such systems, it is common to assume that the breakage of fluid particles is caused by turbulent stresses along the particle surface. Deformations of the particles are often assumed to occur through fluctuations in the surrounding fluid and collisions with turbulent eddies. Breakage criteria can be derived by balancing the external disruptive stresses and surface restoring stresses acting on the fluid particles.

Solsvik et al. (2013) identified six different breakage criteria for turbulent systems, based on different forms of stress or kinetic energy balances:

(a) A particle will break if the turbulent kinetic energy transmitted to the dispersed phase particle from turbulent eddies exceeds a critical value.

(b) Breakage occurs if the turbulent velocity fluctuations around the surface of the particle exceeds a critical value.

(c) If the turbulent kinetic energy of arriving turbulent eddies exceeds a critical value, breakage will occur.

(d) A particle will break if the turbulent inertial stress of the colliding eddy exceeds the interfacial restoring stress of the smallest daughter particle.

(e) A combination of the criteria in (c) and (d)

(f) Breakage will occur if the turbulent inertial stresses exceed the interfacial surface restoring stress of a parent particle of comparable size. This criterion is purely kinematic, thus avoiding the eddy concept of turbulence entirely.

1.2.2 Viscous Shear Stresses

In laminar systems there are no turbulent contributions to the breakage of fluid particles. In such systems, the degree of momentum diffusion is high and the degree of momentum convection is low. Viscous shear stresses in the continuous phase can induce velocity gradients around the interface of the dispersed phase particles. Such velocity gradients can cause deformations, which could lead to breakage of the fluid particles (Solsvik et al., 2013).

Viscous effects on breakage are often neglected in turbulent systems. However, this assumption might not always be valid in all ranges of turbulence. In turbulent systems, viscous and turbulent stresses can both act on the dispersed phase particles, thus increasing the deformation of the particles and leading to a higher probability of breakage. A generalized breakage mechanism can be expressed as a balance between the deforming external viscous stresses and the restoring surface stresses acting on the dispersed phase particles (Solsvik et al., 2013). The ratio between these two stresses is quantified by the capillary number, given by (Janssen and Meijer, 1993; Janssen et al., 1994):

$$\mathrm{Ca} = \frac{\text{viscous stresses}}{\text{surface stresses}} = \frac{\overline{\sigma}_{\mu,c}}{\overline{\sigma}_s} \tag{1.11}$$

1.2.3 Shearing-Off Processes and Interfacial Instabilities

For larger particles, the breakage mechanisms become more complicated. In addition to turbulent and viscous stresses, shearing-off processes and interfacial instabilities can contribute to breakage. In a shearing-off process, several small daughter particles are sheared off from a large mother particle due to a velocity gradient across the mother particle surface (Solsvik et al., 2013). Shearing-off processes are also known as erosive breakage processes (Liao and Lucas, 2009).

Breakage due to interfacial instabilities is also caused by velocity differences across the fluid particle surface. This mechanism can occur both in stagnant and flowing media, and in systems where bubbles are rising or droplets are falling in a stagnant liquid. Solsvik et al. (2013) mentions the Rayleigh-Taylor instability, which occurs when a low-density fluid is accelerated into a high-density fluid, and the Kelvin-Helmholtz instability, which occurs when the density of the phases are approximately equal.

1.3 Domains of Turbulence

Turbulence is assumed to consist of *vortices* or *eddies*, associated with a size λ or wave number $\kappa = 2\pi/\lambda$. There are three sub-ranges of turbulence. The largest eddies are located in the energy-containing range, where the majority of the kinetic energy is located. The integral length scale L represents the largest eddies. In the energy-containing range, the turbulent eddies receive their kinetic energy from velocity gradients in the mean flow, and the turbulence is anisotropic and non-universal. Kinetic energy is transferred to successively smaller scales in a cascade process (Solsvik and Jakobsen, 2016a). In the dissipation range, viscous effects are dominating and the kinetic energy is dissipated to heat via the molecular viscosity (Mockett, 2009). The smallest vortices are characterized by the Kolmogorov length, time and velocity scale, defined in the book of Jakobsen (2014) as:

$$\eta = \left(\frac{\nu^3}{\varepsilon}\right)^{1/4} \tag{1.12}$$

$$\tau_\eta = \left(\frac{\nu}{\varepsilon}\right)^{1/2} \tag{1.13}$$

$$v_\eta = (\nu\varepsilon)^{1/4} \tag{1.14}$$

In the inertial subrange, viscous effects are negligible. Pope (2000) suggested that the transition between the energy-containing and inertial subrange occurs at the eddy size $L/6$ and the transition between the inertial and dissipation subrange occurs at eddies of size 60η.

The inertial and dissipation subrange have a universal character and are together referred to as the universal equilibrium range. According to *Kolmogorov's first similarity hypothesis*, the statistics of the small-scale motions at sufficiently high Reynolds numbers are uniquely determined by the dissipation rate ε and viscosity ν. Similarly, for sufficiently high Reynolds numbers, *Kolmogorov's second similarity hypothesis* states that there exists a region in which the statistics of the motions have a universal form that is uniquely determined by ε (Solsvik and Jakobsen, 2016a). Figure 1.2 shows the energy flow and regions of the turbulent energy cascade.

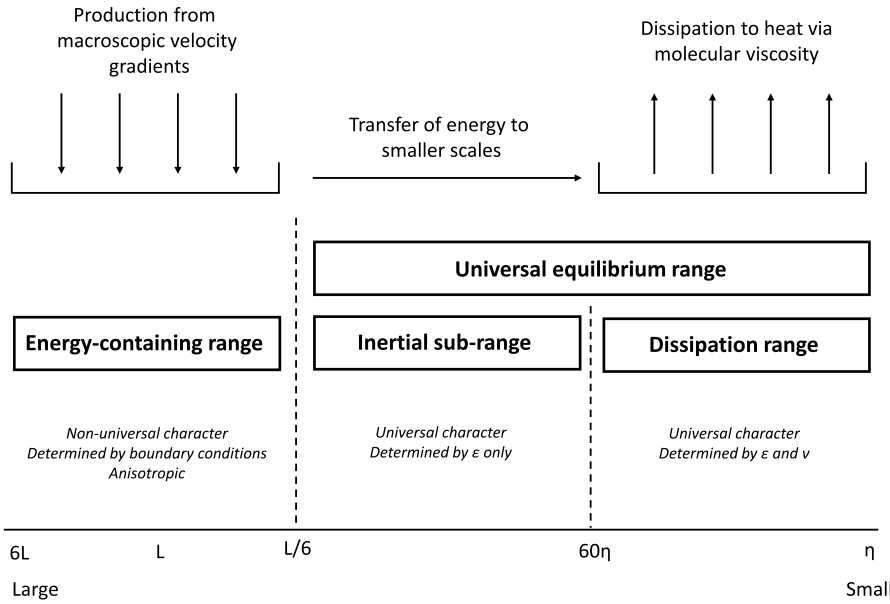

Figure 1.2: Energy flow and regions of the turbulent energy cascade (Solsvik and Jakobsen, 2016a; Mockett, 2009).

The turbulent energy spectrum, $E(\kappa)$, gives the kinetic energy contained in eddies of wave number between κ and $\kappa + \mathrm{d}\kappa$. In Figure 1.3, the energy spectrum of Pope (2000) is shown for a highly turbulent system. This energy spectrum will be explained in further detail in chapter 3.

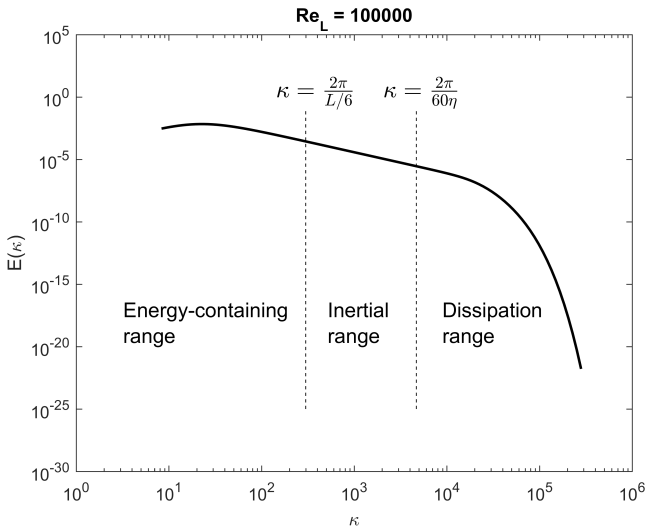

Figure 1.3: The energy spectrum of Pope (2000) for an air-water system at $\mathrm{Re}_L = 100000$.

This energy spectrum demonstrates that the inertial subrange for the air-water system is quite wide at high Reynolds numbers. However, as pointed out by Solsvik et al. (2016b), the inertial range narrows at lower Reynolds numbers. In some cases it might disappear entirely. This effect is indicated in Figure 1.4, where the energy spectrum for the same air-water system is shown for a less turbulent system.

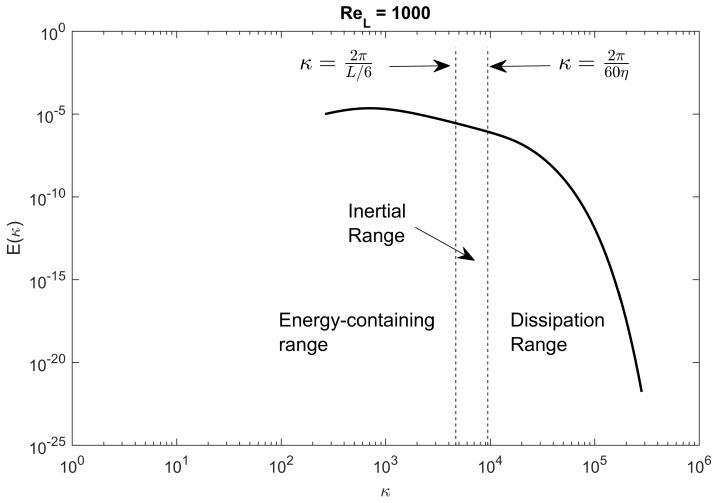

Figure 1.4: The energy spectrum of Pope (2000) for an air-water system at $\mathrm{Re}_L = 1000$.

Notice that the kinetic energy contained in the turbulent eddies decreases when the sys-

tem becomes less turbulent, and that the inertial subrange narrows. Most of the breakage closures available in the literature are only valid in the inertial subrange. As indicated by Figure 1.3 and 1.4, these models might not be valid for all types of turbulent systems, especially when the degree of turbulence decreases.

1.4 Thesis Objectives

Despite the considerable efforts that have been invested in developing models for the breakup of fluid particles, there does not seem to be consensus in the literature on the underlying physics of the breakage mechanism. It is uncertain whether a set of complementary criteria must be applied or a single criteria is sufficient to accurately describe the breakup process.

The objective of this thesis is to perform an evaluation of a set of breakage closures, to determine their suitability as constitutive equations in the population balance equation. Emphasis is placed on selecting regularly used or newly presented closures from the literature that represent the most commonly applied breakage mechanisms and criteria. Suggestions to improvements of the closures are presented, and extended versions of the studied closures are implemented and included in the evaluation along with the original models. Based on the evaluation, a recommendation of which closures are most suitable to give accurate descriptions of multiphase systems through the PBE is given. Additionally, suggestions to further improvements of the studied closures are made.

Chapter 2

Studied Closures

Most of the breakage closures available in the literature are developed for turbulent systems. Therefore, the study was limited to models that identify turbulent motions and stresses as the dominant breakage mechanism. At least one breakage closure from each of the six categories of breakage mechanisms due to turbulent motions and stresses was chosen. The reader is referred to section 1.2.1 for a detailed description of the categories. Emphasis was placed on choosing closures that are frequently used in scientific research or recently made available in scientific literature. A presentation of the closures that were chosen is given in this chapter.

2.1 Coulaloglou and Tavlarides (1977)

A phenomenological model to describe drop breakup in turbulently agitated liquid-liquid dispersions was developed by Coulaloglou and Tavlarides (1977). It was assumed that the turbulent flow field was locally isotropic, and only binary breakage in the inertial subrange of turbulence was considered. Viscous effects on breakup were neglected. Breakup of an oscillating, deformed drop was assumed to occur *if the turbulent kinetic energy transferred to the droplet by turbulent eddies exceeds the drop surface energy*. This breakage criterion was expressed as:

$$b\left(\xi\right) = \left(\frac{1}{\text{breakage time}}\right) \times \left(\frac{\text{fraction of}}{\text{drops breaking}}\right) = \frac{1}{t_b}\frac{\Delta N\left(\xi\right)}{N\left(\xi\right)} \tag{2.1}$$

Where $N\left(\xi\right)$ is the total number of drops of size ξ.

In accordance with the breakage mechanism, the fraction of drops breaking was assumed to be proportional to the fraction of colliding eddies with a turbulent kinetic energy greater

than the surface energy of the droplet. The velocity distribution of the droplets and the turbulent eddies was assumed to be equal. Applying the assumption of random motion, the fraction of energetic collisions was given by a two-dimensional speed distribution:

$$P_{|\mathbf{v}|_{2D}}(v)\,\mathrm{d}v = \frac{2}{v_{\text{rms, 2D}}^2}\exp\left(-\frac{v^2}{v_{\text{rms, 2D}}^2}\right)v\mathrm{d}v \tag{2.2}$$

As shown in Solsvik et al. (2013), this speed distribution can be converted to an exponential distribution in terms of energy by using the relation:

$$P_{E,2D}(E)\,\mathrm{d}E = P_{|\mathbf{v}|_{2D}}(v)\left(\frac{\partial v}{\partial E}\right)\mathrm{d}E \tag{2.3}$$

The turbulent kinetic energy and mean turbulent kinetic energy of droplets is defined as $E = \frac{1}{2}\rho_d\left(\frac{\pi}{6}\xi^3\right)v^2$ and $\bar{E} = \frac{1}{2}\rho_d\left(\frac{\pi}{6}\xi^3\right)v_{\text{rms, 2D}}^2$, respectively. This gives the distribution in terms of energy:

$$P_{E,2D}(E)\,\mathrm{d}E = \frac{1}{\bar{E}}\exp\left(-\frac{E}{\bar{E}}\right)\mathrm{d}E \tag{2.4}$$

The fraction of eddies with a kinetic energy greater than a critical value E_{crit} corresponds to the number fraction of drops breaking. Thus, the fraction of drops breaking introduced in equation (2.1) can be calculated:

$$\frac{\Delta N(\xi)}{N(\xi)} = \int_{E_{\text{crit}}}^{\infty} P_{E,2D}(E)\,\mathrm{d}E = \exp\left(-\frac{E_{\text{crit}}}{\bar{E}}\right) \tag{2.5}$$

The critical energy is taken as the surface energy of a droplet of size ξ, $E_{\text{crit}} = c_1\sigma\xi^2$. The mean turbulent kinetic energy is defined by the two-point Kolmogorov structure function:

$$\bar{E} = c_2\rho_d\xi^3\overline{\delta v^2(\xi)} \tag{2.6}$$

The structure function denotes the mean square of the relative velocity between two points separated by a distance ξ. It was assumed that only eddies smaller or equal to the droplet size contribute to breakup. Larger eddies transport the droplets without breaking them. With the droplet size ξ within the inertial subrange, the structure function was given by:

$$\overline{\delta v^2(\xi)} = c_3\varepsilon^{2/3}\xi^{2/3} \tag{2.7}$$

The fraction of drops breaking can thus be expressed as:

$$\frac{\Delta N(\xi)}{N(\xi)} = \exp\left(-\frac{c_4\sigma}{\rho_d\varepsilon^{2/3}\xi^{5/3}}\right) \tag{2.8}$$

The breakage time was estimated by assuming that the motion of the daughter particles was similar to the motion of eddies in a turbulent flow field. Coulaloglou and Tavlarides (1977) arrived at the following expression:

$$t_b \propto \xi^{2/3}\varepsilon^{-1/3} = c_5\xi^{2/3}\varepsilon^{-1/3} \tag{2.9}$$

Inserting the breakage time from equation (2.9) and the fraction of drops breaking from equation (2.8) in the definition from equation (2.1) gives the final expression for the breakage frequency[1]:

$$b\left(\xi\right) = c_6 \xi^{-2/3} \varepsilon^{1/3} \exp\left(-\frac{c_4 \sigma}{\rho_d \varepsilon^{2/3} \xi^{5/3}}\right) \tag{2.10}$$

Where c_6 and c_4 are adjustable parameters that must be determined experimentally. Coulaloglou and Tavlarides pointed out that adjustments should be made for large hold-up fractions of the dispersed phase. As shown in Solsvik et al. (2013), the damping effect of large hold-up fractions on the local turbulent intensities can be taken into account by including the dispersed phase volume fraction in the breakage frequency:

$$b\left(\xi\right) = c_6 \xi^{-2/3} \frac{\varepsilon^{1/3}}{\left(1+\alpha_d\right)} \exp\left(-\frac{c_4 \sigma \left(1+\alpha_d\right)^2}{\rho_d \varepsilon^{2/3} \xi^{5/3}}\right) \tag{2.11}$$

The probability density function was based on the truncated normal probability density function of Valentas et al. (1966). Two unequal daughter droplets were assumed to form, and the variance was chosen to ensure that at least 99.6 % of the daughters were formed in a volume conserving manner. The probability density function was given as:

$$P_{\mathrm{DSD}}\left(V_\xi, V_\omega\right) = \frac{2.4}{V_\xi} \exp\left(-\frac{4.5\left(2V_\omega - V_\xi\right)^2}{V_\xi^2}\right) \tag{2.12}$$

Converting from a probability density function to a breakage redistribution density function is achieved by multiplying with the number of daughters. For binary breakage, this becomes:

$$h_{\mathrm{DSD}}\left(V_\xi, V_\omega\right) = 2 \times P_{\mathrm{DSD}}\left(V_\xi, V_\omega\right) \tag{2.13}$$

A diameter based redistribution density function is found from the following relation:

$$h_{\mathrm{DSD}}\left(\xi, \omega\right) = h_{\mathrm{DSD}}\left(V_\xi, V_\omega\right) \times \frac{\mathrm{d}V_\omega}{\mathrm{d}\omega} = h_{\mathrm{DSD}}\left(V_\xi, V_\omega\right) \times \frac{\pi}{2}\omega^2 \tag{2.14}$$

2.2 Narsimhan et al. (1979)

A model for the transitional breakage probability of droplets in agitated liquid-liquid dispersions with low dispersed phase volume fractions was developed by Narsimhan et al. (1979). Droplets were assumed to break *if the turbulent motion provides the minimum increase in the surface energy for breakage*. Such fluctuations were taken to be induced by arriving turbulent eddies of different scales. The effect of viscous forces on breakup was neglected, because the high Reynolds numbers in agitated vessels give turbulent microscales that are much smaller than the droplet sizes.

[1] Solsvik et al. (2013) argued that for gas-liquid systems, e.g. air bubbles in water, the continuous phase density ρ_c should be used instead of the dispersed phase density ρ_d.

One might expect that the surface oscillations caused by one eddy are interrupted by the arrival of subsequent eddies. Narsimhan et al. argued that the occurrence of such interruptions depends on the relative magnitudes of the time scales of the eddy bombardment process and the particle surface oscillation. It was assumed that the time scale of oscillation is smaller than the eddy bombardment time scale. Therefore, once an eddy with sufficient kinetic energy arrives, the bombarded droplet is assumed to break instantly. Additionally, the authors assumed that only eddies smaller or equal to the droplets in size can contribute to breakage. Larger eddies only transport the droplets without breaking them.

Narsimhan et al. assumed that the eddy-droplet collisions were statistically regular events. It was postulated that the number of eddies arriving on the surface of a droplet is a Poisson process, exhibiting the following properties:

(i) The number of eddies arriving on the surface of a droplet in disjoint time intervals are independent.

(ii) The probability of more than one eddy arriving at the surface of a droplet within the time interval $[t, t + \mathrm{d}t]$ is assumed to be zero.

(iii) The probability of one eddy arriving on the surface of a droplet within the time interval $[t, t + \mathrm{d}t]$ is given as $\lambda \mathrm{d}t$. The parameter λ represents the average number of eddies arriving on the surface of a droplet per unit time.

(iv) The intensity λ is assumed constant, i.e. it is independent of the droplet size and energy dissipation rate.

Considering a small time interval, τ, two events A and B were defined as:

- A: An eddy arrives on the surface of the droplet in the time interval τ.
- B: The arriving eddy has sufficient energy to provide the droplet of volume V with the minimum increase in surface energy required for breakage.

The probability $P(A)$ follows directly from the characteristics of the Poisson process, and is given as $P(A) = \lambda\tau$. The probability of a droplet of volume V_ξ breaking within the time interval τ is defined as $P(A)P(B|A)$, where $P(B|A)$ is the conditional probability of event B occuring when event A already has taken place. The breakage frequency was subsequently defined as:

$$b\left(\xi\right) = \frac{P(A)P(B|A)}{\tau} = \frac{\lambda\tau P(B|A)}{\tau} = \lambda P(B|A) \tag{2.15}$$

The conditional probability $P(B|A)$ is estimated by assuming that the kinetic energy of the arriving eddy gives an increase in the relative velocity of oscillation of the droplet. Furthermore, an increased oscillation velocity increases the surface energy of the droplet. The surface energy of a droplet of volume V_ξ and diameter ξ is defined as:

$$E_s = \pi\sigma\xi^2 = \pi\sigma\left(\frac{6V_\xi}{\pi}\right)^{2/3} = \sigma\pi^{1/3}6^{2/3}V_\xi^{2/3}$$

An expression for the minimum relative velocity of oscillation, $\Delta v_{\min}$, was obtained by balancing the change in oscillation velocity and the surface energy increase. It was stated

that the surface energy increase is minimal when equal binary breakage occurs[2]:

$$\frac{1}{2}\left(\rho_c V_\xi\right)\Delta v_{\text{min}}^2 = \Delta E_s = \left(2^{1/3}-1\right)\sigma\pi^{1/3}6^{2/3}V_\xi^{2/3} \tag{2.16}$$

Rearranging the equation gives an expression for the minimum relative velocity of oscillation:

$$\Delta v_{\text{min}}^2 = 2\left(2^{1/3}-1\right)\frac{\sigma}{\rho_c}\pi^{1/3}6^{2/3}V_\xi^{-1/3} \tag{2.17}$$

If the characteristic velocity of an eddy of size ξ is v_ξ, breakage will occur if $\frac{1}{2}v_\xi^2 \geq \frac{1}{2}\Delta v_{\text{min}}^2$. It was assumed that the relative velocity between two points was normally distributed. By applying the Kolmogorov theory of local isotropy, this relative velocity was given by the following structure function:

$$\overline{\delta v^2\left(\xi\right)} = 2\varepsilon^{2/3}\xi^{2/3} \tag{2.18}$$

The normal probability density function was given as:

$$P\left(\Delta v\right) = \frac{1}{\sqrt{2\pi}\sigma_v}\exp\left(-\frac{\Delta v^2}{2\sigma_v^2}\right) \tag{2.19}$$

The variance was given from the structure function as $\sigma_v^2 = \overline{\delta v^2\left(\xi\right)}$. The conditional probability $P(B|A)$ that an incoming eddy will have sufficient energy to break the droplet is calculated from a cumulative distribution, as explained in Solsvik et al. (2013):

$$P(B|A) = P\left(v_\xi^2 \geq \Delta v_{\text{min}}^2\right) = 1 - P\left(v_\xi^2 \leq \Delta v_{\text{min}}^2\right) = 1 - \int_0^{\Delta v_{\text{min}}} P\left(\Delta v\right)\mathrm{d}\left(\Delta v\right) \tag{2.20}$$

Two formulas from statistics are applied (Solsvik et al., 2013) in order to evaluate the integral:

$$\int_0^{\Delta v_{\text{min}}} \exp\left(-\frac{\Delta v^2}{2\sigma_v^2}\right)\mathrm{d}\left(\Delta v\right) = \sqrt{\frac{\pi}{2}}\sigma_v \text{erf}\left[\frac{\Delta v_{\text{min}}}{\sqrt{2}\sigma_v}\right]$$

$$\text{erfc}\left(x\right) = 1 - \text{erf}\left(x\right)$$

The following expression is obtained for the conditional probability $P\left(B|A\right)$:

$$P\left(B|A\right) = 1 - \frac{1}{2}\text{erf}\left[\frac{\Delta v_{\text{min}}}{\sqrt{2}\sigma_v}\right] = \frac{1}{2}\left(1 + \text{erfc}\left[\frac{\Delta v_{\text{min}}}{\sqrt{2}\sigma_v}\right]\right) \tag{2.21}$$

Inserting this into the breakage frequency, defined in equation (2.15), gives the final expression for the breakage frequency. On a volume basis, the expression is:

$$b\left(V_\xi\right) = \frac{\lambda}{2} + \frac{\lambda}{2}\text{erfc}\left(\sqrt{2\left(2^{1/3}-1\right)}\sqrt{\frac{\sigma}{\rho_c}}\frac{\pi^{5/18}6^{2/9}V_\xi^{-5/18}}{2\varepsilon^{1/3}}\right) \tag{2.22}$$

[2]Narsimhan et al. (1979) argued that the surface energy increase is minimal when equal binary breakage occurs. As pointed out in Alopaeus et al. (2002) and Liao and Lucas (2009), this is not correct. The surface energy increase is at its maximum in the case of equal binary breakage.

The breakage frequency can also be given on a diameter basis[3]:

$$b\left(\xi\right) = \frac{\lambda}{2} + \frac{\lambda}{2}\mathrm{erfc}\left(\sqrt{2\left(2^{1/3}-1\right)}\sqrt{\frac{\sigma}{\rho_c}}\frac{\sqrt{6}\xi^{-5/6}}{2\varepsilon^{1/3}}\right) \tag{2.23}$$

The expressions for the breakage frequency given in equation (2.22) and (2.23) differ from the original model in two ways. Firstly, the breakage frequency given in Narsimhan et al. (1979) was erroneously defined without the pre-factor of 1/2. Secondly, it lacks the additional $\lambda/2$ term. The breakage frequency was also defined without the $\lambda/2$ term by Solsvik et al. (2013) and Liao and Lucas (2009), without an explanation of why it was not included in the final expression. The additional term results in a non-zero breakage frequency as the size of the mother particle approaches zero, which is not a physically realistic scenario.

It was assumed that the daughter droplet size distribution was perfectly random, giving the following probability density function:

$$P_{\mathrm{DSD}}\left(V_\xi, V_\omega\right) = \frac{1}{V_\xi} \tag{2.24}$$

This corresponds to the following redistribution density function:

$$h_{\mathrm{DSD}}\left(V_\xi, V_\omega\right) = \frac{2}{V_\xi} \tag{2.25}$$

2.3 Luo and Svendsen (1996)

A theoretical model for the prediction of drop and bubble (fluid particle) breakage rates in turbulent dispersions was developed by Luo and Svendsen (1996). Using principles from isotropic turbulence and probability, they aimed at developing a closure with no adjustable parameters and a daughter size distribution that could be directly calculated from the breakage frequency. Luo and Svendsen criticized previous closures and pointed out that adjustable parameters may involve costly experimental programs and reduce the generality of the models. In the model derivation, the following simplifications and assumptions were made:

(i) The turbulence is assumed to be isotropic.

(ii) Only binary breakage of fluid particles is considered.

(iii) Viscous forces are neglected, as the fluid particles are significantly larger than the microscales of turbulence. Thus, only turbulent effects are assumed to contribute to breakage.

(iv) The breakage can be described by a volume fraction variable describing the daughter particle sizes. This variable is assumed to be stochastic, and is defined as: $f_v = V_\omega/V_\xi$. It can take values from 0 to 1.

[3] In Solsvik et al. (2013), the numerator of the erfc argument is incorrect. The factor of $6^{-1/18}$ should be $\sqrt{6}$, as indicated in equation (2.23).

(v) Breakage occurs *if the energy of an arriving eddy is greater than a critical value*. Similarly to Narsimhan et al. (1979), it is assumed that the eddies affect the fluid particles independently, i.e. only one eddy is present at the particle surface at a given time.

(vi) Only eddies smaller or equal to the fluid particles in size can contribute to breakage. It is assumed that larger eddies carry the fluid particles without breaking them.

It was proposed that the breakage density, $\Omega(\xi,\omega)$, of a fluid particle of size ξ into a daughter particle of size ω could be calculated from the product of a collision frequency and a breakage probability:

$$\Omega(\xi,\omega) = \int_{\lambda_{\min}}^{\xi} P_b(\xi,\omega,\lambda)\,\omega_{\text{col}}(\xi,\lambda)\,\mathrm{d}\lambda \tag{2.26}$$

Here, $P_b(\xi,\omega,\lambda)$ is the probability of a fluid particle of size ξ breaking into a daughter of size ω after colliding with an eddy of size λ. This probability equals the probability of the arriving eddy having a kinetic energy greater than or equal to the minimum energy required for breakage to occur. The collision frequency between eddies of size λ to $\mathrm{d}\lambda$ and fluid particles of size ξ is given by $\omega_{\text{col}}(\xi,\lambda)$. By assuming that the motion of eddies is random, it was written as:

$$\omega_{\text{col}}(\xi,\lambda) = \frac{\pi}{4}(\xi+\lambda)^2\,\overline{v}_{\text{rel}} n_\lambda n \tag{2.27}$$

The relative velocity between fluid particle and eddy is assumed equal to the mean turbulent velocity of the eddy. In the inertial subrange of isotropic turbulence, it can be expressed by the Kolmogorov structure function:

$$\overline{v}_{\text{rel}} \approx \sqrt{\overline{\delta v^2(\lambda)}} \approx (2.045)^{1/2}(\varepsilon\lambda)^{1/3} \tag{2.28}$$

An expression for the number density of eddies is obtained by the following kinetic energy balance:

$$n_\lambda \rho_c \frac{\pi}{6}\lambda^3 \frac{\overline{\delta v^2(\lambda)}}{2}\mathrm{d}\lambda = E(\kappa)\,\rho_c(1-\alpha_d)(-\mathrm{d}\kappa) \tag{2.29}$$

Where the wave number κ is related to the eddy size λ by $\kappa = 2\pi/\lambda$. The energy spectrum in the inertial subrange of turbulence is:

$$E(\kappa) = 1.5\varepsilon^{2/3}\kappa^{-5/3} \tag{2.30}$$

By introducing the energy spectrum into the kinetic energy balance and converting $(-\mathrm{d}\kappa)$ to $\mathrm{d}\lambda$, the expression for the number density of eddies becomes:

$$n_\lambda \approx \frac{0.822(1-\alpha_d)}{\lambda^4} \tag{2.31}$$

Inserting the expression for the relative velocity and number density of eddies into the definition in equation (2.27) gives the following expression for the collision frequency:

$$\omega_{\text{col}}(\xi,\zeta) = 0.923(1-\alpha_d)\,n\,(\varepsilon\xi)^{1/3}\frac{(1+\zeta)^2}{\zeta^{11/3}\xi^2} \tag{2.32}$$

Where the dimensionless factor $\zeta = \lambda/\xi$ was introduced for simplicity.

By assuming that the velocity distribution of turbulent eddies is a normal density function, Luo and Svendsen (1996) used the following distribution to describe the kinetic energy distribution of the turbulent eddies:

$$P_E(\chi) = \frac{1}{\overline{E}(\lambda)} \exp(-\chi), \quad \chi = \frac{E(\lambda)}{\overline{E}(\lambda)} \tag{2.33}$$

The mean eddy kinetic energy is given by:

$$\overline{E}(\lambda) = \rho_c \frac{\pi}{6} \lambda^3 \frac{\overline{\delta v^2(\lambda)}}{2} = \rho_c \frac{2.045\pi}{12} (\varepsilon\xi)^{2/3} \zeta^{11/3} \xi^3 \tag{2.34}$$

When a particle of size ξ breaks into two particles with volume fractions f_v and $1 - f_v$, the surface energy increase is given by:

$$\Delta E_s = \sum_i E_s(\omega_i) - E_s(\xi) = \pi\sigma\xi^2 \left(f_v^{2/3} + (1 - f_v)^{2/3} - 1 \right) = c_f \pi\sigma\xi^2 \tag{2.35}$$

Where c_f is the surface area increase coefficient. Breakage of a fluid particle occurs if the kinetic energy of the arriving eddy exceeds or equals the increase in surface energy required for breakage. The critical energy is therefore equal to the surface energy increase:

$$E_{\text{crit}} = c_f \pi\sigma\xi^2 \tag{2.36}$$

A critical dimensionless energy can be obtained by dividing the critical energy by the mean eddy kinetic energy:

$$\chi_c = \frac{E_{\text{crit}}}{\overline{E}(\lambda)} = \frac{12 c_f \sigma}{2.045 \rho_c \varepsilon^{2/3} \xi^{5/3} \zeta^{11/3}} \tag{2.37}$$

The breakage probability is equal to the probability that an arriving eddy has a kinetic energy greater than or equal to the critical energy. This can be written as a cumulative exponential function, as described in Solsvik et al. (2013):

$$P_b(\xi, \omega, \lambda) = P_E[\chi \geq \chi_c] = 1 - P_E[\chi \leq \chi_c] \tag{2.38}$$

This is given as:

$$P_b(\xi, \omega, \lambda) = 1 - \int_0^{\chi_c} \exp(-\chi)\, \mathrm{d}\chi = \exp(-\chi_c) \tag{2.39}$$

An expression for the breakage density can be obtained by inserting the expression for the collision frequency and breakage probability into the definition given in equation (2.26):

$$\frac{\Omega(\xi, \omega)}{n(1 - \alpha_d)} = 0.923 \left(\frac{\varepsilon}{\xi^2} \right)^{1/3} \int_{\zeta_{\min}}^1 \exp\left(-\frac{12 c_f \sigma}{2.045 \rho_c \varepsilon^{2/3} \xi^{5/3} \zeta^{11/3}} \right) \frac{(1 + \zeta)^2}{\zeta^{11/3}} \mathrm{d}\zeta \tag{2.40}$$

Where the dimensionless lower limit $\zeta_{\min}$ is given as $\lambda_{\min}/\xi$. The total breakage density of fluid particles of size ξ is calculated by integrating the partial breakage density over the daughter volume fraction domain:

$$\Omega(\xi) = \frac{1}{2} \int_0^1 \Omega(\xi, f_v)\, \mathrm{d}f_v \tag{2.41}$$

Where the pre-factor takes into account that the integrand is symmetrical around $f_v = 0.5$. The breakage density can be converted to a breakage frequency by using the following relation (Solsvik et al., 2013):

$$b(\xi) = \frac{1}{\nu(\xi)} \frac{\Omega(\xi)}{n} \tag{2.42}$$

Where $\nu(\xi)$ is the number of daughters formed in the breakage process. For binary breakage, $\nu(\xi) = 2$.

The daughter size redistribution function is calculated from the partial and total breakage density, using the following relation:

$$h_{\text{DSD}}(\xi, \omega) = \frac{\Omega(\xi, \omega)}{\Omega(\xi)} \tag{2.43}$$

Using this relation and converting to a probability density function by dividing by the number of daughters formed in the breakage process, the following expression is obtained:

$$P^*_{\text{DSD}}(\xi, f_v) = \frac{\int_{\zeta_{\min}}^1 \frac{(1+\zeta)^2}{\zeta^{11/3}} \exp\left(-\frac{12 c_f(f_v)\sigma}{2.045 \rho_c \varepsilon^{2/3} \xi^{5/3} \zeta^{11/3}}\right) \mathrm{d}\zeta}{\int_{\zeta_{\min}}^1 \frac{(1+\zeta)^2}{\zeta^{11/3}} \int_0^1 \exp\left(-\frac{12 c_f(f_v)\sigma}{2.045 \rho_c \varepsilon^{2/3} \xi^{5/3} \zeta^{11/3}}\right) \mathrm{d}f_v \mathrm{d}\zeta} \tag{2.44}$$

The dimensionless probability density function can be converted to a probability density function given per unit of the inner coordinate of the mother particle by the following relation:

$$P^*_{\text{DSD}}(\xi, f_v) = P_{\text{DSD}}(\xi, f_v) \times \xi \tag{2.45}$$

Thus, the probability density function with unit $[1/\mathrm{m}]$ becomes:

$$P_{\text{DSD}}(\xi, f_v) = \frac{\int_{\zeta_{\min}}^1 \frac{(1+\zeta)^2}{\zeta^{11/3}} \exp\left(-\frac{12 c_f(f_v)\sigma}{2.045 \rho_c \varepsilon^{2/3} \xi^{5/3} \zeta^{11/3}}\right) \mathrm{d}\zeta}{\xi \int_{\zeta_{\min}}^1 \frac{(1+\zeta)^2}{\zeta^{11/3}} \int_0^1 \exp\left(-\frac{12 c_f(f_v)\sigma}{2.045 \rho_c \varepsilon^{2/3} \xi^{5/3} \zeta^{11/3}}\right) \mathrm{d}f_v \mathrm{d}\zeta} \tag{2.46}$$

Multiplying with the number of daughters gives the redistribution density function:

$$h_{\text{DSD}}(\xi, f_v) = 2 \times P_{\text{DSD}}(\xi, f_v) \tag{2.47}$$

The redistribution density function on a diameter basis is found from the following relation:

$$h_{\text{DSD}}(\xi, \omega) = h_{\text{DSD}}(\xi, f_v) \times \frac{\mathrm{d}f_v}{\mathrm{d}\omega} = h_{\text{DSD}}(\xi, f_v) \times 3\frac{\omega^2}{\xi^3} \tag{2.48}$$

2.4 Lehr et al. (2002)

A model to predict the breakage of bubbles in turbulent dispersions was developed by Lehr et al. (2002). They adopted the modelling framework of Luo and Svendsen (1996), assuming binary breakage and that only eddies with length scales smaller than or equal to the bubble diameter can cause breakup. Breakage was assumed to occur *if the turbulent*

kinetic energy transferred from an eddy to a bubble is greater than a critical value, calculated from a stress balance. The breakage density of a bubble was given by the product of a collision frequency and breakage probability, as in Luo and Svendsen (1996):

$$\frac{\Omega\left(\xi,\omega\right)}{n}=\int_{\lambda_{\min}}^{\xi}P_b\left(\xi,\omega,\lambda\right)\omega_{\text{col}}\left(\xi,\lambda\right)\mathrm{d}\lambda \tag{2.49}$$

The collision frequency was defined as in Luo and Svendsen (1996), apart from the number density of bubbles:

$$\omega_{\text{col}}\left(\xi,\lambda\right)=\frac{\pi}{4}\left(\xi+\lambda\right)^2\overline{v}_\lambda n_\lambda \tag{2.50}$$

It was assumed that the relative velocity between bubbles and eddies is equal to the turbulent eddy velocity, and that this could be given by the Kolmogorov structure function in the inertial subrange of turbulence[4]:

$$\overline{v}_\lambda\approx\sqrt{\overline{\delta v^2\left(\lambda\right)}}\approx\sqrt{2}\left(\varepsilon\lambda\right)^{1/3} \tag{2.51}$$

The expression for the number density of eddies is given as[5]:

$$n_\lambda=\frac{0.8413}{\lambda^4} \tag{2.52}$$

Inserting the structure function and number density of eddies in equation (2.50) gives:

$$\omega_{\text{col}}\left(\xi,\lambda\right)=0.8413\sqrt{2}\frac{\pi}{4}\varepsilon^{1/3}\frac{\left(\xi+\lambda\right)^2}{\lambda^{11/3}} \tag{2.53}$$

The main difference between the model of Lehr et al. (2002) and Luo and Svendsen (1996) is the estimation of the breakage probability. The critical energy that must be transferred from a turbulent eddy to a bubble to cause breakage is estimated from a stress balance. Immediately before breakage, bubbles were taken to be nearly cylindrical. Balancing the interfacial force of the bubble surface and the inertial force of the arriving eddy gives:

$$\frac{1}{2}\rho_c\overline{v}_\lambda^2=2\frac{\sigma}{\omega_{\text{sm}}} \tag{2.54}$$

Where ω_{sm} is the diameter of the smallest daughter formed in the breakage process. By assuming that the turbulent velocity of eddies is normally distributed around the mean value given by the structure function, Lehr et al. (2002) arrived at the following expression for the breakage probability:

$$P_b\left(\xi,\omega_{\text{sm}},\lambda\right)=\frac{4}{\pi}\frac{\sigma}{\rho_c\left(\varepsilon\lambda\right)^{2/3}\omega_{\text{sm}}^4}\exp\left(-\frac{2\sigma}{\rho_c\left(\varepsilon\lambda\right)^{2/3}\omega_{\text{sm}}}\right) \tag{2.55}$$

[4]Note that the pre-factor used in the structure function is $\sqrt{2}$, which differs from the factor of $\sqrt{2.045}$ used in Luo and Svendsen (1996)

[5]This expression is slightly different than in Luo and Svendsen (1996), where the constant has a value of 0.822 and a factor of $(1-\alpha_d)$ is included.

By inserting the breakage probability and collision frequency into the definition given in equation (2.49), an expression for the breakage density per unit volume of the smallest daughter is obtained:

$$\frac{\Omega\left(\xi,\omega\right)}{n_{\text{sm}}} = C\int_{\lambda_{\text{min}}}^{\xi}\frac{\sigma}{\rho_c\varepsilon^{1/3}\omega_{\text{sm}}^4}\frac{\left(\xi+\lambda\right)^2}{\lambda^{13/3}}\exp\left(-\frac{2\sigma}{\rho_c\left(\varepsilon\lambda\right)^{2/3}\omega_{\text{sm}}}\right)\mathrm{d}\lambda \tag{2.56}$$

Where the constant C is 1.19. Lehr et al. (2002) argued that this integral could be written as a sum of incomplete Γ functions, giving analytical expressions for the breakage frequency and probability density function:

$$b\left(\xi\right) = \frac{1}{2}\xi^{5/3}\varepsilon^{19/15}\left(\frac{\rho_c}{\sigma}\right)^{7/5}\exp\left[-\frac{\sqrt{2}}{\xi^3\varepsilon^{6/5}}\left(\frac{\sigma}{\rho_c}\right)^{9/5}\right] \tag{2.57}$$

In the original article, Lehr et al. (2002) defined a probability density function that was made dimensionless with a length scale L:

$$P_{\text{DSD}}^{*}\left(V_\omega,V_\xi\right) = P_{\text{DSD}}\left(V_\omega,V_\xi\right)L^3 \tag{2.58}$$

This probability density function was incorrectly normalized with the inner coordinate of the daughter particle. Thus, the original probability density function was given per unit volume of the daughter particles. The correct normalization procedure gives the probability density function per unit volume of the mother particle. A modification of the expression in equation (2.58) was made by Liao and Lucas (2009), using the mother particle diameter as the length scale:

$$P_{\text{DSD}}^{*}\left(V_\omega,V_\xi\right) = P_{\text{DSD}}\left(V_\omega,V_\xi\right)\xi^3 \tag{2.59}$$

By converting the expression in Liao and Lucas (2009) from a volume fraction to a diameter basis, Solsvik et al. (2013) arrived at the following expression for the probability density function:

$$P_{\text{DSD}}\left(\xi,\omega\right) = \frac{9\omega^2}{\sqrt{\pi}\xi^3}\frac{\exp\left\{-\frac{9}{4}\left[\ln\left(\frac{2^{2/5}\omega\rho_c^{3/5}\varepsilon^{2/5}}{\sigma^{3/5}}\right)\right]^2\right\}}{\left\{1+\text{erf}\left[\frac{3}{2}\ln\left(\frac{2^{1/15}\xi\rho_c^{3/5}\varepsilon^{2/5}}{\sigma^{3/5}}\right)\right]\right\}} \tag{2.60}$$

The redistribution density function is found by multiplying with the number of daughters:

$$h_{\text{DSD}}\left(\xi,\omega\right) = 2\times P_{\text{DSD}}\left(\xi,\omega\right) \tag{2.61}$$

2.5 Han et al. (2011)

Han et al. (2011) developed a theoretical model for droplet breakup in turbulent dispersions based on the modelling framework of Luo and Svendsen (1996). The following assumptions and simplifications were made in the model development:

(i) Small, low viscous droplets are considered. The breakup is assumed to be caused by turbulence, neglecting the inertial and viscous forces.

(ii) Both eddies larger and smaller than the droplets can cause breakage.

(iii) Binary breakage is assumed.

(iv) Only the inertial subrange of turbulence is considered.

As in Luo and Svendsen (1996), breakage is assumed to occur *if the turbulent kinetic energy of an arriving eddy exceeds a critical value*. In addition to the surface energy increase in Luo and Svendsen (1996), Han et al. (2011) included a surface energy density increase in the definition of the critical energy. For eddies equal to or smaller than the droplet size, this was given as:

$$E_{\text{crit}} = \max\left(c_f, c_d\right)\pi\sigma\xi^2 \tag{2.62}$$

Here, the surface energy density increase coefficient is given as $c_d = \left[\min\left(f_v, 1-f_v\right)\right]^{-1/3} - 1$. For eddies larger than the droplet, it was assumed that only a fraction of the eddy energy is available for transfer to the fluid particle. By assuming a sinusoidal velocity decrease in a turbulent eddy, Han et al. (2011) modified an expression from Andersson and Andersson (2006a) for the available energy of an eddy. The following relation between the eddy energy and available energy was obtained:

$$E_{\text{available}}\left(\lambda\right) = 4\left(\frac{\lambda}{\xi}\right)^2 \sin^4\left(\frac{\pi}{4}\frac{\xi}{\lambda}\right) E\left(\lambda\right) \tag{2.63}$$

Using this relation, the expression for the critical energy for all eddy sizes was given as:

$$E_{\text{crit}} = \max\left(c_f, c_d\right)\pi\sigma\xi^2 \times \begin{cases} 1 & \text{if} \quad \lambda \leq \xi \\ \frac{1}{4\left(\frac{\lambda}{\xi}\right)^2 \sin^4\left(\frac{\pi}{4}\frac{\xi}{\lambda}\right)} & \text{if} \quad \lambda > \xi \end{cases} \tag{2.64}$$

As in Luo and Svendsen (1996), the breakage probability was defined as the probability of an arriving eddy having a kinetic energy greater than or equal to the critical energy:

$$P_b\left(\xi, \omega, \lambda\right) = 1 - \int_0^{\chi_c} \exp\left(-\chi\right) \mathrm{d}\chi = \exp\left(-\chi_c\right) \tag{2.65}$$

Where the dimensionless critical energy was given as:

$$\chi_c = \frac{E_{\text{crit}}}{\overline{E}\left(\lambda\right)} = \frac{\max\left(c_f, c_d\right)\pi\sigma\xi^2}{\frac{1}{2}\rho_c v_\lambda^2 \frac{1}{6}\pi\lambda^3} \times \begin{cases} 1 & \text{if} \quad \lambda \leq \xi \\ \frac{1}{4\left(\frac{\lambda}{\xi}\right)^2 \sin^4\left(\frac{\pi}{4}\frac{\xi}{\lambda}\right)} & \text{if} \quad \lambda > \xi \end{cases} \tag{2.66}$$

The structure function used for the mean eddy velocity in Han et al. (2011) is $v_\lambda = \sqrt{2}\left(\varepsilon\lambda\right)^{1/3}$. From the kinetic theory of gases, the collision frequency between an eddy and a droplet is given by (Luo and Svendsen, 1996):

$$\omega_{\text{col}}\left(\xi, \lambda\right) = \frac{\pi}{4}\left(\xi + \lambda\right)^2 v_\lambda n_\lambda n \tag{2.67}$$

In general, the number density of eddies is a function of the turbulent energy spectrum and the structure function. In the inertial subrange it becomes:

$$n_\lambda \approx \frac{0.822\,(1-\alpha_d)}{\lambda^4} \tag{2.68}$$

The collision frequency in equation (2.67) was modified to include the effect of droplet surface oscillations. These oscillations were assumed to increase the size of the collision tube, giving[6]

$$\omega_{\text{col}}\,(\xi,\lambda) = \frac{\pi}{4}\,(\xi+\lambda+C_0\xi)^2\,v_\lambda n_\lambda n \tag{2.69}$$

The dimensionless oscillation ratio is given by:

$$C_0 = \frac{v_\lambda\,(\xi)}{\xi}\left(\frac{3\rho_d+2\rho_c}{24}\frac{\xi^3}{2\sigma}\right)^{1/2} \tag{2.70}$$

An interaction frequency was used to describe the eddies larger than the droplets in size. Han et al. (2011) modified another expression from Andersson and Andersson (2006a) by including a sinusoidal formula for the transport time. The interaction frequency was given as[7]

$$\omega_{\text{inter}}\,(\xi,\lambda) = \frac{\pi\xi^3 n_\lambda n}{6\times\min\left[\frac{\lambda}{v_\lambda},\frac{\lambda}{2\left(\frac{\lambda}{\xi}\right)\sin^2\left(\frac{\pi}{4}\frac{\xi}{\lambda}\right)v_\lambda}\right]} \tag{2.71}$$

Following Luo and Svendsen (1996), the partial breakage density is calculated from the product of the collision or interaction frequency and the breakage probability:

$$\frac{\Omega\,(V_\xi,f_v)}{n} = \begin{cases}\int_{\lambda_{\min}}^{\lambda_{\max}} P_b\,(V_\xi,f_v,\lambda)\,\frac{\omega_{\text{col}}(V_\xi,\lambda)}{n}\mathrm{d}\lambda & \lambda\le\xi\\ \int_{\lambda_{\min}}^{\lambda_{\max}} P_b\,(V_\xi,f_v,\lambda)\,\frac{\omega_{\text{inter}}(V_\xi,\lambda)}{n}\mathrm{d}\lambda & \lambda>\xi\end{cases} \tag{2.72}$$

The total breakage density is given by (Luo and Svendsen, 1996):

$$\frac{\Omega\,(V_\xi)}{n} = \frac{1}{2}\int_0^1 \frac{\Omega\,(V_\xi,f_v)}{n}\mathrm{d}f_v \tag{2.73}$$

The volume based breakage redistribution density function can be calculated directly from the partial and total breakage density:

$$h_{\text{DSD}}\,(V_\xi,f_v) = \frac{\Omega\,(V_\xi,f_v)}{\Omega\,(V_\xi)} \tag{2.74}$$

This redistribution density function can be given on a diameter basis by applying the following relation:

$$h_{\text{DSD}}\,(\xi,\omega) = h_{\text{DSD}}\,(V_\xi,f_v)\times\frac{\mathrm{d}f_v}{\mathrm{d}\omega} = h_{\text{DSD}}\,(V_\xi,f_v)\times 3\frac{\omega^2}{\xi^3} \tag{2.75}$$

[6]The collision frequency given in the article of Han et al. (2011) has a pre-factor of 0.923, which corresponds to a constant of $\sqrt{2.045}$ in the structure function. The pre-factor should be 0.913, as a constant of $\sqrt{2}$ was used in the structure function in Han et al. (2011).

[7]In the article of Han et al. (2011), the eddy turnover τ_e is incorrectly defined. It lacks a factor of $\sqrt{2}$ from the inertial range structure function.

2.6 Han et al. (2015)

The model proposed by Han et al. (2011) has been extended on multiple occasions after it was published. In Han et al. (2013), the model was extended to multiple breakage in the inertial subrange. In Han et al. (2014), a binary breakage model in the wide energy spectrum was proposed. Finally, the model of Han et al. (2015) considers multiple breakage in the wide energy spectrum.

Han et al. (2015) argues that only two wide energy spectrum models that contain the dissipation range, inertial range and energy containing range are available in the literature. These are the spectra of Pope (2000) and Hinze (1975). The energy spectrum of Pope showed a better agreement with direct numerical simulation (DNS) results, and was therefore used in the simulations of Han et al. (2015). This energy spectrum as a function of the turbulent wave number κ is given as:

$$E(\kappa) = C\varepsilon^{2/3}\kappa^{-5/3}\left(\frac{\kappa L}{\left[(\kappa L)^2 + C_L\right]^{1/2}}\right)^{5/3+P_0} \exp\left(-\beta_2\left[(\kappa\eta)^4 + C_\eta^4\right]^{1/4} + \beta_2 C_\eta\right) \tag{2.76}$$

Where $P_0 = 2$, $\beta_2 = 5.2$, $C_L \approx 6.78$ and $C_\eta \approx 0.40$. The values used for C_L and C_η are only valid in the limit of infinite integral scale Reynolds numbers, as the parameters are not constant for finite Reynolds numbers. The Kolmogorov constant C was set to 1.62, instead of the commonly used value of 1.5.

The structure function and number density of eddies depend on the energy spectrum. The structure function in terms of κ was given as:

$$v_\kappa = C_0\sqrt{\kappa E(\kappa)} \tag{2.77}$$

Where the constant $C_0 = \sqrt{2}(2\pi)^{1/3}/\sqrt{C}$. An expression for the number density of eddies can be found from a kinetic energy balance, as in Luo and Svendsen (1996):

$$\rho_c\frac{\pi}{6}\left(\frac{2\pi}{\kappa}\right)^3\frac{v_\kappa^2}{2}n_\kappa \mathrm{d}\lambda = \rho_c(1-\alpha_d)E(\kappa)\mathrm{d}\kappa \tag{2.78}$$

In Han et al. (2015), the kinetic energy balance was incorrectly given as[8]:

$$\rho_c\frac{\pi}{6}\left(\frac{2\pi}{\kappa}\right)^3\frac{v_\kappa^2}{2}n_\kappa \mathrm{d}\kappa = \rho_c(1-\alpha_d)E(\kappa)\mathrm{d}\kappa \tag{2.79}$$

Han et al. (2015) arrived at the following incorrect expression for the number density of eddies:

$$n_\kappa = \frac{3(1-\alpha_d)}{2\pi^4 C_0^2}\kappa^2 \tag{2.80}$$

[8]Here, $\mathrm{d}\kappa$ has directly replaced $\mathrm{d}\lambda$ without multiplying with the Jacobian of the transformation. Since $\kappa = 2\pi/\lambda$, the Jacobian is $\mathrm{d}\lambda = -\lambda^2/(2\pi)\mathrm{d}\kappa$

The correct expression is found by accounting for the Jacobian of the transformation from λ to κ, giving:

$$n_\kappa = \frac{3\left(1-\alpha_d\right)}{4\pi^5 C_0^2}\kappa^5 \tag{2.81}$$

The breakage mechanism assumed by Han et al. (2015) is shown in Figure 2.1. As in Han et al. (2011), breakage is assumed to occur *if the turbulent kinetic energy of an arriving eddy exceeds a critical value*. The process of binary breakage occurs without the formation of intermediates. In the process of ternary and quaternary breakage, respectively one and two intermediates are formed. As a result of this, the process of forming the first daughter is statistically independent of the formation of the second and third daughter in the ternary case. Similarly, the process of forming the first daughter is statistically independent of the process forming the second daughter and the process forming the third and fourth daughter in the quaternary case.

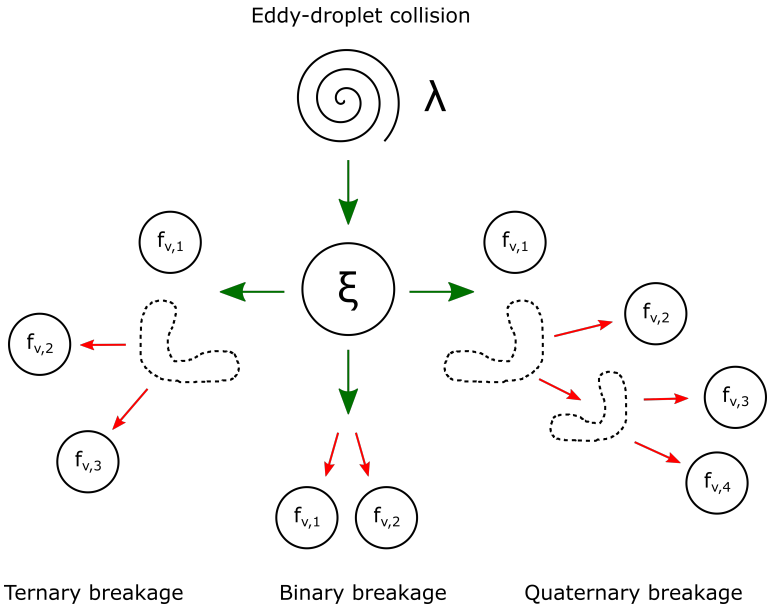

Figure 2.1: A sketch of the breakage mechanism of Han et al. (2015), adapted from the original article.

Each breakage process is associated with its own dimensionless critical energy required for breakup:

$$\chi_{c,m} = \frac{E_{\text{crit}}}{\overline{E}\left(\kappa\right)} = \frac{\max\left(c_{f,m}, c_{d,m}\right)\pi\xi^2\sigma}{\frac{1}{2}\rho_c v_\kappa^2 \frac{1}{6}\pi\left(\frac{2\pi}{\kappa}\right)^3} \times \begin{cases} 1 & \text{if } \frac{2\pi}{\kappa} \leq \xi \\ \frac{1}{4\left(\frac{2\pi}{\kappa\xi}\right)^2 \sin^4\left(\frac{\kappa\xi}{8}\right)} & \text{if } \frac{2\pi}{\kappa} > \xi \end{cases} \tag{2.82}$$

Where $m = 2, 3, 4$ represents the number of daughters formed in the breakage process. To account for the effect of surface oscillations from previous eddy-droplet interactions

on future eddy-droplet interactions, the intermediates were assumed to be ellipsoidal. The surface area of an intermediate was given as:

$$S = 2\pi a^2 \left\{ 1 + \frac{\zeta}{2\sqrt{\zeta - 1}} \times \left[\frac{\pi}{2} + \arcsin\left(\frac{\zeta - 2}{\zeta} \right) \right] \right\} \tag{2.83}$$

Where a and b is, respectively, the short and long semiaxis of the ellipsoid. The dimensionless quantity $\zeta = b^2/a^2$. The semiaxes of the ellipsoid are related to the mean surface oscillation distance of droplets:

$$a = \frac{\xi}{2} \left(1 + \frac{\overline{\delta}}{(\xi/2)} \right)^{-1/2} \tag{2.84}$$

$$b = \frac{\xi}{2} + \overline{\delta} \tag{2.85}$$

Han et al. (2015) defined a shape factor[9] $S_d = S/\left(\pi\xi^2\right)$. This shape factor was used in the definition of the surface energy increase and surface energy density increase for the different processes:

$$c_{f,m} = \left(\sum_{i=1}^{m} f_{v,i}^{2/3} \right) - S_d \quad , \qquad f_{v,m} = 1 - \sum_{j=1}^{m-1} f_{v,j} \tag{2.86}$$

$$c_{d,2} = \max\left[f_{v,1}^{-1/3}, \left(1 - f_{v,1}\right)^{-1/3} \right] - S_d \tag{2.87}$$

$$\begin{aligned} c_{d,3} = &\left\{ \max\left[f_{v,1}^{-1/3}, \left(1 - f_{v,1}\right)^{-1/3} \right] - S_d \right\} \\ +C_t &\left\{ \max\left[f_{v,2}^{-1/3}, \left(1 - f_{v,1} - f_{v,2}\right)^{-1/3} \right] - \left(1 - f_{v,1}\right)^{-1/3} \right\} \end{aligned} \tag{2.88}$$

$$\begin{aligned} c_{d,4} = &\left\{ \max\left[f_{v,1}^{-1/3}, \left(1 - f_{v,1}\right)^{-1/3} \right] - S_d \right\} \\ + C_q &\left\{ \max\left[f_{v,2}^{-1/3}, \left(1 - f_{v,1} - f_{v,2}\right)^{-1/3} \right] - \left(1 - f_{v,1}\right)^{-1/3} \right. \\ + \max&\left. \left[f_{v,3}^{-1/3}, \left(1 - f_{v,1} - f_{v,2} - f_{v,3}\right)^{-1/3} \right] - \left(1 - f_{v,1} - f_{v,2}\right)^{-1/3} \right\} \end{aligned} \tag{2.89}$$

Where C_t and C_q are constants set to 0.039 and 0.11, respectively. The probability of a mother of size ξ to break into m daughters with volume fractions $f_{v,1}, ..., f_{v,m}$ when colliding with an eddy with wave number κ was taken from Luo and Svendsen (1996):

$$P_{b,m}\left(\xi, f_{v,1}, ..., f_{v,m}, \kappa\right) = 1 - \int_0^{\chi_{c,m}} \exp\left(-\chi\right) \mathrm{d}\chi = \exp\left(\chi_{c,m}\right) \tag{2.90}$$

For eddies smaller or equal to the droplets in size, the collision frequency was given as:

$$\omega_{\text{col}}\left(\xi, \kappa\right) \approx \frac{3\kappa^{5/2}\left(1 - \alpha_d\right) n}{2\pi^3 C_0} \left(a + \frac{\pi}{\kappa} \right) \left(b + \frac{\pi}{\kappa} \right) \sqrt{E\left(\kappa\right)} \tag{2.91}$$

[9] The shape factor has been incorrectly defined as $S_d = S/\left(\pi\xi^2\sigma\right)$ multiple times in Han et al. (2015).

For eddies larger than the droplets, an interaction frequency is used. The following expression was obtained by applying the same expression for the available energy in a turbulent eddy as in Han et al. (2011):

$$\omega_{\text{inter}}\left(\xi,\kappa\right) \approx \frac{\left(1-\alpha_d\right)\kappa^{7/2}\xi^3 n}{8\pi^4 C_0}\max\left[1,\frac{4\pi}{\kappa\xi}\sin^2\left(\frac{\kappa\xi}{8}\right)\right]\sqrt{E\left(\kappa\right)} \tag{2.92}$$

Following Luo and Svendsen (1996), the breakage density is calculated from the product of the breakage probability and the collision or interaction frequency, depending on the size of the arriving eddy:

$$\frac{\Omega_m\left(\xi,f_{v,1},...,f_{v,m}\right)}{n} = \begin{cases} \int_{2\pi/\xi}^{\kappa_{\max}} P_{b,m}\left(\xi,f_{v,1},...,f_{v,m},\kappa\right)\frac{\omega_{\text{col}}(\xi,\kappa)}{n}\mathrm{d}\kappa & , \quad \frac{2\pi}{\kappa}\leq\xi \\ \int_{\kappa_{\min}}^{2\pi/\xi} P_{b,m}\left(\xi,f_{v,1},...,f_{v,m},\kappa\right)\frac{\omega_{\text{inter}}(\xi,\kappa)}{n}\mathrm{d}\kappa & , \quad \frac{2\pi}{\kappa}>\xi \end{cases} \tag{2.93}$$

For binary breakage, only one statistically independent volume fraction exists. The binary breakage density can therefore be written as:

$$\frac{\Omega_2\left(\xi,f_{v,1},...,f_{v,m}\right)}{n} = \frac{\Omega_2\left(\xi,f_v\right)}{n} \tag{2.94}$$

In the case of ternary and quaternary breakage, integration over all statistically independent volume fractions must be performed in order to obtain breakage densities that only depend on the generic volume fraction f_v:

$$\frac{\Omega_3\left(\xi,f_v\right)}{n} = \frac{1}{2}\int_0^{1-f_v}\frac{\Omega_3\left(\xi,f_v,f_{v,1},f_{v,2}\right)}{n}\mathrm{d}f_{v,2} + \int_0^{1-f_v}\frac{\Omega_3\left(\xi,f_v,f_{v,1},f_{v,2}\right)}{n}\,\mathrm{d}f_{v,1} \tag{2.95}$$

$$\begin{aligned}\frac{\Omega_4\left(\xi,f_v\right)}{n} = {} & \frac{1}{2}\int_0^{1-f_v}\int_0^{1-f_v-f_{v,2}}\frac{\Omega_4\left(\xi,f_v,f_{v,1},f_{v,2},f_{v,3}\right)}{n}\,\mathrm{d}f_{v,3}\,\mathrm{d}f_{v,2} \\ & + \frac{1}{2}\int_0^{1-f_v}\int_0^{1-f_v-f_{v,1}}\frac{\Omega_4\left(\xi,f_v,f_{v,1},f_{v,2},f_{v,3}\right)}{n}\,\mathrm{d}f_{v,3}\,\mathrm{d}f_{v,1} \\ & + \int_0^{1-f_v}\int_0^{1-f_v-f_{v,1}}\frac{\Omega_4\left(\xi,f_v,f_{v,1},f_{v,2},f_{v,3}\right)}{n}\,\mathrm{d}f_{v,2}\,\mathrm{d}f_{v,1}\end{aligned} \tag{2.96}$$

The total breakage density is obtained by integrating these expressions over the generic volume fraction f_v:

$$\frac{\Omega_m\left(\xi\right)}{n} = \int_0^1\frac{\Omega_m\left(\xi,f_v\right)}{n}\mathrm{d}f_v \tag{2.97}$$

As in Han et al. (2011), the volume based breakage redistribution density functions are calculated from the partial and total breakage densities:

$$h_{m,\text{DSD}}\left(\xi,f_v\right) = \frac{\Omega_m\left(\xi,f_v\right)}{\Omega_m\left(\xi\right)} \tag{2.98}$$

Converting from a volume fraction based to a diameter based redistribution density function is done by applying the following relation:

$$h_{m,\text{DSD}}\left(\xi,\omega\right) = h_{m,\text{DSD}}\left(\xi,f_v\right)\times\frac{\mathrm{d}f_v}{\mathrm{d}\omega} = h_{m,\text{DSD}}\left(\xi,f_v\right)\times 3\frac{\omega^2}{\xi^3} \tag{2.99}$$

2.7 Becker et al. (2014)

A model for the breakage of droplets in turbulent high-viscosity dispersed phases was developed by Becker et al. (2014). They adopted the phenomenological modelling framework of Luo and Svendsen (1996) and applied concepts presented by Han et al. (2011). As in Luo and Svendsen (1996), it was assumed that a droplet will break *if the energy transferred to the droplet from a colliding eddy exceeds a critical value*. However, Becker et al. (2014) included the viscous energy during deformation in the critical energy. The breakage criterion can be written as:

$$E_\lambda \geq E_s + E_\mu \tag{2.100}$$

If the Kolmogorov structure function used in Luo and Svendsen (1996) is applied, the mean kinetic energy of an arriving eddy can be estimated by:

$$E_\lambda = \frac{1}{12}\rho_c \pi \lambda^3 \overline{\delta v^2\left(\lambda\right)} = \frac{2.045}{12}\rho_c \pi \varepsilon^{2/3}\lambda^{11/3} \tag{2.101}$$

It was not evident from the original article which definition of the surface energy E_s should be used. By personal communication[10], it was confirmed that the surface energy could be defined in two ways. One alternative is to use the surface energy density increase of Han et al. (2011):

$$E_s = c_d \pi \sigma \xi^2 \tag{2.102}$$

Where the surface energy density increase coefficient is $c_d = \left[\min\left(f_v, 1-f_v\right)\right]^{-1/3} - 1$. Alternatively, both the surface energy increase and the surface energy density increase can be applied, giving:

$$E_s = \max\left(c_f, c_d\right)\pi\sigma\xi^2 \tag{2.103}$$

Here, c_f is the surface energy increase coefficient of Luo and Svendsen (1996). Unless stated otherwise, the latter definition will be used in this work.

By assuming simple shear flow, the viscous energy dissipated inside a drop was given as:

$$E_\mu\left(\xi\right) = \pi\xi^3\tau_\mu = \pi\xi^2\mu_d\overline{v}_\lambda \tag{2.104}$$

Where the mean eddy velocity $\overline{v}_\lambda$ can be estimated by the structure function. Both terms of the criterion in equation (2.100) are included in the expression for the breakage probability, previously defined in equation (2.39):

$$P_b\left(\xi,\omega,\lambda\right) = \exp\left(-\frac{E_s + E_\mu}{E_\lambda}\right) \tag{2.105}$$

Thus, following the model of Luo and Svendsen (1996), the following expression for the

[10]The personal communication was with Nida Sheibat-Othman at Université de Lyon.

breakage density is obtained:

$$\Omega\left(\xi,\omega\right)=\int_{\lambda_{\min}}^{\xi}P_b\left(\xi,\omega,\lambda\right)\omega_{\text{col}}\left(\xi,\lambda\right)\mathrm{d}\lambda=$$
$$0.923\left(\frac{\varepsilon}{\xi^2}\right)^{1/3}\int_{\zeta_{\min}}^{1}\exp\left(-\frac{\max\left[c_f,c_d\right]\pi\sigma\xi^2+\left(2.045\right)^{1/2}\pi\varepsilon^{1/3}\mu_d\xi^{10/3}}{\frac{2.045}{12}\rho_c\pi\varepsilon^{2/3}\left(\zeta\xi\right)^{11/3}}\right)\frac{\left(1+\zeta\right)^2}{\zeta^{11/3}}\mathrm{d}\zeta \tag{2.106}$$

Where the dimensionless variable $\zeta=\lambda/\xi$. The total breakage density is found by integrating the partial breakage density over the daughter size:

$$\Omega\left(\xi\right)=\int_{\xi_{\min}}^{\xi}\Omega\left(\xi,\omega\right)3\frac{\omega^2}{\xi^3}\mathrm{d}\omega \tag{2.107}$$

The probability density function is given as the ratio between the partial and total breakage density:

$$P_{\text{DSD}}\left(\xi,\omega\right)=3\frac{\omega^2}{\xi^3}\frac{\Omega\left(\xi,\omega\right)}{\Omega\left(\xi\right)} \tag{2.108}$$

The redistribution density function is given as:

$$h_{\text{DSD}}\left(\xi,\omega\right)=2\times P_{\text{DSD}}\left(\xi,\omega\right) \tag{2.109}$$

2.8 Martínez-Bazán et al. (1999a,b, 2010)

A phenomenological model for the breakup of an air bubble into a fully developed turbulent flow was developed by Martínez-Bazán et al. (1999a). The probability density function for the same system was presented in Martínez-Bazán et al. (1999b). Approximately a decade later, Martínez-Bazán et al. (2010) modified the original model to enhance its volume conserving properties. It was assumed that the turbulence was locally isotropic and fully developed, and that the void fraction of the dispersed phase was small. The size of the mother particles was assumed to be within the inertial subrange of turbulence. The basic premise is that breakage is caused by surface deformation. A bubble will break *if the deformation energy provided by the turbulent stresses from the continuous phase exceeds the surface restoring stresses of the fluid particle*. By assuming that the viscous forces are negligible compared to the turbulent forces, the minimum energy required to deform a bubble of size ξ is:

$$\overline{E}_s\left(\xi\right)=\pi\sigma\xi^2 \tag{2.110}$$

The surface restoring pressure was given as the minimum energy required for deformation per unit volume of the bubble:

$$\overline{\sigma}_s\left(\xi\right)=\frac{\overline{E}_s\left(\xi\right)}{\frac{\pi}{6}\xi^3}=\frac{6\sigma}{\xi} \tag{2.111}$$

The average deformation force per unit surface, resulting from the turbulent velocity fluctuations in the continuous phase, can in the inertial subrange be estimated as:

$$\overline{\sigma}_t(\xi) = \frac{1}{2}\rho_c\overline{\delta v^2(\xi)} = \frac{1}{2}\rho_c\beta(\varepsilon\xi)^{2/3} \tag{2.112}$$

When $\overline{\sigma}_s(\xi) > \overline{\sigma}_t(\xi)$, breakage will occur. Equivalently, a bubble will break if its diameter exceeds a critical value. The critical diameter is found by equating the two stresses, giving:

$$\xi_{\text{crit}} = \left(\frac{12\sigma}{\beta\rho_c}\right)^{3/5}\varepsilon^{-2/5} \tag{2.113}$$

Martínez-Bazán et al. used dimensional analysis to define a characteristic time scale for breakage:

$$t_b \propto \frac{\xi}{\Delta v_b} \tag{2.114}$$

Where the characteristic velocity is determined from the difference between the surface deforming and restoring stresses (Solsvik et al., 2013):

$$\frac{1}{2}\rho_c(\Delta v_b)^2 \approx \overline{\sigma}_t(\xi) - \overline{\sigma}_s(\xi) \tag{2.115}$$

Solving for the characteristic velocity and inserting it into equation (2.114) gives:

$$t_b \propto \frac{\xi}{\sqrt{\beta(\varepsilon\xi)^{2/3} - \frac{12\sigma}{\rho_c\xi}}} \tag{2.116}$$

The breakage frequency was given as the inverse of the breakup time:

$$b(\xi) = \frac{1}{t_b} = K_g\frac{\sqrt{\beta(\varepsilon\xi)^{2/3} - \frac{12\sigma}{\rho_c\xi}}}{\xi} \tag{2.117}$$

The constants β and K_g were given as 8.2 and 0.25, respectively. The breakup frequency of bubbles of size $\xi < \xi_{\text{crit}}$ is set to zero, to avoid numerical problems (Solsvik et al., 2013).

Martínez-Bazán et al. (1999b) assumed a binary breakage process, where a daughter of size ω and its complement of size $\left(\xi^3 - \omega^3\right)^{1/3}$ in the range $\omega_{\min} \leq \omega \leq \omega_{\max}$ is formed. The probability density of forming a certain sized pair of daughter particles is related to the product of the excess stresses associated with the daughter sizes:

$$P_{\text{DSD}}(\xi,\omega) \propto [\Delta\sigma_{t1}][\Delta\sigma_{t2}] \tag{2.118}$$

The surplus stresses are given as:

$$[\Delta\sigma_{t1}] = \frac{1}{2}\beta\rho_c(\varepsilon\omega)^{2/3} - \frac{6\sigma}{\xi}$$
$$[\Delta\sigma_{t2}] = \frac{1}{2}\beta\rho_c\left[\varepsilon\left(\xi^3 - \omega^3\right)^{1/3}\right]^{2/3} - \frac{6\sigma}{\xi}$$

Thus, the probability density function can be written as:

$$P_{\text{DSD}}\left(\xi,\omega\right) \propto \left[\frac{1}{2}\beta\rho_c\left(\varepsilon\omega\right)^{2/3} - \frac{6\sigma}{\xi}\right]\left[\frac{1}{2}\beta\rho_c\left[\varepsilon\left(\xi^3-\omega^3\right)^{1/3}\right]^{2/3} - \frac{6\sigma}{\xi}\right] \tag{2.119}$$

This equation can also be expressed in terms of dimensionless variables:

$$P^*_{\text{DSD}}\left(1,\omega^*\right) \propto \left[\frac{1}{2}\beta\rho_c\left(\varepsilon\xi\right)^{2/3}\right]^2\left[\left(\omega^*\right)^{2/3} - \Lambda^{5/3}\right]\left[\left(1-\left(\omega^*\right)^3\right)^{2/9} - \Lambda^{5/3}\right] \tag{2.120}$$

Where $\omega^* = \omega/\xi$ and $\Lambda = \xi_{\text{crit}}/\xi$, using ξ_{crit} as defined in equation (2.113). The dimensionless lower limit is given by $\omega^*_{\text{min}} = \left[12\sigma/\left(\beta\rho_c\right)\right]^{3/2}\xi^{-5/2}\varepsilon^{-1}$ and the dimensionless upper limit is $\omega^*_{\text{max}} = \left(1-\left(\omega^*_{\text{min}}\right)^3\right)^{1/3}$. As pointed out by Martínez-Bazán et al. (2010), the normalization performed in Martínez-Bazán et al. (1999b) was incorrect, leading to the model not conserving volume. They presented a modified closure, where the probability density function was expressed in terms of dimensionless volume before the normalization. By introducing a new variable $V^*_\omega = V_\omega/V_\xi$ they gave the correct form of equation (2.120):

$$P^*_{\text{DSD}}\left(1,V^*_\omega\right) \propto \left[\frac{1}{2}\beta\rho_c\left(\varepsilon\xi\right)^{2/3}\right]^2\left[\left(V^*_\omega\right)^{2/9} - \Lambda^{5/3}\right]\left[\left(1-V^*_\omega\right)^{2/9} - \Lambda^{5/3}\right] \tag{2.121}$$

The normalization that ensures volume conservation was given as:

$$\int_{V^*_{\omega,\text{min}}}^{V^*_{\omega,\text{max}}} P^*_{\text{DSD}}\left(1,V^*_\omega\right)\mathrm{d}V^*_\omega = 1 \tag{2.122}$$

Applying this normalization condition gives the volume conserving probability density function:

$$\begin{aligned} P_{\text{DSD}}\left(V_\xi,V_\omega\right)V_\xi &= \frac{P^*_{\text{DSD}}\left(1,V^*_\omega\right)}{\int_{V^*_{\omega,\text{min}}}^{V^*_{\omega,\text{max}}} P^*_{\text{DSD}}\left(1,V^*_\omega\right)\mathrm{d}V^*_\omega} \\ &= \frac{\left[\left(V^*_\omega\right)^{2/9} - \Lambda^{5/3}\right]\left[\left(1-V^*_\omega\right)^{2/9} - \Lambda^{5/3}\right]}{\int_{V^*_{\omega,\text{min}}}^{V^*_{\omega,\text{max}}}\left[\left(V^*_\omega\right)^{2/9} - \Lambda^{5/3}\right]\left[\left(1-V^*_\omega\right)^{2/9} - \Lambda^{5/3}\right]\mathrm{d}V^*_\omega} \end{aligned} \tag{2.123}$$

The diameter based probability density function is given as:

$$P_{\text{DSD}}\left(\xi,\omega\right) = P_{\text{DSD}}\left(V_\xi,V_\omega\right)\times\frac{\pi}{2}\omega^2 \tag{2.124}$$

This is converted to a redistribution density function by multiplying with the number of daughters:

$$h_{\text{DSD}}\left(\xi,\omega\right) = 2\times P_{\text{DSD}}\left(\xi,\omega\right) \tag{2.125}$$

2.9 Solsvik et al. (2013)

Solsvik et al. (2013) modified the breakage frequency of Martínez-Bazán et al. (1999a) by including the effect of viscous stresses on breakage. The stress balance in Martínez-Bazán et al. (1999a) consisted of a surface restoring and a surface deforming term, given respectively as:

$$\overline{\sigma}_s(\xi) = \frac{6\sigma}{\xi} \tag{2.126}$$

$$\overline{\sigma}_t(\xi) = \frac{1}{2}\rho_c \overline{\delta v^2(\xi)} \tag{2.127}$$

Solsvik et al. (2013) added a term for the restoring viscous effect of the dispersed phase and the deforming stress of the continuous phase, given respectively as:

$$\overline{\sigma}_{\mu,c}(\xi) = \mu_c \overline{S} = \mu_c \sqrt{\frac{\varepsilon}{\nu_c}} \tag{2.128}$$

$$\overline{\sigma}_{\mu,d}(\xi) = \mu_d \overline{S} = \mu_d \sqrt{\frac{\varepsilon}{\nu_c}} \tag{2.129}$$

Similarly to Martínez-Bazán et al. (1999a), the characteristic velocity is determined by the difference between surface deforming and restoring stresses:

$$\frac{1}{2}\rho_c (\Delta v_b)^2 \approx \overline{\sigma}_t(\xi) + \overline{\sigma}_{\mu,c}(\xi) - \overline{\sigma}_s(\xi) - \overline{\sigma}_{\mu,d}(\xi) \tag{2.130}$$

An expression for the breakage time is obtained by solving for the characteristic velocity and inserting it into the definition given in equation (2.114):

$$t_b \propto \frac{\xi}{\sqrt{\frac{2}{\rho_c}\left(\overline{\sigma}_t(\xi) + \overline{\sigma}_{\mu,c}(\xi) - \overline{\sigma}_s(\xi) - \overline{\sigma}_{\mu,d}(\xi)\right)}} \tag{2.131}$$

The breakup frequency is given as:

$$b(\xi) = \frac{1}{t_b} = c_1 \frac{\sqrt{\frac{2}{\rho_c}\left(\overline{\sigma}_t(\xi) + \overline{\sigma}_{\mu,c}(\xi) - \overline{\sigma}_s(\xi) - \overline{\sigma}_{\mu,d}(\xi)\right)}}{\xi} \tag{2.132}$$

By defining the dimensionless groups $\mathrm{We_t} = \overline{\sigma}_t/\overline{\sigma}_s$, $\mathrm{Ca_c} = \overline{\sigma}_{\mu,c}/\overline{\sigma}_s$ and $\mathrm{Ca_d} = \overline{\sigma}_{\mu,d}/\overline{\sigma}_s$, this can be written as:

$$b(\xi) = \frac{c_1}{\xi}\sqrt{\frac{12\sigma}{\rho_c \xi}}\sqrt{\mathrm{We_t} + \mathrm{Ca_c} - \mathrm{Ca_d} - 1} \tag{2.133}$$

Solsvik et al. (2013) added adjustable parameters to this expression, most likely in order to obtain a better agreement with experimental data. The modified expression was:

$$b(\xi) = \frac{c_1}{\xi}\sqrt{\frac{12\sigma}{\rho_c \xi}}\sqrt{\frac{\mathrm{We_t}}{c_2\beta} + c_3\mathrm{Ca_c} - (c_3\mathrm{Ca_d} + 1)} \tag{2.134}$$

Where the adjustable parameters were given as $c_1 = 0.11$, $c_2 = 0.028$ and $c_3 = 75$. An alternative expression for the breakage frequency can be obtained by removing the adjustable parameter on $\mathrm{We_t}$, i.e. only adjusting the viscous effects:

$$b(\xi) = \frac{c_1}{\xi}\sqrt{\frac{12\sigma}{\rho_c \xi}}\sqrt{\mathrm{We_t} + c_3\mathrm{Ca_c} - (c_3\mathrm{Ca_d} + 1)} \tag{2.135}$$

The introduction of these constants implies that the different terms in the stress balance are weighted separately. This affects the calculation of minimum fluid particle size, critical particle diameter and the daughter size distribution function. Following Martínez-Bazán et al. (1999a), the minimum fluid particle size is found by equating the surface energy of a particle of size ξ and the deformation energy between two points separated by a distance ξ_{min}:

$$\frac{1}{2}\beta\rho_c\left(\varepsilon\xi_{\mathrm{min}}\right)^{2/3} + c_3\mu_c\sqrt{\frac{\varepsilon}{\nu_c}} = \frac{6\sigma}{\xi} + c_3\mu_d\sqrt{\frac{\varepsilon}{\nu_c}} \tag{2.136}$$

Solving for the minimum fluid particle size gives:

$$\xi_{\mathrm{min}} = \left[\frac{2\left(\frac{6\sigma}{\xi} - c_3\mu_c\sqrt{\frac{\varepsilon}{\nu_c}} + c_3\mu_d\sqrt{\frac{\varepsilon}{\nu_c}}\right)}{\beta\rho_c\varepsilon^{2/3}}\right]^{3/2} \tag{2.137}$$

The critical particle diameter, ξ_{crit}, is found by equating the deforming and restoring stresses:

$$\overline{\sigma}_t\left(\xi_{\mathrm{crit}}\right) + \overline{\sigma}_{\mu,c}\left(\xi_{\mathrm{crit}}\right) = \overline{\sigma}_s\left(\xi_{\mathrm{crit}}\right) + \overline{\sigma}_{\mu,d}\left(\xi_{\mathrm{crit}}\right) \tag{2.138}$$

Inserting the expressions for the different stresses and including the weights gives:

$$\frac{1}{2}\beta\rho_c\left(\varepsilon\xi_{\mathrm{crit}}\right)^{2/3} + c_3\mu_c\sqrt{\frac{\varepsilon}{\nu_c}} = \frac{6\sigma}{\xi_{\mathrm{crit}}} + c_3\mu_d\sqrt{\frac{\varepsilon}{\nu_c}} \tag{2.139}$$

This equation must be solved iteratively, e.g. using Picard-iteration. A fluid particle will only break if its diameter exceeds ξ_{crit}.

As in Martínez-Bazán et al. (2010), the probability density function is related to the excess stresses associated with each daughter size:

$$P_{\mathrm{DSD}}(\xi,\omega) \propto \left[\Delta\sigma_{t1}(\xi,\omega)\right]\left[\Delta\sigma_{t2}(\xi,\omega)\right] \tag{2.140}$$

When taking the weighting of the different stresses into account, the excess stresses can be written as:

$$\Delta\sigma_{t1}(\xi,\omega) = \frac{1}{2}\beta\rho_c\left(\varepsilon\omega\right)^{2/3} + c_3\mu_c\sqrt{\frac{\varepsilon}{\nu_c}} - \frac{6\sigma}{\xi} - c_3\mu_d\sqrt{\frac{\varepsilon}{\nu_c}} \tag{2.141}$$

$$\Delta\sigma_{t2}(\xi,\omega) = \frac{1}{2}\beta\rho_c\left[\varepsilon\left(\xi^3 - \omega^3\right)^{1/3}\right]^{2/3} + c_3\mu_c\sqrt{\frac{\varepsilon}{\nu_c}} - \frac{6\sigma}{\xi} - c_3\mu_d\sqrt{\frac{\varepsilon}{\nu_c}} \tag{2.142}$$

On a volume basis, the excess stresses can be given as:

$$\Delta\sigma_{t1}\left(V_\xi, V_\omega\right) = \frac{1}{2}\beta\rho_c\left(\frac{6}{\pi}\right)^{2/9}\varepsilon^{2/3}V_\omega^{2/9} - \frac{6\sigma}{V_\xi^{1/3}}\left(\frac{\pi}{6}\right)^{1/3} + c_3\sqrt{\frac{\varepsilon}{\nu_c}}\left(\mu_c - \mu_d\right) \tag{2.143}$$

$$\Delta\sigma_{t2}\left(V_\xi, V_\omega\right) = \frac{1}{2}\beta\rho_c\left(\frac{6}{\pi}\right)^{2/9}\varepsilon^{2/3}\left(V_\xi - V_\omega\right)^{2/9} - \frac{6\sigma}{V_\xi^{1/3}}\left(\frac{\pi}{6}\right)^{1/3} + c_3\sqrt{\frac{\varepsilon}{\nu_c}}\left(\mu_c - \mu_d\right) \tag{2.144}$$

To conserve volume, the probability density function must be normalized according to the following criterion:

$$\int_{V_{\omega,\min}}^{V_{\omega,\max}} P_{\text{DSD}}\left(V_\xi, V_\omega\right)\mathrm{d}V_\omega = 1 \tag{2.145}$$

After normalization, the expression for the probability density function becomes:

$$P_{\text{DSD}}\left(V_\xi, V_\omega\right) = \frac{\left[\Delta\sigma_{t1}\left(V_\xi, V_\omega\right)\right]\left[\Delta\sigma_{t2}\left(V_\xi, V_\omega\right)\right]}{\int_{V_{\omega,\min}}^{V_{\omega,\max}}\left[\Delta\sigma_{t1}\left(V_\xi, V_\omega\right)\right]\left[\Delta\sigma_{t2}\left(V_\xi, V_\omega\right)\right]\mathrm{d}V_\omega} \tag{2.146}$$

$V_{\omega,\max}$ is given as $V_\xi - V_{\omega,\min}$. The diameter based probability density function can be obtained by applying the following relation:

$$P_{\text{DSD}}\left(\xi, \omega\right) = P_{\text{DSD}}\left(V_\xi, V_\omega\right) \times \frac{\pi}{2}\omega^2 \tag{2.147}$$

This is converted to a redistribution density function by multiplying with the number of daughters:

$$h_{\text{DSD}}\left(\xi, \omega\right) = 2 \times P_{\text{DSD}}\left(\xi, \omega\right) \tag{2.148}$$

2.10 Liao (2013) and Liao et al. (2015)

A generalization of the closure of Martínez-Bazán et al. (1999a) was proposed by Liao et al. (2011). In addition to the turbulent stresses considered by Martínez-Bazán et al., Liao et al. (2011) considered viscous and interfacial friction stresses. Modifications to the model of Liao et al. (2011) were made by Liao (2013) and Liao et al. (2015).

The critical stress required to cause breakage was calculated by following the model of Wang et al. (2003), including both the surface energy increase and capillary constraint. The capillary constraint was included because the required disruptive stresses for breakup becomes very large when the size of the smallest daughter particle approaches zero. The critical stress was given as:

$$\overline{\sigma}_{\text{crit}} = \frac{\sigma}{\xi}\max\left(6\left[\left(\frac{\omega}{\xi}\right)^2 + \left(1 - \left(\frac{\omega}{\xi}\right)^3\right)^{2/3} - 1\right], \frac{1}{\min\left[\frac{\omega}{\xi}, \left(1 - \frac{\omega^3}{\xi^3}\right)^{1/3}\right]}\right) \tag{2.149}$$

Breakage was assumed to occur *if the disruptive stresses acting on the bubble exceeds the critical stress*. Liao et al. (2015) considered four different disruptive stresses: turbulent fluctuations, interfacial slip, laminar velocity shear and eddy velocity shear. The turbulent fluctuations and interfacial slip were referred to as inertial stresses, and given as:

$$\overline{\sigma}_{\text{turb}} = \frac{1}{2}\rho_c v_\lambda^2 = \rho_c \left(\varepsilon\xi\right)^{2/3} \tag{2.150}$$

$$\overline{\sigma}_{\text{inter}} = \frac{1}{8}\rho_c c_{\text{D}} v_{\text{T}}^2 \tag{2.151}$$

An expression for the terminal velocity v_{T} of bubbles as a function of particle diameter is given in Fan and Tsuchiya (1990):

$$v_{\text{T}} = \left(\frac{\sigma g}{\rho_c}\right)^{1/4} \left[\left(\frac{\text{Mo}^{-1/4}}{K_b}\left(\xi'\right)^2\right)^{-n} + \left(\frac{2c}{\xi'} + \frac{\xi'}{2}\right)^{-\frac{n}{2}}\right]^{-\frac{1}{n}} \tag{2.152}$$

Where the adjustable parameters K_b, c and n were set to 37, 1.2 and 0.8, respectively. The Morton number and dimensionless bubble diameter was given by:

$$\text{Mo} = \frac{g\mu_c^4|\rho_c - \rho_d|}{\rho_c^2\sigma^3} \tag{2.153}$$

$$\xi' = \xi\left(\frac{\rho_c g}{\sigma}\right)^{1/2} \tag{2.154}$$

Liao et al. (2015) referred to the laminar velocity shear and eddy velocity shear as viscous stresses. The laminar velocity shear was estimated as a purely viscous effect, even though it is applied to turbulent systems:

$$\overline{\sigma}_{\text{shear}} = \mu_c \dot{\gamma}_{\text{shear}} \tag{2.155}$$

Where the mean shear strain rate of the bulk flow is given by the following relation:

$$\dot{\gamma}_{\text{shear}} = \left[2\left(\frac{\partial v_x}{\partial x}\right)^2 + 2\left(\frac{\partial v_y}{\partial y}\right)^2 + 2\left(\frac{\partial v_z}{\partial z}\right)^2 + \left(\frac{\partial v_x}{\partial y} + \frac{\partial v_y}{\partial x}\right)^2 \left(\frac{\partial v_x}{\partial z} + \frac{\partial v_z}{\partial x}\right)^2 + \left(\frac{\partial v_x}{\partial z} + \frac{\partial v_z}{\partial y}\right)^2\right]^{1/2} \tag{2.156}$$

In Liao (2013), the value of $\dot{\gamma}_{\text{shear}}$ was specified to be 10, 50 and 100 s^{-1} in order to demonstrate the characteristics of the model. If the closure is to be used in a computational fluid dynamics (CFD) simulation, local values of the shear rate would be determined by solving equation (2.156).

Around the Kolmogorov length scale a gradual transition between turbulent and laminar flow takes place. In this area, viscous effects become significant. Bubbles smaller than the Kolmogorov length scale will be contained by the smallest eddies. The bubbles will

experience almost laminar flow conditions with a shear rate that is uniquely determined by the Kolmogorov micro-scales. Liao et al. (2015) proposed that the following deforming stress acts on these small bubbles:

$$\overline{\sigma}_{\text{eddy}} = \mu_c \dot{\gamma}_{\text{eddy}} \tag{2.157}$$

Where the eddy shear strain is given as the inverse of the Kolmogorov time scale:

$$\dot{\gamma}_{\text{eddy}} = \frac{1}{\tau_\eta} = \sqrt{\frac{\varepsilon}{\nu_c}} \tag{2.158}$$

The partial breakage density of a mother bubble of size ξ into a daughter of size ω and its complement was given as a sum of the inverse breakage time for each disruptive mechanism[11]:

$$\frac{\Omega(\xi,\omega)}{n} = \sum_k \frac{1}{t_{b,k}} = \sum_k \frac{v_{b,k}}{\omega} \tag{2.159}$$

The breakage velocity associated with the disruptive mechanism of type k was given as a stress difference (Martínez-Bazán et al., 1999a)

$$v_{b,k} = \left(\frac{\overline{\sigma}_k - \overline{\sigma}_{\text{crit}}}{\rho_c}\right)^{0.5} \tag{2.160}$$

Thus, the partial breakage density becomes:

$$\begin{aligned}\frac{\Omega(\xi,\omega)}{n} = \frac{1}{\omega\sqrt{\rho_c}}\Bigg[&\left(\rho_c\left(\varepsilon\xi\right)^{2/3} - \overline{\sigma}_{\text{crit}}\right)^{0.5} + \left(\frac{1}{8}\rho_c c_{\text{D}} v_{\text{T}}^2 - \overline{\sigma}_{\text{crit}}\right)^{0.5} \\ &+ \left(\mu_c\dot{\gamma}_{\text{shear}} - \overline{\sigma}_{\text{crit}}\right)^{0.5} + \left(\mu_c\dot{\gamma}_{\text{eddy}} - \overline{\sigma}_{\text{crit}}\right)^{0.5}\Bigg]\end{aligned} \tag{2.161}$$

As described in Liao (2013), the dimensionless probability density function can be obtained directly from the breakage density. It is assumed that the probability density function is symmetrical around the volume fraction $\omega^3/\xi^3 = 0.5$, giving:

$$P^*_{\text{DSD}}(\xi,\omega) = \frac{\Omega(\xi,\omega)}{\Omega(\xi)} = \frac{\Omega(\xi,\omega)}{\int_0^{\xi/2^{1/3}} 3\frac{\omega^2}{\xi^3}\Omega(\xi,\omega)\,\mathrm{d}\omega} \tag{2.162}$$

The probability density function per unit of the mother particle is given by:

$$P_{\text{DSD}}(\xi,\omega) = \frac{1}{\xi} P^*_{\text{DSD}}(\xi,\omega) \tag{2.163}$$

The redistribution density function is obtained by multiplying with the number of daughters:

$$h_{\text{DSD}}(\xi,\omega) = 2 \times P_{\text{DSD}}(\xi,\omega) \tag{2.164}$$

The breakage frequency is calculated from the total breakage density, given in Liao (2013) as:

$$b(\xi) = \frac{\Omega(\xi)}{n} = \int_0^{\xi/2^{1/3}} 3\frac{\omega^2}{\xi^3}\frac{\Omega(\xi,\omega)}{n}\mathrm{d}\omega \tag{2.165}$$

[11] In Liao (2013) and Liao et al. (2015), the breakage density was erroneously defined without dividing by the number density of fluid particles.

2.11 Xing et al. (2015)

Xing et al. (2015) proposed a unified breakup model that was valid for both bubbles and droplets by including the effect of pressure on the breakup process. The basic premise of the model is that a fluid particle is deformed when it collides with a turbulent eddy. Internal flow within the neck of the deformed fluid particle will lead to breakage. This is illustrated in Figure 2.2.

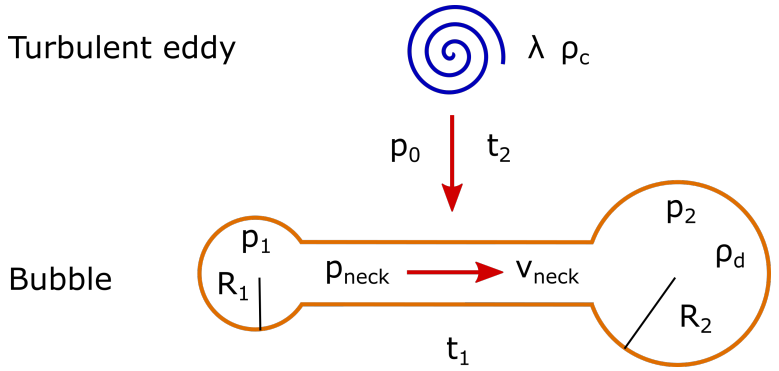

Figure 2.2: A sketch of the fluid particle breakup mechanism, adapted from Xing et al. (2015).

In the model development, the following simplifications and assumptions were made:

(i) Only binary breakup was considered.

(ii) The breakup of bubbles and droplets is mainly caused by collision with turbulent eddies.

(iii) The deformed fluid particle is assumed to divide into three separate parts, as indicated in Figure 2.2. The smaller spherical part has a radius of curvature of R_1 and the larger spherical part has a radius of curvature of R_2. They are connected by a cylindrical neck with a diameter ξ_{neck}.

(iv) The frictional loss along the neck is ignored, because it is small compared to the entrance and exit losses through the neck. An average velocity v_{neck} is used to estimate the internal time scale t_1. Thus, the change in radius of the two spheres is not directly taken into account.

(v) The fluid inside the bubble or droplet is assumed to instantly accelerate due to the pressure difference within the deformed particle. This is because the time scale of the acceleration is negligible compared to the time scale of internal flow.

(vi) To avoid a singularity point when $R_1 = R_2$, R_1 is set to $0.98R_2$ in all cases when the two spheres are equally sized.

In the first step of the model development, the internal flow through the neck of the fluid particle was not considered. The modelling framework of Luo and Svendsen (1996) was

adapted. The breakage density of a fluid particle of size ξ into a daughter particle with volume fraction f_v' and its complement was calculated from the product of a breakage probability and collision frequency:

$$\Omega\left(\xi, f_v'\right) = \int_{\lambda_{\min}}^{\lambda_{\max}} P_b\left(\xi, f_v', \lambda\right) \omega_{\text{col}}\left(\xi, \lambda\right) \mathrm{d}\lambda \tag{2.166}$$

Where the integration limits $\lambda_{\min}$ and $\lambda_{\max}$ were taken as $11.4-31.4$ times the Kolmogorov length scale and 3ξ, respectively. By assuming a normal velocity distribution, the breakage probability was given as (Luo and Svendsen, 1996):

$$P_b\left(\xi, f_v', \lambda\right) = 1 - \int_0^{\chi_c} \exp\left(-\chi\right) \mathrm{d}\chi = \exp\left(-\chi_c\right) \tag{2.167}$$

The critical dimensionless energy for breakup was taken from Han et al. (2011), using both the surface energy increase and surface energy density increase in the breakage criterion[12]:

$$\chi_c = \frac{E_{\text{crit}}\left(\lambda\right)}{\overline{E}\left(\lambda\right)} = \frac{\max\left(c_f, c_d\right) \pi \xi^2 \sigma}{\frac{1}{2} \rho_c \bar{v}_\lambda^2 \lambda^3} \times \begin{cases} 1 & \text{if } \lambda \leq \xi \\ \frac{1}{4\left(\frac{\lambda}{\xi}\right)^2 \sin^4\left(\frac{\pi}{4} \frac{\xi}{\lambda}\right)} & \text{if } \lambda > \xi \end{cases} \tag{2.168}$$

An expression for the collision frequency for eddies smaller or equal to the bubble or droplet size was taken from Luo and Svendsen (1996). This expression is only valid in the inertial subrange of turbulence, and was given as:

$$\omega_{\text{col}}\left(\xi, \zeta\right) = 0.923 \left(1 - \alpha_d\right) n \left(\varepsilon \xi\right)^{1/3} \frac{\left(1 + \zeta\right)^2}{\zeta^{11/3} \xi^2} \tag{2.169}$$

Where the dimensionless variable $\zeta = \lambda / \xi$. To arrive at this expression, the inertial subrange structure function was used. This can be written as $\overline{v}_\lambda^2 = 2\left(\varepsilon\xi\right)^{2/3}$. For eddies larger than the fluid particle, the collision frequency is replaced by an interaction frequency. Following Han et al. (2011), this was given as[13]:

$$\omega_{\text{inter}}\left(\xi, \zeta\right) = \frac{0.43 \left(1 - \alpha_d\right) n \varepsilon^{1/3}}{\zeta^{14/3} \xi^{5/3} \min\left[1, \frac{1}{2\sqrt{2}\zeta \sin^2\left(\pi/\left(4\zeta\right)\right)}\right]} \tag{2.170}$$

In the second step of the model development, Xing et al. (2015) developed a physical model for the flow through the neck of the fluid particle. The pressure inside spherical part i of the deformed bubble or droplet was given by the Young-Laplace equation:

$$p_i = p_0 + \frac{2\sigma}{R_i} \qquad i = 1, 2 \tag{2.171}$$

[12]Compared to Han et al. (2015), the expression presented in Xing et al. (2015) lacks a $\pi/6$ term in the expression for the mean eddy kinetic energy.

[13]The expression for ω_{inter} in the article of Xing et al. (2015) used max instead of min in the denominator. This mistake has been corrected in the model used in this work.

Here, p_0 is the pressure outside the fluid particle, i.e. the pressure in the continuous medium. The pressure difference between the two parts is:

$$p_1 - p_2 = 2\sigma \left(\frac{1}{R_1} - \frac{1}{R_2} \right) \tag{2.172}$$

The two radii of curvature are calculated from the volume fraction f_v':

$$R_1 = \frac{\xi}{2} \left(f_v' \right)^{1/3} \tag{2.173}$$

$$R_2 = \frac{\xi}{2} \left(1 - f_v' \right)^{1/3} \tag{2.174}$$

The internal flow through the neck was estimated using the Bernoulli equation with expansion and contraction loss. From sphere 1 to the neck, the Bernoulli equation gives:

$$p_1 = p_{\text{neck}} + \rho_d \frac{v_{\text{neck}}^2}{2} \left[1 + K_c \right] \tag{2.175}$$

Where K_c is a contraction loss coefficient. Similarly, the transport from the neck to sphere 2 gives:

$$p_{\text{neck}} + \rho_d \frac{v_{\text{neck}}^2}{2} = p_2 + K_e \rho_d \frac{v_{\text{neck}}^2}{2} \tag{2.176}$$

Here, K_e is an expansion loss coefficient. Combining equation (2.175) and (2.176) and solving for the neck velocity gives:

$$v_{\text{neck}} = \sqrt{\frac{2 \left(p_1 - p_2 \right)}{\rho_d \left(K_c + K_e \right)}} \tag{2.177}$$

Inserting for the pressure difference from equation (2.172) gives:

$$v_{\text{neck}} = \sqrt{\frac{4\sigma}{\rho_d \left(K_c + K_e \right)} \left(\frac{1}{R_1} - \frac{1}{R_2} \right)} \tag{2.178}$$

The value of K_c and K_e was set to 0.2 and 0.3, respectively. The time for the smaller sphere to completely flow into the larger sphere is estimated by applying dimensional analysis:

$$t_1 = \frac{4V_1}{v_{\text{neck}} \pi \xi_{\text{neck}}^2} \tag{2.179}$$

According to Wilkinson et al. (1993), the pressure in the neck will decrease due to the internal gas flow. This acts as a suction force, causing the bubble or droplet neck to contract faster. The pressure difference between the neck and the continuous fluid can be calculated by inserting the expression from equation (2.178) into equation (2.175):

$$p_0 - p_{\text{neck}} = \frac{2\sigma}{K_c + K_e} \left(\frac{1 - K_e}{R_1} - \frac{1 + K_c}{R_2} \right) \tag{2.180}$$

The difference $p_0 - p_{\text{neck}}$ can be both positive and negative, thus either enhancing or preventing the contraction of the fluid particle neck. This net dynamic pressure exerts an additional shrinking velocity on the surface of the neck, given by:

$$v_{\text{plus}} = \begin{cases} \sqrt{\frac{2(p_0 - p_{\text{neck}})}{\rho_d}} & p_0 - p_{\text{neck}} > 0 \\ -\sqrt{\frac{-2(p_0 - p_{\text{neck}})}{\rho_c}} & p_0 - p_{\text{neck}} \leq 0 \end{cases} \tag{2.181}$$

The shrinking velocity of the bubble or droplet is the sum of the continuous phase velocity and the additional velocity. Again, dimensional analysis can be applied to calculate the shrinking time of the neck:

$$t_2 = \begin{cases} \frac{\xi_{\text{neck}}}{v_{\text{plus}} + U_\lambda} & v_{\text{plus}} + U_\lambda > 0 \\ +\infty & v_{\text{plus}} + U_\lambda \leq 0 \end{cases} \tag{2.182}$$

The continuous phase velocity can be interpreted as the velocity fluctuations over the fluid particle neck, and is not the same as the structure function. Xing et al. (2015) assumed spherical particles and that all the energy in the energy spectrum is available in one particle. It was given as:

$$U_\lambda = \sqrt{\frac{12E\left(\xi_{\text{neck}}\right)}{\pi \rho_c \xi_{\text{neck}}^3}} \tag{2.183}$$

The third step of the model development consisted of introducing the effect of internal flow on the breakup frequency and daughter size distribution of Luo and Svendsen (1996). Xing et al. (2015) assumed that a bubble or droplet will break *if the shrinking time is short compared to the internal flow time*. Following the probability function for bubble coalescence from Coulaloglou and Tavlarides (1977) and Prince and Blanch (1990), the following breakup probability function was proposed:

$$\gamma = \exp\left(-\frac{t_2}{t_1}\right) \tag{2.184}$$

The minimum and maximum breakup fraction was set to $f'_{v,\text{min}} = 0$ and $f'_{v,\text{max}} = 0.5$, respectively. The effect of the internal flow on the breakage density was taken into account by multiplying with the breakage probability γ. An additional factor was introduced to ensure that the probability of forming small daughters was large. An exponential decay function was used to describe this trend. Introducing these two modifications, the partial breakage density was given as:

$$\Omega\left(\xi, f_v\right) = \int_{f'_{v,\text{min}}}^{f'_{v,\text{max}}} \Omega\left(\xi, f'_v\right) \frac{5\gamma \exp\left(-5 f_v\right)}{\exp\left(-5 f_{v,\text{min}}\right) - \exp\left(-5 f_{v,\text{max}}\right)} \mathrm{d}f'_v \tag{2.185}$$

The total breakage density can be calculated directly from the partial breakage density:

$$\Omega\left(\xi\right) = \int_0^{0.5} \Omega\left(\xi, f_v\right) \mathrm{d}f_v \tag{2.186}$$

The breakage frequency is given as [14]:

$$b\left(\xi\right) = \frac{\Omega\left(\xi\right)}{n} \tag{2.187}$$

The probability density function given per unit of the mother particle size is calculated directly as the ratio between the partial and total breakage density:

$$P_{\text{DSD}}\left(\xi, f_v\right) = \frac{\Omega\left(\xi, f_v\right)}{\Omega\left(\xi\right)} \tag{2.188}$$

The diameter based probability density function is obtained by applying the following relation:

$$P_{\text{DSD}}\left(\xi, \omega\right) = P_{\text{DSD}}\left(\xi, f_v\right) \times \frac{\mathrm{d}f_v}{\mathrm{d}\omega} = P_{\text{DSD}}\left(\xi, f_v\right) \times 3\frac{\omega^2}{\xi^3} \tag{2.189}$$

This can easily be converted to a redistribution density function by multiplying with the number of daughters:

$$h_{\text{DSD}}\left(\xi, \omega\right) = 2 \times P_{\text{DSD}}\left(\xi, \omega\right) \tag{2.190}$$

[14] Note that the breakage frequency is defined differently than in Solsvik et al. (2013). It lacks the number of daughters, ν, because Xing et al. (2015) uses the number of mother particles that break rather than the number of daughters that are formed in the definition of the breakage density.

Chapter 3

Extensions and Modifications of Studied Closures

In order to improve the numerical properties of the breakage closures or make the models applicable to a wider range of systems and conditions, most of the breakage closures presented in chapter 2 were modified before they were evaluated. In this chapter, a description of how the models were modified will be given. Additionally, the expressions for the breakage frequencies and redistribution functions from the extended models are presented.

3.1 Structure Function and Number Density of Eddies in Entire Energy Spectrum

With the exception of Han et al. (2015), all of the breakage closures studied in this work apply the Kolmogorov turbulence energy spectrum and the Kolmogorov second order longitudinal structure function, which are exclusively valid in the inertial subrange of turbulence. As pointed out by Solsvik and Jakobsen (2016b), these models are limited to fully developed turbulent flows in the limit of infinite integral scale Reynolds numbers. However, in chemical reactors, separators and other types of equipment, the Reynolds numbers are generally finite. For finite Reynolds numbers, the inertial subrange of turbulence narrows, and in some cases it might even disappear. To give more accurate descriptions of chemical engineering equipment, the breakage closures should therefore be extended to the wide energy spectrum. This ensures that the models are always valid for the systems they are applied to.

In order to extend the closures to the entire energy spectrum, the inertial range structure function and number density of eddies must be replaced by their equivalents from the entire

energy spectrum. There are several different wide energy spectrum models available in the literature. A detailed review of the different models is given in Solsvik and Jakobsen (2016a). In this work, the semi-empirical structure function for the entire spectrum of turbulence of Sawford and Hunt (1986) is applied. This structure function was chosen due to its computational efficiency and reasonable accuracy for all Reynolds numbers studied in Solsvik and Jakobsen (2016a). It is given by (Solsvik and Jakobsen, 2016a):

$$\overline{\delta v^2(\lambda)} = \frac{4}{3}k\left(\frac{\lambda^2}{r_d^2+\lambda^2}\right)^{2/3}\left(\frac{\lambda^2}{\lambda^2+r_L^2}\right)^{1/3} \tag{3.1}$$

Where k is the turbulent kinetic energy of eddies. The length scale $r_d = (15C_1)^{3/4}\eta_e$ determines the crossover from the viscous to the inertial subrange. The Kolmogorov structure function parameter C_1 is fixed a value of 2.0. The crossover scale r_L is given as $(2/3)^{3/2}L$, where L is the integral length scale.

An expression for the number density of turbulent eddies can be obtained from an energy balance, as described in Solsvik and Jakobsen (2016a) and Luo and Svendsen (1996). It is assumed that the energy spectrum, $E(\kappa)$, represents the turbulent kinetic energy per unit mass contained in vortices with wave numbers between κ and $\kappa + \mathrm{d}\kappa$. This kinetic energy is balanced by the translational kinetic energy for a collection of spherical vortices in the Lagrangian framework, giving:

$$n_\lambda \rho_c \frac{\pi}{6}\lambda^3 \frac{\overline{v}_\lambda(\lambda)^2}{2}\mathrm{d}\lambda = E(\kappa)\,\rho_c\,(1-\alpha_d)\,(-\mathrm{d}\kappa) \tag{3.2}$$

The wave number κ and eddy size λ are related by $\kappa = 2\pi/\lambda$. If the mean translational velocity $\overline{v}_\lambda$ is approximated by the structure function $\overline{\delta v^2(\lambda)}$, the number density of eddies is given by:

$$n_\lambda = \frac{24E\left(\frac{2\pi}{\lambda}\right)}{\lambda^5\overline{\delta v^2(\lambda)}}(1-\alpha_d) \tag{3.3}$$

In this work, the energy spectrum of Pope (2000) for the entire range of isotropic turbulence was applied. This is given as (Solsvik and Jakobsen, 2016a):

$$E(\kappa) = C\varepsilon^{2/3}\kappa^{-5/3} f_L(\kappa L)\, f_\eta(\eta\kappa) \tag{3.4}$$

Where the dimensionless functions $f_L(\kappa L)$ and $f_\eta(\eta\kappa)$ determine the shape of the energy containing and dissipation subrange, respectively. They both tend to unity in the inertial subrange, thus essentially recovering the Kolmogorov inertial range energy spectrum. The dimensionless functions are given as:

$$f_L(\kappa L) = \left\{\frac{\kappa L}{\left[(\kappa L)^2 + c_L\right]^{1/2}}\right\}^{5/3+p_0} \tag{3.5}$$

$$f_\eta(\eta\kappa) = \exp\left\{-\beta_2\left(\left[(\kappa\eta)^4 + c_\eta^4\right]^{1/4} - c_\eta\right)\right\} \tag{3.6}$$

Where $p_0 = 2$ and $\beta_2 = 5.2$. The parameters c_L and c_η are determined in order to fulfill two integral constraints, given in Solsvik and Jakobsen (2016a) as:

$$\kappa = \int_0^\infty E(\kappa)\,\mathrm{d}\kappa \tag{3.7}$$

$$\varepsilon = \int_0^\infty 2v\kappa^2 E(\kappa)\,\mathrm{d}\kappa \tag{3.8}$$

Where v is the root mean square fluctuating velocity. In Solsvik (2016), approximate explicit relations for computing C_L and C_η were derived. These relations were applied in this work, to avoid cumbersome optimization routines. The relations were given as:

$$C_L(\mathrm{Re}_L, C) = \exp\left[-\frac{4.478 + 18.362C}{\mathrm{Re}_L^{1.075-0.070C}} - 1.342 + 2.024C\right] - 1.913 + 2.169C \tag{3.9}$$

$$C_\eta(\mathrm{Re}_L, C) = \exp\left[\frac{14.043 - 4.222C}{\mathrm{Re}_L^{1.986-0.363C}}\right] - [0.089 + 0.339C] \tag{3.10}$$

The integral scale L, turbulent kinetic energy per unit mass, k, and integral scale Reynolds number Re_L must be known in order to evaluate the structure function and number density of eddies in the wide energy spectrum. Following Solsvik et al. (2016b), the integral scale L has been specified in this work. The two other quantities can be calculated from:

$$k = (L\varepsilon)^{2/3} \tag{3.11}$$

$$\mathrm{Re}_L = \frac{k^2}{\varepsilon\nu_c} \tag{3.12}$$

3.2 Martínez-Bazán et al. Models: Including Breakage Probability

In the closures of Martínez-Bazán et al., the breakage frequency is given as the inverse breakage time:

$$b(\xi) = \frac{1}{t_b} \tag{3.13}$$

In this definition of the breakage frequency, it is implicitly assumed that the breakage probability of fluid particles is equal to unity, i.e. all fluid particles will break. This assumption is reasonable in the highly turbulent water jet system studied by Martínez-Bazán et al. (1999a), but might not be correct in other, less turbulent systems. In the model of Coulaloglou and Tavlarides (1977), the breakage probability was included in the definition of the breakage frequency:

$$b(\xi) = \frac{1}{t_b} \times P_{\text{breakage}} \tag{3.14}$$

Thus, applying the framework of Coulaloglou and Tavlarides (1977) on the closures based on Martínez-Bazán et al. (1999a) might give more physically realistic predictions of less turbulent systems. As explained in section 2.1, the breakage probability was defined by Coulaloglou and Tavlarides as the fraction of drops breaking, given as:

$$P_{\text{breakage}}(\xi) = \frac{\Delta N(\xi)}{N(\xi)} = \int_{E_{\text{crit}}(\xi)}^{\infty} P_{E,2\text{D}}(E)\,\mathrm{d}E = \exp\left(-\frac{E_{\text{crit}}(\xi)}{\bar{E}(\xi)}\right) \tag{3.15}$$

Where $E_{\text{crit}}(\xi)$ is the total restoring energy that must be exceeded by the total deforming energy $\overline{E}(\xi)$ in order to cause breakage.

As described in section 2.8, the breakage frequency of the Martínez-Bazán et al. models is set to zero when the fluid particle size ξ is smaller than the critical size ξ_{crit}. This results in a steep breakage frequency profile that might cause numerical difficulties. The introduction of a breakage probability therefore has a secondary advantage. It spreads the peak of the breakage frequency profile over several particle sizes, which might improve the numerical properties of the models. This effect is illustrated in Figure 3.1.

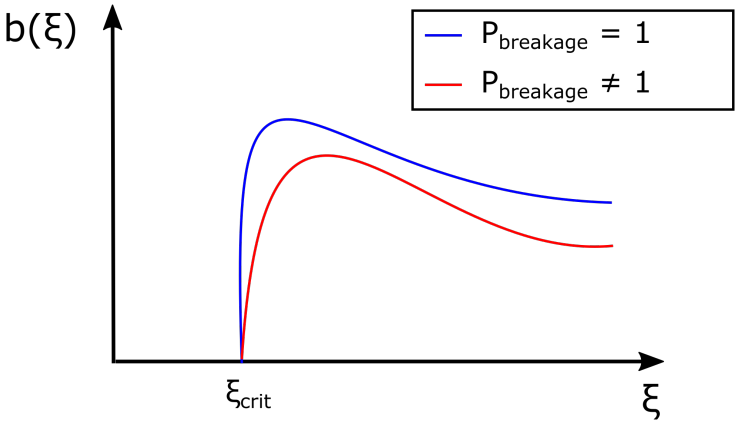

Figure 3.1: The effect of breakage probability on the breakage frequency of models based on Martínez-Bazán et al. When including the breakage probability, the breakage frequency profile becomes less steep.

For fluid particles smaller than or equal to ξ_{crit}, no breakage will occur, and the breakage probability is set to zero. For fluid particles larger than the critical size, the breakage probability is shifted ξ_{crit} along the positive ξ-axis. This means that the breakage probability starts increasing at ξ_{crit}. The general expression for the breakage probability is:

$$P_{\text{breakage}} = \begin{cases} 0 & \text{if } \xi \leq \xi_{\text{crit}} \\ \exp\left(-\frac{E_{\text{crit}}(\xi-\xi_{\text{crit}})}{\bar{E}(\xi-\xi_{\text{crit}})}\right) & \text{if } \xi > \xi_{\text{crit}} \end{cases} \tag{3.16}$$

If the critical diameter is smaller than the minimum fluid particle size, all particles will

break. In this case, the breakage probability is not shifted, and therefore calculated from equation (3.15).

3.2.1 Martínez-Bazán et al. (1999a)

The original model of Martínez-Bazán et al. (1999a) is only valid in the inertial subrange of turbulence. The critical energy required for breakage is given by the deformation energy:

$$E_{\text{crit}}(\xi) = \pi\sigma\xi^2 \tag{3.17}$$

The deformation energy resulting from turbulent velocity fluctuations in the continuous phase, can in the inertial subrange be estimated as:

$$\overline{E}(\xi) = \frac{1}{2}\rho_c\frac{\pi}{6}\xi^3\overline{\delta v^2(\xi)} = \frac{\pi}{12}\rho_c\beta\xi^3(\varepsilon\xi)^{2/3} \tag{3.18}$$

Inserting these expressions into equation (3.16) gives:

$$P_{\text{breakage}} = \begin{cases} 0 & \text{if } \xi \leq \xi_{\text{crit}} \\ \exp\left(-\frac{12\sigma}{\rho_c\beta\varepsilon^{2/3}(\xi-\xi_{\text{crit}})^{5/3}}\right) & \text{if } \xi > \xi_{\text{crit}} \end{cases} \tag{3.19}$$

3.2.2 Martínez-Bazán et al. (1999a) Entire Energy Spectrum

By replacing the inertial range structure function in equation (3.18) with the structure function of Sawford and Hunt (1986), valid in the entire spectrum of turbulence, the following expression for the breakage frequency is obtained:

$$P_{\text{breakage}} = \begin{cases} 0 & \text{if } \xi \leq \xi_{\text{crit}} \\ \exp\left(-\frac{12\sigma}{\rho_c(\xi-\xi_{\text{crit}})\overline{\delta v^2(\xi-\xi_{\text{crit}})}}\right) & \text{if } \xi > \xi_{\text{crit}} \end{cases} \tag{3.20}$$

3.2.3 Solsvik et al. (2013)

In the model of Solsvik et al. (2013), the effect of viscous forces on the breakage frequency are included. The critical energy required for breakage is calculated from the sum of the restoring stresses:

$$E_{\text{crit}}(\xi) = \left[\overline{\sigma}_s(\xi) + c_3\overline{\sigma}_{\mu,d}(\xi)\right]V_\xi = \left[\frac{6\sigma}{\xi} + c_3\mu_d\sqrt{\frac{\varepsilon}{\nu_c}}\right]\frac{\pi}{6}\xi^3 \tag{3.21}$$

Similarly, the deformation energy is calculated from the sum of deforming stresses:

$$\overline{E}(\xi) = \left[\overline{\sigma}_t(\xi) + c_3\overline{\sigma}_{\mu,c}(\xi)\right]V_\xi = \left[\frac{1}{2}\rho_c\overline{\delta v^2(\xi)} + c_3\mu_c\sqrt{\frac{\varepsilon}{\nu_c}}\right]\frac{\pi}{6}\xi^3 \tag{3.22}$$

In the inertial range, the expression for the deformation energy becomes:

$$\overline{E}(\xi) = \left[\frac{1}{2}\rho_c\beta\left(\varepsilon\xi\right)^{2/3} + c_3\mu_c\sqrt{\frac{\varepsilon}{\nu_c}}\right]\frac{\pi}{6}\xi^3 \tag{3.23}$$

Inserting the expressions into equation (3.16) gives:

$$P_{\text{breakage}} = \begin{cases} 0 & \text{if } \xi \leq \xi_{\text{crit}} \\ \exp\left(-\frac{\frac{6\sigma}{\xi-\xi_{\text{crit}}}+c_3\mu_d\sqrt{\frac{\varepsilon}{\nu_c}}}{\frac{1}{2}\rho_c\beta\varepsilon^{2/3}(\xi-\xi_{\text{crit}})^{2/3}+c_3\mu_c\sqrt{\frac{\varepsilon}{\nu_c}}}\right) & \text{if } \xi > \xi_{\text{crit}} \end{cases} \tag{3.24}$$

3.2.4 Solsvik et al. (2013) Entire Energy Spectrum

The expression for the breakage probability of Solsvik et al. (2013) in the entire energy spectrum is easily obtained by replacing the structure function for the inertial subrange with the entire energy spectrum structure function of Sawford and Hunt (1986):

$$P_{\text{breakage}} = \begin{cases} 0 & \text{if } \xi \leq \xi_{\text{crit}} \\ \exp\left(-\frac{\frac{6\sigma}{\xi-\xi_{\text{crit}}}+c_3\mu_d\sqrt{\frac{\varepsilon}{\nu_c}}}{\frac{1}{2}\rho_c\overline{\delta v^2}(\xi-\xi_{\text{crit}})+c_3\mu_c\sqrt{\frac{\varepsilon}{\nu_c}}}\right) & \text{if } \xi > \xi_{\text{crit}} \end{cases} \tag{3.25}$$

3.3 Breakage Frequencies and Redistribution Functions in the Wide Energy Spectrum

In this section, the expressions for the breakage frequencies and redistribution functions for all closures in the wide energy spectrum will be given. The models of Narsimhan et al. (1979) and Lehr et al. (2002) were left out of the evaluation, and therefore not extended to the wide spectrum. The closure of Han et al. (2011) and Liao et al. were previously given explicitly as a function of the turbulent quantities, and are therefore not repeated in this section.

3.3.1 Coulaloglou and Tavlarides (1977)

As explained in section 2.1, the daughter size distribution function used in the semi-empirical model of Coulaloglou and Tavlarides (1977) is independent of the energy spectrum. Only the breakage frequency is affected when the model is extended to the wide energy spectrum. This was given as the product of the inverse breakage time and the fraction of drops breaking:

$$b(\xi) = \left(\frac{1}{\text{breakage time}}\right) \times \left(\frac{\text{fraction of}}{\text{drops breaking}}\right) = \frac{1}{t_b}\frac{\Delta N(\xi)}{N(\xi)} \tag{3.26}$$

The fraction of drops breaking was defined in terms of a critical and mean turbulent kinetic energy. The critical energy in the entire energy spectrum is identical to the original model, and the mean turbulent kinetic energy is calculated from the structure function:

$$\frac{\Delta N\left(\xi\right)}{N\left(\xi\right)} = \exp\left(-\frac{E_{\text{crit}}}{\overline{E}}\right) = \exp\left(-\frac{c_1\sigma\xi^2}{c_2\rho_d\xi^3\overline{\delta v^2\left(\xi\right)}}\right) \tag{3.27}$$

The breakage time is calculated using dimensional analysis as the ratio between a length and velocity scale. The length scale is the particle size ξ and the structure function is used to calculate the velocity scale:

$$t_b \propto \frac{\text{length scale}}{\text{velocity scale}} = \frac{\xi}{\sqrt{\overline{\delta v^2\left(\xi\right)}}} \tag{3.28}$$

The wide energy spectrum breakage frequency of Coulaloglou and Tavlarides (1977) can therefore be written as:

$$b\left(\xi\right) = c_6\frac{\sqrt{\overline{\delta v^2\left(\xi\right)}}}{\xi}\exp\left(-\frac{c_4\sigma}{\rho_d\xi\overline{\delta v^2\left(\xi\right)}}\right) \tag{3.29}$$

3.3.2 Luo and Svendsen (1996)

As previously described in section 2.3, the breakage density of a fluid particle of size ξ into a daughter of size ω is calculated from the product of a breakage probability and collision frequency:

$$\Omega\left(\xi,\omega\right) = \int_{\lambda_{\min}}^{\xi} P_b\left(\xi,\omega,\lambda\right)\omega_{\text{col}}\left(\xi,\lambda\right)\mathrm{d}\lambda \tag{3.30}$$

Both the breakage probability and the collision frequency is affected by the extension to the wide energy spectrum. The collision frequency is explicitly written as a function of the number density of eddies and structure function:

$$\frac{\omega_{\text{col}}}{n} = \frac{\pi}{4}\left(\xi+\lambda\right)^2 n_\lambda\sqrt{\overline{\delta v^2\left(\lambda\right)}} \tag{3.31}$$

The breakage probability is given as:

$$P_b\left(\xi,\omega,\lambda\right) = 1 - \int_0^{\chi_c}\exp\left(-\chi\right)\mathrm{d}\chi = \exp\left(-\chi_c\right) \tag{3.32}$$

Where the critical dimensionless energy is calculated from a critical energy and mean kinetic energy:

$$\chi_c = \frac{E_{\text{crit}}}{\overline{E}\left(\lambda\right)} = \frac{c_f\pi\sigma\xi^2}{\overline{E}\left(\lambda\right)} \tag{3.33}$$

The critical energy is independent of the energy spectrum, but the mean kinetic energy depends on the structure function:

$$\overline{E}(\lambda) = \rho_c \frac{\pi}{6} \lambda^3 \frac{\overline{\delta v^2(\lambda)}}{2} \tag{3.34}$$

This gives the following expression for the critical dimensionless energy:

$$\chi_c = \frac{12 c_f \sigma \xi^2}{\rho_c \lambda^3 \overline{\delta v^2(\lambda)}} \tag{3.35}$$

The total breakage density is found by integrating the partial breakage density over the daughter size. If the daughter diameter is used, the equation becomes (Solsvik et al., 2013):

$$\Omega(\xi) = \int_0^{\xi} \Omega(\xi, \omega) \frac{3\omega^2}{\xi^3} \mathrm{d}\omega \tag{3.36}$$

The breakage frequency and daughter size redistribution function is calculated as in the original model:

$$b(\xi) = \frac{1}{\nu(\xi)} \frac{\Omega(\xi)}{n} \tag{3.37}$$

$$h_{\mathrm{DSD}}(\xi, \omega) = \frac{\Omega(\xi, \omega)}{\Omega(\xi)} \tag{3.38}$$

3.3.3 Becker et al. (2014)

The model of Becker et al. (2014) strongly resembles the model of Luo and Svendsen (1996), and is therefore affected similarly by the extension to the wide energy spectrum. The breakage density of a bubble or droplet of size ξ into a daughter of size ω was given by:

$$\Omega(\xi, \omega) = \int_{\lambda_{\min}}^{\xi} P_b(\xi, \omega, \lambda) \omega_{\mathrm{col}}(\xi, \lambda) \mathrm{d}\lambda \tag{3.39}$$

The collision frequency used in Becker et al. is taken directly from Luo and Svendsen (1996). In the wide energy spectrum, this was previously defined in equation (3.31) as:

$$\frac{\omega_{\mathrm{col}}}{n} = \frac{\pi}{4} (\xi + \lambda)^2 n_\lambda \sqrt{\overline{\delta v^2(\lambda)}} \tag{3.40}$$

Compared to Luo and Svendsen (1996), the breakage probability of Becker et al. (2014) contains an extra term in the denominator, due to the introduction of viscous effects:

$$P_b(\xi, \omega, \lambda) = \exp(-\chi_c) = \exp\left(-\frac{E_s + E_\mu}{E_\lambda}\right) \tag{3.41}$$

The surface energy is not affected by the energy spectrum, and is therefore the same as in the original model:

$$E_s = \max(c_f, c_d) \pi \sigma \xi^2 \tag{3.42}$$

Where the surface energy increase coefficient $c_f = \left(\omega^3/\xi^3\right)^{2/3} + \left(1 - \left(\omega^3/\xi^3\right)\right)^{2/3} - 1$ and the surface energy density increase coefficient $c_d = \left[\min\left(\omega^3/\xi^3, 1 - \omega^3/\xi^3\right)\right]^{-1/3} - 1$.

The viscous energy depends on the structure function, and can be written as:

$$E_\mu = \pi\xi^2\mu_d\sqrt{\overline{\delta v^2\left(\lambda\right)}} \tag{3.43}$$

Naturally, the mean kinetic energy of an arriving eddy is affected by the change of structure function. It can be expressed as:

$$E_\lambda = \frac{\pi}{12}\rho_c\lambda^3\overline{\delta v^2\left(\lambda\right)} \tag{3.44}$$

As in the original model, the total breakage density is found by integrating the partial breakage density over the daughter size.

$$\Omega\left(\xi\right) = \int_0^\xi \Omega\left(\xi,\omega\right)\frac{3\omega^2}{\xi^3}\mathrm{d}\omega \tag{3.45}$$

The breakage frequency and redistribution function is found by following the framework of Luo and Svendsen:

$$b\left(\xi\right) = \frac{1}{\nu\left(\xi\right)}\frac{\Omega(\xi)}{n} \tag{3.46}$$

$$h_{\mathrm{DSD}}\left(\xi,\omega\right) = \frac{\Omega\left(\xi,\omega\right)}{\Omega\left(\xi\right)} \tag{3.47}$$

3.3.4 Han et al. (2015)

The model of Han et al. (2015) applied the energy spectrum of Pope (2000) without taking into account that the parameters C_L and C_η vary with the integral scale Reynolds number. In the extended model of Han et al. (2015), equations (3.9) and (3.10) have been used for C_L and C_η to account for the Reynolds number dependency.

As previously described in section (2.6), a structure function depending on the energy spectrum was employed in the model of Han et al. (2015). In the extended model derived in this work, the structure function of Sawford and Hunt (1986), given in equation (3.1) is used. The number density of eddies depends on the structure function, and therefore the expression for the number density of eddies in the extended model also differs from the original model. The number density of eddies from equation (3.2) is used in the extended model.

Similarly to the model of Luo and Svendsen (1996), the breakage probabilities in Han et al. (2015) are affected by the change of structure function. The breakage probability of a process forming m daughters was given previously as:

$$P_{b,m}\left(\xi, f_{v,1}, ..., f_{v,m}, \kappa\right) = 1 - \int_0^{\chi_{c,m}} \exp\left(-\chi\right)\mathrm{d}\chi = \exp\left(\chi_{c,m}\right) \tag{3.48}$$

The critical dimensionless energy depends on the structure function, and can be written as:

$$\chi_{c,m} = \frac{E_{\text{crit}}}{\overline{E}\left(\kappa\right)} = \frac{\max\left(c_{f,m}, c_{d,m}\right)\pi\xi^2\sigma}{\frac{1}{2}\rho_c\overline{\delta v^2\left(\frac{2\pi}{\kappa}\right)}\frac{1}{6}\pi\left(\frac{2\pi}{\kappa}\right)^3} \times \begin{cases} 1 & \text{if } \frac{2\pi}{\kappa} \leq \xi \\ \frac{1}{4\left(\frac{2\pi}{\kappa\xi}\right)^2\sin^4\left(\frac{\kappa\xi}{8}\right)} & \text{if } \frac{2\pi}{\kappa} > \xi \end{cases} \tag{3.49}$$

The collision frequency from Han et al. (2015) can be written explicitly as a function of the structure function and number density of eddies:

$$\omega_{\text{col}}\left(\xi,\kappa\right) = \pi\left(a+\frac{\pi}{\kappa}\right)\left(b+\frac{\pi}{\kappa}\right)\sqrt{\overline{\delta v^2\left(\frac{2\pi}{\kappa}\right)}}n_\kappa n \tag{3.50}$$

Han et al. (2015) employed an expression from Han et al. (2011) for the interaction frequency. This was previously defined in section 2.5. In terms of the wave number, the interaction frequency can be written as:

$$\omega_{\text{inter}}\left(\xi,\kappa\right) = \frac{\pi\xi^3 n_\kappa n}{6 \times \min\left[\frac{\left(2\pi/\kappa\right)}{\sqrt{\overline{\delta v^2\left(\frac{2\pi}{\kappa}\right)}}}, \frac{\left(2\pi/\kappa\right)}{\left(\frac{4\pi}{\kappa\xi}\right)\sin^2\left(\frac{\kappa\xi}{8}\right)\sqrt{\overline{\delta v^2\left(\frac{2\pi}{\kappa}\right)}}}\right]} \tag{3.51}$$

As in the original model, the partial breakage density is calculated from the product of a breakage probability and a collision or interaction frequency:

$$\frac{\Omega_m\left(\xi, f_{v,1}, ..., f_{v,m}\right)}{n} = \begin{cases} \int_{2\pi/\xi}^{\kappa_{\max}} P_{b,m}\left(\xi, f_{v,1}, ..., f_{v,m}, \kappa\right)\frac{\omega_{\text{col}}(\xi,\kappa)}{n}\mathrm{d}\kappa & , \quad \frac{2\pi}{\kappa} \leq \xi \\ \int_{\kappa_{\min}}^{2\pi/\xi} P_{b,m}\left(\xi, f_{v,1}, ..., f_{v,m}, \kappa\right)\frac{\omega_{\text{inter}}(\xi,\kappa)}{n}\mathrm{d}\kappa & , \quad \frac{2\pi}{\kappa} > \xi \end{cases} \tag{3.52}$$

The breakage frequencies and redistribution functions are calculated as in the original model. The binary breakage density is given as:

$$\frac{\Omega_2\left(\xi, f_{v,1}, ..., f_{v,m}\right)}{n} = \frac{\Omega_2\left(\xi, f_v\right)}{n} \tag{3.53}$$

The ternary and quaternary breakage densities are found by integrating over all statistically independent volume fractions:

$$\frac{\Omega_3\left(\xi, f_v\right)}{n} = \frac{1}{2}\int_0^{1-f_v}\frac{\Omega_3\left(\xi, f_v, f_{v,1}, f_{v,2}\right)}{n}\mathrm{d}f_{v,2} + \int_0^{1-f_v}\frac{\Omega_3\left(\xi, f_v, f_{v,1}, f_{v,2}\right)}{n}\,\mathrm{d}f_{v,1} \tag{3.54}$$

$$\begin{aligned}\frac{\Omega_4\left(\xi, f_v\right)}{n} = {} & \frac{1}{2}\int_0^{1-f_v}\int_0^{1-f_v-f_{v,2}}\frac{\Omega_4\left(\xi, f_v, f_{v,1}, f_{v,2}, f_{v,3}\right)}{n}\,\mathrm{d}f_{v,3}\,\mathrm{d}f_{v,2} \\ & + \frac{1}{2}\int_0^{1-f_v}\int_0^{1-f_v-f_{v,1}}\frac{\Omega_4\left(\xi, f_v, f_{v,1}, f_{v,2}, f_{v,3}\right)}{n}\,\mathrm{d}f_{v,3}\,\mathrm{d}f_{v,1} \\ & + \int_0^{1-f_v}\int_0^{1-f_v-f_{v,1}}\frac{\Omega_4\left(\xi, f_v, f_{v,1}, f_{v,2}, f_{v,3}\right)}{n}\,\mathrm{d}f_{v,2}\,\mathrm{d}f_{v,1}\end{aligned} \tag{3.55}$$

The total breakage density is found by integrating over the generic volume fraction f_v:

$$\frac{\Omega_m(\xi)}{n} = \int_0^1 \frac{\Omega_m(\xi, f_v)}{n} \mathrm{d}f_v \tag{3.56}$$

The breakage frequency is found by dividing by the number of daughters formed in the breakage process:

$$b_m(\xi) = \frac{1}{m} \frac{\Omega_m(\xi)}{n} \tag{3.57}$$

The redistribution density functions are given as the ratio between the partial and total breakage densities:

$$h_{m,\mathrm{DSD}}(\xi, f_v) = \frac{\Omega_m(\xi, f_v)}{\Omega_m(\xi)} \tag{3.58}$$

3.3.5 Martínez-Bazán et al. (1999a,b, 2010)

The breakage frequency from the original model was extended by introducing a probability of breakage, as explained in section 3.2. The following expression for the breakage frequency was applied:

$$b(\xi) = \frac{1}{t_b} \times P_{\text{breakage}} \tag{3.59}$$

Following the original model, the breakage time is calculated from dimensional analysis:

$$t_b \propto \frac{\xi}{\Delta v_b} \tag{3.60}$$

Where the characteristic velocity is found from the difference between the surface deforming and restoring stresses. In the wide energy spectrum, this becomes:

$$\frac{1}{2}\rho_c (\Delta v_b)^2 \approx \overline{\sigma}_t(\xi) - \overline{\sigma}_s(\xi) = \frac{1}{2}\rho_c \overline{\delta v^2(\xi)} - \frac{6\sigma}{\xi} \tag{3.61}$$

Solving for the characteristic velocity and inserting the expression into the definition of the breakage time gives:

$$t_b \propto \frac{\xi}{\sqrt{\overline{\delta v^2(\xi)} - \frac{12\sigma}{\rho_c \xi}}} \tag{3.62}$$

Inserting the expression for the breakage time and the breakage probability from section 3.2.2 gives the breakage frequency in the wide energy spectrum:

$$b(\xi) = K_g \frac{\sqrt{\overline{\delta v^2(\xi)} - \frac{12\sigma}{\rho_c \xi}}}{\xi} \times \begin{cases} 0 & \text{if } \xi \leq \xi_{\text{crit}} \\ \exp\left(-\frac{12\sigma}{\rho_c(\xi - \xi_{\text{crit}})\overline{\delta v^2(\xi - \xi_{\text{crit}})}}\right) & \text{if } \xi > \xi_{\text{crit}} \end{cases} \tag{3.63}$$

In the case where ξ_{min} is larger than ξ_{crit}, fluid particles of all sizes can break, and the breakage probability is not shifted. This gives the following expression for the breakage frequency:

$$b(\xi) = K_g \frac{\sqrt{\overline{\delta v^2(\xi)} - \frac{12\sigma}{\rho_c \xi}}}{\xi} \times \exp\left(-\frac{12\sigma}{\rho_c \xi \overline{\delta v^2(\xi)}}\right) \tag{3.64}$$

The probability density function of Martínez-Bazán et al. is found from the product of two excess stresses. On a diameter basis, these are given as:

$$\Delta\sigma_{t1}\left(\xi,\omega\right)=\frac{1}{2}\rho_c\overline{\delta v^2\left(\omega\right)}-\frac{6\sigma}{\xi} \tag{3.65}$$

$$\Delta\sigma_{t2}\left(\xi,\omega\right)=\frac{1}{2}\rho_c\overline{\delta v^2\left(\left(\xi^3-\omega^3\right)^{1/3}\right)}-\frac{6\sigma}{\xi} \tag{3.66}$$

Following Martínez-Bazán et al. (2010), the excess stresses are written in terms of volume in order to obtain a volume conserving probability density function:

$$\Delta\sigma_{t1}\left(V_\xi,V_\omega\right)=\frac{1}{2}\rho_c\overline{\delta v^2\left(\left(\frac{6V_\omega}{\pi}\right)^{1/3}\right)}-\frac{6\sigma}{V_\xi^{1/3}}\left(\frac{\pi}{6}\right)^{1/3} \tag{3.67}$$

$$\Delta\sigma_{t2}\left(V_\xi,V_\omega\right)=\frac{1}{2}\rho_c\overline{\delta v^2\left[\left(\frac{6}{\pi}\right)^{1/3}\left(V_\xi-V_\omega\right)^{1/3}\right]}-\frac{6\sigma}{V_\xi^{1/3}}\left(\frac{\pi}{6}\right)^{1/3} \tag{3.68}$$

The probability density function on a volume basis after normalization is given by:

$$P_{\text{DSD}}\left(V_\xi,V_\omega\right)=\frac{\left[\Delta\sigma_{t1}\left(V_\xi,V_\omega\right)\right]\left[\Delta\sigma_{t2}\left(V_\xi,V_\omega\right)\right]}{V_\xi\int_{V_{\omega,\min}}^{V_{\omega,\max}}\left[\Delta\sigma_{t1}\left(V_\xi,V_\omega\right)\right]\left[\Delta\sigma_{t2}\left(V_\xi,V_\omega\right)\right]\mathrm{d}V_\omega} \tag{3.69}$$

The diameter based probability density function is easily obtained by applying the following relation:

$$P_{\text{DSD}}\left(\xi,\omega\right)=P_{\text{DSD}}\left(V_\xi,V_\omega\right)\times\frac{\pi}{2}\omega^2 \tag{3.70}$$

3.3.6 Solsvik et al. (2013)

The model of Solsvik et al. (2013) is based on the framework of Martínez-Bazán et al.. After introducing a breakage probability, as described in section 3.2, the expression for the breakage frequency becomes:

$$b\left(\xi\right)=\frac{1}{t_b}\times P_{\text{breakage}} \tag{3.71}$$

Where the breakage time is calculated from dimensional analysis:

$$t_b\propto\frac{\xi}{\Delta v_b} \tag{3.72}$$

The characteristic velocity is determined by the difference between surface deforming and restoring stresses:

$$\frac{1}{2}\rho_c\left(\Delta v_b\right)^2\approx\overline{\sigma}_t\left(\xi\right)+\overline{\sigma}_{\mu,c}\left(\xi\right)-\overline{\sigma}_s\left(\xi\right)-\overline{\sigma}_{\mu,d}\left(\xi\right) \tag{3.73}$$

In the wide energy spectrum, only the turbulent stress from the continuous phase is changed compared to the original model. The stresses can be written as:

$$\overline{\sigma}_s(\xi) = \frac{6\sigma}{\xi} \tag{3.74}$$

$$\overline{\sigma}_t(\xi) = \frac{1}{2}\rho_c\overline{\delta v^2(\xi)} \tag{3.75}$$

$$\overline{\sigma}_{\mu,c}(\xi) = \mu_c\sqrt{\frac{\varepsilon}{\nu_c}} \tag{3.76}$$

$$\overline{\sigma}_{\mu,d}(\xi) = \mu_d\sqrt{\frac{\varepsilon}{\nu_c}} \tag{3.77}$$

Solving for the breakage time t_b and inserting the expression for the breakage probability from section 3.2.4 gives an expression for the breakage frequency. In the case where $\xi > \xi_{\text{crit}}$, this becomes:

$$b(\xi) = \frac{c_1}{\xi}\sqrt{\frac{12\sigma}{\rho_c\xi}}\sqrt{\text{We}_\text{t} + c_3\text{Ca}_\text{c} - (c_3\text{Ca}_\text{d}+1)}\times\exp\left(-\frac{\frac{6\sigma}{\xi-\xi_{\text{crit}}} + c_3\mu_d\sqrt{\frac{\varepsilon}{\nu_c}}}{\frac{1}{2}\rho_c\overline{\delta v^2(\xi-\xi_{\text{crit}})} + c_3\mu_c\sqrt{\frac{\varepsilon}{\nu_c}}}\right) \tag{3.78}$$

Where the adjustable parameters c_1 and c_3 are introduced by following the original model. When $\xi \leq \xi_{\text{crit}}$, the breakage frequency is set to zero. In the case where ξ_{min} is larger than ξ_{crit}, particles of all sizes can break, and the breakage probability is not shifted. The breakage frequency in this case becomes:

$$b(\xi) = \frac{c_1}{\xi}\sqrt{\frac{12\sigma}{\rho_c\xi}}\sqrt{\text{We}_\text{t} + c_3\text{Ca}_\text{c} - (c_3\text{Ca}_\text{d}+1)}\times\exp\left(-\frac{\frac{6\sigma}{\xi} + c_3\mu_d\sqrt{\frac{\varepsilon}{\nu_c}}}{\frac{1}{2}\rho_c\overline{\delta v^2(\xi)} + c_3\mu_c\sqrt{\frac{\varepsilon}{\nu_c}}}\right) \tag{3.79}$$

As in Martínez-Bazán et al. (2010), the probability density function is calculated from the product of two excess stresses:

$$P_{\text{DSD}}(V_\xi, V_\omega) \propto \left[\Delta\sigma_{t1}(V_\xi, V_\omega)\right]\left[\Delta\sigma_{t2}(V_\xi, V_\omega)\right] \tag{3.80}$$

In the wide energy spectrum, the excess stresses can be written as:

$$\Delta\sigma_{t1}(V_\xi, V_\omega) = \frac{1}{2}\rho_c\delta v^2\overline{\left(\left(\frac{6V_\omega}{\pi}\right)^{1/3}\right)} - \frac{6\sigma}{V_\xi^{1/3}}\left(\frac{\pi}{6}\right)^{1/3} + c_3\sqrt{\frac{\varepsilon}{\nu_c}}(\mu_c - \mu_d) \tag{3.81}$$

$$\Delta\sigma_{t2}(V_\xi, V_\omega) = \frac{1}{2}\rho_c\delta v^2\overline{\left[\left(\frac{6}{\pi}\right)^{1/3}(V_\xi - V_\omega)^{1/3}\right]} - \frac{6\sigma}{V_\xi^{1/3}}\left(\frac{\pi}{6}\right)^{1/3}c_3\sqrt{\frac{\varepsilon}{\nu_c}}(\mu_c - \mu_d) \tag{3.82}$$

The normalized volume based probability density function is given by:

$$P_{\text{DSD}}(V_\xi, V_\omega) = \frac{\left[\Delta\sigma_{t1}(V_\xi, V_\omega)\right]\left[\Delta\sigma_{t2}(V_\xi, V_\omega)\right]}{\int_{V_{\omega,\text{min}}}^{V_{\omega,\text{max}}}\left[\Delta\sigma_{t1}(V_\xi, V_\omega)\right]\left[\Delta\sigma_{t2}(V_\xi, V_\omega)\right]\mathrm{d}V_\omega} \tag{3.83}$$

As in the model of Martínez-Bazán et al., the diameter based probability density function is obtained by using the following relation:

$$P_{\text{DSD}}(\xi,\omega) = P_{\text{DSD}}(V_\xi, V_\omega) \times \frac{\pi}{2}\omega^2 \tag{3.84}$$

3.3.7 Xing et al. (2015)

In Xing et al. (2015), the partial breakage density of a fluid particle of size ξ into a daughter particle with volume fraction f_v' and its complement was given as:

$$\Omega(\xi, f_v') = \int_{\lambda_{\min}}^{\lambda_{\max}} P_b(\xi, f_v', \lambda)\, \omega_{\text{col}}(\xi,\lambda)\, \mathrm{d}\lambda \tag{3.85}$$

In the wide energy spectrum, the breakage probability can be written as:

$$\chi_c = \frac{E_{\text{crit}}(\lambda)}{\overline{E}(\lambda)} = \frac{\max(c_f, c_d)\,\pi\xi^2\sigma}{\frac{1}{2}\rho_c\overline{\delta v^2(\lambda)}\lambda^3} \times \begin{cases} 1 & \text{if } \lambda \le \xi \\ \frac{1}{4\left(\frac{\lambda}{\xi}\right)^2 \sin^4\left(\frac{\pi}{4}\frac{\xi}{\lambda}\right)} & \text{if } \lambda > \xi \end{cases} \tag{3.86}$$

For eddies smaller or equal to the fluid particle, the collision frequency from Luo and Svendsen (1996) was applied. In the wide energy spectrum, this can be written as:

$$\omega_{\text{col}}(\xi,\lambda) = \frac{\pi}{4}(\xi+\lambda)^2\sqrt{\overline{\delta v^2(\lambda)}}n_\lambda n \tag{3.87}$$

For eddies larger than the fluid particle, the collision frequency is replaced by an interaction frequency, which can be written as:

$$\omega_{\text{inter}}(\xi,\lambda) = \frac{\pi\xi^3 n_\lambda n}{6 \times \min\left[\frac{\lambda}{\sqrt{\overline{\delta v^2(\lambda)}}}, \frac{\lambda}{2\left(\frac{\lambda}{\xi}\right)\sin^2\left(\frac{\pi}{4}\frac{\xi}{\lambda}\right)\sqrt{\overline{\delta v^2(\lambda)}}}\right]} \tag{3.88}$$

By applying the Bernoulli equation, Xing et al. (2015) arrived at the following expression for the velocity inside the neck of the deformed fluid particle:

$$v_{\text{neck}} = \sqrt{\frac{4\sigma}{\rho_d(K_c+K_e)}\left(\frac{1}{R_1}-\frac{1}{R_2}\right)} \tag{3.89}$$

The neck velocity was used to find the time for the smaller sphere to completely empty into the larger sphere, t_1:

$$t_1 = \frac{4V_1}{v_{\text{neck}}\pi\xi_{\text{neck}}^2} \tag{3.90}$$

In addition to the emptying time, Xing et al. (2015) found an expression for the shrinking time of the fluid particle neck, t_2:

$$t_2 = \begin{cases} \frac{\xi_{\text{neck}}}{v_{\text{plus}}+U_\lambda} & v_{\text{plus}} + U_\lambda > 0 \\ +\infty & v_{\text{plus}} + U_\lambda \le 0 \end{cases} \tag{3.91}$$

Where the additional shrinking velocity, v_{plus}, was given as:

$$v_{\text{plus}} = \begin{cases} \sqrt{\frac{2(p_0 - p_{\text{neck}})}{\rho_d}} & p_0 - p_{\text{neck}} > 0 \\ -\sqrt{\frac{-2(p_0 - p_{\text{neck}})}{\rho_c}} & p_0 - p_{\text{neck}} \leq 0 \end{cases} \tag{3.92}$$

The continuous phase velocity, U_λ, is a function of the energy spectrum, and is therefore affected by the extension to the entire turbulent spectrum:

$$U_\lambda = \sqrt{\frac{12E\left(\xi_{\text{neck}}\right)}{\pi \rho_c \xi_{\text{neck}}^3}} \tag{3.93}$$

The rest of the extended model of Xing et al. (2015) is the same as explained in section 2.11, but it is repeated briefly here as well, for completeness. The modified partial breakage density was given as:

$$\Omega\left(\xi, f_v\right) = \int_{f'_{v,\min}}^{f'_{v,\max}} \Omega\left(\xi, f'_v\right) \frac{5\gamma \exp\left(-5 f_v\right)}{\exp\left(-5 f_{v,\min}\right) - \exp\left(-5 f_{v,\max}\right)} \mathrm{d}f'_v \tag{3.94}$$

Where $\gamma = \exp\left(-t_2/t_1\right)$. The total breakage density is obtained by integrating the partial breakage density over the daughter volume fraction:

$$\Omega\left(\xi\right) = \int_0^{0.5} \Omega\left(\xi, f_v\right) \mathrm{d}f_v \tag{3.95}$$

The breakage frequency is found directly from the total breakage density:

$$b\left(\xi\right) = \frac{\Omega\left(\xi\right)}{n} \tag{3.96}$$

Finally, the probability density function is calculated as:

$$P_{\text{DSD}}\left(\xi, f_v\right) = \frac{\Omega\left(\xi, f_v\right)}{\Omega\left(\xi\right)} \tag{3.97}$$

Chapter 4

Evaluation of Closures

In order to be suitable as a constitutive equation in the PBE, a breakage closure must exhibit a handful of important properties. These properties were used to make an overall assessment of the closures. Four different systems were used in the evaluation. The physical parameters for the air-water, petroleum-water, toluene-water and dodecane-water systems are given in Table 4.1. As shown in chapter 2, some of the closures have adjustable parameters. In Table 4.2, the value of these parameters for the different systems are given.

Table 4.1: Physical parameters for the systems used in the closure evaluation. AW is the air-water system, PW I is the petroleum-water system I, PW II is petroleum-water system II, TW is the toluene-water system and DW is the dodecane-water system.

Symbol	Unit	AW	PW I	PW II	TW	DW
ρ_d	kg/m^3	1.21	790	760	870	750
ρ_c	kg/m^3	1000	1000	1000	1000	1000
μ_d	mPa s	0.0186	0.65	1.9	0.55	1.34
μ_c	mPa s	1	0.89	0.89	0.89	0.89
σ	N/m	0.072	0.0385	0.028	0.036	0.053
ε	W/kg	1 and 4	6.027	2.5	6.027	8.5
α_d	-	0.05	0	0	0	0.1
ξ_{min} [a]	m	η	η	η	η	η
ξ_{max}	m	0.035	0.01	variable	0.01	0.01

[a] In some models, the minimum fluid particle size is given as 11.4 $\times\eta$.

Table 4.2: The value of the adjustable parameters for all of the systems used in the closure evaluation.

Closure	Parameter	AW	PW I	PW II	TW	DW
CT[a]	c_4	5.25	0.75	0.75	0.75	0.75
CT[a]	c_6	0.014	0.075	0.075	0.075	0.075
MB	K_g	0.3	0.3	0.3	0.3	0.3
SO	c_1	0.11	0.11	0.11	0.11	0.11
SO	c_3	1.0	1.0	1.0	1.0	1.0

[a] For the model of Coulaloglou and Tavlarides (1977), the same values as in Solsvik et al. (2013) were used.

4.1 Evaluation Criteria

The population balance equation is often coupled with mass, momentum and energy balances, giving equation systems that are computationally demanding to solve. In order to avoid bottlenecks in the simulations, it is important that the breakage closures are computationally efficient.

To avoid mass disappearing from the system, the closures must also conserve number and volume. The equations used to compute the conserving properties are given in section 4.3. For each of the four systems, the conserving properties for each closure were calculated for 20 and 100 collocation points. In each case, all possible particle sizes, i.e. from ξ_{min} to ξ_{max} were considered. The reported conserving properties were taken from the particle size that gave the largest error.

Another important characteristic of a breakage closure is the ability to accurately reproduce experimental data. For the breakage frequency of droplets in the toluene-water and petroleum-water system I, the experimental data of Maaß and Kraume (2012) was applied. Data for the breakage frequency of droplets in the dodecane-water system was taken from Andersson and Andersson (2006b). Experimental data for the breakage frequency of bubbles in the air-water system was taken from Wilkinson et al. (1993). The only available source of experimental data for the probability density functions is Zaccone et al. (2007), who used the petroleum-water system II.

The main purpose of the breakage closures is to function as constitutive equations in the population balance equation. Therefore, it is important that the breakage closures, when used as a part of the PBE, give plausible solutions of the density function without causing numerical difficulties. A test case consisting of a two-dimensional PBE with breakage and growth terms was used to test the closures. The test case was solved using orthogonal collocation, and is explained in section 4.4.

It is likely that the number of daughter particles formed in a breakage process can vary with the system parameters and conditions. Therefore, the breakage closures should predict the number of daughters formed, instead of simply assuming a fixed number of daughters for all conditions. Finally, the closures should be based on physical principles and possible to validate experimentally. Adjustable parameters should be avoided.

The criteria used to evaluate the breakage closures are summarized below:

(1) The breakage closures should be computationally efficient. Closures with a computational time over five seconds with 50 collocation points were considered inefficient.

(2) The closures must be number and volume conserving. An error of less than 1 % was considered acceptable.

(3) The breakage closures should be able to accurately reproduce experimental data.

(4) The breakage closures should give plausible solutions of the population balance equation without causing numerical difficulties.

(5) The breakage closures should predict the number of daughters formed in the breakage process, instead of assuming a fixed number of daughters for all conditions.

(6) The models should be based on physical principles and possible to validate experimentally. Adjustable parameters should be avoided.

4.2 Closures Excluded From the Evaluation

In the closure of Narsimhan et al. (1979), the following expression was given for the breakage frequency:

$$b\left(\xi\right)=\frac{\lambda}{2}+\frac{\lambda}{2}\mathrm{erfc}\left(\sqrt{2\left(2^{1/3}-1\right)}\sqrt{\frac{\sigma}{\rho_c}}\frac{\sqrt{6}\xi^{-5/6}}{2\varepsilon^{1/3}}\right) \tag{4.1}$$

The $\lambda/2$ term results in a non-zero breakage frequency as the mother particle size approaches zero, which is not a physically realistic scenario. The model of Narsimhan et al. (1979) was therefore excluded from the evaluation.

In the model of Lehr et al. (2002), the following expression for the partial breakage density per unit volume of the smallest daughter particle was given as:

$$\frac{\Omega\left(\xi,\omega\right)}{n_{\mathrm{sm}}}=C\int_{\lambda_{\mathrm{min}}}^{\xi}\frac{\sigma}{\rho_c\varepsilon^{1/3}\omega_{\mathrm{sm}}^4}\frac{\left(\xi+\lambda\right)^2}{\lambda^{13/3}}\exp\left(-\frac{2\sigma}{\rho_c\left(\varepsilon\lambda\right)^{2/3}\omega_{\mathrm{sm}}}\right)\mathrm{d}\lambda \tag{4.2}$$

The exponential breakage probability used in this expression causes confusion. It deviates from the modelling framework of Luo and Svendsen (1996), because it is not derived from a cumulative exponential distribution, and does not satisfy the normalization condition (Solsvik et al., 2013).

Instead of integrating the partial breakage density over the daughter particle size, Lehr et al. (2002) provided an analytical solution for the breakage frequency by expressing the integral as a sum of incomplete Γ functions. This rough approximation gave the following breakage frequency:

$$b\left(\xi\right)=\frac{1}{2}\xi^{5/3}\varepsilon^{19/15}\left(\frac{\rho_c}{\sigma}\right)^{7/5}\exp\left[-\frac{\sqrt{2}}{\xi^3\varepsilon^{6/5}}\left(\frac{\sigma}{\rho_c}\right)^{9/5}\right] \tag{4.3}$$

Similarly, an analytical expression for the probability density function was provided, instead of calculating the probability density function as the ratio between the partial and total breakage density. These approximations lead to a more computationally efficient model. Nevertheless, due to the inconsistencies in the model derivation, the model of Lehr et al. (2002) was also omitted from the evaluation.

4.3 Number and Volume Conservation

The number and volume conservation is related to the zeroth and first moments of the breakage redistribution density function, respectively. The formula for calculating the number and volume conservation can on a volume basis be written as (Solsvik et al., 2013):

$$\mathrm{mom}_{K=0}\left(V_\xi\right) = \int_{V_{\xi,\min}}^{V_\xi} h_{\mathrm{DSD}}\left(V_\xi, V_\omega\right) \mathrm{d}V_\omega = \nu \tag{4.4}$$

$$\mathrm{mom}_{K=1}\left(V_\xi\right) = \int_{V_{\xi,\min}}^{V_\xi} V_\omega h_{\mathrm{DSD}}\left(V_\xi, V_\omega\right) \mathrm{d}V_\omega = V_\xi \tag{4.5}$$

If the breakage redistribution density function is diameter based, the equations for the number and volume conservation become:

$$\mathrm{mom}_{K=0}\left(\xi\right) = \int_{\xi_{\min}}^{\xi} h_{\mathrm{DSD}}\left(\xi, \omega\right) \mathrm{d}\omega = \nu \tag{4.6}$$

$$\mathrm{mom}_{K=1}\left(\xi\right) = \int_{\xi_{\min}}^{\xi} \frac{\pi}{6}\omega^3 h_{\mathrm{DSD}}\left(\xi, \omega\right) \mathrm{d}\omega = V_\xi \tag{4.7}$$

4.4 Two-Dimensional Population Balance Test Case with Breakage and Growth Terms

The PBE used in the test case was expressed in terms of the statistical mass density function instead of the number density function used in section 1.1. These two are related as follows (Solsvik and Jakobsen, 2013):

$$f_{d,m}\left(\xi, \mathbf{r}, t\right) = f_{d,n}\left(\xi, \mathbf{r}, t\right) \rho_d\left(\mathbf{r}, t\right) V\left(\xi\right) \tag{4.8}$$

This gives the following PBE before simplifications:

$$\begin{aligned} &\frac{\partial f_{d,m}\left(\xi, \mathbf{r}, t\right)}{\partial t} + \nabla_{\mathbf{r}} \cdot \left[\mathbf{v}_{\mathbf{r}}\left(\xi, \mathbf{r}, t\right) f_{d,m}\left(\xi, \mathbf{r}, t\right)\right] - \\ &\frac{f_{d,m}\left(\xi, \mathbf{r}, t\right)}{\rho_d\left(\mathbf{r}, t\right)} \left[\frac{\partial \rho_d\left(\mathbf{r}, t\right)}{\partial t} + \mathbf{v}_{\mathbf{r}}\left(\xi, \mathbf{r}, t\right) \cdot \nabla_{\mathbf{r}} \rho_d\left(\mathbf{r}, t\right)\right] + \\ &\frac{\partial}{\partial \xi}\left[v_\xi\left(\xi, \mathbf{r}, t\right) f_{d,m}\left(\xi, \mathbf{r}, t\right)\right] - \frac{3}{\xi} v_\xi\left(\xi, \mathbf{r}, t\right) f_{d,m}\left(\xi, \mathbf{r}, t\right) = J\left(\xi, \mathbf{r}, t\right) \end{aligned} \tag{4.9}$$

Following Solsvik and Jakobsen (2013), steady state and a constant continuous phase velocity was assumed. Additionally, the equation was cross-sectionally averaged, giving one independent spatial coordinate z. As previously mentioned, only breakage and growth terms were included. The simplified PBE can be written as:

$$v_z \frac{\partial f_{d,m}(\xi,z)}{\partial z} - v_z \frac{f_{d,m}(\xi,z)}{\rho_d(z)} \frac{\partial \rho_d(z)}{\partial z} + \frac{\partial}{\partial \xi}\left[v_\xi(\xi,z) f_{d,m}(\xi,z)\right] - \frac{3}{\xi} v_\xi(\xi,z) f_{d,m}(\xi,z) = J(\xi,z) \tag{4.10}$$

Inserting for the breakage death and breakage birth terms in $J(\xi,z)$ gives:

$$v_z \frac{\partial f_{d,m}(\xi,z)}{\partial z} - v_z \frac{f_{d,m}(\xi,z)}{\rho_d(z)} \frac{\partial \rho_d(z)}{\partial z} + \frac{\partial}{\partial \xi}\left[v_\xi(\xi,z) f_{d,m}(\xi,z)\right] - \frac{3}{\xi} v_\xi(\xi,z) f_{d,m}(\xi,z) = \frac{\pi}{6}\xi^3 \int_\xi^{\xi_{\max}} h_{\text{DSD}}(\xi,\zeta)\, b(\zeta) \frac{f_{d,m}(\zeta,z)}{\frac{\pi}{6}\zeta^3} \mathrm{d}\zeta - b(\xi) f_{d,m}(\xi,z) \tag{4.11}$$

The constitutive equation for the bubble growth velocity can be taken from Morel et al. (2010):

$$v_\xi(\xi,z) = -\frac{\xi v_z}{3\rho_d(z)} \frac{\partial \rho_d(z)}{\partial z} \tag{4.12}$$

The dispersed phase density as a function of z can be estimated from the ideal gas law if the dispersed phase is a gas (Solsvik and Jakobsen, 2013):

$$\rho_d(z) = \frac{M_d p(z)}{RT} \tag{4.13}$$

For liquid-liquid systems, ρ_d is assumed to be constant, i.e. the dispersed phase is assumed to be incompressible. An expression for the pressure was given in Solsvik and Jakobsen (2013):

$$p(z) = p_0 + g\rho_c\left[z_{\max} - z\right] \tag{4.14}$$

By inserting the growth velocity from equation (4.12) into the equation (4.4), the final expression for the PBE used in the test case is obtained:

$$v_z \frac{\partial f_{d,m}(\xi,z)}{\partial z} - \frac{\xi v_z}{3\rho_d(z)} \frac{\partial \rho_d(z)}{\partial z} \frac{\partial f_{d,m}(\xi,z)}{\partial \xi} - f_{d,m}(\xi,z) \frac{v_z}{3\rho_d(z)} \frac{\partial \rho_d(z)}{\partial z} = \xi^3 \int_\xi^{\xi_{\max}} h_{\text{DSD}}(\xi,\zeta)\, b(\zeta) \frac{f_{d,m}(\zeta,z)}{\zeta^3} \mathrm{d}\zeta - b(\xi) f_{d,m}(\xi,z) \tag{4.15}$$

The closures based on the framework of Martínez-Bazán et al. apply a critical diameter, ξ_{crit}. Particles smaller than or equal to the critical diameter will not break, i.e. $b(\xi \leq \xi_{\text{crit}}) = 0$. To avoid numerical problems, the breakage birth integral for these models is modified to ensure that the integration variable ζ never starts below ξ_{crit}. The breakage birth term can be written as:

$$B_B(\xi,z) = \begin{cases} \xi^3 \int_{\xi_{\text{crit}}}^{\xi_{\max}} h_{\text{DSD}}(\xi,\zeta)\, b(\zeta) \frac{f_{d,m}(\zeta,z)}{\zeta^3} \mathrm{d}\zeta & \text{if } \xi \leq \xi_{\text{crit}} \\ \xi^3 \int_{\xi}^{\xi_{\max}} h_{\text{DSD}}(\xi,\zeta)\, b(\zeta) \frac{f_{d,m}(\zeta,z)}{\zeta^3} \mathrm{d}\zeta & \text{if } \xi > \xi_{\text{crit}} \end{cases} \tag{4.16}$$

For closures that assume multiple breakage, e.g. the model of Han et al. (2015), the breakage birth term of the PBE must be slightly modified. Three integrals are needed to separately take into account the contributions to breakage birth from binary, ternary and quaternary events. The PBE in the case of multiple breakage becomes:

$$\begin{aligned} & v_z \frac{\partial f_{d,m}(\xi,z)}{\partial z} - \frac{\xi v_z}{3\rho_d(z)} \frac{\partial \rho_d(z)}{\partial z} \frac{\partial f_{d,m}(\xi,z)}{\partial \xi} - f_{d,m}(\xi,z) \frac{v_z}{3\rho_d(z)} \frac{\partial \rho_d(z)}{\partial z} \\ & = -\left[b_2(\xi) + b_3(\xi) + b_4(\xi)\right] f_{d,m}(\xi,z) + \xi^3 \left[\int_\xi^{\xi_{\max}} h_{2,\mathrm{DSD}}(\xi,\zeta)\, b_2(\zeta) \frac{f_{d,m}(\zeta,z)}{\zeta^3} \mathrm{d}\zeta \right. \\ & \left. + \int_\xi^{\xi_{\max}} h_{3,\mathrm{DSD}}(\xi,\zeta)\, b_3(\zeta) \frac{f_{d,m}(\zeta,z)}{\zeta^3} \mathrm{d}\zeta + \int_\xi^{\xi_{\max}} h_{4,\mathrm{DSD}}(\xi,\zeta)\, b_4(\zeta) \frac{f_{d,m}(\zeta,z)}{\zeta^3} \mathrm{d}\zeta \right] \end{aligned} \tag{4.17}$$

For a given system, the boundary condition for the dispersed phase density, $\rho_d(z=0)$ was set to the value given in Table 4.1. Additionally, one boundary condition in z and ξ is needed for the mass density function. From Solsvik and Jakobsen (2013), the following boundary conditions were chosen:

$$f_{d,m}(\xi_{\min}, \forall z) = 0 \tag{4.18}$$

$$\begin{aligned} f_{d,}(\forall \xi, z_{\min}) = 29.4 & \left[0.001 + \frac{2.999}{\xi_{\max} - \xi_{\min}} (\xi - \xi_{\min}) \right]^3 \times \\ & \exp\left[-0.7 \left(0.001 + \frac{2.999}{\xi_{\max} - \xi_{\min}} (\xi - \xi_{\min}) \right)^4 \right] \end{aligned} \tag{4.19}$$

The system of equations for the PBE test case was solved using an in-house solver based on orthogonal collocation, the simplest weighted residual method. As this thesis is not mainly focused on numerics, an explanation of the numerical method is not given here. A description of weighted residual methods in general and orthogonal collocation specifically is given in Solsvik and Jakobsen (2014).

Chapter 5

Results and Discussion

In this chapter, the breakage frequencies, probability density functions and mass density functions from the PBE test case for the original and extended versions of all closures are given. The implementations of Liao et al. (2015) and Xing et al. (2015) from this work produced results that were different from the original articles. Correspondence with the article authors did not reveal the reason behind the differences. Regardless of the differences, it was decided to include the models of Liao et al. (2015) and Xing et al. (2015) in the evaluation, as they are recently published and therefore not yet evaluated in the literature.

5.1 Volume and Number Conservation

Table 5.1 shows the volume and number conserving properties of the original breakage closures. If a closure is volume conserving, it returns a value of 1.0. A number conserving closure returns the number of daughters, i.e. 2.0 for binary breakage, 3.0 for ternary breakage and 4.0 for quaternary breakage.

Table 5.1: Volume and number conserving properties of the original breakage closures at 20 and 100 collocation points. The physical parameters of the air-water system were used in the calculations.

	Alias	Volume	Number
20 collocation points			
Coulaloglou and Tavlarides (1977)	CT	0.9999	1.9999
Luo and Svendsen (1996)	LS	1.9883	2.0000
Han et al. (2011)	H11	1.0006	2.0000
Han et al. (2015) binary	H15	0.5189	1.0434
Han et al. (2015) ternary	H15	0.8698	2.7033
Han et al. (2015) quaternary	H15	0.9836	3.9491
Becker et al. (2014)	BE	0.9987	2.0000
Martínez-Bazán et al. (2010)	MB	0.9972	1.9978
Solsvik et al. (2013)	SO	0.9958	1.9973
Liao et al. (2015)	LI	0.9282	8.7197
Xing et al. (2015)	XI	0.7943	2.6460
100 collocation points			
Coulaloglou and Tavlarides (1977)		0.9999	1.9999
Luo and Svendsen (1996)		1.7208	2.0000
Han et al. (2011)		1.0000	2.0000
Han et al. (2015) binary		1.0005	2.0011
Han et al. (2015) ternary		1.0001	3.0002
Han et al. (2015) quaternary		1.0000	4.0001
Becker et al. (2014)		1.0000	2.0000
Martínez-Bazán et al. (2010)		1.0001	2.0001
Solsvik et al. (2013)		1.0001	2.0002
Liao et al. (2015)		0.9667	8.4346
Xing et al. (2015)		0.7977	2.6437

The majority of the original breakage closures conserve both volume and number within the 1 % error margin for both 20 and 100 collocation points, and are considered acceptable in terms of conserving properties. The model of Han et al. (2015) did not conserve number or volume with 20 collocation points, and should therefore only be applied when a sufficient amount of numerical points is used. The closure of Luo and Svendsen (1996) demonstrated weak volume conserving properties for both numerical resolutions. Further testing showed that this model needed 500 collocation points to give a volume conserving error of less than 10 %. The sensitivity towards the number of collocation points indicates that the redistribution function of Luo and Svendsen (1996) is steep. This is confirmed in section 5.4, where the probability density functions are plotted.

The volume conservation error of the original version of Liao et al. (2015) was approximately 7 % and 3 % for 20 and 100 collocation points, respectively. The model is therefore almost volume conserving. The number conserving errors, however, were far from acceptable. For both 20 and 100 collocation points, the number conservation was over 4 times the correct value of 2.0. The model of Liao et al. (2015) is comparable to the closure

of Martínez-Bazán et al. and Solsvik et al. (2013). The main difference between these models is that Liao et al. (2015) uses the daughter particle size as the characteristic length scale in the definition of the breakage time, and that the probability density function is calculated from the partial and total breakage density. This deviation from the framework of Martínez-Bazán et al. might cause the number conserving errors.

The original model of Xing et al. (2015) was neither number or volume conserving for 20 or 100 collocation points. This model returned approximately equal values for the volume and number conservation for all particle sizes that were studied. This might indicate that the breakage frequency and probability density function is scaled with an incorrect value, and that the model has the potential of being conserving if it is scaled correctly.

In Table 5.2, the volume and number conserving properties of the extended breakage closures are given.

Table 5.2: Volume and number conserving properties of the extended breakage closures at 20 and 100 collocation points. The physical parameters of the air-water system were used in the calculations, and the integral length scale L was set to 0.1 m.

	Alias	**Volume**	**Number**
20 collocation points			
Coulaloglou and Tavlarides (1977)[a]	CTW	0.9999	1.9999
Luo and Svendsen (1996)	LSW	1.9817	2.0000
Han et al. (2011)	H11W	0.9989	2.0000
Han et al. (2015) binary	H15M	0.9914	1.9855
Han et al. (2015) ternary	H15M	1.0044	3.0132
Han et al. (2015) quaternary	H15M	1.0071	4.0277
Becker et al. (2014)	BEW	0.9988	2.0000
Martínez-Bazán et al. (2010)	MBW	1.0073	2.0150
Solsvik et al. (2013)	SOW	0.9885	1.9819
Liao et al. (2015)	LIW	0.9285	8.4182
Xing et al. (2015)	XIW	0.7943	2.6460
100 collocation points			
Coulaloglou and Tavlarides (1977)		0.9999	1.9999
Luo and Svendsen (1996)		1.6681	2.0000
Han et al. (2011)		1.0000	2.0000
Han et al. (2015) binary		0.9999	1.9998
Han et al. (2015) ternary		1.0000	3.0001
Han et al. (2015) quaternary		1.0000	4.0000
Becker et al. (2014)		1.0000	2.0000
Martínez-Bazán et al. (2010)		1.0001	2.0001
Solsvik et al. (2013)		1.0002	2.0001
Liao et al. (2015)		0.9669	8.2909
Xing et al. (2015)		0.7977	2.6437

[a] The extended and original redistribution functions of Coulaloglou and Tavlarides (1977) are identical.

The conserving properties of the extended versions are similar to the original models, indicating that the energy spectrum does not have a large impact on the redistribution functions. Only the closure of Luo and Svendsen (1996), Liao et al. (2015) and Xing et al. (2015) give large errors. The extended model of Han et al. (2015) gives acceptable results also for 20 collocation points, suggesting that it is less sensitive to the numerical resolution than the original model.

5.2 Computational Time

The implementations of the breakage closures have not been optimized with regard to computational efficiency. Nevertheless, a comparison of the relative computational efficiency of the closures is useful, as it gives an indication of which closures are suitable as kernels in the PBE. The relative computational efficiency of the original closures is shown in Figure 5.1.

As the figure indicates, the model of Han et al. (2015) is clearly the most computationally demanding closure, taking around 1500 times longer than most of the other closures. This model contains many integrals that are cumbersome to evaluate, and is therefore only suitable for simple systems, e.g. where the population balance is solved without coupling with other equations and the numerical resolution is not an issue. The closure of Han et al. (2011) is far less computationally demanding. However, it takes approximately four times longer than the other models, which use around 0.01 seconds each time they are called upon.

Figure 5.2 shows the relative computational time of the extended breakage closures. The extended models exhibit the same behavior as the original models, with the model of Han et al. (2015) clearly being the least computationally efficient. The relative magnitudes of the computational times are similar to the original models.

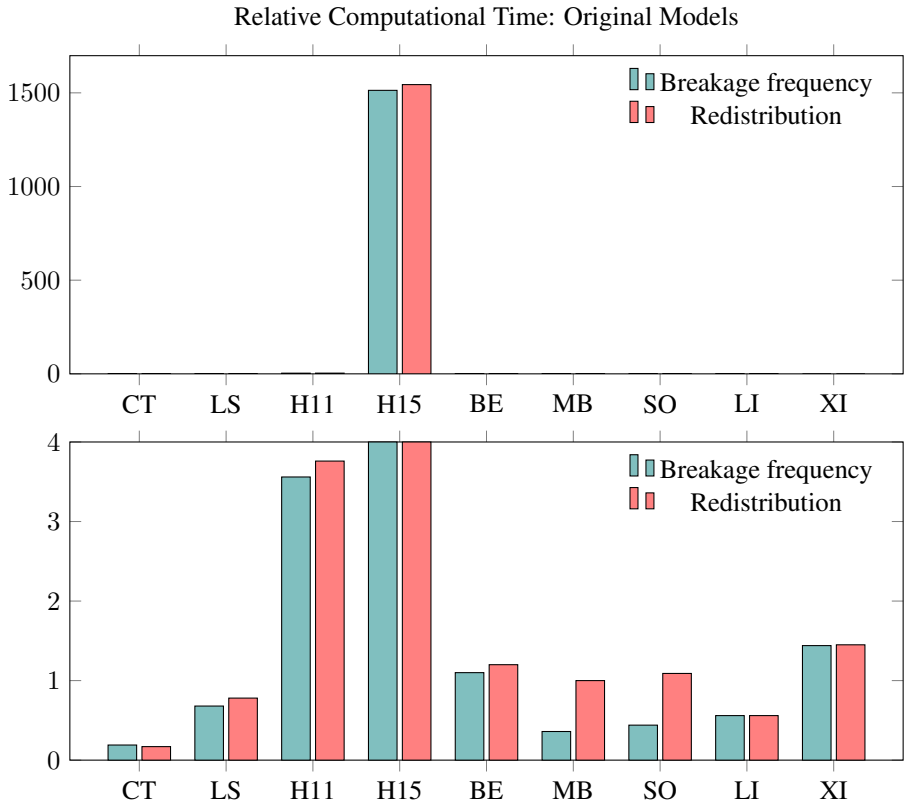

Figure 5.1: A comparison of the relative computational times of the breakage frequencies and redistribution functions of the original breakage closures. The computational time was measured using the air-water system and 50 collocation points. The lower graph is a zoom of the upper graph. The aliases are given in Table 5.1.

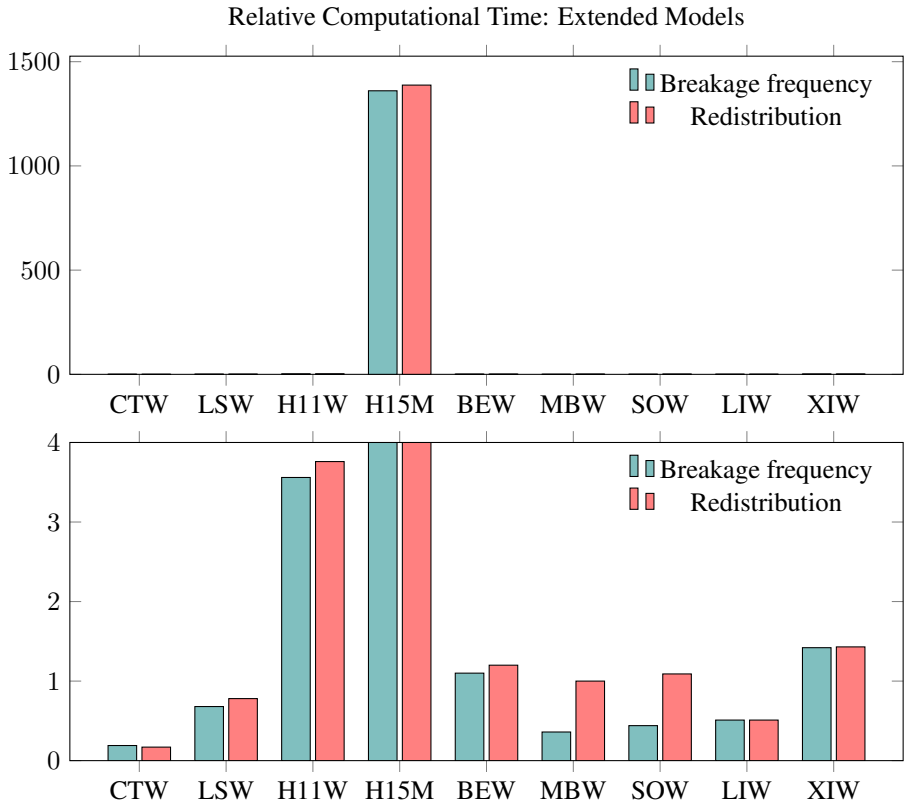

Figure 5.2: A comparison of the relative computational times of the breakage frequencies and redistribution functions of the extended breakage closures. The computational time was measured using the air-water system and 50 collocation points. The lower graph is a zoom of the upper graph. The aliases are given in Table 5.2.

5.3 Breakage Frequencies

In the literature, there is a lack of experimental data on the breakage frequencies of bubbles and droplets in turbulent dispersions. The few available sources of experimental data contain very few data points, making it difficult to evaluate the breakage closures over a sufficiently wide range of particle sizes. In order to evaluate the closures properly, there is a need for experiments measuring the breakage frequency of both bubbles and droplets in several systems over large particle size ranges. In this section, the breakage frequencies of the original and extended versions of all breakage closures are compared with the available experimental data.

5.3.1 Air-Water System

The breakage frequencies of all closures except the models of Liao et al. (2015) and Xing et al. (2015) are shown in Figure 5.3 with an integral scale of 0.1 m.

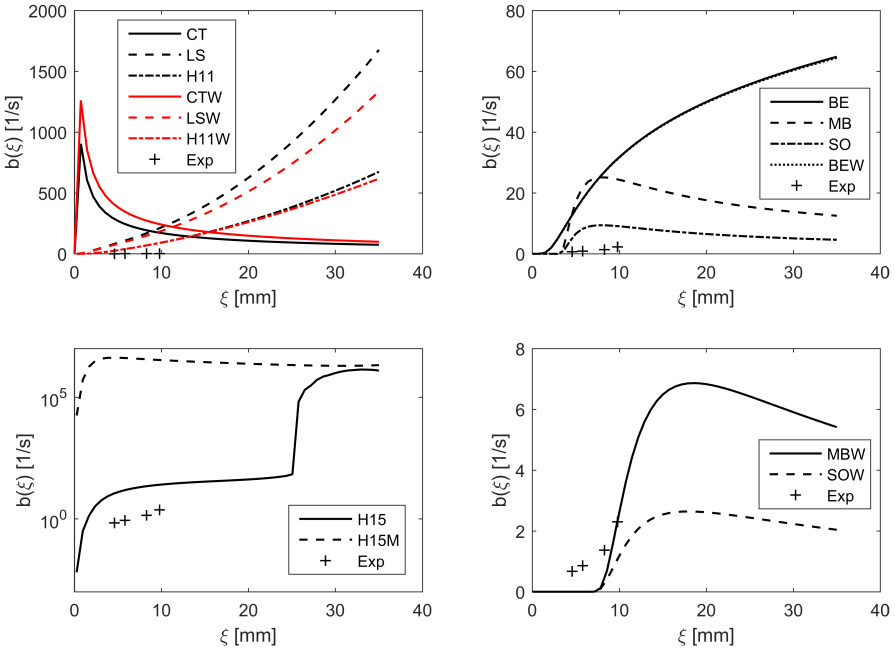

Figure 5.3: Breakage frequencies for the air-water system. The integral scale L has been set to 0.1 m in the wide energy spectrum models. Exp is the experimental data of Wilkinson et al. (1993).

Most of the closures fail to predict the breakage frequencies measured by Wilkinson et al. (1993). All models except the extended model of Martínez-Bazán et al. (1999a) and Solsvik et al. (2013) overpredict the breakage frequency. The best agreement with the experimental data is achieved by the extended model of Martínez-Bazán et al. (1999a), even though the model fails to predict the breakage frequency for the smallest particle sizes. The original model of Han et al. (2015) gives a non-physical peak in the breakage frequency profile around $\xi = 25$ mm. However, it should be mentioned that this model was not originally developed for gas-liquid systems.

The wide energy spectrum versions of the closures are affected by the integral scale. It can be seen from Figure 5.3 that when the integral scale is 0.1 m, the original and extended models give almost identical results. As shown in appendix A.1.1, most of the original and extended models give very similar profiles also for an integral scale of 1 m. This indicates that the air-water system with $L = 0.1$ m and 1 m is located within the inertial subrange of turbulence. The original and extended versions of Han et al. (2015), Martínez-Bazán et al. (1999a) and Solsvik et al. (2013) predict different breakage frequencies in

the inertial subrange. For Han et al. (2015), this difference is most likely a result of the inconsistent turbulent energy spectrum applied in the original model. For Martínez-Bazán et al. (1999a) and Solsvik et al. (2013), the difference might be caused by the introduced breakage probability, explained in section 3.2, which can differ between the original and extended model due to the change in structure function.

When the integral scale is set to 0.01 m, all of the wide models predict lower breakage frequencies than for $L = 0.1$ and 1 m. This is shown in appendix A.1.1, and is an indication that for $L = 0.01$ m, the air-water system has shifted from the inertial subrange to the dissipation subrange of the turbulent energy spectrum. In this domain, the deforming energy acting on the bubbles is lower, which can explain the decrease in predicted breakage frequency in the wide spectrum models. The decrease in breakage frequency results in a better agreement with the experimental data, but none of the models are able to reproduce the data of Wilkinson et al. (1993) with acceptable accuracy for $L = 0.01$ m.

In Figure 5.4, the breakage frequencies for the models of Liao et al. (2015) and Xing et al. (2015) are shown. The figure shows that both models fail to reproduce the experimental data of Wilkinson et al. (1993), and that for $L = 0.1$ m, the wide and inertial range models give almost identical results. The sensitivity analysis shown in appendix A.1.1 gave similar results for Liao et al. (2015) and Xing et al. (2015) as for the other models. An integral scale of 1 m gives similar results as 0.1 m, and an integral scale of 0.01 m gives a reduction in the predicted breakage frequency.

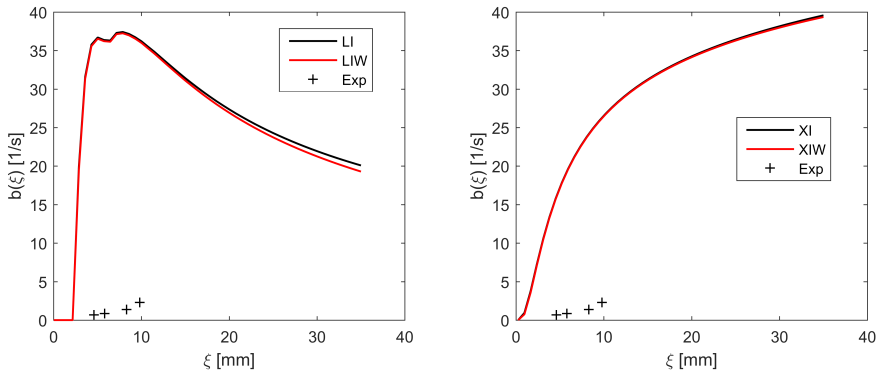

Figure 5.4: Breakage frequencies of Liao et al. (2015) and Xing et al. (2015) for the air-water system. The integral scale L has been set to 0.1 m in the wide energy spectrum models and the value of $\dot{\gamma}_{\text{shear}}$ was set to 10 s^{-1}. Exp is the experimental data of Wilkinson et al. (1993).

5.3.2 Petroleum-Water System I

The breakage frequencies of most models for the petroleum-water system I are given in Figure 5.5. The integral scale has been set to 0.1 m.

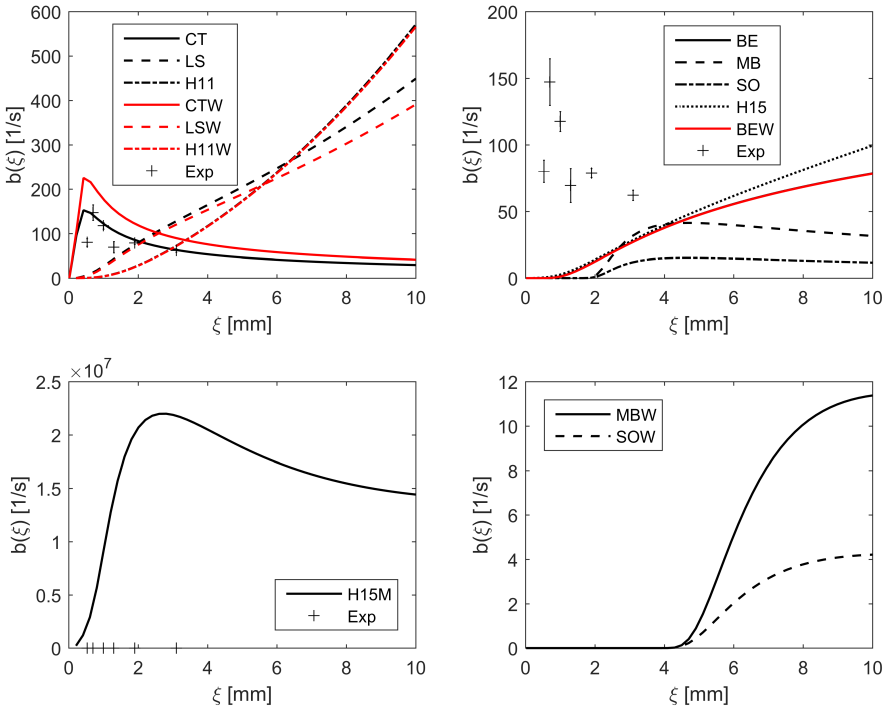

Figure 5.5: Breakage frequencies for the petroleum-water system I. The integral scale L has been set to 0.1 m in the wide energy spectrum models. Exp is the experimental data of Maaß and Kraume (2012).

For the petroleum-water system I, it is the original and extended version of Coulaloglou and Tavlarides (1977) that show the best agreement with the experimental data of Maaß and Kraume (2012)[1]. However, it should be kept in mind that these models have adjustable parameters that have been tuned for this specific system. Therefore, a good fit to the experimental data is easier to achieve than for the phenomenological models. Both models of Luo and Svendsen (1996) and Han et al. (2011) also fit the experimental data fairly well. The modified model of Han et al. (2015) overpredicts the breakage frequency with several orders of magnitude, and the rest of the models predict a lower breakage frequency than the experimental data.

[1] Some of the experimental data points reported in the article of Maaß and Kraume (2012) are incorrect. This was verified by personal communication, and the correct values have been used in this work.

The sensitivity analysis for the breakage frequencies of the petroleum-water system I with regard to the integral scale is given in appendix A.1.2. The analysis shows similar results as in the air-water system from the previous section. When the integral scale is 0.1 and 1 m, the original and extended models give similar results, indicating that the petroleum-water system I with these integral scales is within the inertial subrange. For an integral scale of 0.01 m, the wide spectrum models predict lower breakage frequencies, indicating that the system is within the dissipation subrange for this value of L.

In Figure 5.6, the breakage frequencies of Liao et al. (2015) and Xing et al. (2015) are shown. Both models are in the same order of magnitude as the experimental data, and agree well with the last data point. However, most of the data points are higher than the breakage frequencies predicted by Liao et al. (2015) and Xing et al. (2015). The sensitivity analysis from appendix A.1.2 gives the same results as for the other closures. Integral scales of 0.1 and 1 m seem to give a system within the inertial subrange, and an integral scale of 0.01 m shifts the system into the dissipation subrange. The agreement with the experimental data is worse in the dissipation subrange, because the predicted breakage frequencies are lower, and therefore further from the data points.

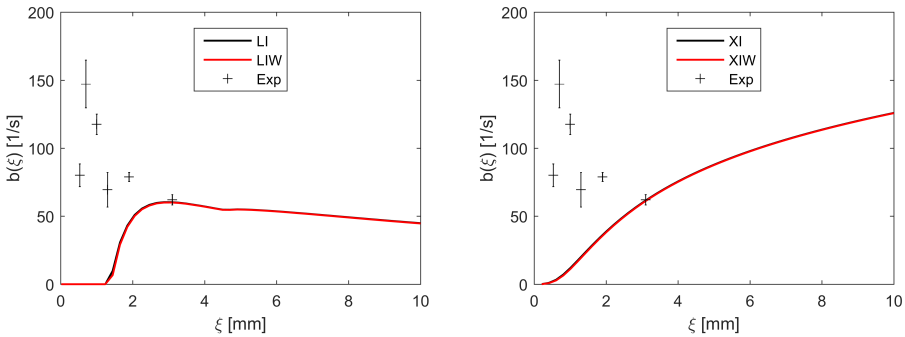

Figure 5.6: Breakage frequencies of Liao et al. (2015) and Xing et al. (2015) for the petroleum-water system I. The integral scale L has been set to 0.1 m in the wide energy spectrum models and the value of $\dot{\gamma}_{\text{shear}}$ was set to 10 s^{-1}. Exp is the experimental data of Maaß and Kraume (2012).

5.3.3 Toluene-Water System

The breakage frequencies of most models for the toluene-water system are given in Figure 5.7. The integral scale has been set to 0.1 m.

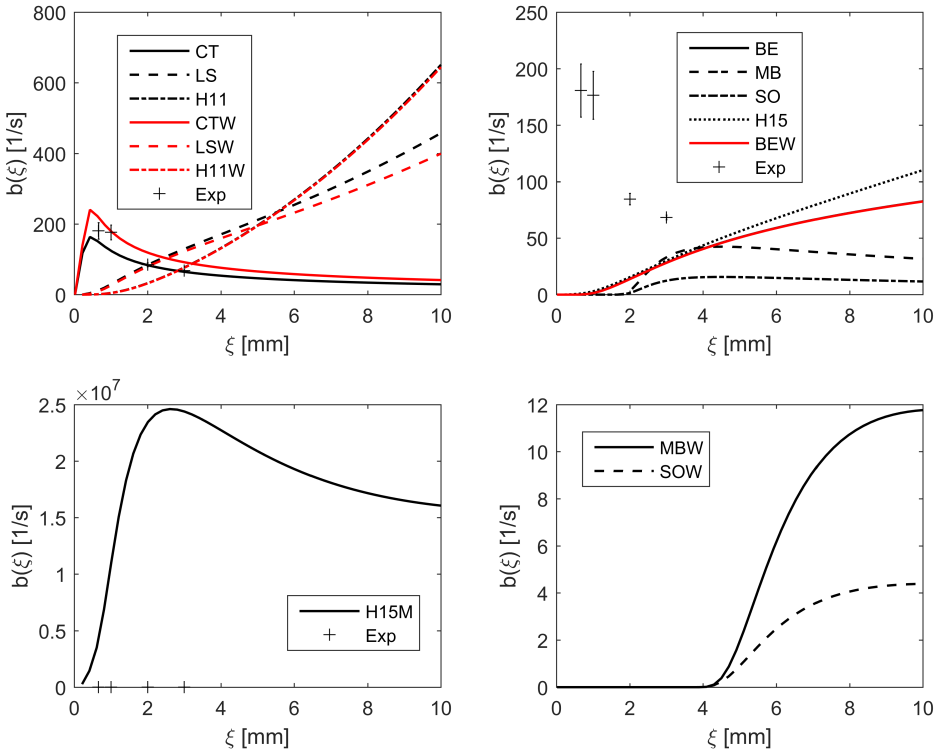

Figure 5.7: Breakage frequencies for the toluene-water system. The integral scale L has been set to 0.1 m in the wide energy spectrum models. Exp is the experimental data of Maaß and Kraume (2012).

The parameters of the toluene-water system are similar to the petroleum-water system, and the models therefore show similar trends. The original and extended model of Coulaloglou and Tavlarides (1977) shows the best agreement with the experimental data of Maaß and Kraume (2012)[2]. The original and extended model of Luo and Svendsen (1996) and Han et al. (2011) also match the data acceptably. As in the petroleum-water system, the other models fail to reproduce the experimental data. The sensitivity analysis given in appendix A.1.3 shows the same sensitivity towards the integral scale as in the petroleum-water system I.

[2]For the toluene-water system, there were also errors in the experimental data reported in the article of Maaß and Kraume (2012). The correct values have been used in this work, and were verified by personal communication.

In Figure 5.8, the breakage frequencies of Liao et al. (2015) and Xing et al. (2015) for an integral scale of 0.1 m are given. As in the petroleum-water system I, the last data point of Maaß and Kraume (2012) fits well with both models. However, the rest of the experimental data is higher than the values predicted by Liao et al. (2015) and Xing et al. (2015). Also for these models, the sensitivity analysis in appendix A.1.3 shows similar results as for the petroleum-water system I.

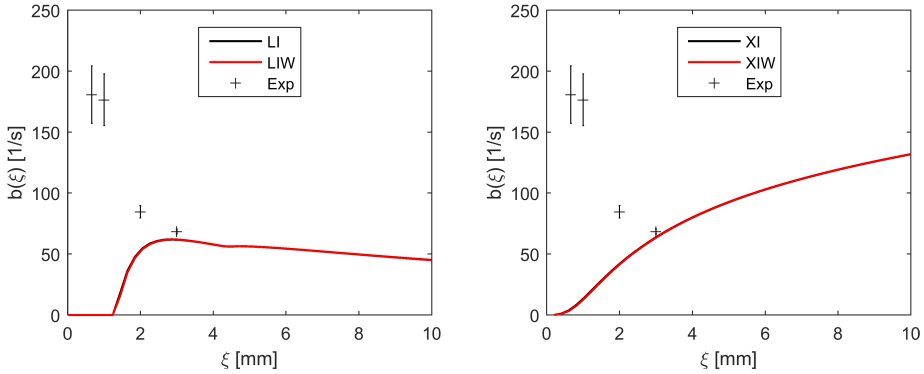

Figure 5.8: Breakage frequencies of Liao et al. (2015) and Xing et al. (2015) for the toluene-water system. The integral scale L has been set to 0.1 m in the wide energy spectrum models and the value of $\dot{\gamma}_{\text{shear}}$ was set to 10 s^{-1}. Exp is the experimental data of Maaß and Kraume (2012).

5.3.4 Dodecane-Water System

The breakage frequencies for the dodecane-water system are shown in Figure 5.9. The integral scale was set to 0.1 m.

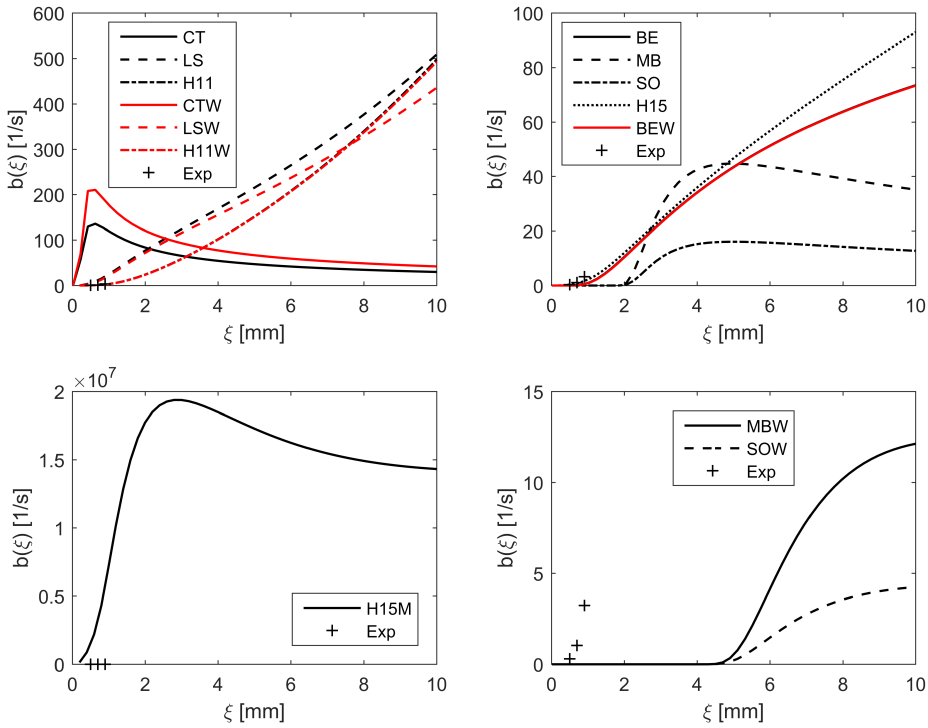

Figure 5.9: Breakage frequencies for the dodecane-water system. The integral scale L has been set to 0.1 m in the wide energy spectrum models. Exp is the experimental data of Andersson and Andersson (2006b).

The trends in the dodecane-water system are similar to the two previously discussed liquid-liquid systems. The original model of Han et al. (2015) and both models of Han et al. (2011) and Becker et al. (2014) are in close agreement with the experimental data. The models of Luo and Svendsen (1996) slightly overpredict the breakage frequency measured by Andersson and Andersson (2006b). The other models fail to reproduce the experimental data. As in the petroleum-water and toluene-water system, the modified model of Han et al. (2015) predicts a breakage frequency several orders of magnitude higher than the experimental data. The sensitivity towards the integral scale is similar as for the other systems, as shown in appendix A.1.4. The model of Han et al. (2011) is in better agreement with the experimental data in the dissipation subrange, because the predicted breakage frequency is slightly lower than in the inertial subrange.

In Figure 5.10, the breakage frequencies of Liao et al. (2015) and Xing et al. (2015) are given. From the figure, it is evident that both models fail to reproduce the experimental data of Andersson and Andersson (2006b). The breakage frequencies are, however, in the same order of magnitude as the experimental data. In appendix A.1.4, it can be seen that the models demonstrate the same sensitivity towards the integral scale as seen in the previous systems.

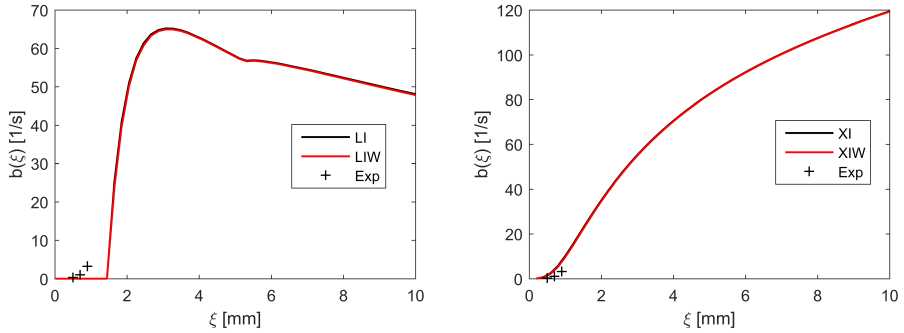

Figure 5.10: Breakage frequencies of Liao et al. (2015) and Xing et al. (2015) for the dodecane-water system. The integral scale L has been set to 0.1 m in the wide energy spectrum models and the value of $\dot{\gamma}_{\text{shear}}$ was set to 10 s^{-1}. Exp is the experimental data of Andersson and Andersson (2006b).

5.4 Probability Density Functions

In this section the probability density functions of the breakage closures are given for the petroleum-water system II and the air-water system. The toluene-water and dodecane-water systems are not included, because they are similar to the petroleum-water system II, and there is no experimental data available for the probability density functions in these systems. The air-water system is included because the parameters are substantially different from the petroleum-water system II. The probability density functions in this section are given as a function of the diameter fraction f_d, given as ω/ξ.

5.4.1 Petroleum-Water System II

Figure 5.11 shows the dimensionless diameter based probability density functions of most of the closures for a parent droplet with a diameter of 2 mm. The model predictions are compared with the experimental data of Zaccone et al. (2007), using petroleum-water system II.

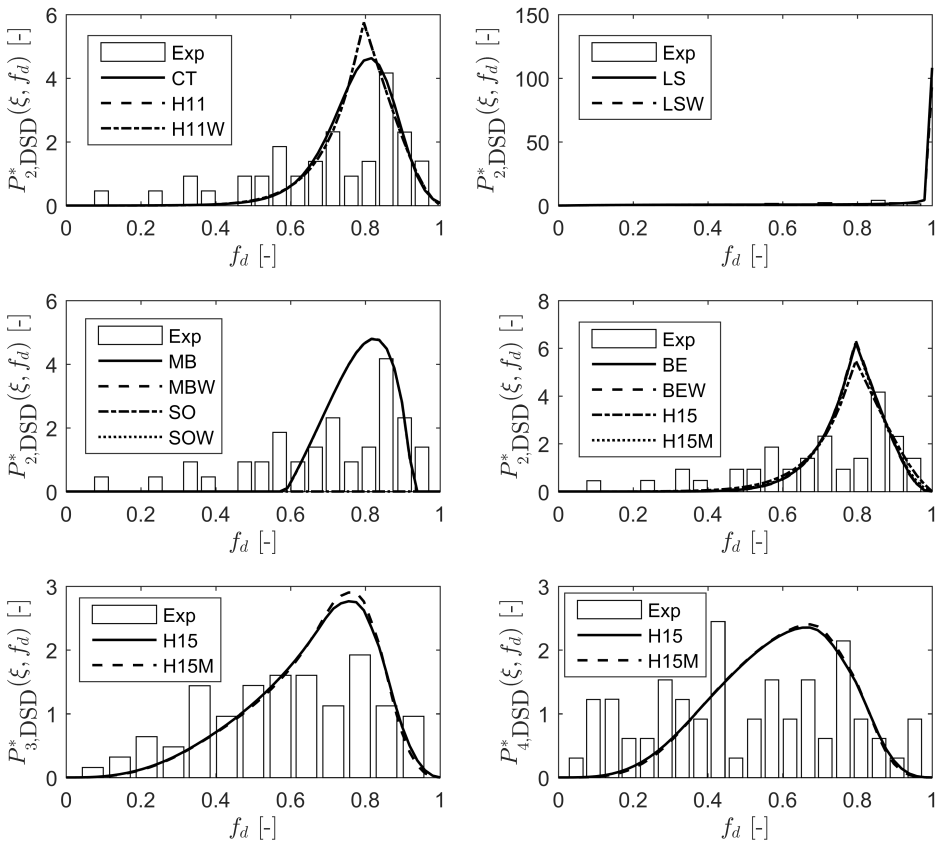

Figure 5.11: Probability density functions for the petroleum-water system II with a parent droplet diameter of 2 mm. The integral scale L has been set to 0.1 m in the wide energy spectrum models. Exp is the binary, ternary and quaternary experimental data of Zaccone et al. (2007).

Most of the probability density functions are Λ-shaped, meaning that the most likely scenario is equal breakage. On a diameter basis, a diameter fraction of $f_d = 0.794$ corresponds to a volume fraction of $f_v = 0.5$. As can be seen from Figure 5.11, all models except Luo and Svendsen (1996) and the quaternary probability density function of Han et al. (2015) have peaks around $f_d = 0.8$. In the extended model of Martínez-Bazán et al. (2010) and Solsvik et al. (2013), the mother diameter of 2 mm is smaller than ξ_{crit}, meaning that no breakage and therefore no redistribution occurs. Although none of the binary redistribution functions fit excellently with the experimental data, all closures except the models of Luo and Svendsen (1996) and the extended model of Martínez-Bazán et al. (2010) and Solsvik et al. (2013) have similar trends as the data of Zaccone et al. (2007).

The shape of the probability density function of both models of Luo and Svendsen (1996) is different than the other models. It is U-shaped, meaning that the most probable case is unequal breakage, where one large and one small daughter particle is formed. This is

not in agreement with the experimental data of Zaccone et al. (2007). A steep probability density function can cause numerical difficulties, in addition to problems with conserving properties. As previously discussed in section 5.1, the original and extended version of Luo and Svendsen (1996) needed significantly more collocation points than the other models in order to become volume conserving. This is most likely caused by the steep probability density functions.

The ternary and quaternary probability density functions of the original and extended model of Han et al. (2015) are almost identical. None of the models are in excellent agreement with the data of Zaccone et al. (2007), but the ternary model gives an acceptable fit.

The sensitivity analysis in appendix A.2.2 shows that the probability density functions are almost independent of the integral length scale, unlike the breakage frequencies. All of the studied closures except Coulaloglou and Tavlarides (1977) are phenomenological, and the redistributions are calculated from a fraction. The effect of the integral scale might be almost equal in the numerator and denominator, and thus the effect on the redistribution is marginalized.

In Figure 5.12, the probability density functions for the petroleum-water system II of Liao et al. (2015) and Xing et al. (2015) are given for a parent droplet with a diameter of 2 mm. The figure shows that the redistribution functions are M-shaped and that none of the models are able to predict the peak located around f_d = 0.8 from the experimental data. From appendix A.2.2, it can be seen that the integral scale has almost no effect on the redistribution of Liao et al. (2015) and Xing et al. (2015).

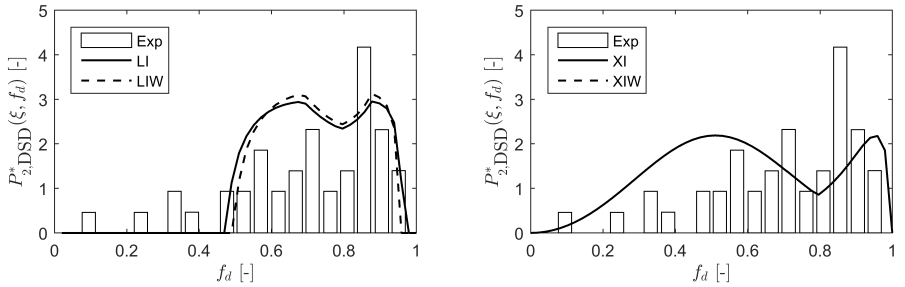

Figure 5.12: Probability density functions of Liao et al. (2015) and Xing et al. (2015) for the petroleum-water system II with a parent droplet diameter of 2 mm. The integral scale L has been set to 0.1 m in the wide energy spectrum models. Exp is the binary, ternary and quaternary experimental data of Zaccone et al. (2007).

In Figure 5.13, the probability density functions for the petroleum-water system II are shown for a parent droplet with a diameter of 1 mm.

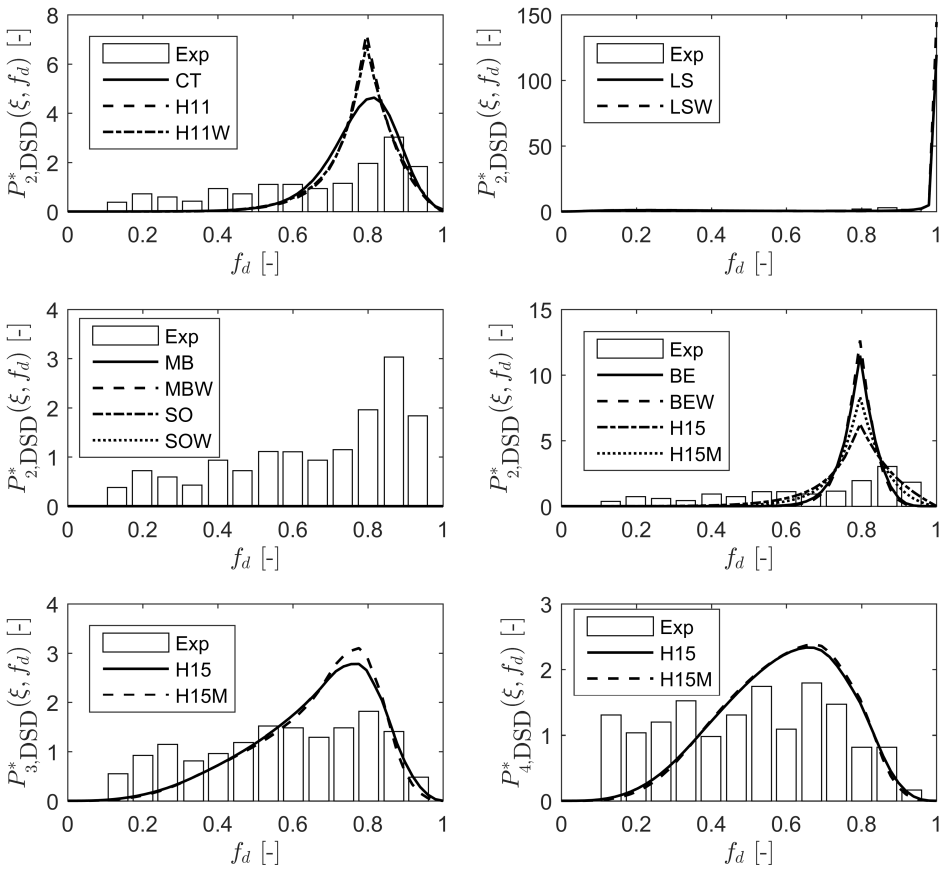

Figure 5.13: Probability density functions for the petroleum-water system II with a parent droplet diameter of 1 mm. The integral scale L has been set to 0.1 m in the wide energy spectrum models. Exp is the binary, ternary and quaternary experimental data of Zaccone et al. (2007).

As the size of the mother particle decreases, the size range where mother particles redistribute to daughter particles narrows. This leads to an increase in the function values of the probability density functions, because the area under the curves must remain the same, regardless of mother size. This effect is seen in Figure 5.13, where the function values are higher than in Figure 5.11. Otherwise, the probability density function profiles are similar to the case with 2 mm as the mother particle diameter. As 1 mm is smaller than ξ_{crit} for all versions of Martínez-Bazán et al. (2010) and Solsvik et al. (2013), all of these models predict zero redistribution.

Compared to Figure 5.11, the ternary and quaternary models of Han et al. (2015) are in better agreement with the experimental data of Zaccone et al. (2007) for a mother particle diameter of 1 mm than 2 mm. The binary probability density functions show an opposite trend.

In Figure 5.14, the probability density functions for the petroleum-water system II of Liao et al. (2015) and Xing et al. (2015) are given for a parent droplet with a diameter of 1 mm. From the figure it can be seen that both models of Liao et al. (2015) predict no redistribution, because no breakup occurs at this particle size. The probability density function of Xing et al. (2015) is identical to the one from Figure 5.12. The sensitivity analysis in appendix A.2.2 shows that, for all models, the integral scale has almost no effect on the redistribution functions also for a mother particle with 1 mm diameter.

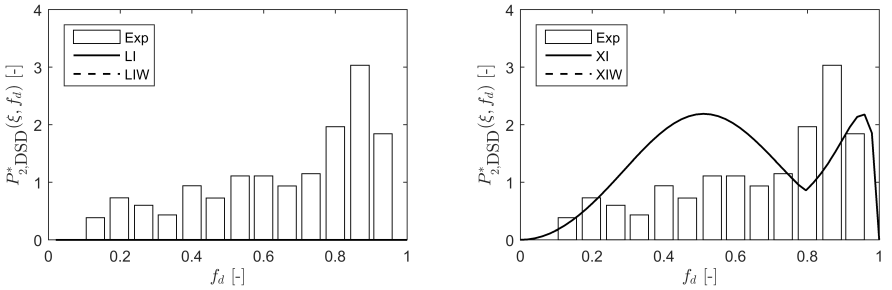

Figure 5.14: Probability density functions of Liao et al. (2015) and Xing et al. (2015) for the petroleum-water system II with a parent droplet diameter of 1 mm. The integral scale L has been set to 0.1 m in the wide energy spectrum models. Exp is the binary, ternary and quaternary experimental data of Zaccone et al. (2007).

In Figure 5.15, the probability density functions for the petroleum-water system II are shown for a parent droplet with a diameter of 0.6 mm. Decreasing the mother particle diameter from 1 mm to 0.6 mm results in a further increase in the function values of the probability density functions. Compared to Figure 5.13, the binary, ternary and quaternary redistribution functions agree less with the experimental data, even though the trends are similar.

In Figure 5.16, the probability density functions for the petroleum-water system II of Liao et al. (2015) and Xing et al. (2015) are given for a parent droplet with a diameter of 0.6 mm. The trends are very similar to the previous cases. As in the two previous cases, the integral scale has almost no effect on the redistribution functions for a parent particle with a diameter of 0.6 mm.

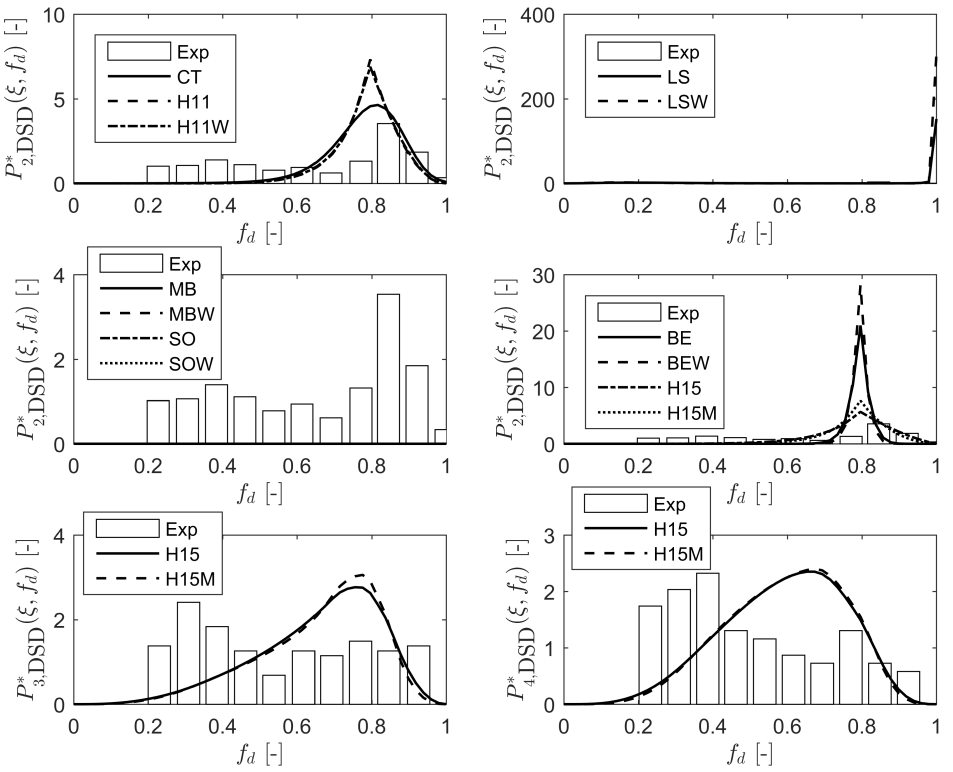

Figure 5.15: Probability density functions for the petroleum-water system II with a parent droplet diameter of 0.6 mm. The integral scale L has been set to 0.1 m in the wide energy spectrum models. Exp is the binary, ternary and quaternary experimental data of Zaccone et al. (2007).

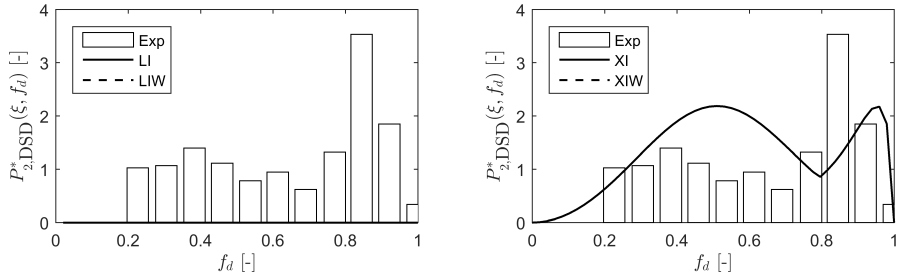

Figure 5.16: Probability density functions of Liao et al. (2015) and Xing et al. (2015) for the petroleum-water system II with a parent droplet diameter of 0.6 mm. The integral scale L has been set to 0.1 m in the wide energy spectrum models. Exp is the binary, ternary and quaternary experimental data of Zaccone et al. (2007).

5.4.2 Air-Water System

In Figure 5.17 and Figure 5.18, the probability density functions are shown for the air-water system with a dissipation rate of 1 W/kg, an integral scale of 0.1 m and a mother particle diameter of 20 mm.

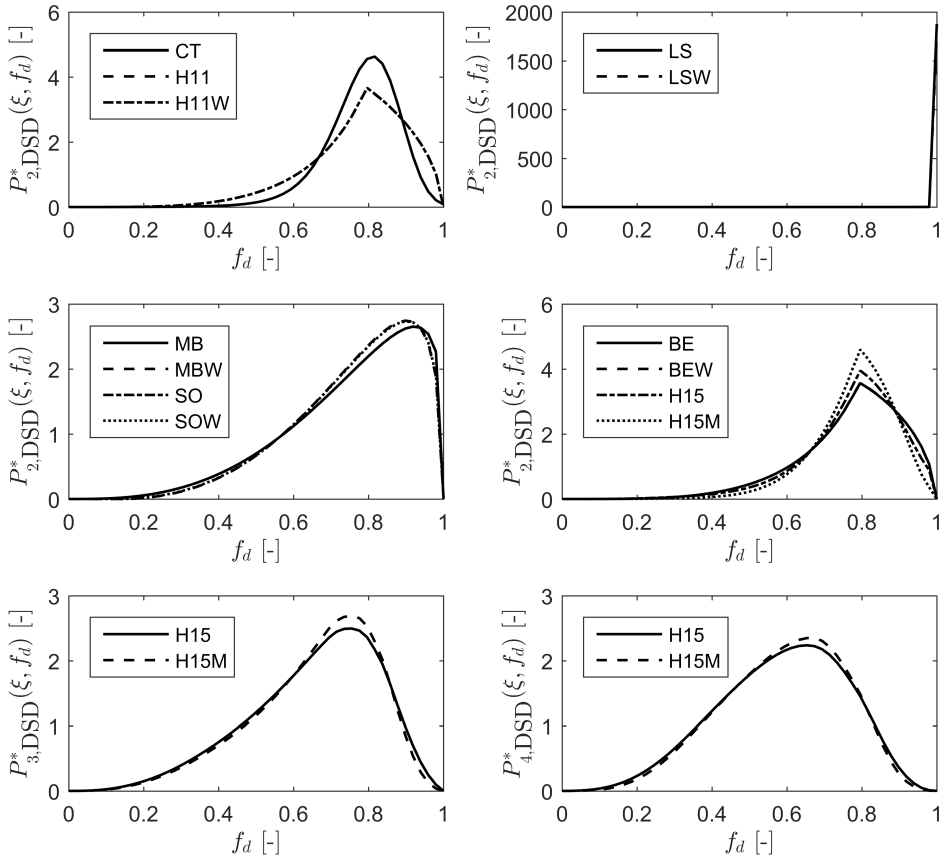

Figure 5.17: Probability density functions for the air-water system with a parent bubble diameter of 20 mm. The integral scale L has been set to 0.1 m in the wide energy spectrum models, and a dissipation rate of 1 W/kg has been used.

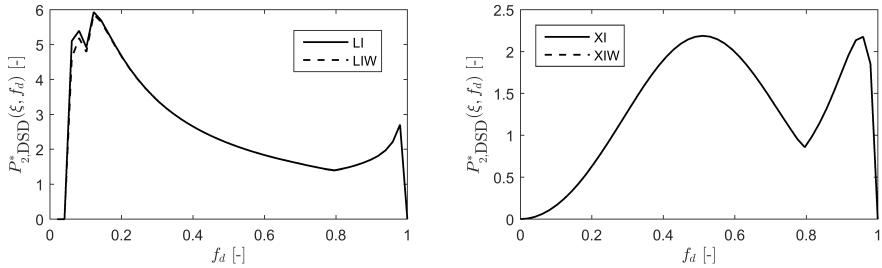

Figure 5.18: Probability density functions of Liao et al. (2015) and Xing et al. (2015) for the air-water system with a parent bubble diameter of 20 mm. The integral scale L has been set to 0.1 m in the wide energy spectrum models, and a dissipation rate of 1 W/kg has been used.

The probability density functions in the air-water system give similar results as in the petroleum-water system II. The original and extended versions of all closures give almost equal probability density functions, indicating that the energy spectrum has little effect on the redistribution. The sensitivity analysis in appendix A.2.1 confirms this. The effect of the integral scale is, however, slightly larger in the air-water system than in the petroleum-water system II.

5.5 Population Balance Test Case

In this section, mass density functions from the PBE test case using the air-water system and petroleum-water system I are given. The toluene-water and dodecane-water system is not included, due to their similarity to the petroleum-water system. A numerical grid consisting of 15 points in the z-direction and 50 points in the ξ-direction was used. Simulations involving the closure of Han et al. (2015) were performed with 20 points in the ξ-direction, due to the high computational demand of the model.

5.5.1 Air-Water System

In Figure 5.19, the mass density functions from the PBE test case using the original and extended versions of Han et al. (2015) and Becker et al. (2014) are shown.

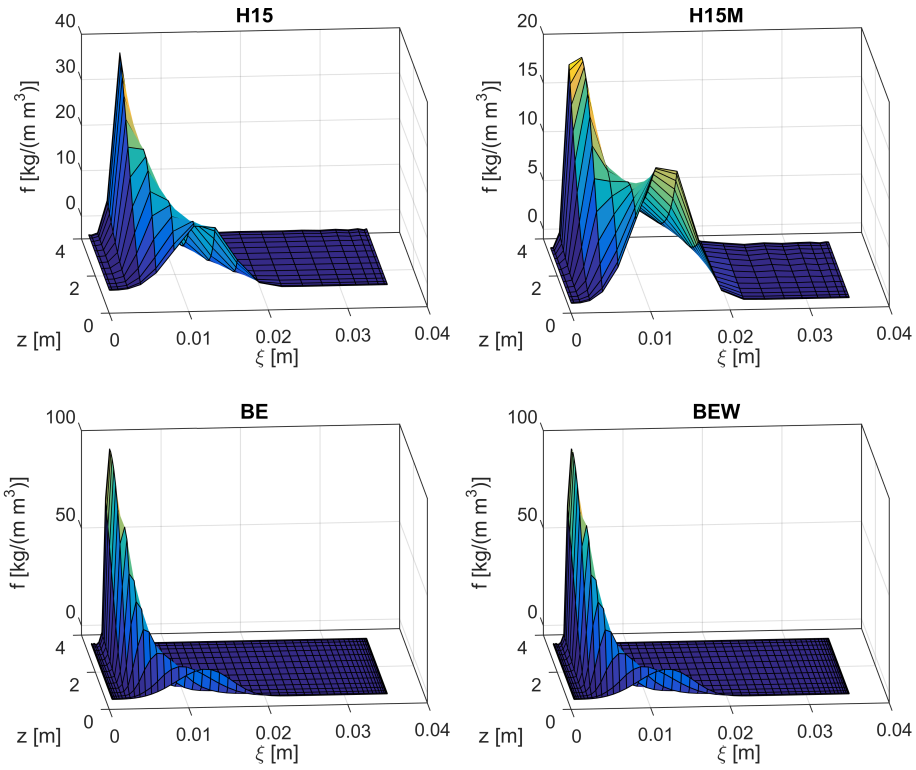

Figure 5.19: Mass density functions from the PBE test case using the original and extended versions of Han et al. (2015) and Becker et al. (2014). Physical parameters from the air-water system with ε = 1 W/kg were used, and the integral scale L was set to 0.1 m. To avoid numerical issues, the breakage frequency of the original and modified model of Han et al. (2015) was scaled with a factor of 0.1 and 1e-6, respectively.

The mass density functions generated by using the models of Han et al. (2015) and Becker et al. (2014) as closures in the PBE show similar trends. The fluid particles contained in the initial profile break into smaller particles, shifting the mass density functions toward smaller particle sizes. Due to the lack of coalescence terms, this effect can only be counteracted by the pressure drop-induced growth of fluid particles. It is evident from Figure 5.19 that the effect of breakage is larger than the growth effect. The height of the mass density function profiles increases because the mass contained in the initial profile must be redistributed within a narrower size range. Notice that the peak of the profiles is not located at the smallest particle size. This is a result of the capillary breakage constraint which is included in both the model of Han et al. (2015) and Becker et al. (2014). This constraint causes the energy required for breakage to increase asymptotically towards infinity as the daughter particle sizes approach zero, and therefore creates a lower bound for the size of the fluid particles.

The difference between the profiles generated by the original and extended model of

Becker et al. (2014) is small. The two versions will produce similar results if the considered system is located within the inertial subrange of turbulence. The integral scale Reynolds number of the air-water system with a dissipation rate of 1 W/kg is approximately 46 000, which is relatively high. As discussed in section 1.3, the inertial subrange of the air-water system is wide at high Reynolds numbers. Therefore, it is likely that the considered system is located in the inertial subrange. The model of Becker et al. (2014) provides a plausible mass density function without scaling the breakage frequency, making it suitable as a closure in the PBE.

The mass density profiles of Han et al. (2015) seem similar, but it is important to notice that the breakage frequencies have been scaled down in order to avoid numerical difficulties. A large breakage frequency leads to a steep mass density function, which can cause problems when the equation system is solved. The original and extended version were scaled by a factor of 0.1 and 1e-6, respectively. As previously discussed in section 5.3, the extended version of Han et al. (2015) predicts a breakage frequency that is several orders of magnitude larger than the available experimental data. It is therefore unlikely that the extended model of Han et al. (2015) is physically realistic, which makes it ineligible as a PBE closure.

Both models of Han et al. (2015) and the extended model of Becker et al. (2014) apply the wide turbulent energy spectrum, and are therefore affected by changes in the integral scale. In appendix A.3.1, it is seen that the mass density function profiles of the wide spectrum models when L is 1 m are very similar to the ones obtained with the integral scale set to 0.1 m. This is consistent with the results for the breakage frequencies and probability density functions, and indicates that the air-water system with an integral scale of 1 m is also located in the inertial subrange of turbulence. With an integral scale of 0.001 m, the mass density function of Becker et al. (2014) was almost identical to the initial profile throughout the column. This value of the integral scale shifts the system to the dissipation subrange, where the breakage frequency is very low.

The original model of Han et al. (2015) was very sensitive towards integral scales in the inertial subrange. When the integral scale was set to 0.001 m, the mass density function diverged. As a consequence of this, the value was set to 0.01 m, which gave a plausible profile. If the original model of Han et al. (2015) is to be used as a closure in the PBE, care must be taken to accurately estimate the integral scale. The extended model of Han et al. (2015) was more robust for low integral scales, giving a mass density function similar to the wide model of Becker et al. (2014) for $L = 0.001$ m. A possible explanation for the differences between the original and extended model of Han et al. (2015) is that the energy spectrum in the original model is not consistent, and only valid for infinite Reynolds numbers. When the integral scale is small, the Reynolds number is small, which might cause problems when the energy spectrum is only valid for very turbulent systems.

In Figure 5.20, the mass density functions from the PBE test case using the original and extended versions of Coulaloglou and Tavlarides (1977), Luo and Svendsen (1996) and Han et al. (2011) are shown.

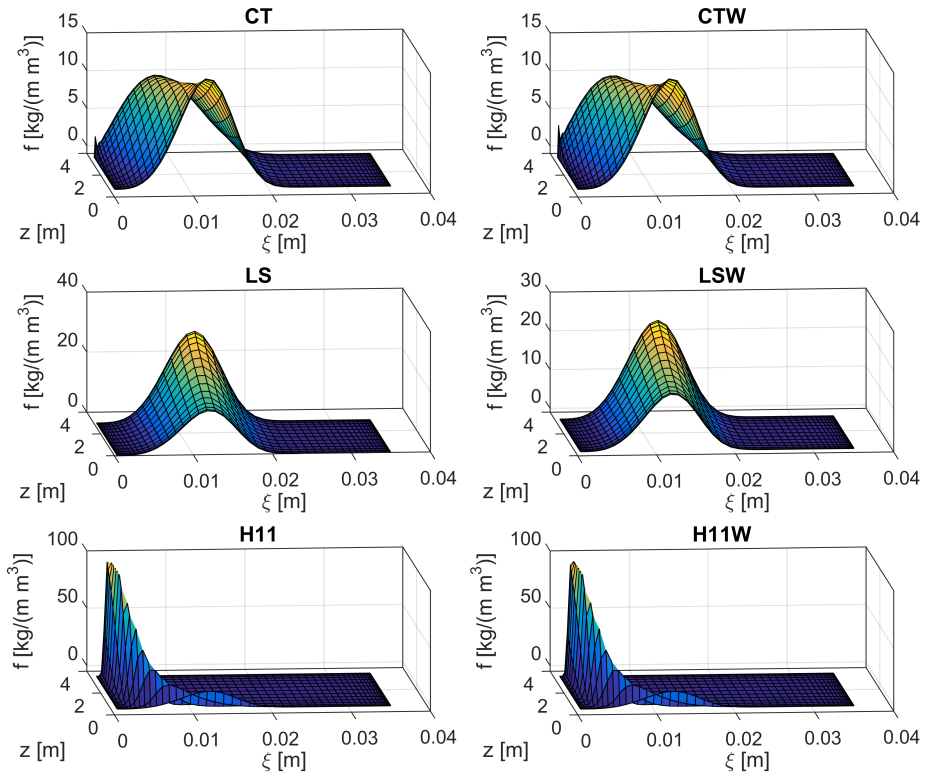

Figure 5.20: Mass density functions from the PBE test case using the original and extended versions of Coulaloglou and Tavlarides (1977), Luo and Svendsen (1996) and Han et al. (2011). Physical parameters from the air-water system with ε = 1 W/kg were used, and the integral scale L was set to 0.1 m. To avoid numerical issues, the breakage frequency of the original and extended model of Coulaloglou and Tavlarides (1977) was scaled with a factor of 0.003 and 0.0025, respectively. The breakage frequency of the original and extended model of Luo and Svendsen (1996) was scaled with a factor of 0.001.

Similarly to the closure of Han et al. (2015), the breakage frequency of both versions of Coulaloglou and Tavlarides (1977) and Luo and Svendsen (1996) was scaled down in order to avoid problems in the solution of the mass density function. Neither of these models contain a capillary constraint, which results in accumulation of bubbles at the smallest particle size if the breakage frequency is sufficiently high. This effect can be seen in the mass density functions from Coulaloglou and Tavlarides (1977), where a small peak is located at the smallest ξ and largest z. For high breakage frequencies, the mass density profiles would eventually become a single peak next to the z-axis. In the simulations involving Luo and Svendsen (1996), the mass density profiles become more wide as z increases, even though the profiles become higher. This is due to the fact that the closure is not volume conserving, and mass is generated in every breakage process.

The profiles generated by Han et al. (2011) strongly resemble the profiles of Becker et al.

(2014) from 5.19. This model includes the capillary constraint, causing accumulation of particles at a ξ-value larger than ξ_{min}. The mass density function in plausible, and no scaling of the breakage frequency is necessary. The mass density functions generated by the original and extended models are quite similar, because the air-water system considered in the test case is likely in the inertial subrange of turbulence. As shown in appendix A.3.1, the mass density function profiles with an integral scale of 1 m were also for these models very similar to the ones generated with an integral scale of 0.1 m. When L was set to 0.001 m, the peaks of the mass density profiles were lower, due to the reduced breakage frequency in the dissipation subrange compared to the inertial subrange.

In Figure 5.21, the mass density functions from the PBE test case using the original and extended versions of Martínez-Bazán et al. and Solsvik et al. (2013) are shown.

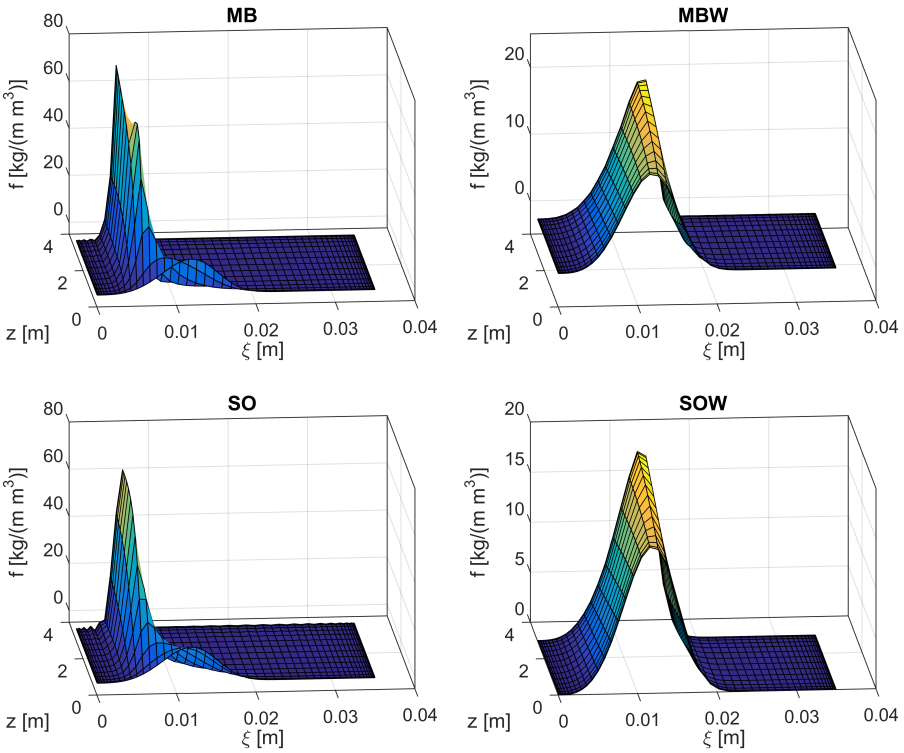

Figure 5.21: Mass density functions from the PBE test case using the original and extended versions of Martínez-Bazán et al. and Solsvik et al. (2013). Physical parameters from the air-water system with ε = 1 W/kg were used, and the integral scale L was set to 0.1 m.

The mass density profiles of the original models of Martínez-Bazán et al. and Solsvik et al. (2013) resemble the profiles obtained using Han et al. (2011) and Becker et al. (2014). A critical diameter, found by equating the deforming and restoring stresses, is applied in these models. If a fluid particle exceeds this critical diameter, it will break. Although it is not directly a capillary constraint, it has a similar effect on the mass density function

profiles, because the fluid particles in a breakage dominated case will accumulate around ξ_{crit}, not at ξ_{min}. Therefore, the profiles are similar to the profiles of Han et al. (2011) and Becker et al. (2014).

It is important to remember that the closures of Martínez-Bazán et al. and Solsvik et al. (2013) were modified by introducing a breakage probability, as explained in section 3.2. Without this modification, the breakage frequency profiles become too steep, leading to a diverging solution of the mass density function. However, when this modification is included, the models produce plausible solutions of the PBE without further scaling.

Unlike the other models, the extended version of Martínez-Bazán et al. and Solsvik et al. (2013) do not produce similar results as the inertial range models. The reason is that when the wide structure function is used, the calculation of ξ_{crit} changes. For the inertial range models, the critical diameter is 0.0041 m, which is smaller than most of the ξ values of the initial profile. This means that most of the particles contained within the initial profile will break. For the wide energy spectrum models, the critical diameter is 0.01 m, which is approximately in the middle of where the initial profile is located. Therefore, not all of the initially present fluid particles can undergo breakage, and the peak of the mass density function is not as high as in the inertial case.

As can be seen in appendix A.3.1, the mass density function profiles are very similar when the integral scale is 1 m and 0.1 m. However, when the integral scale is set to 0.001 m, the extended model of Martínez-Bazán et al. and Solsvik et al. (2013) gives the initial mass density function throughout the whole column. Once again, the explanation is the value of ξ_{crit}. When $L = 0.001$ m, the value of ξ_{crit} becomes approximately 0.056 m, which is higher than the maximum value of the initial profile. Therefore, none of the particles contained in the initial profile can undergo breakage, and only a slight change in the mass density function as a result of growth takes place.

In Figure 5.22, the mass density functions from the PBE test case using the closure of Liao et al. (2015) and Xing et al. (2015) are shown.

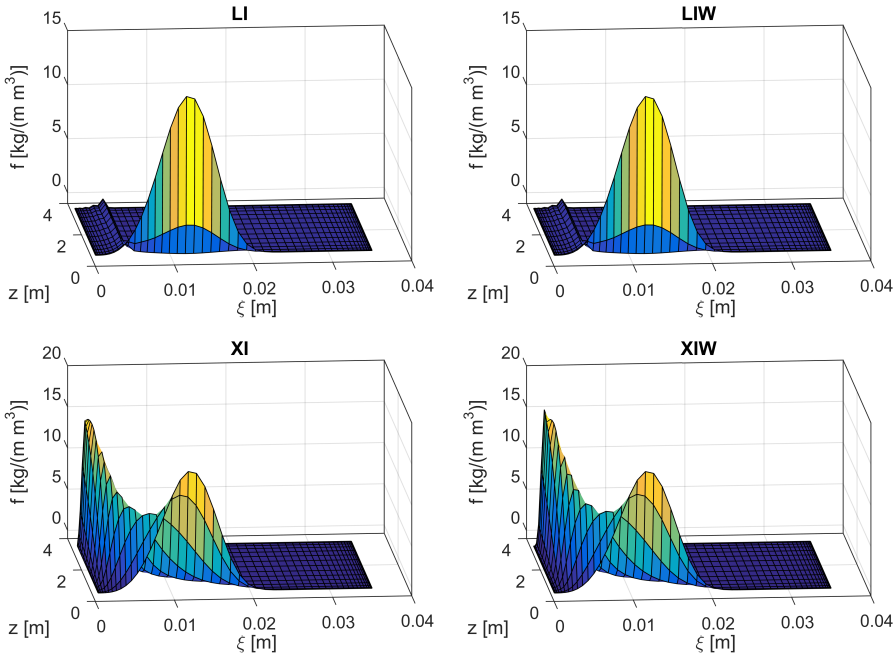

Figure 5.22: Mass density functions from the PBE test case using the original and extended versions of Liao et al. (2015) and Xing et al. (2015). Physical parameters from the air-water system with ε = 1 W/kg were used, and the integral scale L was set to 0.1 m.

The mass density profiles generated by using the model of Liao et al. (2015) as a closure in the PBE quickly approach zero due to the non-conserving nature of the model. Naturally, this makes the model of Liao et al. (2015) unsuitable as a closure in the PBE. The profiles generated by Xing et al. (2015) are also not physically realistic. Due to the volume conserving error of this model, the peak of the mass density function is not as high as it should be. Notice that the particles accumulate at a particle size larger than ξ_{min}, due to the capillary constraint included in Xing et al. (2015). The results from the sensitivity analysis in appendix A.3.1 are difficult to interpret due to the conserving error of the models. Before they can be applied as closures in the PBE, the closures must be modified to give much smaller conserving errors than the current implementations.

5.5.2 Petroleum-Water System I

In Figure 5.23, the mass density functions from the PBE test case using the original and extended versions of Han et al. (2015) and Becker et al. (2014) are shown.

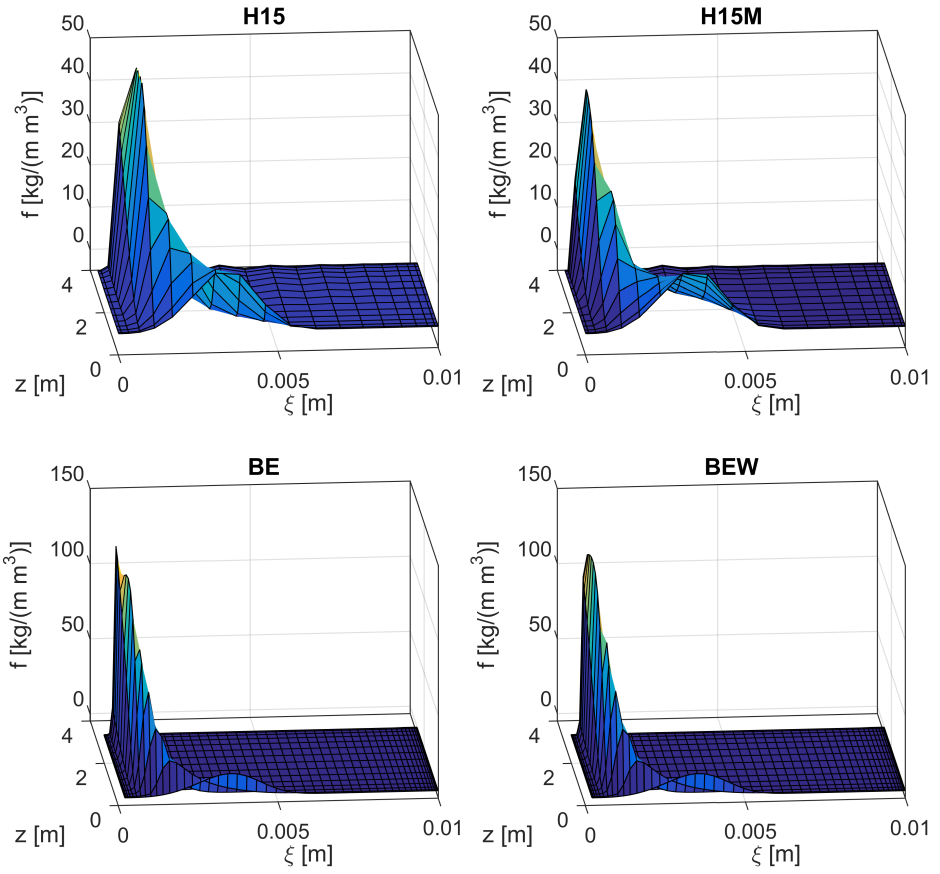

Figure 5.23: Mass density functions from the PBE test case using the original and extended versions of Han et al. (2015) and Becker et al. (2014). Physical parameters from the petroleum-water system I were used, and the integral scale L was set to 0.1 m. To avoid numerical issues, the breakage frequency of the original and modified model of Han et al. (2015) was scaled with a factor of 0.1 and 1e-7, respectively.

The trends of the mass density functions are very similar to the air-water system. The breakage frequency of the extended version of Han et al. (2015) was scaled with a factor of 1e-7, which is lower than the factor of 1e-6 used in the air-water system. This is due to the fact that the breakage frequency in the petroleum-water system I is higher than in the air-water system. The sensitivity analysis in appendix A.3.2 gave similar results as for the air-water system. An integral scale of 1 m likely gives a system within the inertial

subrange, because the mass density profiles are very similar to the ones generated with an integral scale of 0.1 m. Using an integral scale of 0.001 m gave profiles that resembled the initial profile, because the breakage frequency is lower in the dissipation subrange.

In Figure 5.24, the mass density functions from the PBE test case using the original and extended versions of Coulaloglou and Tavlarides (1977), Luo and Svendsen (1996) and Han et al. (2011) are shown.

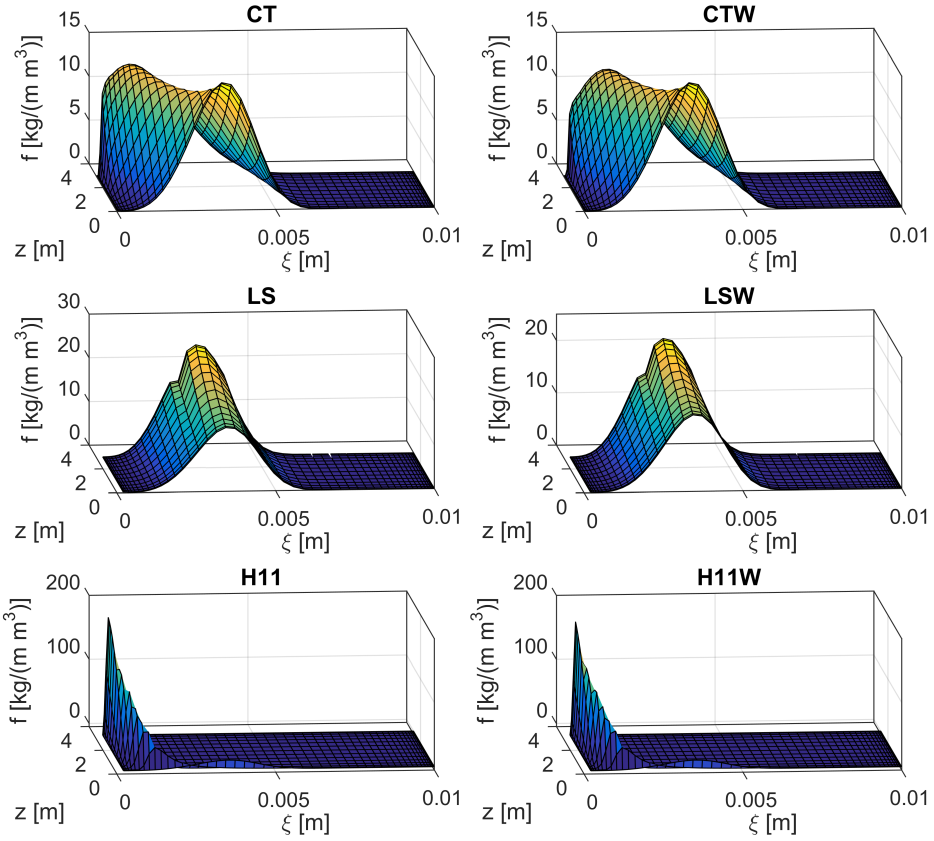

Figure 5.24: Mass density functions from the PBE test case using the original and extended versions of Coulaloglou and Tavlarides (1977), Luo and Svendsen (1996) and Han et al. (2011). Physical parameters from the petroleum-water system I were used, and the integral scale L was set to 0.1 m. To avoid numerical issues, the breakage frequency of the original and extended model of Coulaloglou and Tavlarides (1977) was scaled with a factor of 0.008 and 0.005, respectively. The breakage frequency of the original and extended model of Luo and Svendsen (1996) was scaled with a factor of 0.001.

The mass density profiles are also in this case similar to the air-water system. The profile generated by Luo and Svendsen (1996) widens even though the height increases, which is not physically realistic. The model is not volume conserving, and because mass is

generated in every breakage process, more mass must be distributed underneath the mass density profile as z increases. In appendix A.3.2, the sensitivity analysis shows that the mass density profiles of the wide spectrum models depends similarly on the integral scale as in the air-water system.

In Figure 5.25, the mass density functions from the PBE test case using the original and extended versions of Martínez-Bazán et al. and Solsvik et al. (2013) are shown. Figure 5.26 shows the mass density functions from the PBE test case using the original and extended versions of Liao et al. (2015) and Xing et al. (2015). The mass density profiles are very similar to the ones generated in the air-water system, and the sensitivity analysis in appendix A.3.2 demonstrates the same dependency on the integral scale as in the air-water system. Notice that the models of Liao et al. (2015) and Xing et al. (2015) give non-physical mass density profiles, due to the large conserving errors of these models.

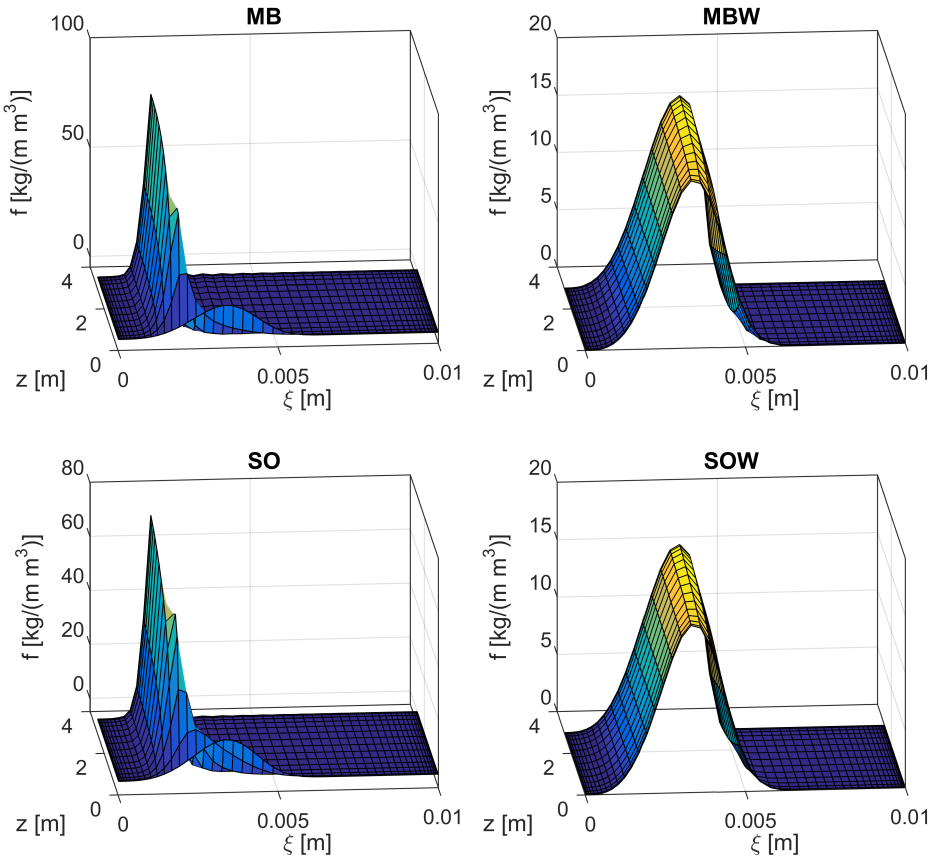

Figure 5.25: Mass density functions from the PBE test case using the original and extended versions of Martínez-Bazán et al. and Solsvik et al. (2013). Physical parameters from the petroleum-water system I were used, and the integral scale L was set to 0.1 m.

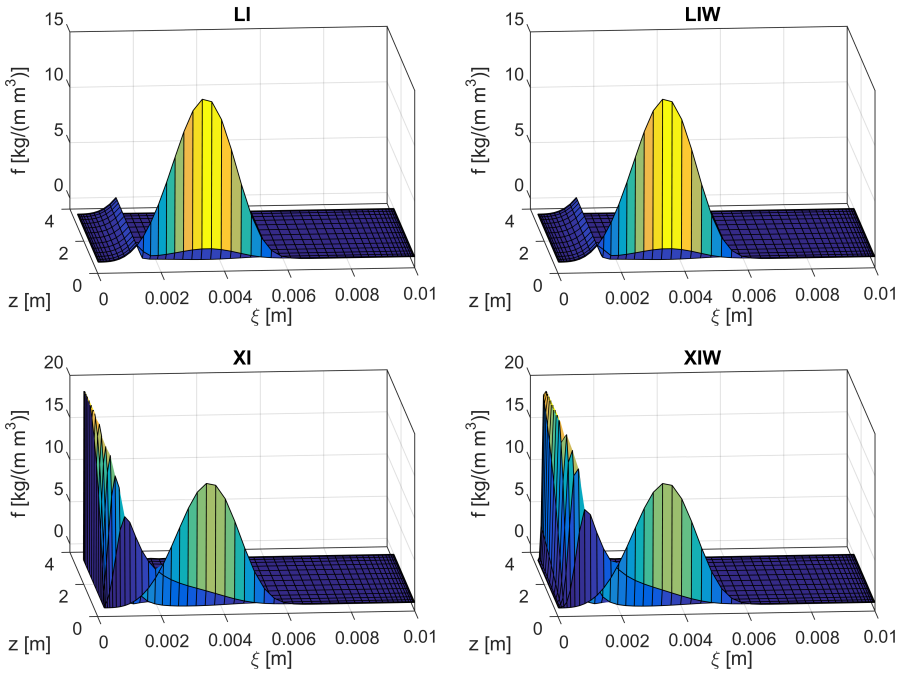

Figure 5.26: Mass density functions from the PBE test case using the original and extended versions of Liao et al. (2015) and Xing et al. (2015). Physical parameters from the petroleum-water system I were used, and the integral scale L was set to 0.1 m.

5.6 Conclusions and Additional Remarks

The majority of the studied closures were both volume and number conserving in their original and extended form at 20 and 100 collocation points. Being volume and number conserving is an important fundamental property of a breakage closure, and is a requirement in order to be suitable as a constitutive equation in the PBE. The original model of Han et al. (2015) was not conserving at 20 collocation points, and should therefore not be applied when it is important to use few numerical points in the simulation. The steep redistribution function of Luo and Svendsen (1996) leads to weak volume conserving properties for both the original and extended version. Further analysis showed that this closure needed approximately 500 collocation points to give a volume conserving error of less than 10 %. Both versions of Liao et al. (2015) and Xing et al. (2015) also demonstrated unacceptable conserving properties, making them ineligible as closures in the PBE.

The original and extended versions of the closures required similar computational times. In this work the semi-empirical structure function of Sawford and Hunt (1986) was applied. The computational demand of this function is similar to the inertial subrange structure function of Kolmogorov, causing the extended models to be as efficient as the original

ones. The model of Han et al. (2015) was clearly the most computationally demanding closure, taking around 1500 times longer than most of the other closures. This makes the model of Han et al. (2015) suitable only for simple systems, e.g. where few particle sizes are considered. The closure of Han et al. (2011) took approximately four times longer than the other models, which used around 0.01 seconds each time they were called upon.

In the air-water system, most of the models failed to predict the breakage frequencies measured by Wilkinson et al. (1993). The extended model of Martínez-Bazán et al. (1999a) achieved the best agreement with the experimental data, especially for the largest particle sizes in the experimental data series. In the petroleum-water system I and toluene-water system, the original model of Coulaloglou and Tavlarides (1977) provided the best fit to the experimental data of Maaß and Kraume (2012). It should, however, be kept in mind that this model has adjustable parameters that are tuned specifically for each system it is applied to. It is therefore easier to achieve a good agreement with the experimental data. Both models of Luo and Svendsen (1996), Han et al. (2011), Liao et al. (2015) and Xing et al. (2015) were also close to the experimental data, particularly for the largest particle sizes in the experimental data. In the dodecane-water system, best fit to the experimental data of Andersson and Andersson (2006b) was achieved by the original model of Han et al. (2015) and both models of Han et al. (2011) and Becker et al. (2014). In all of the studied systems, the extended model of Han et al. (2015) predicted breakage frequencies that were several orders of magnitude higher than the experimental data and the other models.

The probability density functions of most of the studied closures are Λ-shaped, meaning that the most likely scenario is equal breakage. The U-shaped probability density function of Luo and Svendsen (1996) favors uneven breakage, and for the M-shaped probability density functions of Liao et al. (2015) and Xing et al. (2015) the most probable scenario is between those of the Λ and U-shaped functions. Most of the breakage closures fit reasonably well with the experimental data of Zaccone et al. (2007) for a parent droplet with a diameter of 2 mm, although none of the models provided an excellent fit. Both versions of Luo and Svendsen (1996) and the extended model of Martínez-Bazán et al. (2010) and Solsvik et al. (2013) did not agree well with the experimental data. For decreasing mother particle size, the binary redistribution models were not able to predict the experimental data as well as for the largest parent size. The probability density functions from the air-water system were similar to the petroleum-water system II.

The mass density functions generated by applying the studied closures as constitutive equations in the PBE test case were quite similar in the air-water and petroleum-water system I. As no experimental data was available, it was most important that the closures contributed to plausible mass density profiles without causing numerical difficulties. This was achieved by Becker et al. (2014), the original model of Han et al. (2015), Coulaloglou and Tavlarides (1977), Han et al. (2011), Martínez-Bazán et al. and Solsvik et al. (2013). In order to avoid numerical difficulties and oscillations in the mass density profiles, the breakage frequency of some of the models had to be scaled down. This effect was most clear for the extended model of Han et al. (2015), which had to be scaled with factors of 1e-6 and 1e-7. It should also be mentioned that the closures of Martínez-Bazán et al. and Solsvik et al. (2013) were modified by introducing a breakage probability, as explained in section 3.2. Without this modification, the solution of the mass density function diverged.

Luo and Svendsen (1996), Liao et al. (2015) and Xing et al. (2015) produced non-physical profiles of the mass density function, due to the conserving errors of these closures. Before they can be applied as closures in the PBE, these models must be modified to reduce the conserving errors.

The sensitivity analysis given in appendix A showed that the integral scale has the same effect on the breakage frequencies and mass density profiles. The probability density functions were only slightly affected by changes in the integral scale. This can be explained by the fact that most of the probability density functions are phenomenological, and therefore calculated from a fraction. As a result of this, the effect of the integral scale might be marginalized. For integral scales of 1 m and 0.1 m, the wide spectrum models gave similar results as the inertial range models, indicating that for these integral scales, the studied systems are located within the inertial subrange of turbulence. For integral scales of 0.01 and 0.001 m, however, the predicted breakage frequency was reduced, because the systems were most likely shifted to the dissipation subrange. Due to the sensitivity towards the integral scale, the wide energy spectrum versions of the closures should be used. This ensures that the closures are always applicable, regardless of system conditions and degree of turbulence.

The sensitivity analysis indicates that to ensure that the breakage closures are valid to all systems they are applied to, the wide versions of the breakage closures should be applied in all cases.

From the evaluation, it can be concluded that the models of Coulaloglou and Tavlarides (1977), Han et al. (2011), Becker et al. (2014) and the model of Martínez-Bazán et al. with the introduced breakage probability are most suitable as closures in the PBE. They are computationally efficient, volume and number conserving, fit at least one of the experimental data series acceptably well and give plausible solutions of the PBE test case. The wide energy spectrum versions of these closures should be applied, because they are valid in all ranges of turbulence.

A weakness of the model of Coulaloglou and Tavlarides (1977) is that it is not phenomenological, and has adjustable parameters that must be adjusted specifically for each system. Additionally, the breakage frequency of this model was scaled down in the PBE test case in order to avoid numerical difficulties due to the non-physical scenario of all particles accumulating at the smallest particle size. Including the capillary constraint in the breakage frequency avoids this issue, and therefore seems to be an important criterion. It is important to notice that none of the studied closures predict the number of daughters formed in the breakage process as a function of system parameters and mother particle size. It is unrealistic that an *a priori* assumption of how many daughters are formed will be correct for all systems and particle sizes. Therefore, introducing a relation for the number of daughters has the potential of making the closures significantly more physically realistic.

Chapter 6

Introducing a Relation for the Number of Daughters

As mentioned in section 5.6, the closures studied in this work make *a priori* assumptions about the number of daughters formed in the breakage process. It is likely that this quantity will vary with the system conditions and the size of the parent particle. Therefore, calculating the number of daughters based on the system conditions and parent particle size has the potential of making the closures more physically realistic. However, introducing such a relation involves some challenges, and the modifications must be consistent with the framework to which they are made. In this chapter, the challenges that arise when introducing a relation for the number of daughters into the breakage closures will be briefly discussed.

6.1 Excisting Relations for the Number of Daughters

In the review of Solsvik et al. (2013), two empirical relations from the literature for the number of daughters were presented. The simplest of the two relations was given by Lee et al. (1987a,b):

$$\nu\left(V_\xi\right) = 2 + c_1\left(V_\xi\right)^{c_2} \tag{6.1}$$

Where c_1 and c_2 was set to 10.0 and 0.5, respectively. On a diameter basis, this can be written as:

$$\nu\left(\xi\right) = 2 + c_3\xi^{c_4} \tag{6.2}$$

Where the new constants c_3 and c_4 become 7.236 and 1.5, respectively.

The other relation was given by Kuriyama et al. (1995) for agitated vessels with high-viscosity liquid droplets[1]:

$$\nu\left(\xi\right) = c_1 \left(\frac{\mu_d}{\mu_c}\right)^{1/2} \left[\mathrm{Re}_\mathrm{D}^2 \mathrm{We}_\mathrm{D} \left(\frac{\rho_d}{\rho_c}\right) \left(\frac{\mu_c}{\mu_d}\right)^2 \left(\frac{\xi}{D}\right)^{13/3}\right]^{0.14} \tag{6.3}$$

Here, Re_D and We_D is the Reynolds and Weber number for the agitation system. They are given as $D^2 n_r \rho_c / \mu_c$ and $\rho_c n_r^2 D^3 / \sigma$, respectively, where n_r and D is the rotational speed and diameter of the impeller. The constant c_1 was given as 0.68.

As there are few excisting relations for the number of daughters in the literature, new relations must be developed. In general, there are two main alternatives for developing such relations. One possibility is to apply theoretical principles to develop a predictive model without empirical parameters that predicts the number of daughters. However, it might be difficult to develop a relation of this type that is accurate for several systems and conditions, without the possibility of adjusting parameters to fit available experimental data. The other alternative is to develop empirical relations solely based on experimental data. Models developed in this manner will most likely give better agreement with experimental data, but a relation for each type of system must probably be developed, and the relations must be tuned to fit each specific system, which requires time and effort.

Another aspect that should be considered when developing relations for the number of daughters formed in a breakage process is the definition of the breakup event. Most of the experiments on single fluid particle breakage in the literature, e.g. Maaß and Kraume (2012), apply the *initial breakup* definition of the breakage event. By this definition, the breakup event ends at the initial breakup, and no fragmentation after this point is considered. However, as discussed in the recent article of Solsvik et al. (2016a), the breakup event can also be defined as a *breakage cascade*. Using this definition, the breakup event is considered as a sequence of breakups. The breakup event does not end after the initial breakup, but follows the fluid particles until a final population is formed. The two definitions of the breakage event lead to different interpretations of the experimental data, and therefore result in different breakage times and daughter size distributions.

6.2 Example: Extension of Martínez-Bazán et al. to Ternary Breakage

To illustrate the challenges that arise when a relation for the number of daughters is introduced, the model of Martínez-Bazán et al., which was one of the most promising models in the evaluation, will be extended to ternary breakage. The breakage frequency of the model is only a function of the parent size, and is therefore not affected by the extension to ternary breakage. The probability density of forming N daughters from a parent particle of size ξ is, by following the article of Martínez-Bazán et al. (2010), given as a product of

[1] The expression of $\nu\left(\xi\right)$ given in Solsvik et al. (2013) lacks the exponent of 13/3.

the excess stresses associated with each daughter size:

$$P_{\mathrm{DSD}}\left(V_\xi, V_{\omega,1}, ..., V_{\omega,N-1}\right) \propto \prod_{i=1}^{N} \left[\Delta\sigma_{ti}\left(\xi, V_{\omega,i}\right)\right] \tag{6.4}$$

When N daughters are formed, there are $N-1$ independent daughter variables. The volume of the final daughter is given as:

$$V_{\omega,N} = V_\xi - \left(\sum_{j=1}^{N-1} V_{\omega,j}\right) \tag{6.5}$$

For ternary breakage, i.e. $N = 3$, the expression for the probability density function becomes:

$$P_{\mathrm{DSD}}\left(V_\xi, V_{\omega,1}, V_{\omega,2}\right) \propto \left[\Delta\sigma_{t1}\left(\xi, V_{\omega,1}\right)\right]\left[\Delta\sigma_{t2}\left(\xi, V_{\omega,2}\right)\right]\left[\Delta\sigma_{t3}\left(\xi, V_{\omega,3}\right)\right] \tag{6.6}$$

Where $V_{\omega,3} = V_\xi - V_{\omega,1} - V_{\omega,2}$. The excess stresses are given as the difference between the deforming stresses evaluated in the daughter size and the surface restoring stress acting on the parent particle:

$$\Delta\sigma_{t1}\left(V_\xi, V_{\omega,1}\right) = \frac{1}{2}\rho_c\delta v^2\overline{\left(\frac{6V_{\omega,1}}{\pi}\right)^{1/3}} - \frac{6\sigma}{V_\xi^{1/3}}\left(\frac{\pi}{6}\right)^{1/3} \tag{6.7}$$

$$\Delta\sigma_{t2}\left(V_\xi, V_{\omega,2}\right) = \frac{1}{2}\rho_c\delta v^2\overline{\left(\frac{6V_{\omega,2}}{\pi}\right)^{1/3}} - \frac{6\sigma}{V_\xi^{1/3}}\left(\frac{\pi}{6}\right)^{1/3} \tag{6.8}$$

$$\Delta\sigma_{t3}\left(V_\xi, V_{\omega,3}\right) = \frac{1}{2}\rho_c\delta v^2\overline{\left(\frac{6V_{\omega,3}}{\pi}\right)^{1/3}} - \frac{6\sigma}{V_\xi^{1/3}}\left(\frac{\pi}{6}\right)^{1/3} \tag{6.9}$$

The probability density function on a volume basis is normalized by the integral of the excess stresses over all independent daughter sizes:

$$P_{\mathrm{DSD}}\left(V_\xi, V_{\omega,1}, V_{\omega,2}\right) = \frac{\left[\Delta\sigma_{t1}\right]\left[\Delta\sigma_{t2}\right]\left[\Delta\sigma_{t3}\right]}{V_\xi \int_{V_{\min}}^{V_{\omega,1,\max}} \int_{V_{\min}}^{V_{\omega,2,\max}} \left[\Delta\sigma_{t1}\right]\left[\Delta\sigma_{t2}\right]\left[\Delta\sigma_{t3}\right] \mathrm{d}V_{\omega,2}\mathrm{d}V_{\omega,1}} \tag{6.10}$$

The maximum value of the second independent daughter size is restricted by the value of the first. This can be written as:

$$V_{\omega,2,\max} = V_\xi - V_{\omega,1} - V_{\min} \tag{6.11}$$

Converting the probability density function to a redistribution density function is easily achieved by multiplying with the predicted number of daughters:

$$h_{\mathrm{DSD}}\left(V_\xi, V_{\omega,1}, V_{\omega,2}\right) = \nu\left(V_\xi\right) \times P_{\mathrm{DSD}}\left(V_\xi, V_{\omega,1}, V_{\omega,2}\right) \tag{6.12}$$

The redistribution density function is a part of the breakage birth integral in the PBE. The breakage birth term was previously given in section 4.4 as:

$$B_B\left(\xi, z\right) = \xi^3 \int_\xi^{\xi_{\max}} h_{\mathrm{DSD}}\left(\xi, \zeta\right) b\left(\zeta\right) \frac{f_{d,m}\left(\zeta, z\right)}{\zeta^3} \mathrm{d}\zeta \tag{6.13}$$

Notice that in the PBE, the redistribution density function contains only two arguments, the parent size and one daughter size. Therefore, the function in equation (6.12) must be manipulated to give a redistribution density function that can be used in the population balance. By integrating the function in equation (6.12) over all independent daughter sizes except one, the correct form of the redistribution density function is obtained. This gives an additional integral, that for N daughters will consist of $N-2$ nested integrals.

$$h_{\mathrm{DSD}}\left(V_{\xi}, V_{\omega,1}\right) = \int_{V_{\mathrm{min}}}^{V_{\omega,2,\mathrm{max}}} h_{\mathrm{DSD}}\left(V_{\xi}, V_{\omega,1}, V_{\omega,2}\right) \mathrm{d}V_{\omega,2} \tag{6.14}$$

It is evident from the above example that the number of daughters must be an integer. A relation for the mean number of daughters might return a decimal value. In this case, the number of daughters must be rounded off before it is used in a phenomenological framework like that of Martínez-Bazán et al.

6.3 Potential Challenges

From the above example it is seen that the model of Martínez-Bazán et al. becomes significantly more complex than the original binary model when even the simplest form of multiple breakage is considered. The comparison of computational times of the studied closures from section 5.2 showed that the model of Han et al. (2015), which contains a triple integral, was approximately 1500 times more computationally demanding than the other closures. Therefore, it is likely that a phenomenological model considering more than four or five daughters will be too computationally demanding to be suitable as a closure in the PBE. A relation for the number of daughters will probably, for some conditions and parent particle sizes, return more than four or five daughters. If the formation of 10 daughters is predicted, the normalization in the model of Martínez-Bazán et al. will consist of 9 nested integrals. In such cases, it is evident that simplifications must be applied to reduce the model complexity. Another challenge is that the closure must be adaptive, i.e. able to deal with any number of daughters that is predicted for the given parent particle size and system conditions.

6.4 Reducing the Model Complexity

When the predicted number of daughters becomes large, the models become complex, and the computational time increases significantly. Thus, to make it possible to use the closures as constitutive equations in the PBE, attempts should be made to make them simpler. As the model complexity is caused by the large number of integrals, such attempts should focus on either reducing the number of integrals or finding more efficient methods for evaluating them.

One alternative for efficient evaluation of the integrals is to find analytical solutions. If this is possible, it is only necessary to perform the integration once for every number of

daughters, after which the analytical solutions can be used. However, finding analytical solutions might require complex mathematics and it is uncertain whether this is possible for the closures that are considered in this work. Another possibility for simplifying the models is to make assumptions about how the sizes of the daughter particles are related. Assuming that all daughters are equally sized will give one independent daughter variable, i.e. the same complexity as binary breakage.

Another possibility for reducing the model complexity is based on a novel classification of the daughter particles. Consider a breakage event that follows the *breakage cascade* definition of Solsvik et al. (2016a). A large number of daughters is formed, because the breakage event is made up of several sequential breakage processes. Instead of treating the daughter particles separately, they are divided into *groups* with a mean particle size and a certain number of particles. This concept takes advantage of the fact that several daughters are often formed within the same size range to reduce the number of daughter variables. An illustration of the concept is shown in Figure 6.1.

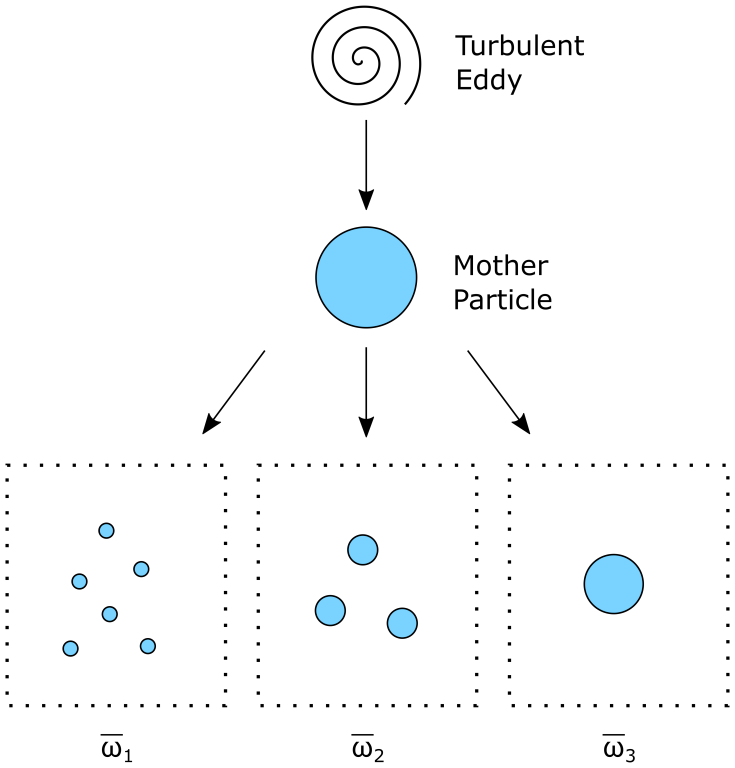

Figure 6.1: Sketch of a breakage process forming 10 daughters divided into three groups with mean diameters $\overline{\omega}_1$, $\overline{\omega}_2$ and $\overline{\omega}_3$.

Evidently, this procedure only works for breakage processes where several daughters of

approximately the same size are formed. It requires empirical relations for the number of *groups* that are formed, and the number of daughters in each group. By following the framework described in section 6.2, a redistribution density function for each group can be obtained. For the breakage process illustrated in Figure 6.1, the three groups require the evaluation of five, two and one integrals, respectively. This is most likely less computationally demanding than treating the whole daughter population at once, which would require the evaluation of nine nested integrals.

The redistribution density functions must be combined into one redistribution function that can be used in the breakage birth term in the PBE. This is not a trivial procedure, and care must be taken to ensure that the combined redistribution density function is volume conserving and that it conserves the number of daughters formed in the breakage process. For the process illustrated in Figure 6.1, the zeroth moment of the combined redistribution density function should return a value of 10.

Chapter 7

Conclusions and Recommendations for Further Work

In this thesis, a set of regularly used breakage closures from the literature were implemented and evaluated, to determine their suitability as constitutive equations in the population balance equation. Extended versions of the models were also included in the evaluation. The closures were evaluated with regard to computational time, conserving properties, ability to reproduce experimental data and performance as closures in a simplified PBE test case. Based on the evaluation, suggestions for further improvements of the closures were made.

7.1 Closure Evaluation

The majority of the studied closures were both volume and number conserving for both 20 and 100 collocation points. The conserving properties of the original model of Han et al. (2015) were sensitive to the number of collocation points, and this model should not be applied when it is necessary to use few numerical points in the simulation. Luo and Svendsen (1996), Liao et al. (2015) and Xing et al. (2015) demonstrated unacceptable conserving properties, making them ineligible as closures in the PBE. Due to its many integrals, the model of Han et al. (2015) was far more computationally demanding than the other models. This makes it unsuitable for complex simulations were the population balance is coupled with other equations or it is necessary to solve for many particle sizes. Most of the closures took around 0.01 seconds per iteration, which was approximately 1500 times faster than the model of Han et al. (2015).

None of the models were in acceptable agreement with all sets of experimental data. For the air-water system, the breakage frequency predicted by the extended model of

Martínez-Bazán et al. (1999a) provided the best fit with the data of Wilkinson et al. (1993). In the petroleum-water system I and toluene-water system, the semi-empirical model of Coulaloglou and Tavlarides (1977) agreed well with the breakage frequencies measured by Maaß and Kraume (2012). This model has adjustable parameters that are tuned specifically for each system, making it easier to achieve a good fit to the experimental data. For the petroleum-water system I and toluene-water system, both versions of Luo and Svendsen (1996), Han et al. (2011), Liao et al. (2015) and Xing et al. (2015) were acceptably close to the experimental data. In the dodecane-water system, it was the original model of Han et al. (2015), both models of Han et al. (2011) and Becker et al. (2014) that gave the best agreement with the data of Andersson and Andersson (2006b). Most of the closures fit reasonably well to the data of Zaccone et al. (2007) for probability density functions in the petroleum-water system II. However, none of the closures were able to give an excellent reproduction of the data. The U-shaped redistribution function of Luo and Svendsen (1996) was different from the Λ-shaped functions predicted by most other models, and agreed poorly with the experimental data. Additionally, the redistributions of the extended models of Martínez-Bazán et al. (2010) and Solsvik et al. (2013) did not agree well with the experimental data.

The mass density functions generated by applying Becker et al. (2014), Han et al. (2011), Martínez-Bazán et al. and Solsvik et al. (2013) as closures in the PBE test case were plausible and required no scaling of the breakage frequency. However, it is important to notice that the closure of Martínez-Bazán et al. and Solsvik et al. (2013) were modified by introducing a breakage probability, which made the breakage frequency profiles less steep. Without this modification, the solution of the mass density functions diverged. The non-conserving models of Luo and Svendsen (1996), Liao et al. (2015) and Xing et al. (2015) produced non-physical solutions of the mass density function. Before they can be applied as closures in the PBE, these models must be modified to eliminate the conserving errors.

Based on the evaluation, it was concluded that the models of Coulaloglou and Tavlarides (1977), Han et al. (2011), Becker et al. (2014) and the model of Martínez-Bazán et al. with the introduced breakage probability are most suitable as constitutive equations in the PBE. These models are computationally efficient, volume and number conserving, fit at least one of the experimental data series acceptably and give plausible solutions of the PBE test case. The wide energy spectrum extensions should be used instead of the original models, to make sure that the closures are valid in all ranges of the turbulent energy spectrum. The adjustable parameters included in Coulaloglou and Tavlarides (1977) and the fact that it was necessary to scale the breakage frequency of the model in the PBE test case are considered weaknesses of the closure. To avoid accumulation of particles at the smallest particle size, the capillary criterion was identified as an important constraint.

7.2 Relation for the Number of Daughters

In the evaluation of the closures, it was noticed that none of the models predict the number of daughters formed in the breakage process as a function of system parameters and the

mother particle size. In all closures, an *a priori* assumption of the number of daughters is applied. It is unrealistic that such an assumption is correct for all systems and particle sizes. Therefore, introducing a relation for the number of daughter particles was identified as a possible improvement of the breakage closures. However, extending the closures in this manner involves some challenges.

Through an example where the model of Martínez-Bazán et al. (2010) was extended to ternary breakage, it was shown that introducing a relation for the number of daughters makes the model significantly more complex. It was considered likely that without simplifications, the models would be too computationally demanding to be suitable as closures in the PBE. A method for reducing the model complexity by dividing the daughter particles into groups based on the particle sizes was presented. This method has the potential of reducing the computational demand of closures where the number of daughters are predicted, but care must be taken to ensure that the combined redistribution density function that the method returns is both volume and number conserving.

7.3 Recommendations for Further Work

There is a general lack of experimental data for the breakage frequencies and probability density functions for bubbles and droplets in the literature. The few available sources of data contain few data points for a narrow range of particle sizes. In order to evaluate the breakage closures properly, experiments measuring the breakage frequencies and redistribution functions of both bubbles and droplets in several systems for a wide range of particle sizes must be performed. With access to such experimental data, it would be possible to accurately evaluate the trends predicted by the closures over wide particle size ranges, which would greatly help to determine which breakage mechanism and criteria that are physically correct. Attempts should be made to develop new closures that predict the number of daughters formed in the breakage process as a function of system properties and the parent particle size. With sufficient amounts of available experimental data, evaluations should be performed to determine if the prediction of the number of daughters makes the models more physically realistic.

Bibliography

Alopaeus, V., Koskinen, J., Keskinen, K. I., Majander, J., 2002. Simulation of the population balances for liquid-liquid systems in a nonideal stirred tank. Part 2-parameter fitting and the use of the multiblock model for dense dispersions. Chemical Engineering Science 57 (10), 1815–1825.

Andersson, R., Andersson, B., 2006a. Modeling the Breakup of Fluid Particles in Turbulent Flows. AIChE Journal 52 (6), 2031–2038.

Andersson, R., Andersson, B., 2006b. On the Breakup of Fluid Particles in Turbulent Flows. AIChE Journal 52 (6), 2020–2030.

Becker, P. J., Puel, F., Jakobsen, H. A., Sheibat-Othman, N., 2014. Development of an improved breakage kernel for high dispersed viscosity phase emulsification. Chemical Engineering Science 109, 326–338.

Coulaloglou, C., Tavlarides, L., 1977. Description of interaction processes in agitated liquid-liquid dispersions. Chemical Engineering Science 32 (11), 1289–1297.

Fan, L.-S., Tsuchiya, K., 1990. Bubble Wake Dynamics in Liquids and Liquid-Solid Suspensions. Butterworth-Heinemann, Stoneham, MA.

Han, L., Gong, S., Ding, Y., Fu, J., Gao, N., Luo, H., 2015. Consideration of Low Viscous Droplet Breakage in the Framework of the Wide Energy Spectrum and the Multiple Fragments. AIChE Journal 61, 2147–2168.

Han, L., Gong, S., Li, Y., Ai, Q., Luo, H., Liu, Z., Liu, Y., 2013. A novel theoretical model of breakage rate and daughter size distribution for droplet in turbulent flows. Chemical Engineering Science 102, 186–199.

Han, L., Gong, S., Li, Y., Gao, N., Fu, J., Luo, H., Liu, Z., 2014. Influence of energy spectrum distribution on drop breakage in turbulent flows. Chemical Engineering Science 117, 55–70.

Han, L., Luo, H., Liu, Y., 2011. A theoretical model for droplet breakup in turbulent dispersions. Chemical Engineering Science 66 (4), 766–776.

Hinze, J., 1975. Turbulence. McGraw Hill, New York.

Hulburt, M., Katz, S., 1964. Some problems in particle technology. A statistical mechanical formulation. Chemical Engineering Science 19, 555–574.

Jakobsen, H. A., 2014. Chemical Reactor Modeling: Multiphase Reactive Flows, 2nd Edition. Springer International Publishing, Switzerland.

Jakobsen, H. A., Lindborg, H., Dorao, C. A., 2005. Modeling of Bubble Column Reactors: Progress and Limitations. Ind. Eng. Chem. Res. 44, 5107–5151.

Janssen, J. J. M., Boon, A., Agterof, W. G. M., 1994. Influence of Dynamic Interfacial Properties on Droplet Breakup in Simple Shear Flow. AIChE Journal 40 (12), 1929–1939.

Janssen, J. M. H., Meijer, H. E. H., 1993. Droplet breakup mechanisms: Stepwise equilibrium versus transient dispersion. Journal of Rheology 37 (4), 597–608.

Kuriyama, M., Ono, M., Tokanai, H., Konno, H., 1995. The number of daughter drops formed per breakup of a highly viscous mother-drop in turbulent flow. Journal of Chemical Engineering of Japan 28 (4), 477–479.

Lasheras, J. C., Eastwood, C., Martínez-Bazán, C., Montañés, J. L., 2002. A review of statistical models for the break-up of an immiscible fluid immersed into a fully developed turbulent flow. International Journal of Multiphase Flow 28, 247–278.

Lee, C. H., Erickson, L. E., Glasgow, L. A., 1987a. Bubble breakup and coalescence in turbulent gas-liquid dispersions. Chem Eng Commun 59, 65–84.

Lee, C. H., Erickson, L. E., Glasgow, L. A., 1987b. Dynamics of bubble size distribution in turbulent gas-liquid dispersions. Chem Eng Commun 61, 181–195.

Lehr, F., Millies, M., Mewes, D., 2002. Bubble size distributions and flow fields in bubble columns. AIChE Journal 42 (11), 1225–1233.

Liao, Y., 2013. Development and Validation of Models for Bubble Coalescence and Breakup. Ph.D. thesis, Dresden University of Technology.

Liao, Y., Lucas, D., 2009. A literature review of theoretical models for drop and bubble breakup in turbulent dispersions. Chemical Engineering Science 64 (15), 3389–3406.

Liao, Y., Lucas, D., Krepper, E., Schmidtke, M., 2011. Development of a generalized coalescence and breakup closure for the inhomogeneous MUSIG model. Nuclear Engineering and Design 241 (4), 1024–1033.

Liao, Y., Rzehak, R., Lucas, D., Krepper, E., 2015. Baseline closure model for dispersed bubbly flow: Bubble coalescence and breakup. Chemical Engineering Science 122, 336–349.

Luo, H., Svendsen, H. F., 1996. Theoretical Model for Drop and Bubble Breakup in Turbulent Dispersions. AIChE Journal 42 (5), 1225–1233.

Maaß, S., Kraume, M., 2012. Determination of breakage rates using single drop experiments. Chemical Engineering Science 70, 146–164.

Martínez-Bazán, C., Montañés, J. L., Lasheras, J. C., 1999a. On the breakup of an air bubble injected into a fully developed turbulent flow. Part 1. Breakup frequency. Journal of Fluid Mechanics 401, 157–182.

Martínez-Bazán, C., Montañés, J. L., Lasheras, J. C., 1999b. On the breakup of an air bubble injected into a fully developed turbulent flow. Part 2. Size PDF of the resulting daughter bubbles. Journal of Fluid Mechanics 401, 183–207.

Martínez-Bazán, C., Rodríguez-Rodríguez, J., Deane, G. B., Montañes, J. L., Lasheras, J. C., 2010. Considerations on bubble fragmentation models. Journal of Fluid Mechanics 661, 159–177.

Mockett, C. A., 2009. Comprehensive Study of Detached-Eddy Simulation. Ph.D. thesis, Technical University of Berlin, Magdeburg.

Morel, C., Ruyer, P., Seiler, N., Laviéville, J. M., 2010. Comparison of several models for multi-size bubbly flows on an adiabatic experiment. International Journal of Multiphase Flow 36, 25–39.

Narsimhan, G., Gupta, J. P., Ramkrishna, D., 1979. A model for transitional breakage probability of droplets in agitated lean liquid-liquid dispersions. Chemical Engineering Science 34 (2), 257–265.

Pope, S., 2000. Turbulent Flows. Cambridge University Press, Cambridge, UK.

Prince, M. J., Blanch, H. W., 1990. Bubble coalescence and break-up in air-sparged bubble columns. AIChE Journal 36 (10), 1485–1499.

Randolph, A., 1964. A population balance for countable entities. Canadian Journal of Chemical Engineering 42, 280–281.

Sawford, B., Hunt, J., 1986. Effects of turbulence structure, molecular diffusion and source size on scalar fluctuations in homogeneous turbulence. J. Fluid Mech. 165, 373–400.

Solsvik, J., 2016. Turbulence Modeling in the Wide Energy Spectrum. Submitted for publication.

Solsvik, J., Jakobsen, H. A., 2013. On the solution of the population balance equation for bubbly flows using the high-order least squares method: implementation issues. Reviews in Chemical Engineering 29 (2), 63–98.

Solsvik, J., Jakobsen, H. A., 2014. Evaluation of Spectral, Spectral-Element and Finite-Element Methods for the Solution of the Pellet Equation. The Canadian Journal of Chemical Engineering 92, 1396–1413.

Solsvik, J., Jakobsen, H. A., 2015. The Foundation of the Population Balance Equation: A Review. Journal of Dispersion Science and Technology 36 (4), 510–520.

Solsvik, J., Jakobsen, H. A., 2016a. A Review of the Statistical Turbulence Theory Required Extending the Population Balance Closure Models to the Entire Spectrum of Turbulence. AIChE Journal 62 (5), 1795–1820.

Solsvik, J., Jakobsen, H. A., 2016b. Development of Fluid Particle Breakup and Coalescence Closure Models for the Complete Energy Spectrum of Isotropic Turbulence. Ind. Eng. Chem. Res. 55, 1449–1460.

Solsvik, J., Maaß, S., Jakobsen, H. A., 2016a. Definition of the Single Drop Breakup Event. Ind. Eng. Chem. Res. 55, 2872–2882.

Solsvik, J., Skjervold, V. T., Han, L., Luo, H., Jakobsen, H. A., 2016b. A theoretical study on drop breakup modeling in turbulent flows: the inertial subrange versus the entire spectrum of isotropic turbulence. Chemical Engineering Science 149, 249–265.

Solsvik, J., Tangen, S., Jakobsen, H. A., 2013. On the constitutive equations for fluid particle breakage. Reviews in Chemical Engineering 29 (5), 241–356.

Valentas, K. J., Bilous, O., Amundson, N. R., 1966. Analysis of breakage in dispersed phase systems. Industrial & Engineering Chemistry Fundamentals 5 (2), 271–279.

Wang, T., Wang, J., Jin, Y., 2003. A novel theoretical breakup kernel function for bubbles/droplets in a turbulent flow. Chemical Engineering Science 58 (20), 4629–4637.

Wilkinson, P. M., Van Schayk, A., Spronken, J. P. M., Van Dierendonck, L., 1993. The influence of gas density and liquid properties on bubble breakup. Chemical Engineering Science 48 (7), 1213–1226.

Xing, C., Wang, T., Guo, K., Wang, J., 2015. A Unified Theoretical Model for Breakup of Bubbles and Droplets in Turbulent Flows. AIChE Journal 61, 1391–1403.

Zaccone, A., Gäbler, A., Maaß, S., Marchisio, D., Kraume, M., 2007. Drop breakage in liquid liquid stirred dispersions: Modelling of single drop breakage. Chemical Engineering Science 62, 6297–6307.

Appendices

Appendix A

Sensitivity Analysis

In this chapter, the sensitivity of all closures towards the integral length scale L, is studied. Plots are given of the breakage frequencies, probability density functions and mass density functions from the PBE test case.

A.1 Breakage Frequencies

A.1.1 Air-Water System

In Figure A.1, the breakage frequencies of most models in the air-water system with an integral scale of 0.01 m are given.

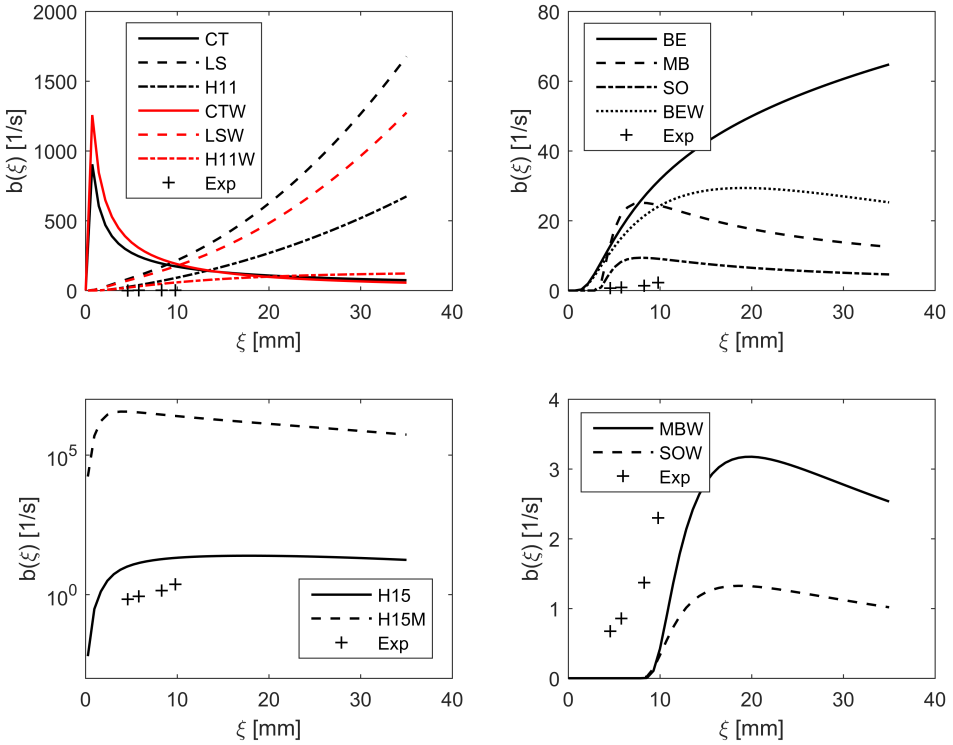

Figure A.1: Breakage frequencies for the air-water system. The integral scale L has been set to 0.01 m. Exp is the experimental data of Wilkinson et al. (1993).

In Figure A.2, a zoom in of the extended model of Han et al. (2011) is given, to give a better view of how well the model fits the experimental data.

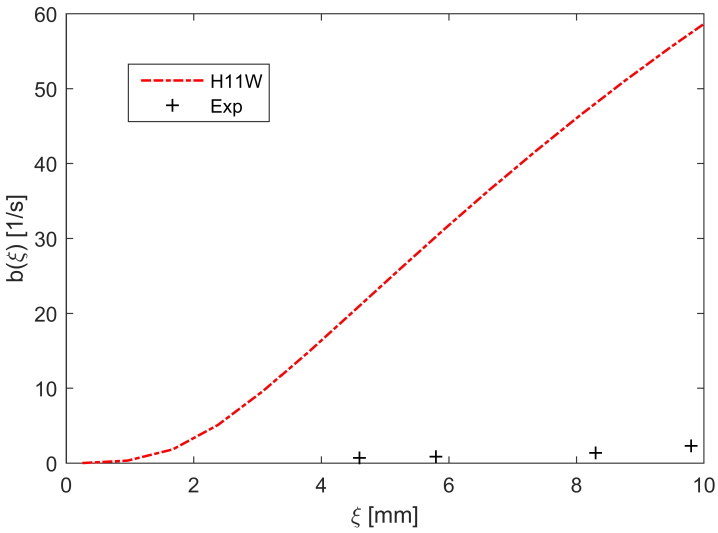

Figure A.2: The breakage frequency of the extended model of Han et al. (2011) for the air-water system with $L = 0.01$ m. Exp is the experimental data of Wilkinson et al. (1993).

In Figure A.3, the breakage frequencies of Liao et al. (2015) and Xing et al. (2015) for an integral scale of 0.01 m are shown.

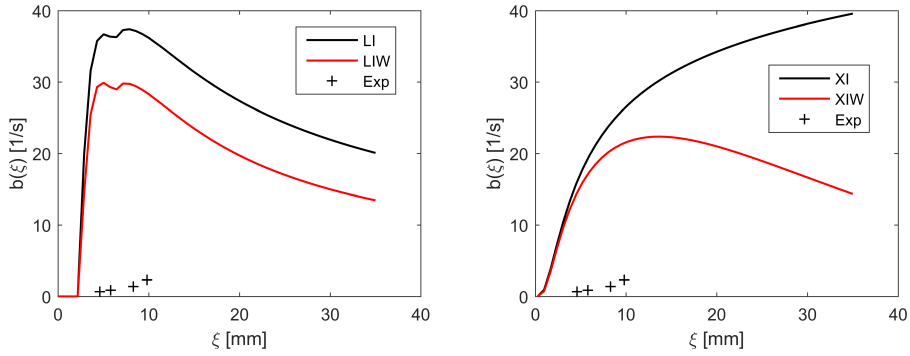

Figure A.3: Breakage frequencies of Liao et al. (2015) and Xing et al. (2015) for the air-water system. The integral scale L has been set to 0.01 m in the wide energy spectrum models and the value of $\dot{\gamma}_{\text{shear}}$ was set to 10 s^{-1}. Exp is the experimental data of Wilkinson et al. (1993).

In Figure A.4, the breakage frequencies of most models with an integral scale of 1 m are shown. In Figure A.5, the breakage frequencies of Liao et al. (2015) and Xing et al. (2015) with an integral scale of 1 m are shown.

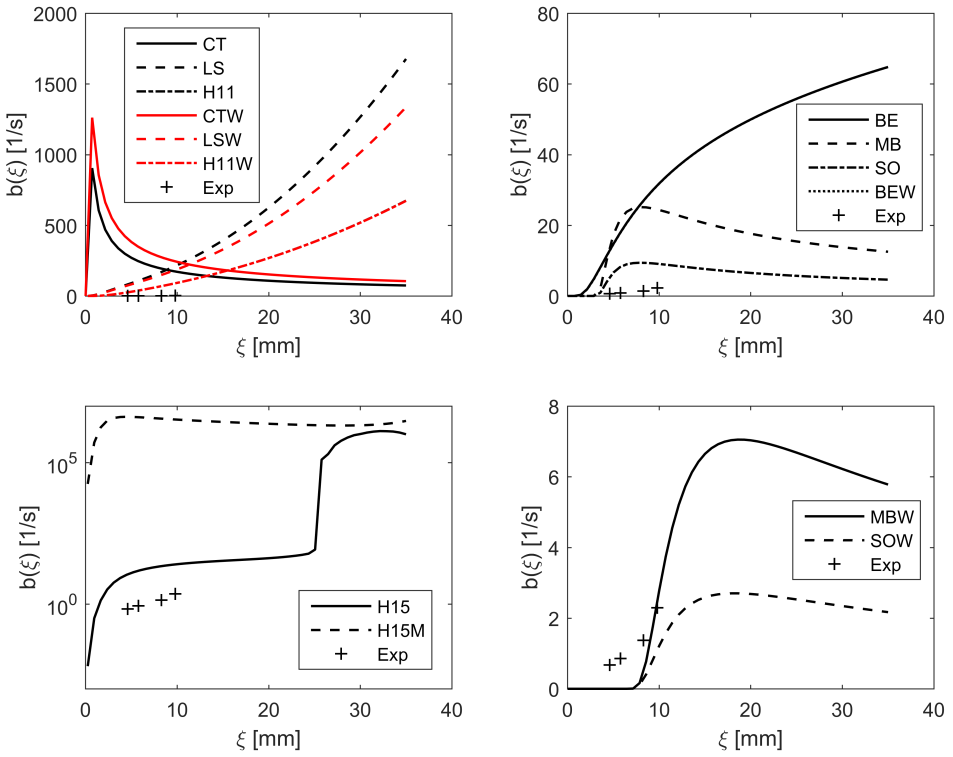

Figure A.4: Breakage frequencies for the air-water system. The integral scale L has been set to 1 m. Exp is the experimental data of Wilkinson et al. (1993).

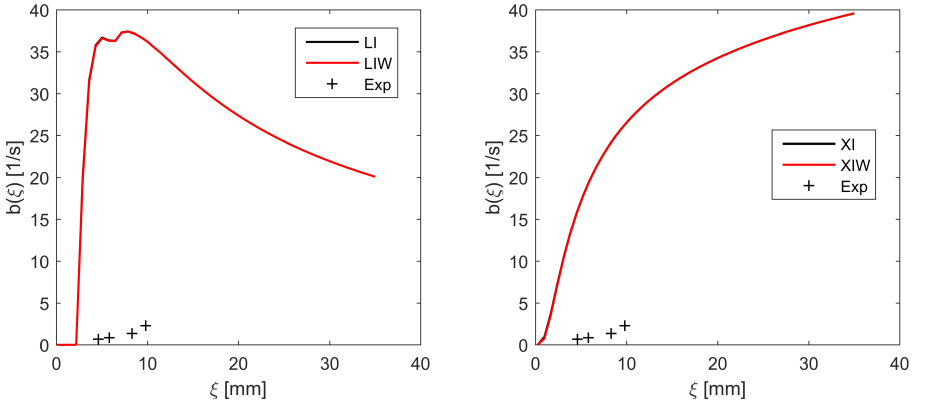

Figure A.5: Breakage frequencies of Liao et al. (2015) and Xing et al. (2015) for the air-water system. The integral scale L has been set to 1 m in the wide energy spectrum models and the value of $\dot{\gamma}_{\text{shear}}$ was set to 10 s^{-1}. Exp is the experimental data of Wilkinson et al. (1993).

A.1.2 Petroleum-Water System I

In Figure A.6, the breakage frequencies of most models in the petroleum-water system I with an integral scale of 0.01 m are shown.

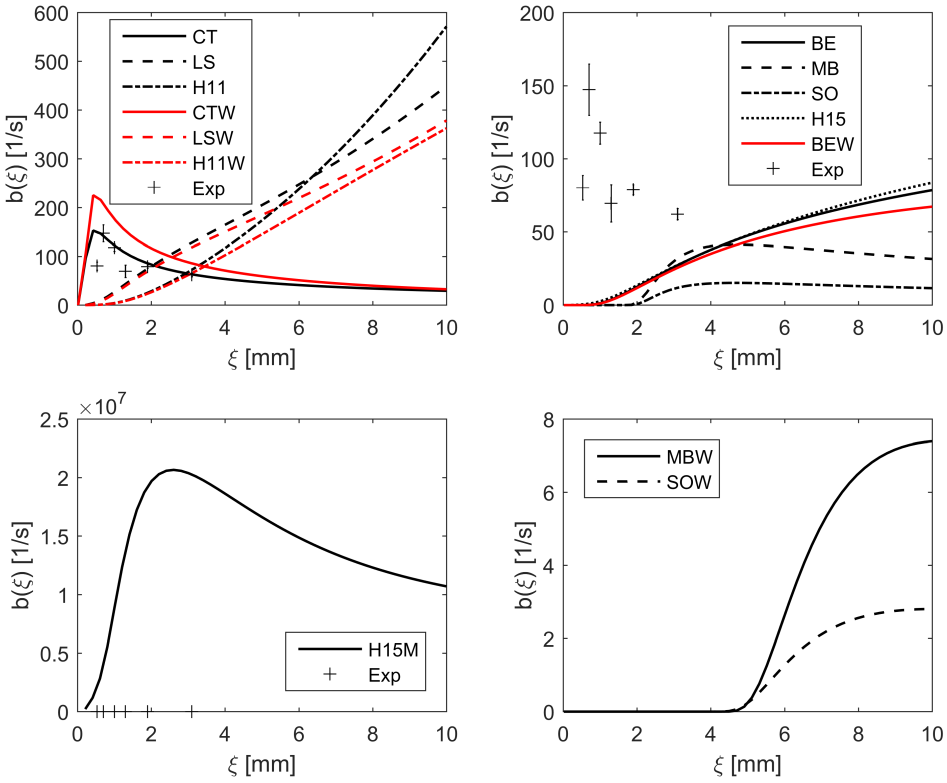

Figure A.6: Breakage frequencies for the petroleum-water system. The integral scale L has been set to 0.01 m. Exp is the experimental data of Maaß and Kraume (2012).

In Figure A.7, the breakage frequencies of Liao et al. (2015) and Xing et al. (2015) in the petroleum-water system I with an integral scale of 0.01 m are shown.

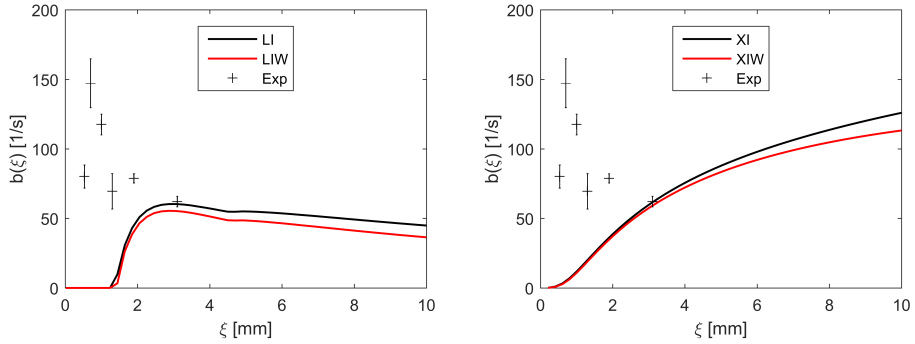

Figure A.7: Breakage frequencies of Liao et al. (2015) and Xing et al. (2015) for the petroleum-water system I. The integral scale L has been set to 0.01 m in the wide energy spectrum models and the value of $\dot{\gamma}_{\text{shear}}$ was set to 10 s^{-1}. Exp is the experimental data of Maaß and Kraume (2012).

Figure A.8 shows the breakage frequencies for most of the closures for an integral scale of 1 m.

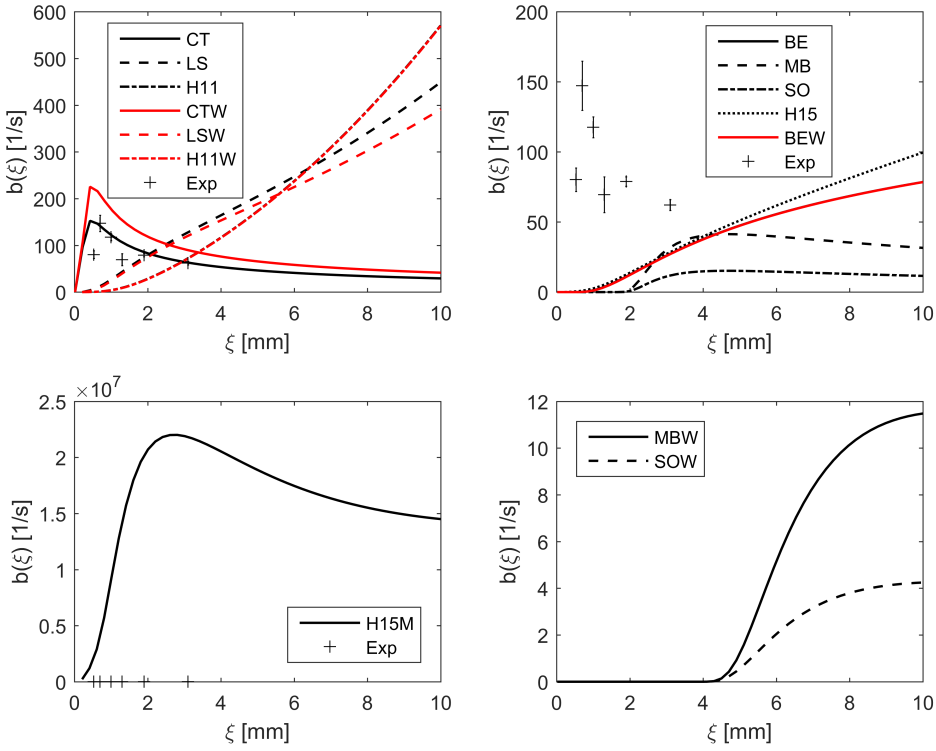

Figure A.8: Breakage frequencies for the petroleum-water system. The integral scale L has been set to 1 m. Exp is the experimental data of Maaß and Kraume (2012).

Figure A.9 gives the breakage frequencies of Liao et al. (2015) and Xing et al. (2015) for an integral scale of 1 m.

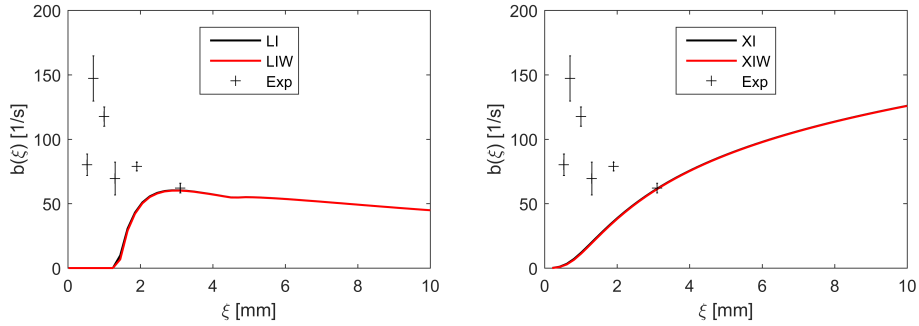

Figure A.9: Breakage frequencies of Liao et al. (2015) and Xing et al. (2015) for the petroleum-water system I. The integral scale L has been set to 1 m in the wide energy spectrum models and the value of $\dot{\gamma}_{\text{shear}}$ was set to 10 s^{-1}. Exp is the experimental data of Maaß and Kraume (2012).

A.1.3 Toluene-Water System

The breakage frequencies for most models in the toluene-water system with an integral scale of 0.01 m are given in Figure A.10.

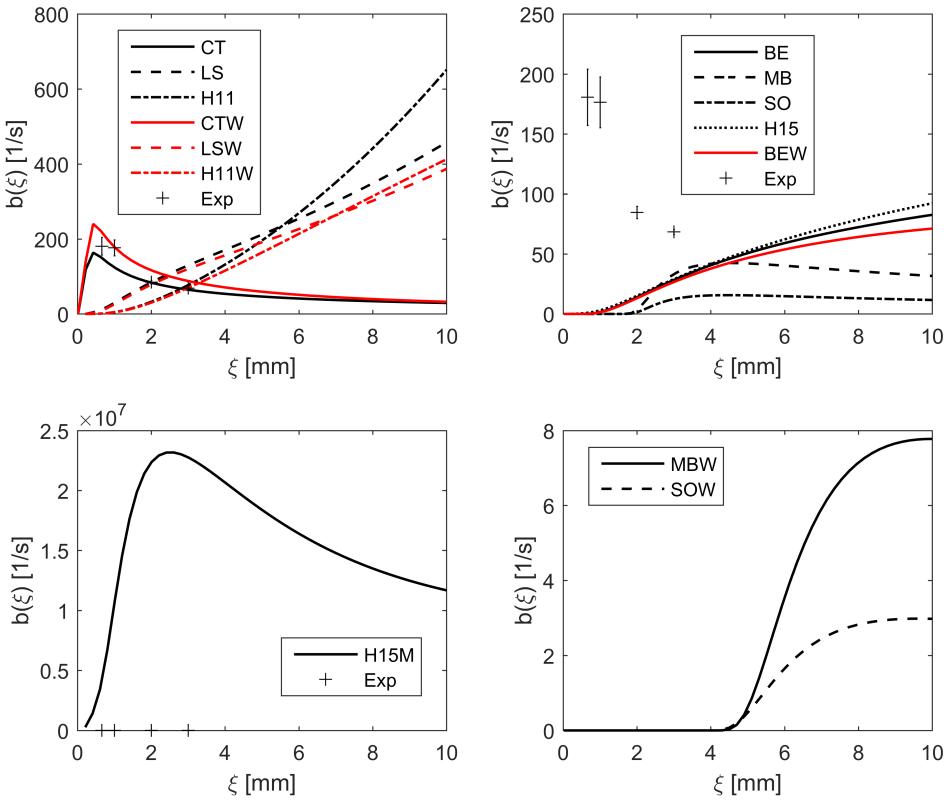

Figure A.10: Breakage frequencies for the toluene-water system. The integral scale L has been set to 0.01 m. Exp is the experimental data of Maaß and Kraume (2012).

In Figure A.11, the breakage frequencies of Liao et al. (2015) and Xing et al. (2015) for an integral scale of 0.01 m are given. The breakage frequencies for most models in the toluene-water system with an integral scale of 1 m are given in Figure A.12.

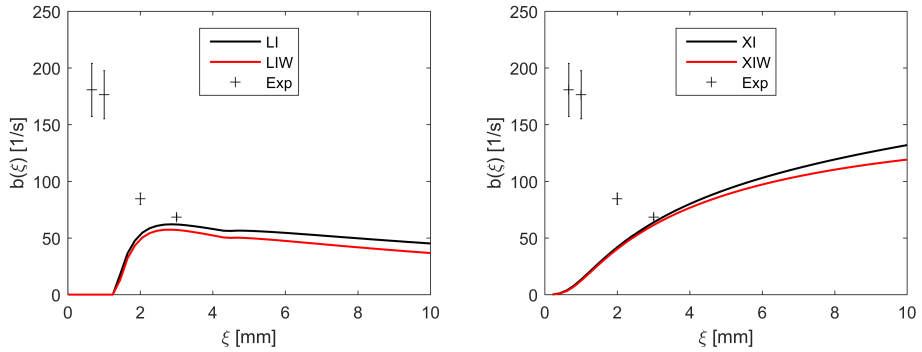

Figure A.11: Breakage frequencies of Liao et al. (2015) and Xing et al. (2015) for the toluene-water system. The integral scale L has been set to 0.01 m in the wide energy spectrum models and the value of $\dot{\gamma}_{\text{shear}}$ was set to 10 s^{-1}. Exp is the experimental data of Maaß and Kraume (2012).

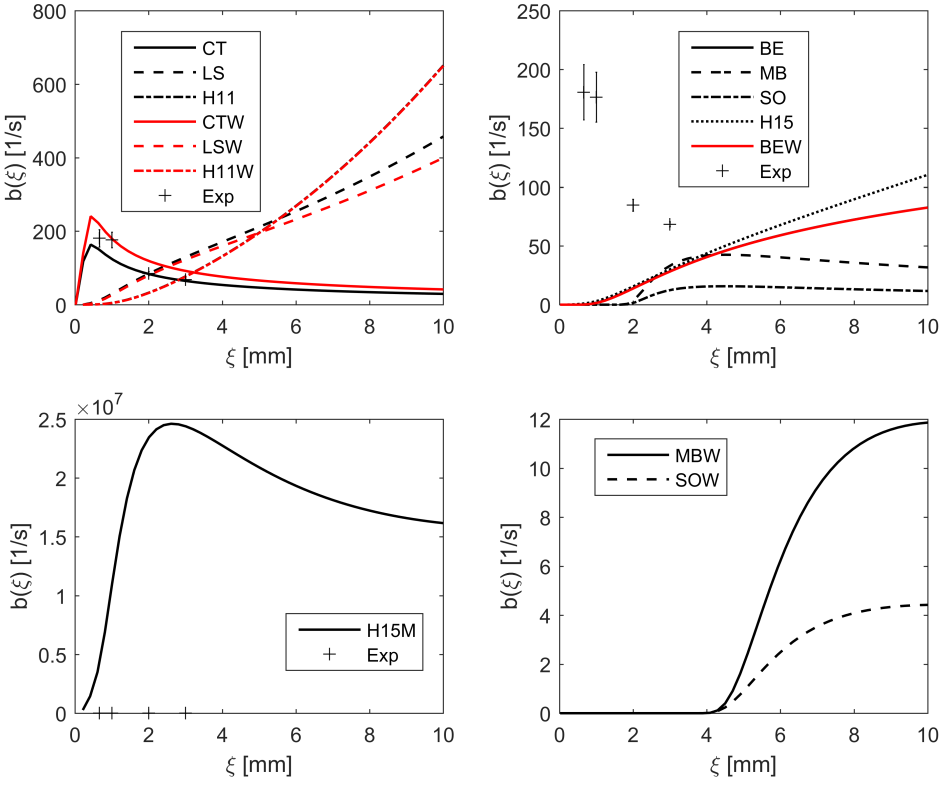

Figure A.12: Breakage frequencies for the toluene-water system. The integral scale L has been set to 1 m. Exp is the experimental data of Maaß and Kraume (2012).

In Figure A.13, the breakage frequencies of Liao et al. (2015) and Xing et al. (2015) for an integral scale of 1 m are given.

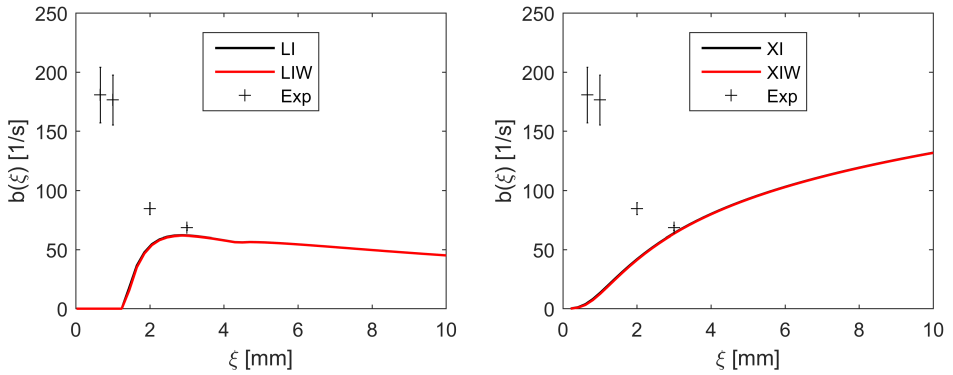

Figure A.13: Breakage frequencies of Liao et al. (2015) and Xing et al. (2015) for the toluene-water system. The integral scale L has been set to 1 m in the wide energy spectrum models and the value of $\dot{\gamma}_{\text{shear}}$ was set to 10 s^{-1}. Exp is the experimental data of Maaß and Kraume (2012).

A.1.4 Dodecane-Water System

The breakage frequencies for most models with an integral scale of 0.01 m are given in Figure A.14.

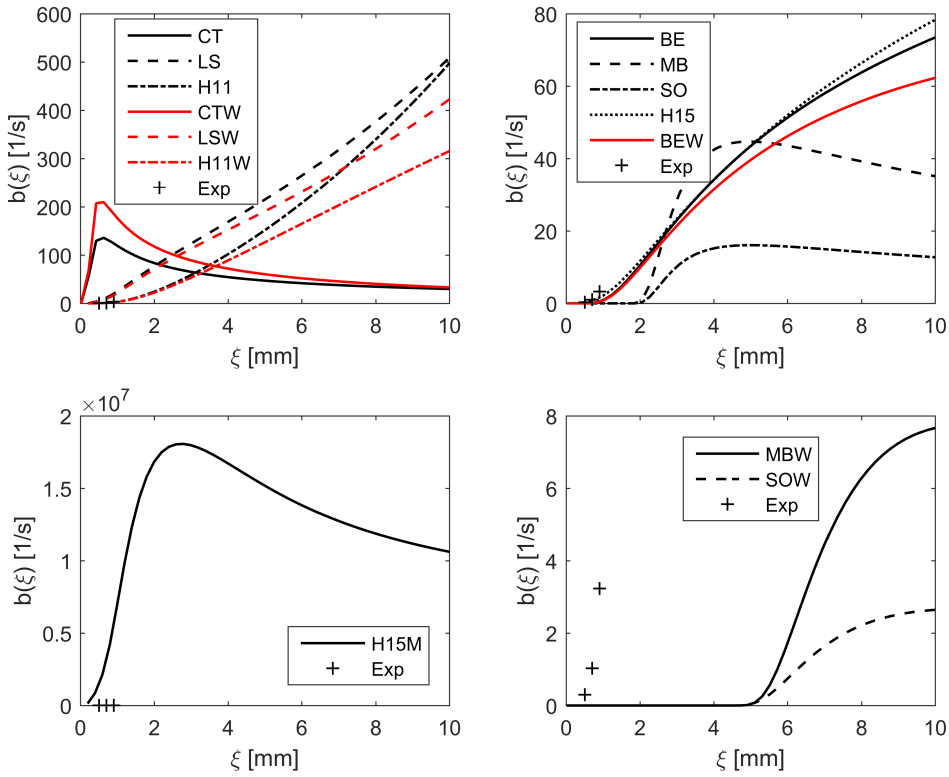

Figure A.14: Breakage frequencies for the dodecane-water system. The integral scale L has been set to 0.01 m. Exp is the experimental data of Andersson and Andersson (2006b).

In Figure A.15, the breakage frequencies of the closures that seem to give the best agreement with the experimental data of Andersson and Andersson (2006b) are given. In order to make it easier to determine which models provide the best fit, the ξ domain has been narrowed.

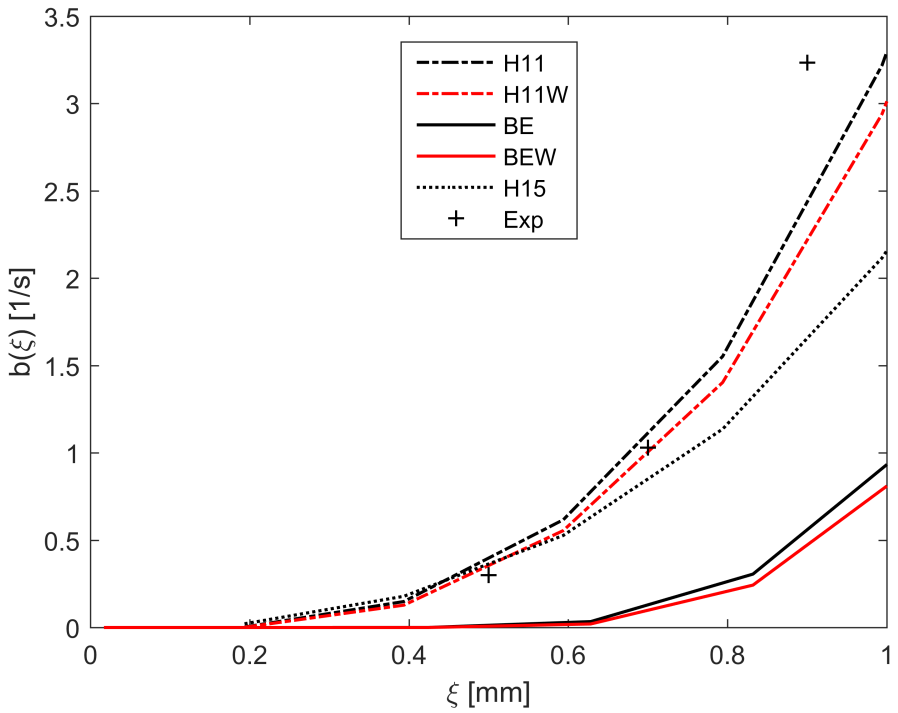

Figure A.15: Breakage frequencies of selected closures in the dodecane-water system. The integral scale L has been set to 0.01 m. Exp is the experimental data of Andersson and Andersson (2006b).

The breakage frequencies of Liao et al. (2015) and Xing et al. (2015) for an integral scale of 0.01 m are given in Figure A.16.

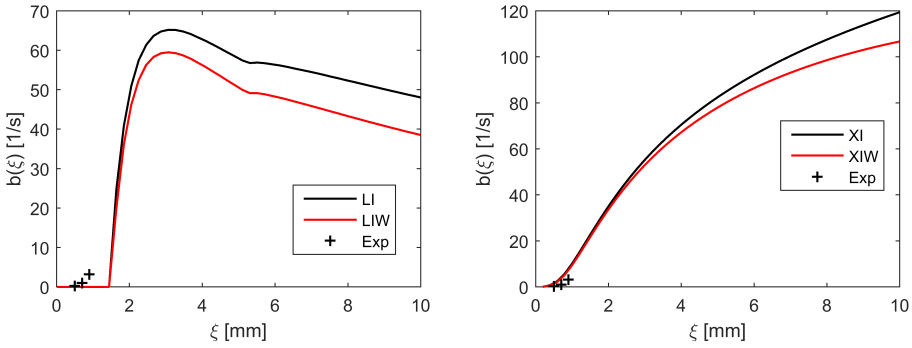

Figure A.16: Breakage frequencies of Liao et al. (2015) and Xing et al. (2015) for the dodecane-water system. The integral scale L has been set to 0.01 m in the wide energy spectrum models and the value of $\dot{\gamma}_{\text{shear}}$ was set to 10 s^{-1}. Exp is the experimental data of Andersson and Andersson (2006b).

The breakage frequencies for an integral scale of 1 m are given in Figure A.17 and Figure A.18.

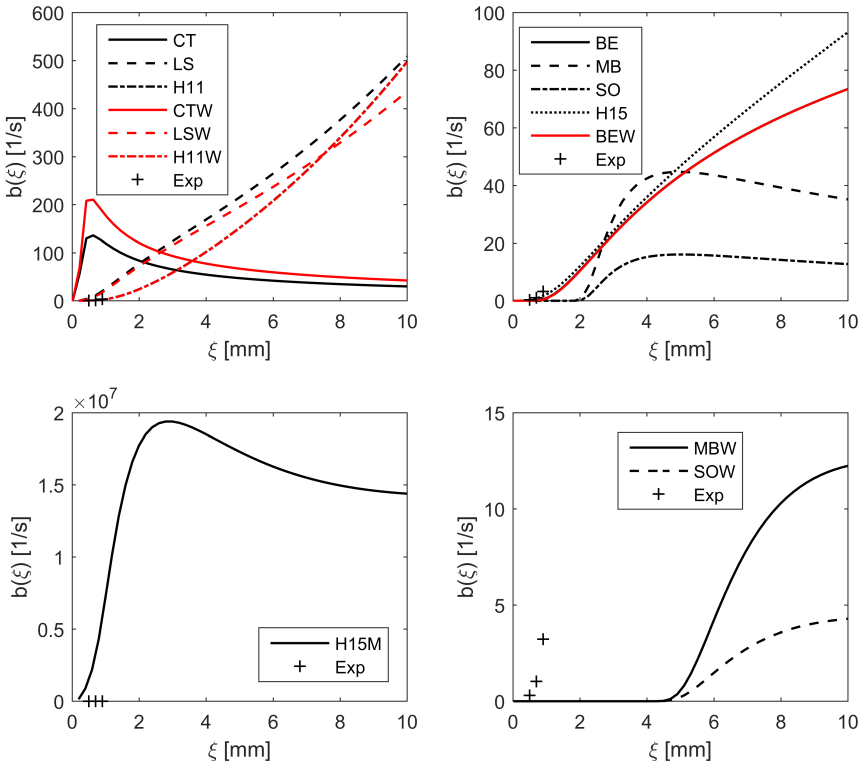

Figure A.17: Breakage frequencies for the dodecane-water system. The integral scale L has been set to 1 m. Exp is the experimental data of Andersson and Andersson (2006b).

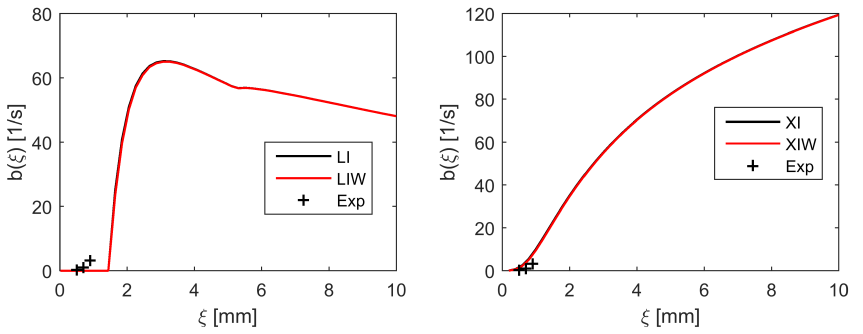

Figure A.18: Breakage frequencies of Liao et al. (2015) and Xing et al. (2015) for the dodecane-water system. The integral scale L has been set to 1 m in the wide energy spectrum models and the value of $\dot{\gamma}_{\text{shear}}$ was set to 10 s^{-1}. Exp is the experimental data of Andersson and Andersson (2006b).

A.2 Probability Density Functions

A.2.1 Air-Water System

In Figure A.19, the probability density functions for most of the closures with L = 0.01 m and a parent particle with a diameter of 20 mm are given.

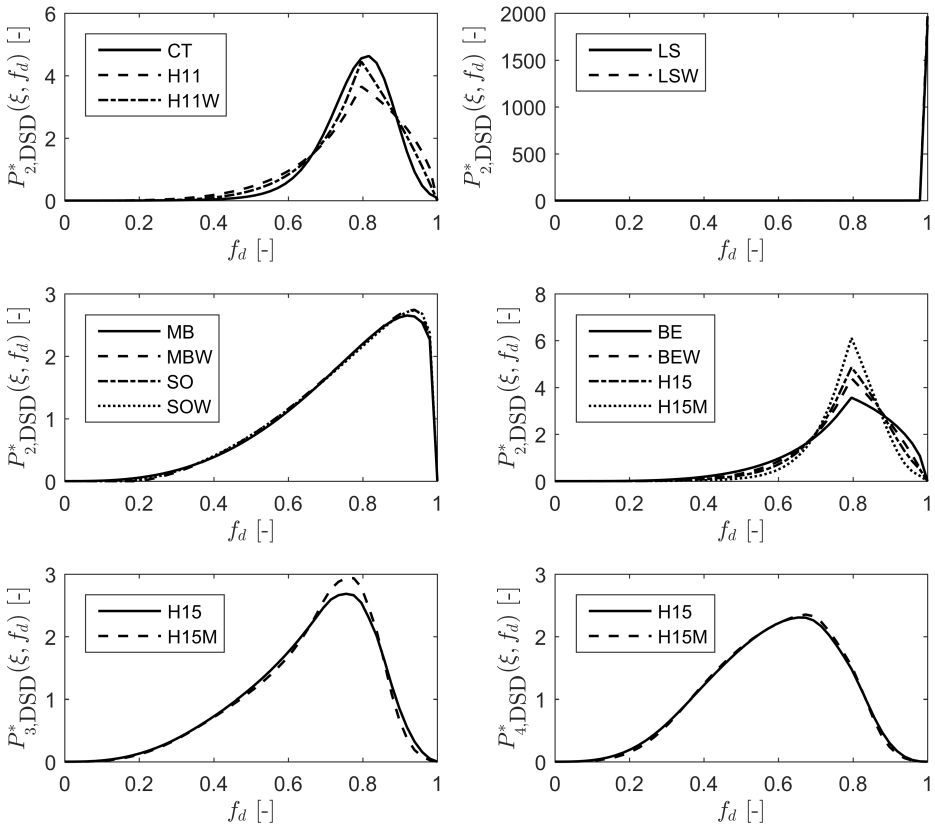

Figure A.19: Probability density functions for the air-water system with a parent bubble diameter of 20 mm. The integral scale L has been set to 0.01 m in the wide energy spectrum models, and a dissipation rate of 1 W/kg has been used.

In Figure A.20, the probability density functions of Liao et al. (2015) and Xing et al. (2015) with a length scale of 0.01 m are shown. In Figure A.21, the probability density functions for most of the closures with L = 1 m and a parent particle with a diameter of 20 mm are given.

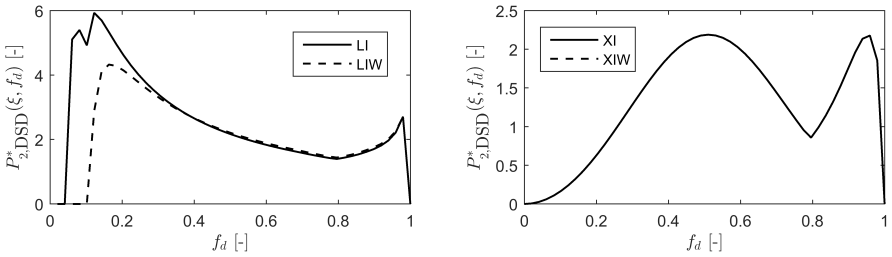

Figure A.20: Probability density functions of Liao et al. (2015) and Xing et al. (2015) for the air-water system with a parent bubble diameter of 20 mm. The integral scale L has been set to 0.01 m in the wide energy spectrum models, and a dissipation rate of 1 W/kg has been used.

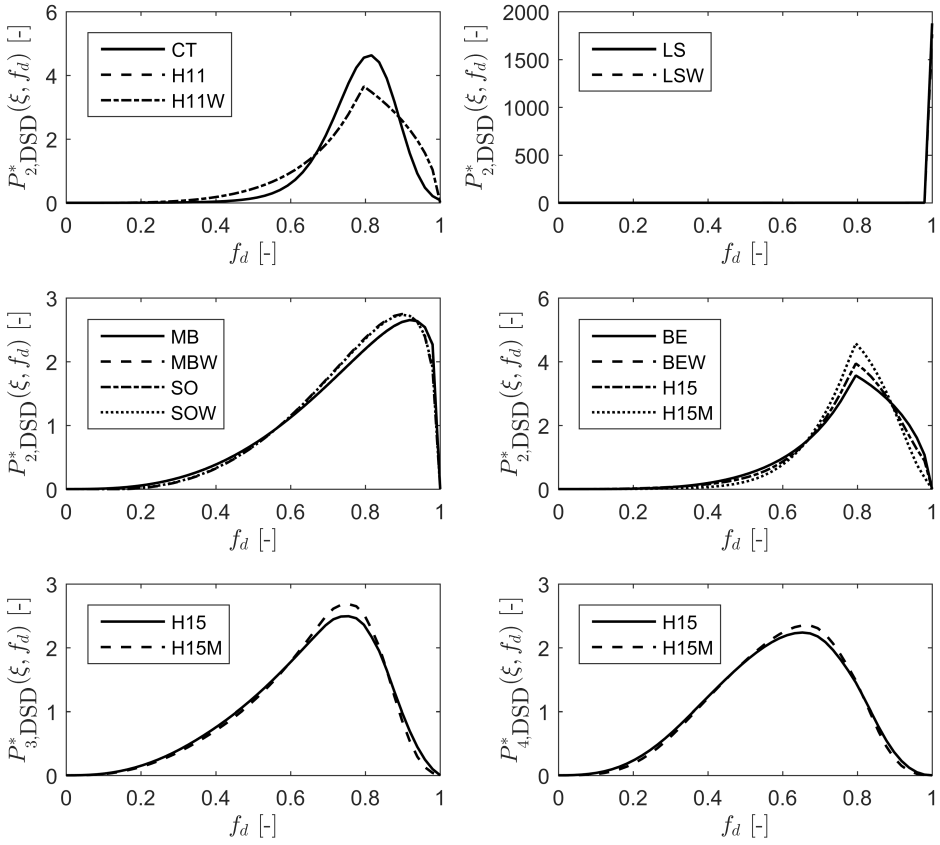

Figure A.21: Probability density functions for the air-water system with a parent bubble diameter of 20 mm. The integral scale L has been set to 1 m in the wide energy spectrum models, and a dissipation rate of 1 W/kg has been used.

In Figure A.22, the probability density functions of Liao et al. (2015) and Xing et al. (2015) with a length scale of 1 m are shown.

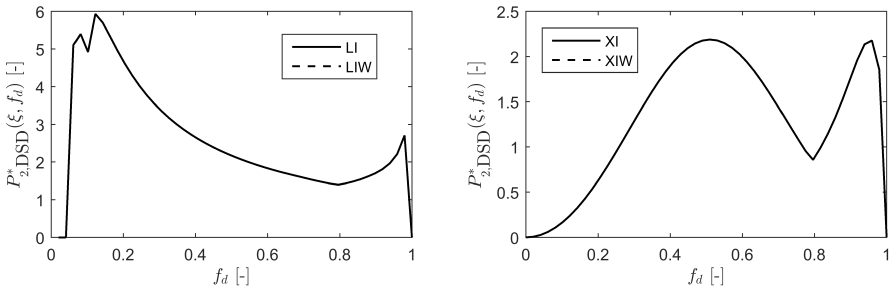

Figure A.22: Probability density functions of Liao et al. (2015) and Xing et al. (2015) for the air-water system with a parent bubble diameter of 20 mm. The integral scale L has been set to 1 m in the wide energy spectrum models, and a dissipation rate of 1 W/kg has been used.

A.2.2 Petroleum-Water System II

The probability density functions for most of the closures for a parent particle of 2 mm and an integral scale of 0.01 m are shown in Figure A.23.

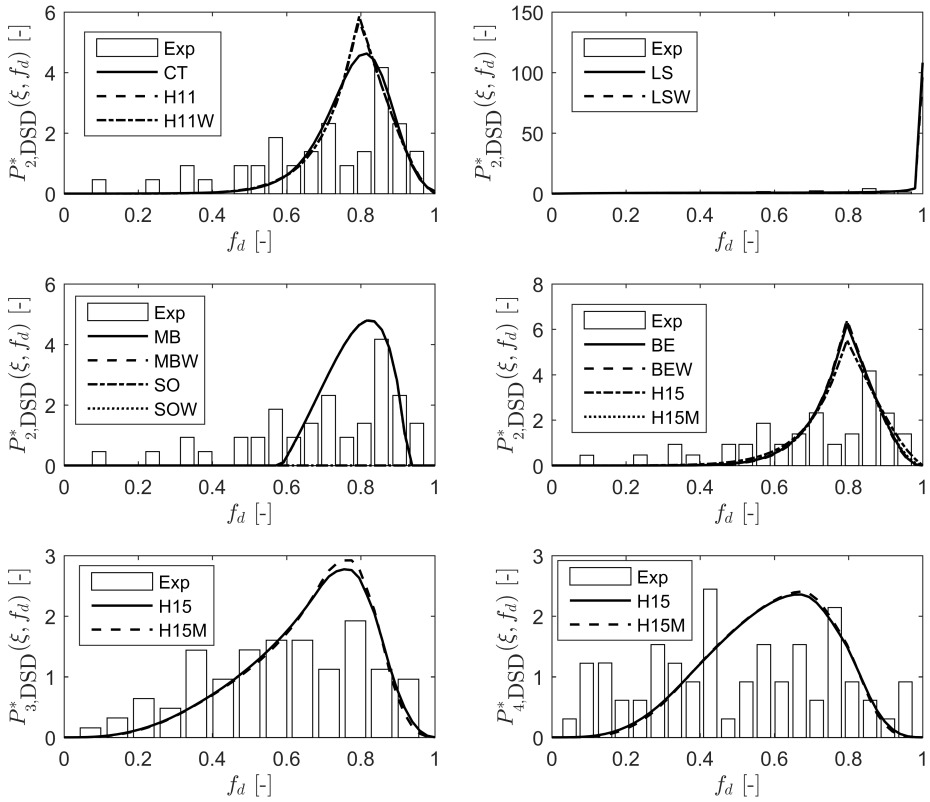

Figure A.23: Probability density functions for the petroleum-water system II with a parent droplet diameter of 2 mm. The integral scale L has been set to 0.01 m in the wide energy spectrum models. Exp is the binary, ternary and quaternary experimental data of Zaccone et al. (2007).

The probability density functions for Liao et al. (2015) and Xing et al. (2015) for a parent particle of 2 mm and an integral scale of 0.01 m are shown in Figure A.24. The probability density functions for most of the closures for a parent particle of 1 mm and an integral scale of 0.01 m are shown in Figure A.25.

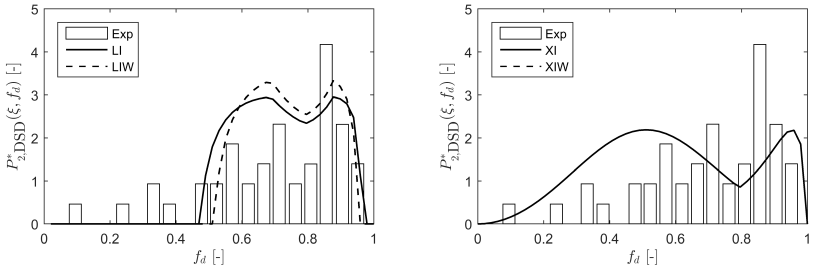

Figure A.24: Probability density functions of Liao et al. (2015) and Xing et al. (2015) for the petroleum-water system II with a parent droplet diameter of 2 mm. The integral scale L has been set to 0.01 m in the wide energy spectrum models. Exp is the binary, ternary and quaternary experimental data of Zaccone et al. (2007).

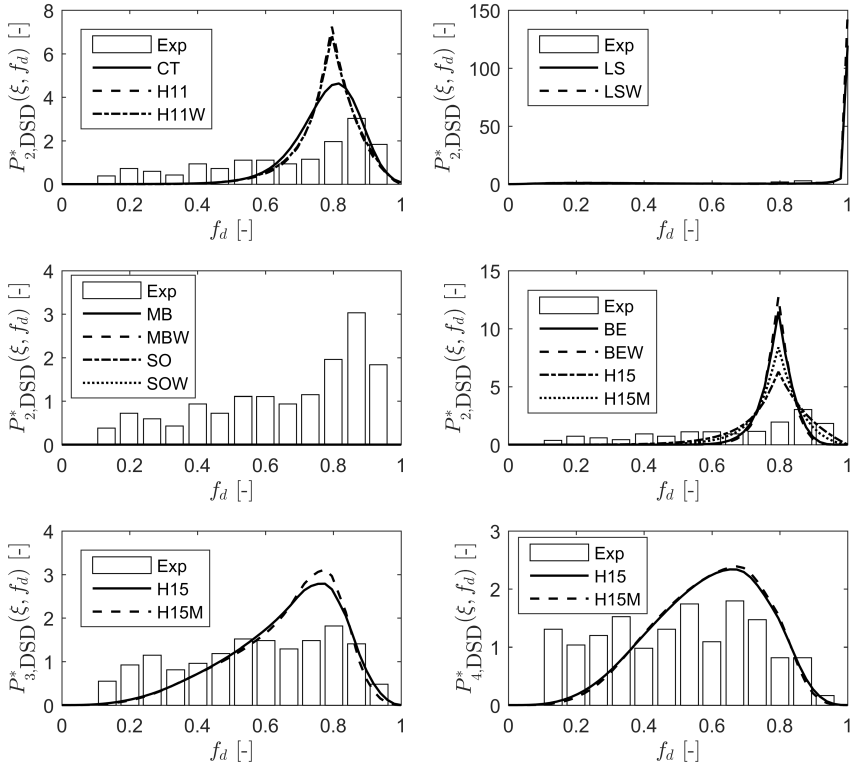

Figure A.25: Probability density functions for the petroleum-water system II with a parent droplet diameter of 1 mm. The integral scale L has been set to 0.01 m in the wide energy spectrum models. Exp is the binary, ternary and quaternary experimental data of Zaccone et al. (2007).

The probability density functions for Liao et al. (2015) and Xing et al. (2015) for a parent particle of 1 mm and an integral scale of 0.01 m are shown in Figure A.26. The probability

density functions for most of the closures for a parent particle of 0.6 mm and an integral scale of 0.01 m are shown in Figure A.27.

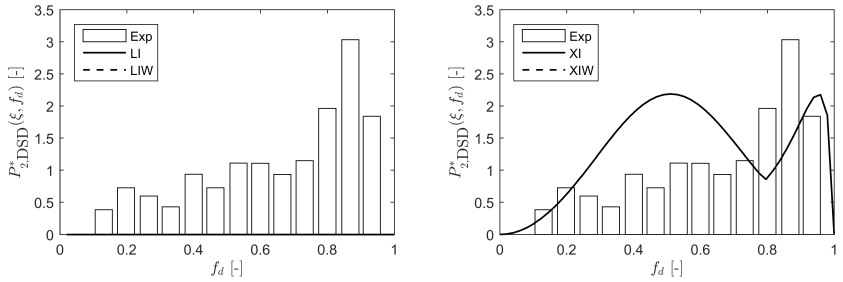

Figure A.26: Probability density functions of Liao et al. (2015) and Xing et al. (2015) for the petroleum-water system II with a parent droplet diameter of 1 mm. The integral scale L has been set to 0.01 m in the wide energy spectrum models. Exp is the binary, ternary and quaternary experimental data of Zaccone et al. (2007).

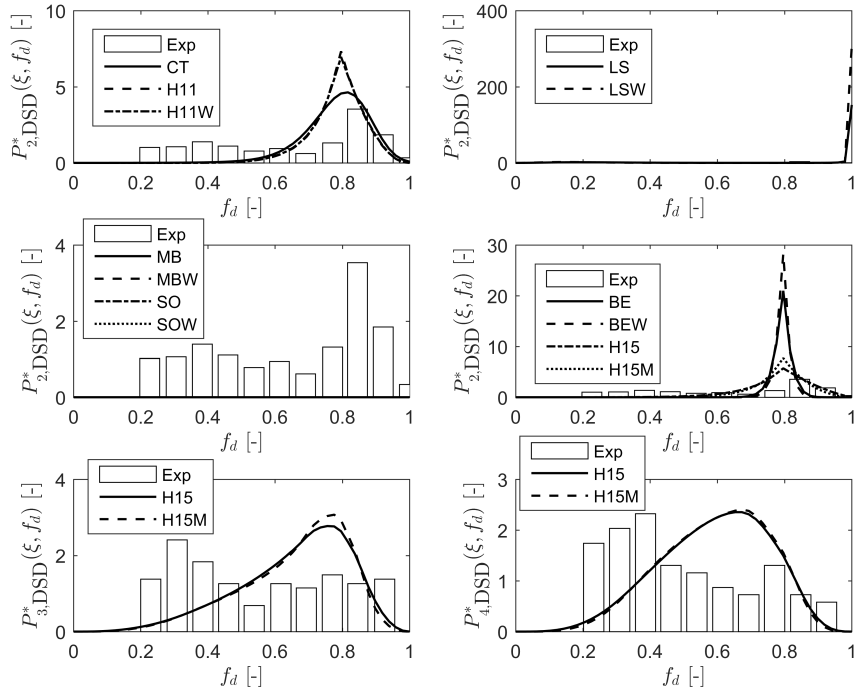

Figure A.27: Probability density functions for the petroleum-water system II with a parent droplet diameter of 0.6 mm. The integral scale L has been set to 0.01 m in the wide energy spectrum models. Exp is the binary, ternary and quaternary experimental data of Zaccone et al. (2007).

The probability density functions for Liao et al. (2015) and Xing et al. (2015) for a parent

particle of 0.6 mm and an integral scale of 0.01 m are shown in Figure A.28. The probability density functions for most of the closures for a parent particle of 2 mm and an integral scale of 1 m are shown in Figure A.29.

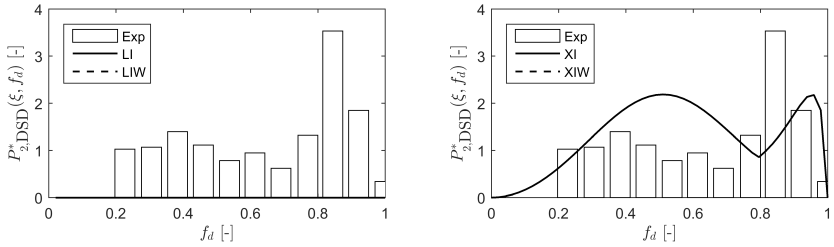

Figure A.28: Probability density functions of Liao et al. (2015) and Xing et al. (2015) for the petroleum-water system II with a parent droplet diameter of 0.6 mm. The integral scale L has been set to 0.01 m in the wide energy spectrum models. Exp is the binary, ternary and quaternary experimental data of Zaccone et al. (2007).

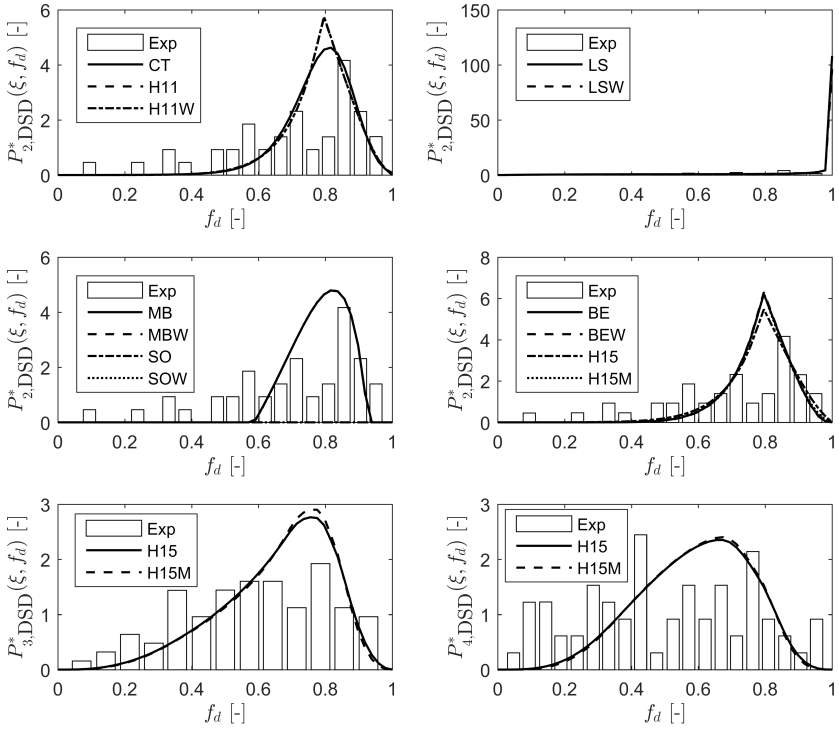

Figure A.29: Probability density functions for the petroleum-water system II with a parent droplet diameter of 2 mm. The integral scale L has been set to 1 m in the wide energy spectrum models. Exp is the binary, ternary and quaternary experimental data of Zaccone et al. (2007).

The probability density functions for Liao et al. (2015) and Xing et al. (2015) for a parent particle of 2 mm and an integral scale of 1 m are shown in Figure A.30.

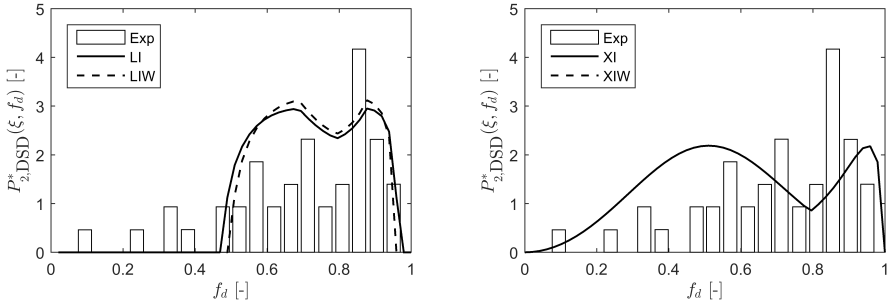

Figure A.30: Probability density functions of Liao et al. (2015) and Xing et al. (2015) for the petroleum-water system II with a parent droplet diameter of 2 mm. The integral scale L has been set to 1 m in the wide energy spectrum models. Exp is the binary, ternary and quaternary experimental data of Zaccone et al. (2007).

The probability density functions for Liao et al. (2015) and Xing et al. (2015) for a parent particle of 1 mm and an integral scale of 1 m are shown in Figure A.31.

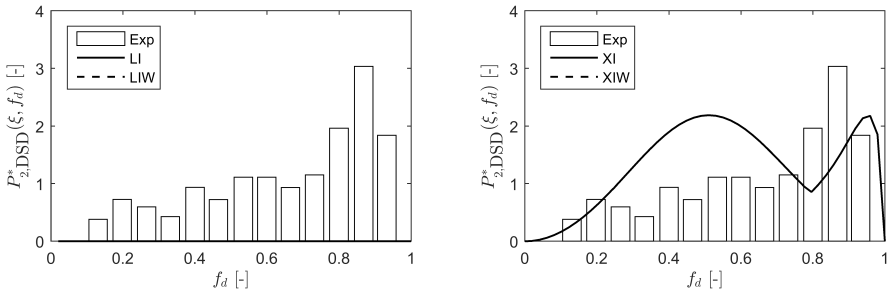

Figure A.31: Probability density functions of Liao et al. (2015) and Xing et al. (2015) for the petroleum-water system II with a parent droplet diameter of 1 mm. The integral scale L has been set to 1 m in the wide energy spectrum models. Exp is the binary, ternary and quaternary experimental data of Zaccone et al. (2007).

The probability density functions for most of the closures for a parent particle of 1 mm and an integral scale of 1 m are shown in Figure A.32.

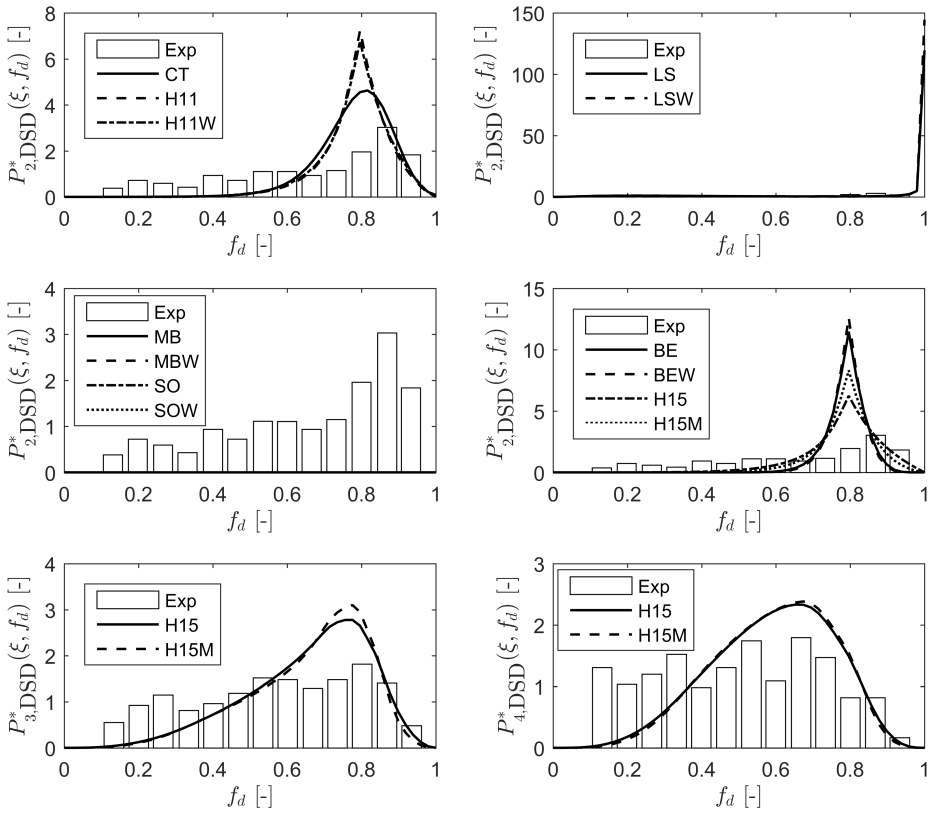

Figure A.32: Probability density functions for the petroleum-water system II with a parent droplet diameter of 1 mm. The integral scale L has been set to 1 m in the wide energy spectrum models. Exp is the binary, ternary and quaternary experimental data of Zaccone et al. (2007).

The probability density functions for most of the closures for a parent particle of 0.6 mm and an integral scale of 1 m are shown in Figure A.33.

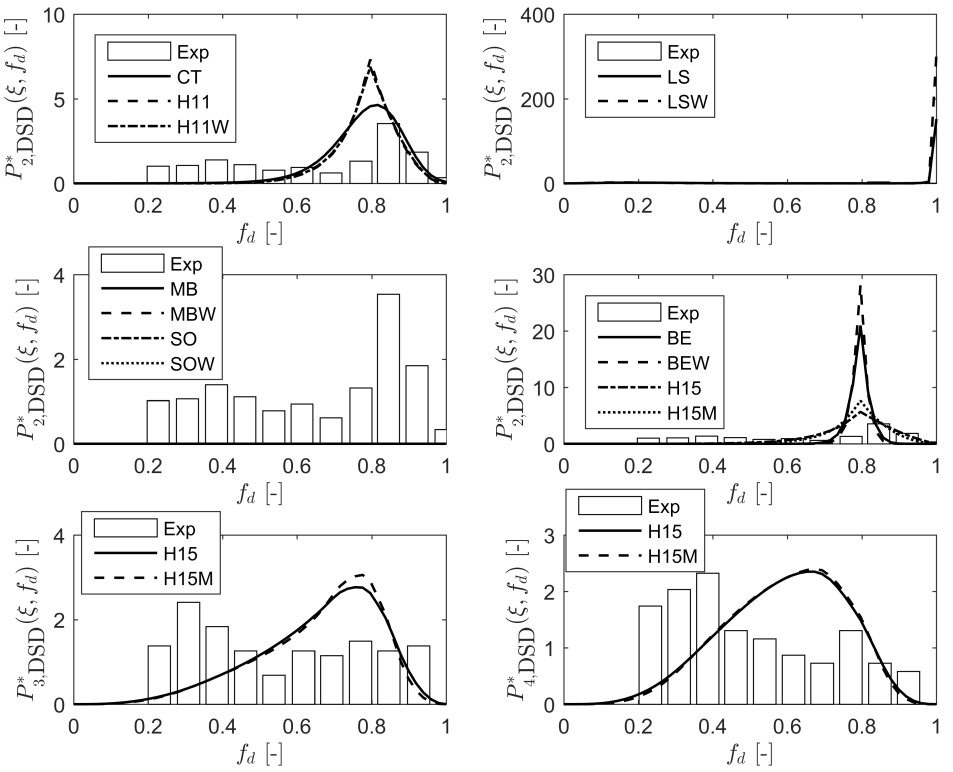

Figure A.33: Probability density functions for the petroleum-water system II with a parent droplet diameter of 0.6 mm. The integral scale L has been set to 1 m in the wide energy spectrum models. Exp is the binary, ternary and quaternary experimental data of Zaccone et al. (2007).

The probability density functions for Liao et al. (2015) and Xing et al. (2015) for a parent particle of 0.6 mm and an integral scale of 1 m are shown in Figure A.34.

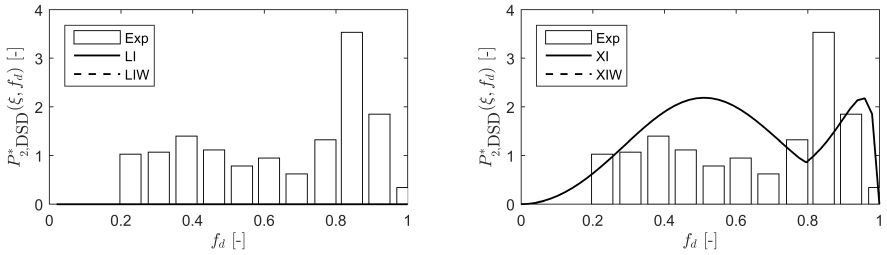

Figure A.34: Probability density functions of Liao et al. (2015) and Xing et al. (2015) for the petroleum-water system II with a parent droplet diameter of 0.6 mm. The integral scale L has been set to 1 m in the wide energy spectrum models. Exp is the binary, ternary and quaternary experimental data of Zaccone et al. (2007).

A.3 Mass Density Functions

In this section, the sensitivity of the mass density functions towards the integral scale L is shown for the air-water system and petroleum-water system I. The inertial range models are included in the graphs, even though they are independent of the integral scale. They were included to make it easier to see the differences between the inertial and wide energy spectrum models.

A.3.1 Air-Water System

In Figure A.35 to A.37, the mass density functions for the air-water system for L = 0.001 m are shown.

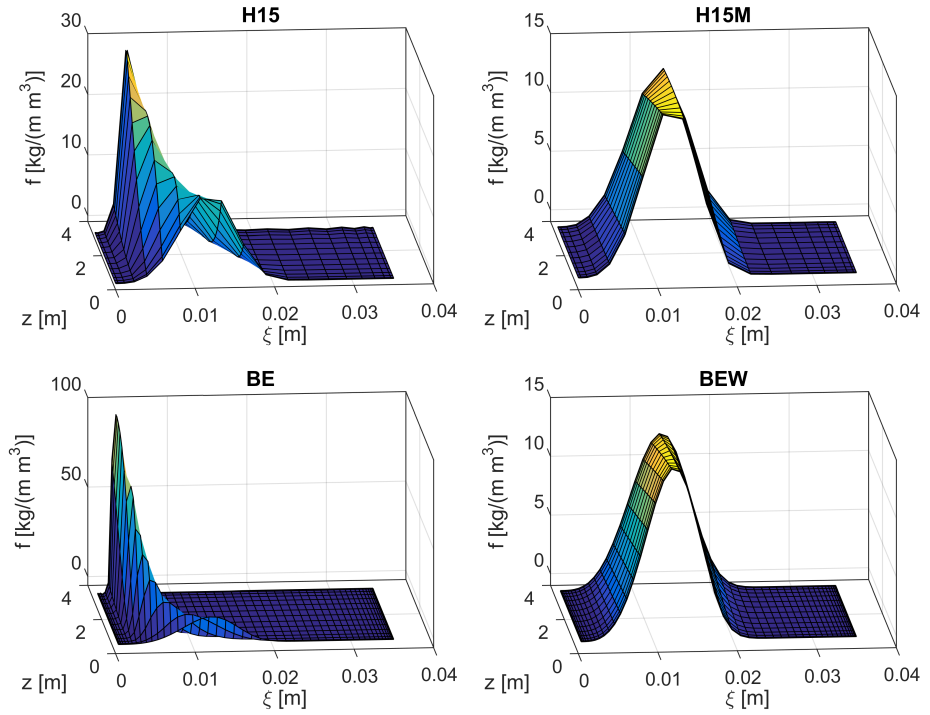

Figure A.35: Mass density functions from the PBE test case using the original and extended versions of Han et al. (2015) and Becker et al. (2014). Physical parameters from the air-water system were used, and the integral scale L was set to 0.001 m for all models except the original model of Han et al. (2015). For H15, L was set to 0.01 m to avoid a diverging solution. The breakage frequency of the original and modified model of Han et al. (2015) was scaled with a factor of 0.1 and 1e-6, respectively.

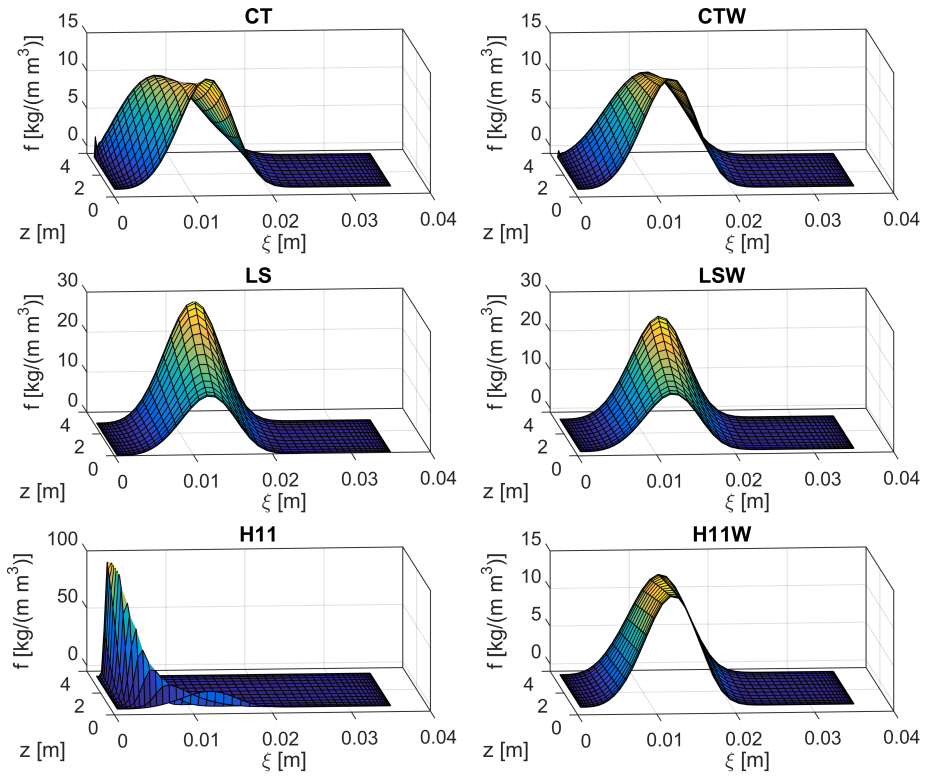

Figure A.36: Mass density functions from the PBE test case using the original and extended versions of Coulaloglou and Tavlarides (1977), Luo and Svendsen (1996) and Han et al. (2011). Physical parameters from the air-water system with $\varepsilon = 1$ W/kg were used, and the integral scale L was set to 0.001 m. To avoid numerical issues, the breakage frequency of the original and extended model of Coulaloglou and Tavlarides (1977) was scaled with a factor of 0.003 and 0.0025, respectively. The breakage frequency of the original and extended model of Luo and Svendsen (1996) was scaled with a factor of 0.001.

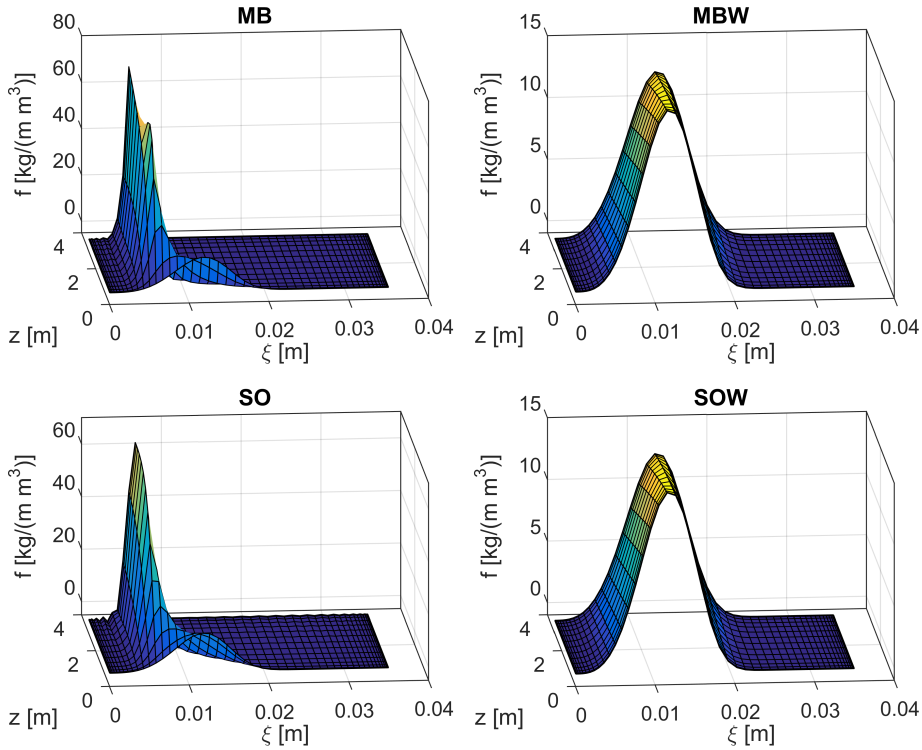

Figure A.37: Mass density functions from the PBE test case using the original and extended versions of Martínez-Bazán et al. and Solsvik et al. (2013). Physical parameters from the air-water system were used, and the integral scale L was set to 0.001 m.

In Figure A.38, the mass density functions for the air-water system using the closure of Liao et al. (2015) and Xing et al. (2015) are given for $L = 0.01$ m.

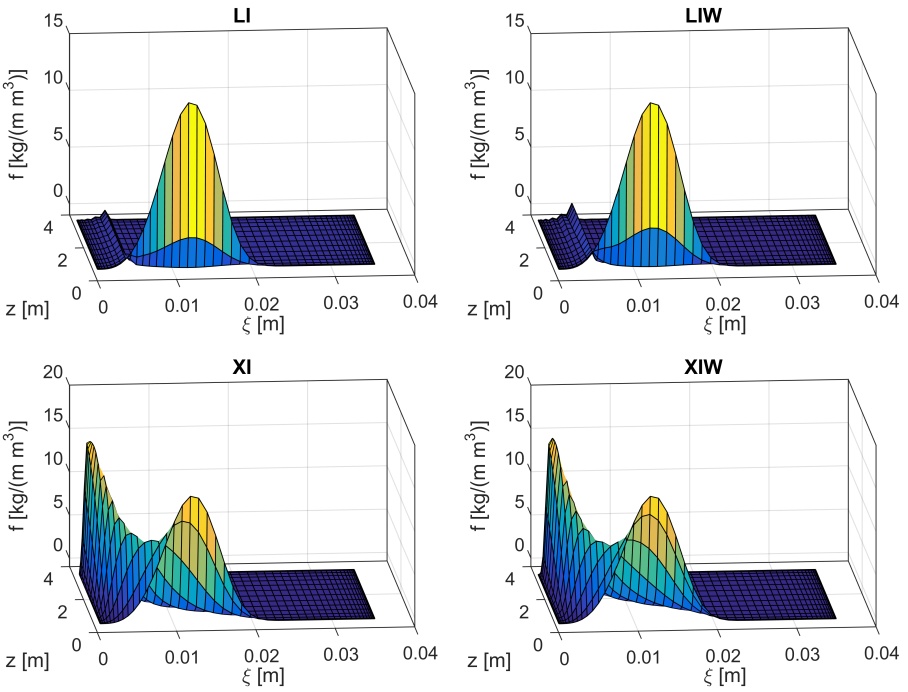

Figure A.38: Mass density functions from the PBE test case using the original and extended versions of Liao et al. (2015) and Xing et al. (2015). Physical parameters from the air-water system were used, and the integral scale L was set to 0.01 m.

In Figure A.39 to A.42, the mass density functions for the air-water system for L = 1 m are shown.

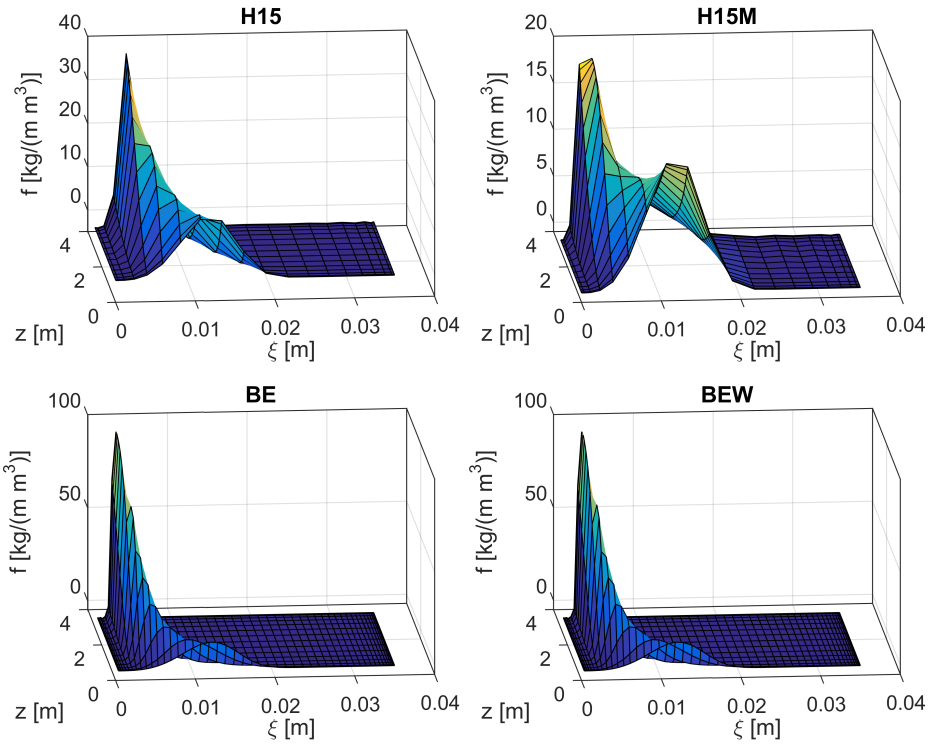

Figure A.39: Mass density functions from the PBE test case using the original and extended versions of Han et al. (2015) and Becker et al. (2014). Physical parameters from the air-water system were used, and the integral scale L was set to 1 m. To avoid numerical issues, the breakage frequency of the original and modified model of Han et al. (2015) was scaled with a factor of 0.1 and 1e-6, respectively.

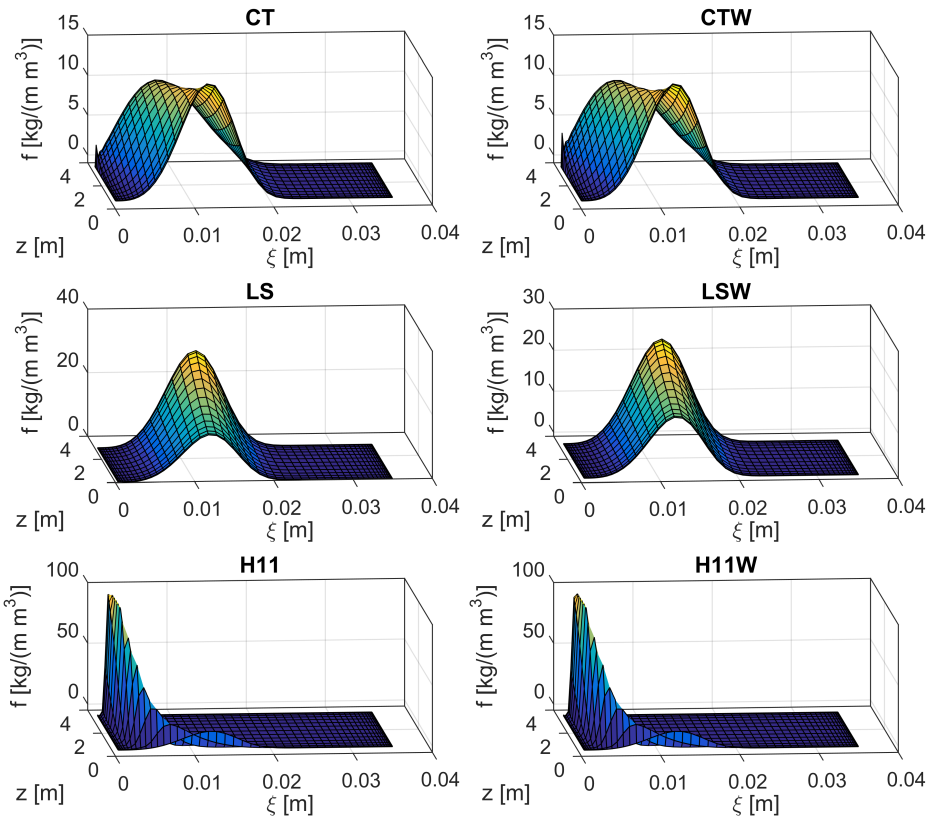

Figure A.40: Mass density functions from the PBE test case using the original and extended versions of Coulaloglou and Tavlarides (1977), Luo and Svendsen (1996) and Han et al. (2011). Physical parameters from the air-water system with ε = 1 W/kg were used, and the integral scale L was set to 1 m. To avoid numerical issues, the breakage frequency of the original and extended model of Coulaloglou and Tavlarides (1977) was scaled with a factor of 0.003 and 0.0025, respectively. The breakage frequency of the original and extended model of Luo and Svendsen (1996) was scaled with a factor of 0.001.

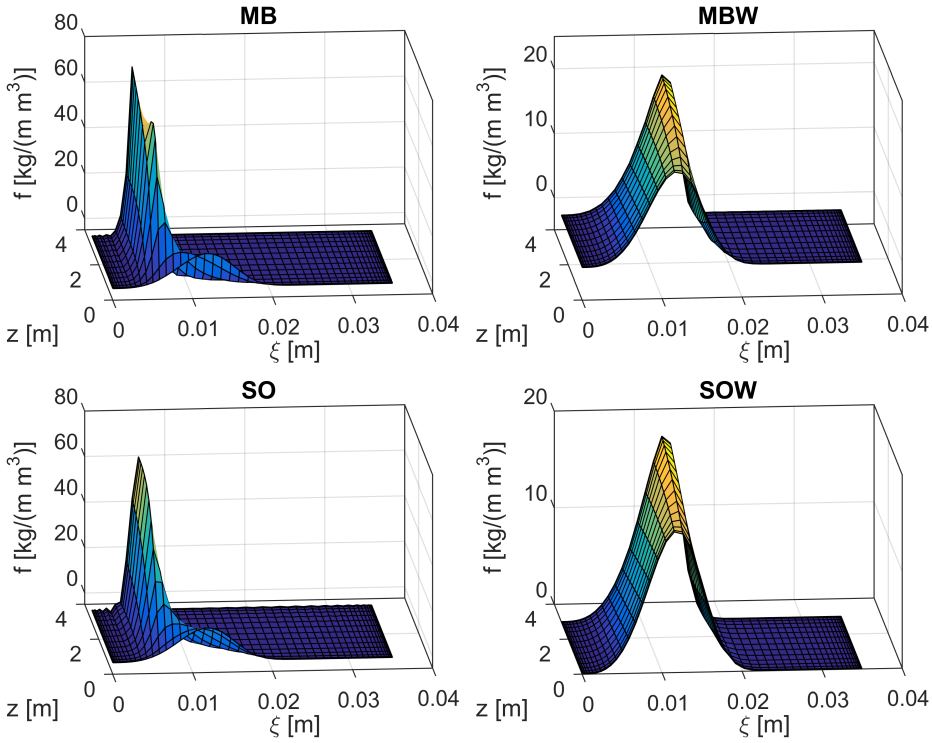

Figure A.41: Mass density functions from the PBE test case using the original and extended versions of Martínez-Bazán et al. and Solsvik et al. (2013). Physical parameters from the air-water system were used, and the integral scale L was set to 1 m.

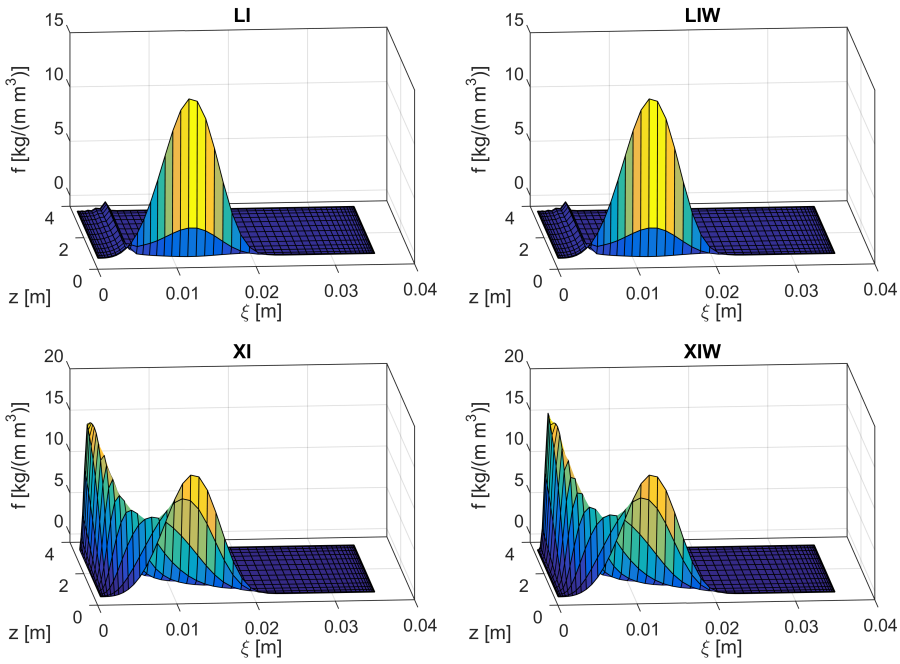

Figure A.42: Mass density functions from the PBE test case using the original and extended versions of Liao et al. (2015) and Xing et al. (2015). Physical parameters from the air-water system were used, and the integral scale L was set to 1 m.

A.3.2 Petroleum-Water System I

In Figure A.43 to A.45, the mass density functions for the petroleum-water system I for L = 0.001 m are shown.

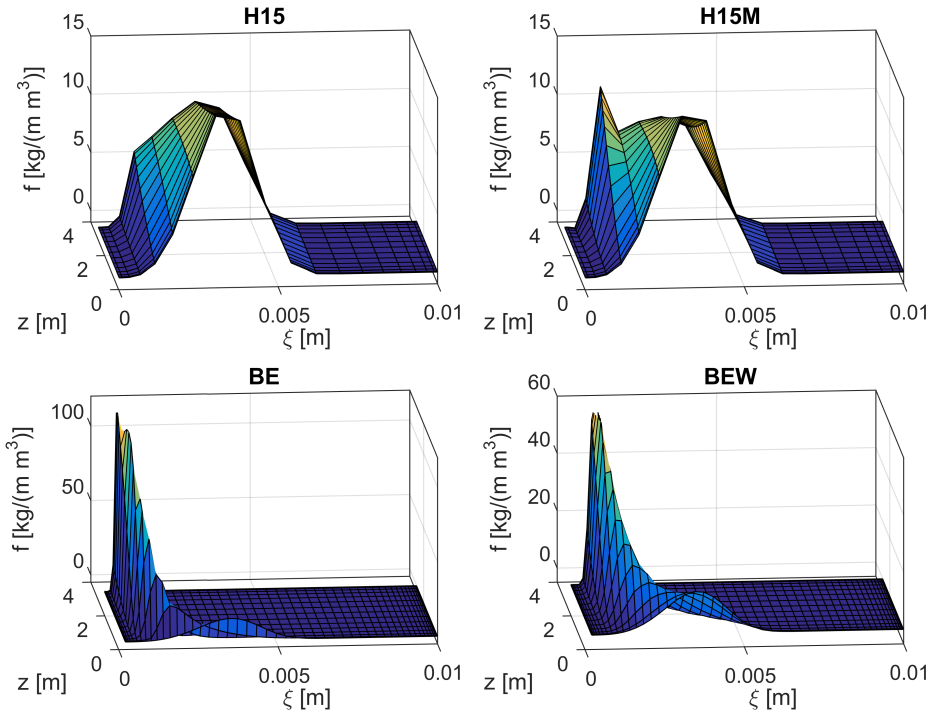

Figure A.43: Mass density functions from the PBE test case using the original and extended versions of Han et al. (2015) and Becker et al. (2014). Physical parameters from the petroleum-water system I were used, and the integral scale L was set to 0.001 m. To avoid numerical issues, the breakage frequency of the original and modified model of Han et al. (2015) was scaled with a factor of 0.1 and 1e-7, respectively.

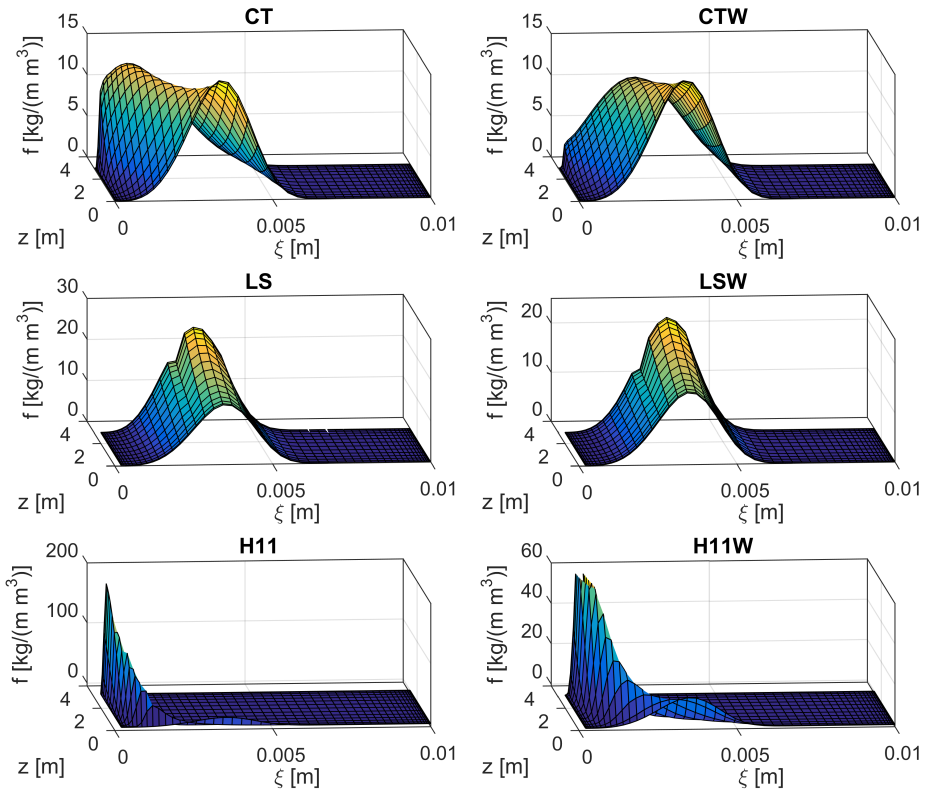

Figure A.44: Mass density functions from the PBE test case using the original and extended versions of Coulaloglou and Tavlarides (1977), Luo and Svendsen (1996) and Han et al. (2011). Physical parameters from the petroleum-water system I were used, and the integral scale L was set to 0.001 m. To avoid numerical issues, the breakage frequency of the original and extended model of Coulaloglou and Tavlarides (1977) was scaled with a factor of 0.008 and 0.005, respectively. The breakage frequency of the original and extended model of Luo and Svendsen (1996) was scaled with a factor of 0.001.

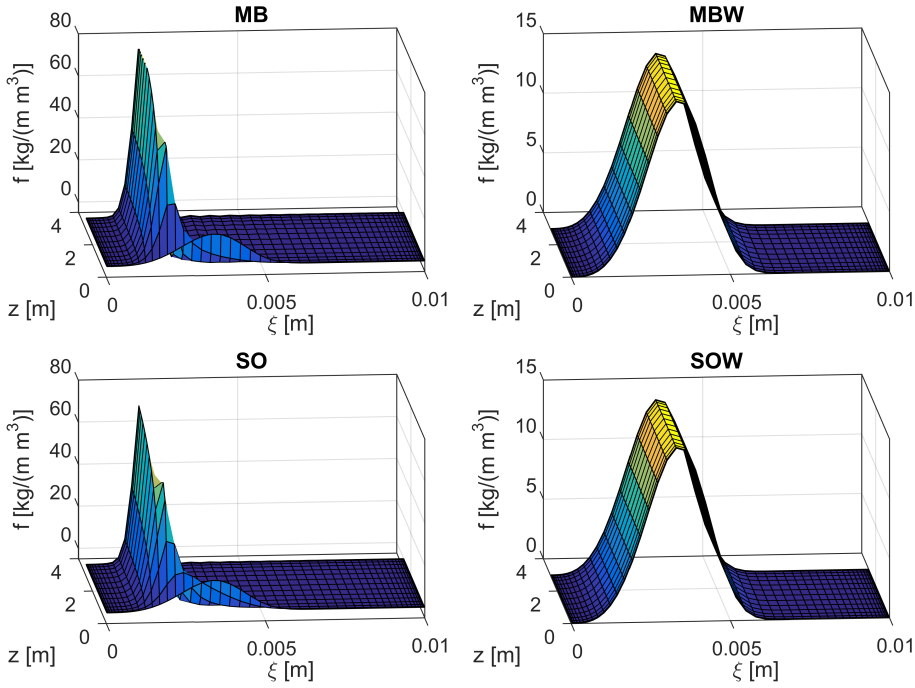

Figure A.45: Mass density functions from the PBE test case using the original and extended versions of Martínez-Bazán et al. and Solsvik et al. (2013). Physical parameters from the petroleum-water system I were used, and the integral scale L was set to 0.001 m.

In Figure A.46, the mass density functions for the petroleum-water system I using the closures of Liao et al. (2015) and Xing et al. (2015) for an integral scale of 0.01 m are shown.

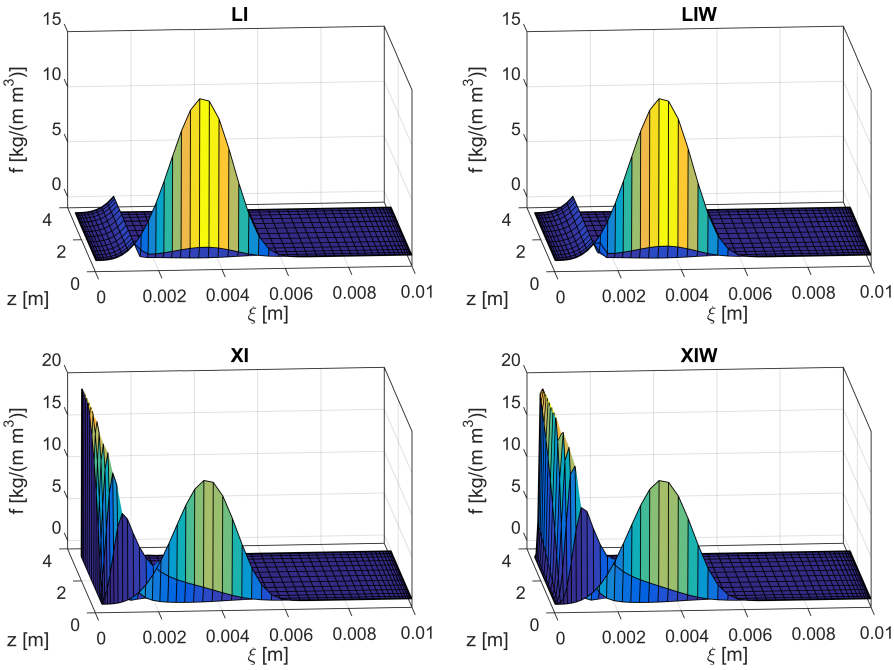

Figure A.46: Mass density functions from the PBE test case using the original and extended versions of Liao et al. (2015) and Xing et al. (2015). Physical parameters from the petroleum-water system I were used, and the integral scale L was set to 0.01 m.

In Figure A.47 to A.50, the mass density functions for the petroleum-water system I for L = 1 m are shown.

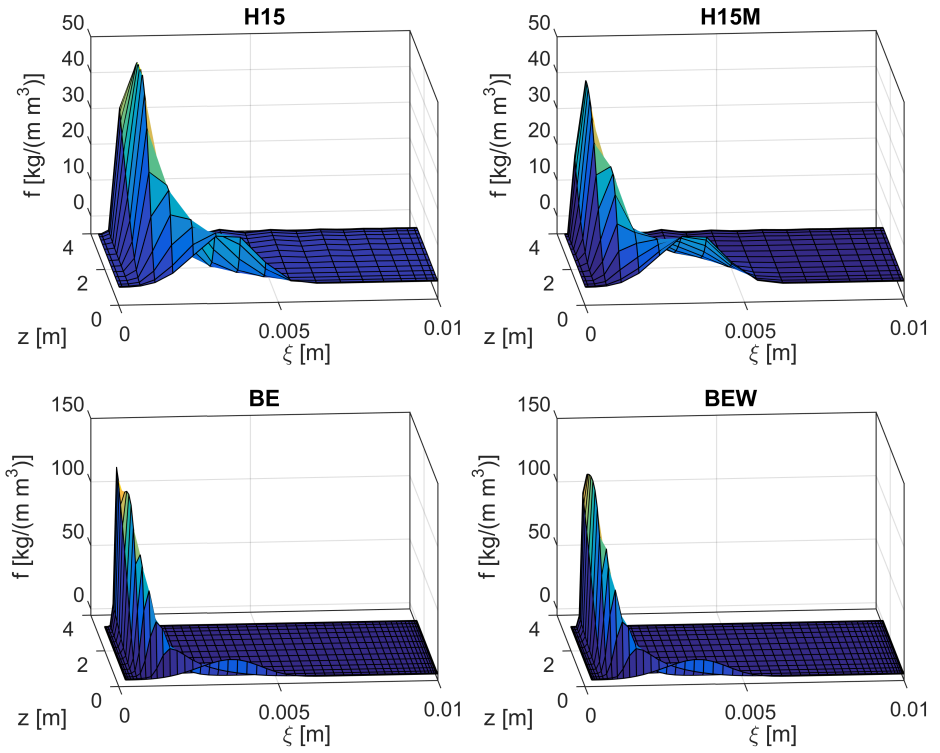

Figure A.47: Mass density functions from the PBE test case using the original and extended versions of Han et al. (2015) and Becker et al. (2014). Physical parameters from the petroleum-water system I were used, and the integral scale L was set to 1 m. To avoid numerical issues, the breakage frequency of the original and modified model of Han et al. (2015) was scaled with a factor of 0.1 and 1e-7, respectively.

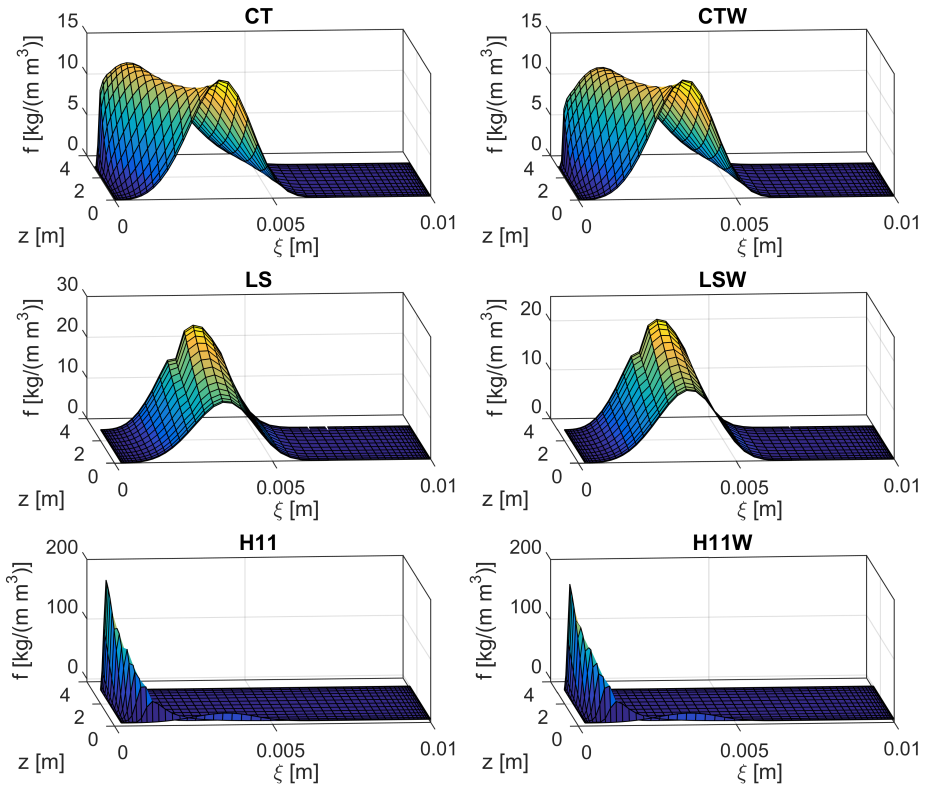

Figure A.48: Mass density functions from the PBE test case using the original and extended versions of Coulaloglou and Tavlarides (1977), Luo and Svendsen (1996) and Han et al. (2011). Physical parameters from the petroleum-water system I were used, and the integral scale L was set to 1 m. To avoid numerical issues, the breakage frequency of the original and extended model of Coulaloglou and Tavlarides (1977) was scaled with a factor of 0.008 and 0.005, respectively. The breakage frequency of the original and extended model of Luo and Svendsen (1996) was scaled with a factor of 0.001.

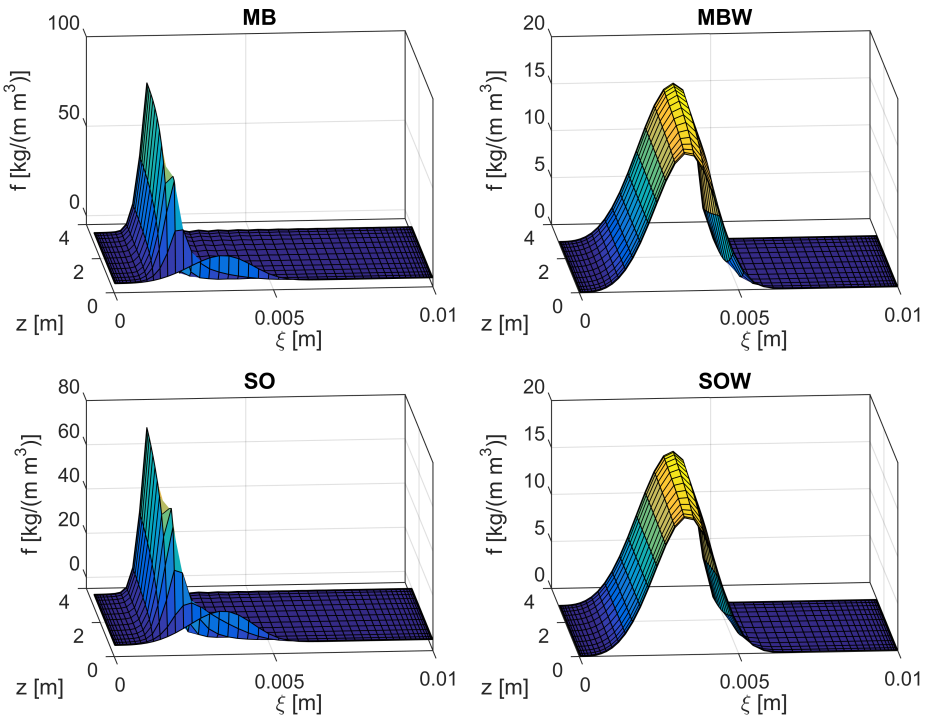

Figure A.49: Mass density functions from the PBE test case using the original and extended versions of Martínez-Bazán et al. and Solsvik et al. (2013). Physical parameters from the petroleum-water system I were used, and the integral scale L was set to 1 m.

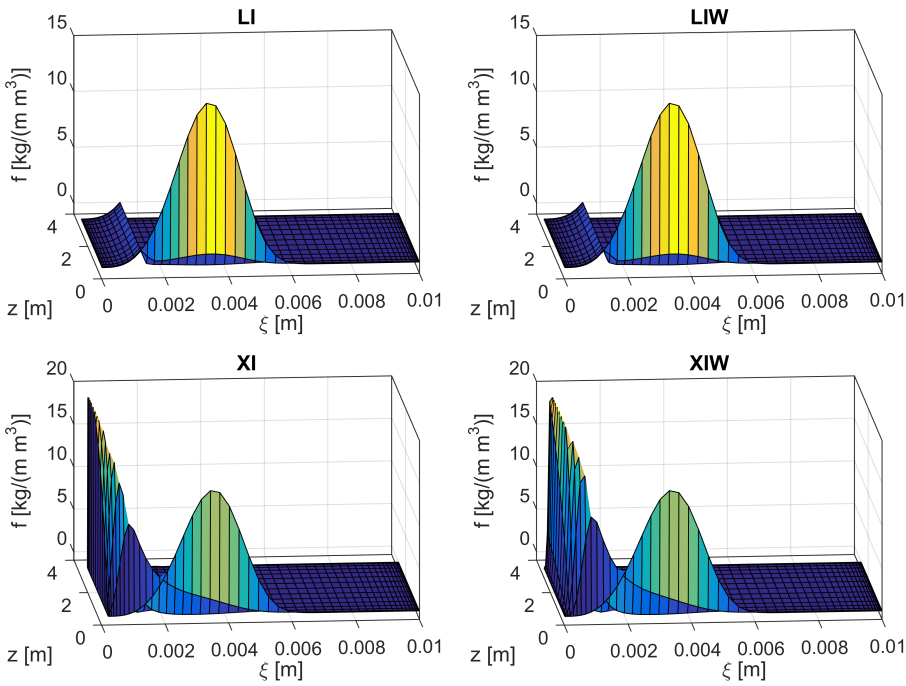

Figure A.50: Mass density functions from the PBE test case using the original and extended versions of Liao et al. (2015) and Xing et al. (2015). Physical parameters from the petroleum-water system I were used, and the integral scale L was set to 1 m.